Exploration of the Chemistry of Macrocycles and Bipyridine Derivatives: Synthesis, Supramolecular Chemistry and Photophysical Aspects

A thesis submitted for the degree of
DOCTOR OF PHILOSOPHY

by

Monima Sarma

School of Chemistry
University of Hyderabad
Hyderabad - 500 046

September, 2012

To

My parents

All My Teachers

Lonima and Nayan Da

My brother Jay

and

Tanmay

Statement

I hereby declare that, the overall material contained in this thesis is the outcome of research accomplished by me in the School of Chemistry, University of Hyderabad, Hyderabad, India, under the supervision of Prof. Samar K. Das.

In keeping with the general trend of reporting scientific observations, due acknowledgements have been made wherever the work described is based on the findings of other investigators. Any omission, which might have occurred by oversight or error, is regretted.

Monima Sarma

Hyderabad
September, 2012

Certificate

Certified that the work pertaining to the thesis entitled "Exploration of the Chemistry of Macrocycles and Bipyridine Derivatives: Synthesis, Supramolecular Chemistry and Photophysical Aspects" has been carried out by Ms. Monima Sarma under my supervision and that the aforementioned work has not been submitted elsewhere for obtaining a degree.

Prof. Samar K. Das
(Supervisor)

Dean
School of Chemistry

Hyderabad
September, 2012

Acknowledgements

At the outset, I would like to express my profound sense of reverence to my supervisor, Prof. Samar Kumar Das, for his constant guidance, motivation and invaluable assistance during the entire tenure of my Ph. D. work and also for providing me with enough liberty to accomplish my research work.

I would like to thank Prof. M. V. Rajasekharan, Dean, School of Chemistry and the former Deans of School of Chemistry for their kind assistance on various instances. Also, I would like to thank the University Grants Commission (UGC), New Delhi for providing me with a research fellowship.

I would also like to thank all the faculty members of School of Chemistry for their kind help on many occasions. Special thanks are due to Prof. Samudranil Pal, Prof. Anunay Samanta, Prof. Sushanta Mahapatra and Prof. K. C. Kumara Swamy (School of Chemistry), Prof. D. N. Rao and Dr. Surajit Dhara (School of Physics), Dr. S. Venugopal Rao (ACHREM) for their valuable help and useful discussion.

Jotting down a 'one line acknowledgement' to my parents, sister, brother, brother-in-law and Tanmay would appear quite preposterous at this moment as their love and back-up has always been the sole motivation of my work.

I would also like to convey my appreciation and thank all the non-teaching staffs of School of Chemistry for their assistance in all the office related matters as well as in the operation of the instruments. Also, I would also like to take this opportunity to convey my heartfelt gratitude and acclaim to all those individuals who have directly or indirectly provided me with invaluable assistance, whether be it guidance, access to materials or any service that had helped me during my stay in the School of Chemistry, University of Hyderabad.

It is my pleasure to acknowledge all my previous and current colleagues: Dr. V. Shivaiah, Dr. V. Madhu, Dr. S. Supriya, Dr. P. Raghavaiah, Dr. T. Arumuganathan, Dr. T. Chatterjee, Dr. B. Rambabu, Dr. A. Srinivas Rao, G. Durga Prasad, Bharat, Kishore, Sridevi, Veeranna, Chinnabbai, Paulami, Krishna, Praveen, Olivia for their cooperation and for creating a soothing ambience during my tenure in the laboratory. I also thank the M.Sc. as well as the UGC networking project students Lavanya, Vindhya, Ashok, Moses,

Sunitha, Pal, Raju, Arti, Shivaiah, Jagadeesh and Y. Mahesh for a congenial environment in the laboratory.

I also thank all my wingmates for their assistance on various occasions, especially, Nayan, Raja, Sanatan, Shesadri, Rama Krishna, Venu, Sudha, Madhusudhan, Pramiti, Ajay, Narayana, Supratim, Chandrasekhar, Viji, Satish, Rama Raju, Ramesh, Ramkumar, Prakash, Anand, Kishore and Prabhu. At this juncture, I would also like to thank Anindita di, Tulika, Nagaraju, Swamy, Balu and Satish for their help during the electrochemical studies, Dinesh for the phosphorescence studies, Sayed Hamad (ACHREM) for the two-photon absorption studies, Gupta and Hari Prasad for helping me on certain occasions. Last but not the least, various cheerful moments with Tridib, Satpal, Bipul da, Sanjeev da, DK Sreenivas, Ranjit Thakuria, and others are worth mentioning.

Monima Sarma

Hyderabad
September, 2012

List of Publications

1. D–π–A–A–π–D prototype 2,2′–bipyridine dyads exhibiting large structure and environment–sensitive fluorescence: synthesis, photophysics, and computation

   Monima Sarma, Tanmay Chatterjee, Susanta Ghanta and Samar K. Das*, *J. Org. Chem.* **2012**, *77*, 432.

2. Spontaneous resolution through helical association of a Cu–azamacrocyclic complex with Lindqvist–type isopolyanion

   Monima Sarma, Tanmay Chatterjee, Hanumanthugari Vindhya and Samar K. Das*, *Dalton Trans.* **2012**, *41*, 1862.

3. Ammonium–crown ether based host–guest systems: N–H···O hydrogen bond directed guest inclusion featuring N–H donor functionalities in angular Geometry

   Monima Sarma, Tanmay Chatterjee and Samar K. Das*, *RSC Adv.* **2012**, *2*, 3920.

4. Cyclometalated iridium(III) complexes containing 4,4'–π–conjugated–2,2'–bipyridine derivatives as the ancillary ligands: synthesis, photophysics and computational studies

   Monima Sarma and Samar K. Das*, **2012** (communicated).

5. Bringing an important macrocycle into a polyoxometalate matrix: synthesis, crystal structure, spectroscopy and electrochemistry of $[Co^{III}(transdiene)(Cl)_2]_2[Mo_6O_{19}]$, $[Ni^{II}(transdiene)][W_6O_{19}]\cdot DMSO\cdot DCM$ and $[Zn^{II}(transdiene)(Cl)]_2[W_6O_{19}]$

   Monima Sarma, Tanmay Chatterjee and Samar K. Das*, *Dalton Trans*. **2011**, *40*, 2954.

6. Inorganic–organic hybrid materials based on Co(III) tetra–aza–macrocyclic complexes and Lindqvist type poly–oxo anions: Synthesis, characterization and spectroscopy of $[Co^{III}(L)(NO_2)_2]_2[Mo_6O_{19}]$ and $[Co^{III}(L)(NCS)_2]_2[W_6O_{19}]\cdot 2CH_3CN$ (L = Transdiene)

   Monima Sarma, Tanmay Chatterjee and Samar K. Das*, *J. Mol. Struct*. **2011**, *1004*, 31.

7. Sterically driven electronic properties of naphthalene– and anthracene–end–capped 2,2'–bipyridine luminophores: synthesis and density functional theory

   Tanmay Chatterjee, **Monima Sarma** and Samar K. Das*, *Tetrahedron Lett.* **2011**, *52*, 5460.

8. Synthesis and photo–physical properties of methoxy–substituted π –conjugated–2,2'–bipyridines

   Tanmay Chatterjee, **Monima Sarma** and Samar K. Das*, *Tetrahedron Lett.* **2010** , *51*, 1985.

9. Donor–acceptor amphiphilic 2,2'–bipyridine chromophores: synthesis, linear optical, and thermal properties

   Tanmay Chatterjee, **Monima Sarma** and Samar K. Das*, *Tetrahedron Lett.* **2010** , *51*, 6906.

10. Supramolecular architectures from ammonium–crown ether inclusion complexes in polyoxometalate association: synthesis, structure and spectroscopy

    Tanmay Chatterjee, **Monima Sarma** and Samar K. Das*, *Cryst. Growth Des.* **2010**, *10*, 3149.

11. Polyoxometalate associated ion–pair solid based on a crown ether inclusion complex: synthesis, structure and spectroscopy

    Tanmay Chatterjee, **Monima Sarma** and Samar K. Das*, *J. Mol. Struct*. **2010**, *981*, 34.

12. A copper–cyclen coordination complex associated with a polyoxometalate anion: synthesis, crystal structure and electrochemistry of [Cu(cyclen)(MeCN)][W_6O_{19}]

    Monima Sarma, Tanmay Chatterjee and Samar K. Das*, *Inorg. Chem. Commun*. **2010**, *13*, 1114.

Posters and Flash Presentations

1. **Monima Sarma** and Samar K. Das*, *D–π–A–A–π–D prototype 2,2'–bipyridine dyads exhibiting large structure and environment–sensitive fluorescence: synthesis, photophysics, and computation.* **Winner of the Flash Presentation at Dr. K V. Rao Scientific Society–2012**, held in March, 2012, KVR Building, Hyderabad, India.

2. **Monima Sarma** and Samar K. Das*, *D–π–A–A–π–D prototype 2,2'–bipyridine dyads exhibiting large structure and environment–sensitive fluorescence: synthesis, photophysics, and computation.* **Winner of the Flash Presentation at Chemfest–2012,** held in February, 2012, School of Chemistry, University of Hyderabad, India.

3. **Monima Sarma** and Samar K. Das*, *D–π–A–A–π–D prototype 2,2'–bipyridine dyads exhibiting large structure and environment–sensitive fluorescence: synthesis, photophysics, and computation.* **Poster Presentation at Chemfest–2012,** held in February, 2012, School of Chemistry, University of Hyderabad, India.

4. **Monima Sarma** and Samar K. Das*, *Stabilization of planar aromatic donors with spherical polyoxoanions: synthesis and characterization of a series of 9,10–bis (imidazolylmethyl)anthracene hexamolybdates and hexatungstates,* **Poster Presentation at 11th CRSI National Symposium in Chemistry,** held in National Chemical Laboratory, Pune, India.

Contents

CHAPTER–1

An Introduction to the Chemistry of Macrocycles and Bipyridine Derivatives: Supramolecular and Photophysical Aspects and Motivation of the Present Work

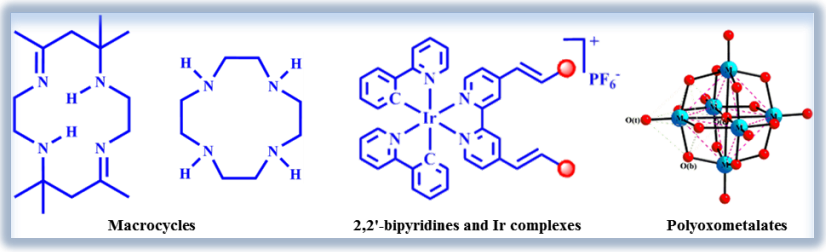

CHAPTER–2

Transition Metal Complexes of Tetra-aza Macrocycles in Polyoxometalate Association: Racemization or Conglomeration?

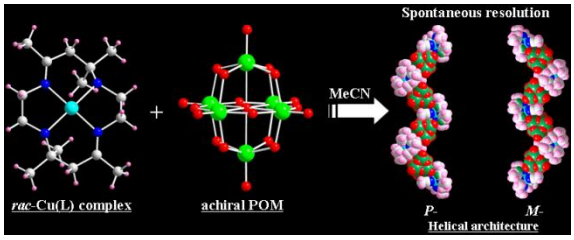

CHAPTER–3

Ammonium-Crown Ether Based Host-Guest Systems: N–H···O Hydrogen Bond Directed Guest Inclusion Featuring N–H Donor Functionalities in Angular Geometry

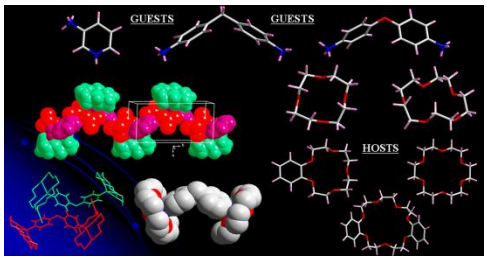

CHAPTER–4

D–π–A–A–π–D Prototype 2,2'-Bipyridine Dyads Exhibiting Large Structure and Environment Sensitive Fluorescence: Synthesis, Photophysics and Computation

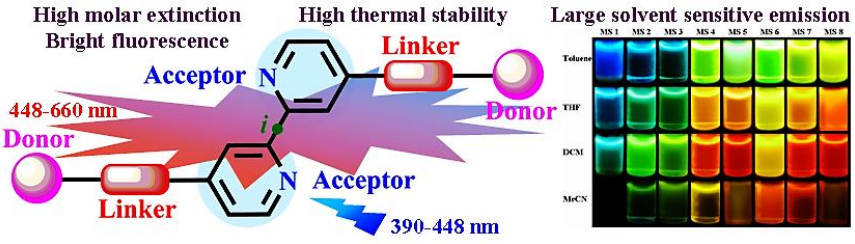

CHAPTER–5

Cyclometalated Iridium(III) Complexes Containing 4,4'–π–Conjugated–2,2'–Bipyridine Derivatives as the Ancillary Ligands : Synthesis, Photophysics and Computational Studies

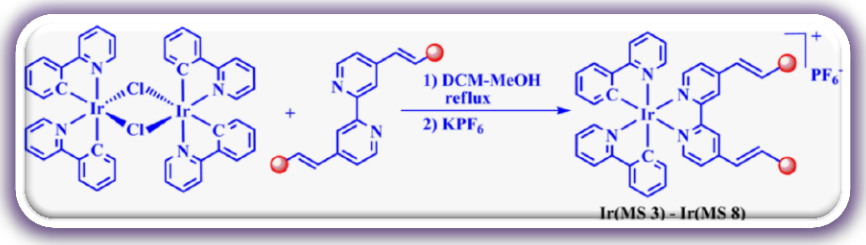

CHAPTER–6

Concluding Remarks and Future Scopes of the Present Work

Chapter-1

An Introduction to the Chemistry of Macrocycles and Bipyridine Derivatives: Supramolecular and Photophysical Aspects and Motivation of the Present Work

ABSTRACT: The present work is mainly subdivided into two broad categories, (a) supramolecular chemistry, and (b) photophysical chemistry. The Chapters 2 and 3 essentially describe the non-covalent intermolecular interactions of macrocyclic cations with external anions whereas, the Chapters 4 and 5 correspond to the syntheses and photophysical properties of 2,2'–bipyridine-based donor–acceptor systems and their transition metal complexes. An important class of inorganic materials namely, polyoxometalates, has been introduced as the anionic counterparts to the supramolecular complexes depicted in Chapter 2. Alternatively, it can be said that, the thesis represents three types of important molecular systems *viz.*, the macrocycles, polyoxometalates and 2,2'–bipyridines, the chemistry of which, has been briefly reviewed in this "Introduction" chapter. Although, an elaborate discussion about the concerned systems is beyond the scope of the thesis, we have made an attempt to focus on the significant aspects of the aforesaid materials relevant to our work. The basic chemistry of the pertinent systems i.e. the synthetic procedures, structural features and their applications etc., has been emphasized in this chapter. On the basis of this background information, we have put across the motivating features behind the present work at the end of this chapter.

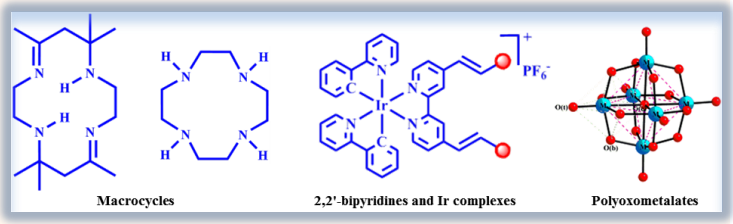

● 1.1. INTRODUCTION

The research in experimental chemistry was probably initiated by the Alchemists long before Christ. The integral parts of experimental research or 'wet' research lies in the design of molecules with desired properties, synthesis of the target molecules using appropriate synthetic strategies and eventually, characterization of the synthesized compounds via available analytical tools. The 'modern chemistry' research was however, fueled up and accelerated with the important inventions such as X-ray, LASER, etc. which paved the way to manufacture various sophisticated instruments for easy characterization and data analyses.

Supramolecular chemistry is a broader subject of modern chemical research which was first brought in by Jean-Marie Lehn in 1978 and was defined as *the chemistry of molecular assemblies and of the intermolecular bond*.[1] Supramolecules are considered as

aggregates in which, a number of components come together, either spontaneously or by design, to form a larger entity, whose properties are generally derived from its precursors. The field of supramolecular chemistry has produced several instances of chemically attractive and aesthetically pleasing self-assembled structures with greater complexity than molecules themselves.[2] The distinction between large molecules and supramolecular species is based on interactions involving the independent molecular parts, i.e., systems where the individual parts or molecules are held together by coordination or covalent bonds are termed as large molecules whereas those, in which intermolecular forces come into play, are termed as supramolecules. Supramolecules are administered by virtue of intermolecular non-covalent forces such as hydrogen bond, dipolar interaction, π–stacking, Van der Waals interaction, donor–acceptor interaction etc.[3–4] The stabilizing energy of non-covalent complexes is generally said to comprise, contributions from an attractive (e.g. electrostatic, induction, charge transfer, dispersion etc.) as well as a repulsive (exchange-repulsion) term. These two forces work in harmony, thereby bringing stability to such supramolecular complexes in which the existence of the repulsive force prevents the subsystems from drawing too close together. Furthermore, it is worth mentioning that supramolecular chemistry forms the basis of life, which is quite evident from the intensive hydrogen bonding interactions between the nucleic bases which are prevalent in the double helical structure of DNA. Therefore, the study of non-covalent interactions is crucial to comprehend many biological processes from cell structure to vision that rely on these forces. In a nutshell, it can be aptly said that the biological systems are often the inspiration for supramolecular research.

Spectroscopy is another broad subject of modern research, the basis of which relates to the interaction between matter and electromagnetic radiation. The electronic nature of the substrates called *chromophores* can be comprehended from the UV-visible and emission spectroscopy. The molecular processes, *Fluorescence* and *phosphorescence* are well-known emission processes that occur upon electronic excitation of a *chromophore*. A substantial growth in the electronics market in the past few decades have aided in devising ultra sensitive detectors for gaining information, even up to the single molecular level. Lately, the design and syntheses of new organic chromophores with tunable photophysical properties are drawing immense notice due to their fascinating applications

in the optoelectronic devices. The work carried out in the present thesis mainly accentuates two broad subjects of chemical research i.e. supramolecular chemistry and synthetic photochemistry. Aza-macrocycles and oxy-crown ethers are the supramolecular synthons used in Chapters 2 and 3, to build various network structures. The other part of the thesis (Chapters 4 and 5) involves syntheses and photophysical aspects of the 2,2'–bipyridine derivatives along with their transition metal complexes. The related chemistry of the focused substrates of the present work is briefly discussed before delving into the main contents of the thesis.

● 1.2. SUPRAMOLECULAR CHEMISTRY AND THE MACROCYCLES

The formation of supramolecular aggregates or supramolecules is generally governed by molecular recognition of a guest component (substrate) by a host (receptor) through non-covalent intermolecular forces. Thus, the supramolecules are also termed as host-guest complexes. Several types of host molecules have been reported so far, some common representative examples being cyclodextrins, calixarenes, cucurbiturils, porphyrins, metallacrowns, crown ethers, zeolites, cyclophanes, aza-macrocycles etc.

As the non-covalent interactions in supramolecules are usually weak, therefore the only way to achieve strong and specific complexation (recognition) of a guest molecule is the presence of several binding sites in the host or receptor molecule. Though the principle of multi-site complexation is very familiar in biological systems, the same can also be viewed from the generalized chelate effect. Macrocycles are regarded as excellent building blocks for providing multi-complexing sites and the whole cavity for guest encapsulation through non-covalent interactions. An important prerequisite for multi-site binding is that, the binding sites of host and guest molecules must be complementary, i.e. complexation is most efficient when the shapes and arrangements of binding sites in host and guest molecules match each other in congruence with the general lock and key principle by Emil Fischer.[5]

In the present work we have chosen tetra-aza macrocycles and crown ethers as components (see Chart 1) to derive the target supramolecular complexes. A brief overview of the concerned macrocycles will be given in the next few sections of this chapter. The interlaying supramolecular chemistry of the synthesized compounds will be discussed in the respective chapters.

● 1.2.1. Chemistry of transdiene

The 14–membered aza-macrocycle 5,7,7,12,14,14–hexamethyl–1,4,8,11–tetraazacyclo tetradeca–4,11–diene (commonly known as transdiene) was first synthesized by N. F. Curtis.[6] The master thesis of Curtis described a yellow diamagnetic solid, that was prepared from the reaction between paramagnetic $[Ni(en)_3]^{2+}$ and acetone. In 1961, the yellow solid was recognized as the square planar Ni^{II} complex of transdiene (hereafter L). After the discovery of synthetic routes for obtaining the protonated form of the free macrocyclic ligand, coordination complexes of L were extensively explored in terms of electron transfer reactions,[7] as model systems towards understanding the active sites of some biologically active metallo–proteins (e.g. vitamin B_{12}),[8] in terms of catalysis (e.g. H_2O and CO_2 reduction) etc.[9] The macrocycle, L is generally characterized by two NH(*sec*) protons and based on their orientation, the ligand L generates two chiral centers

Chart 1. List of the macrocycles used in the present work.

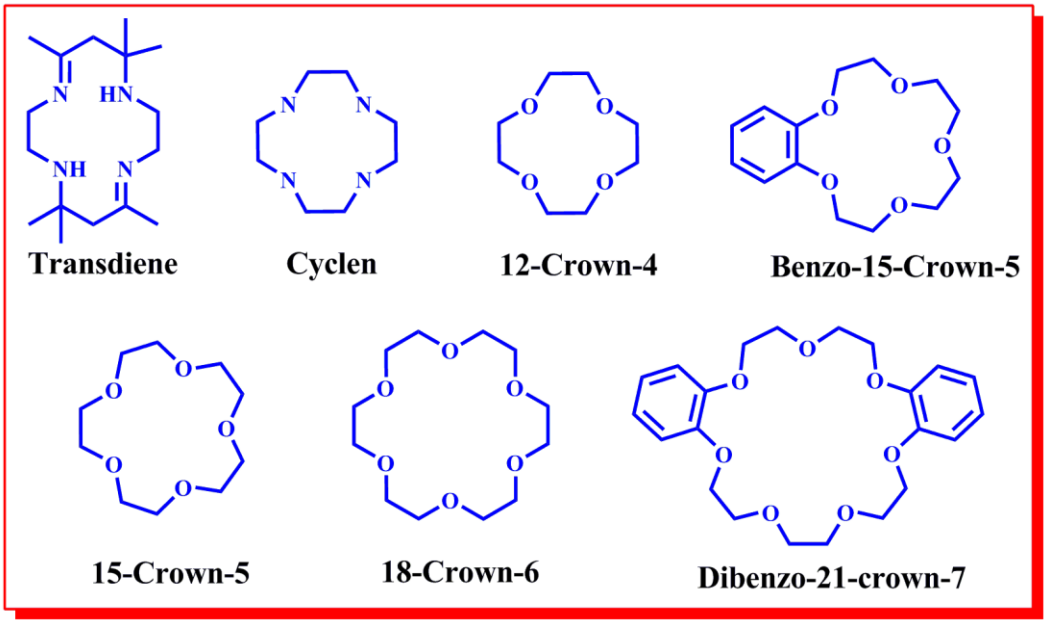

when it coordinates to a metal atom. Thus, the relevant coordination complexes exist as two diastereomers *viz*. *racemic*– (*RR*– or *SS*–) if both the NH(*sec*) protons are on the same face of the macrocycle and *meso*– (*RS*–) if they project to different faces as shown in Scheme 1.[10] This macrocycle is mostly isolated as its perchlorate salt in which N(amine)–H···N(imine) hydrogen bonding between the two ethylenediamine type

fragments stabilize the system. It is evident from Scheme 1 that, there are two types of nitrogen atoms in the molecular structure of L and its metal complexes: (a) the amine nitrogen atoms and (b) the imine nitrogen atoms. The amine (>NH) and imine (>C=N–) functionalities can be clearly distinguished by IR spectroscopy. Therefore, two types of C–N bonds exist in the molecular structure of L and its complexes i.e., the longer C–N(amine) and shorter C=N(imine) bonds. Similarly, there are three different types of peripheral methyl groups in L: (a) axial, (b) equatorial and (c) directly attached with the imine functionality. Although, the structure of L resembles a Schiff base, it has been found to be highly stable even in acidic or basic media in contrast to the conventional Schiff bases which are prone to hydrolysis in these media.

Scheme 1. Molecular structure of L and its coordination complex, showing two diastereomers of the M–L complexes.

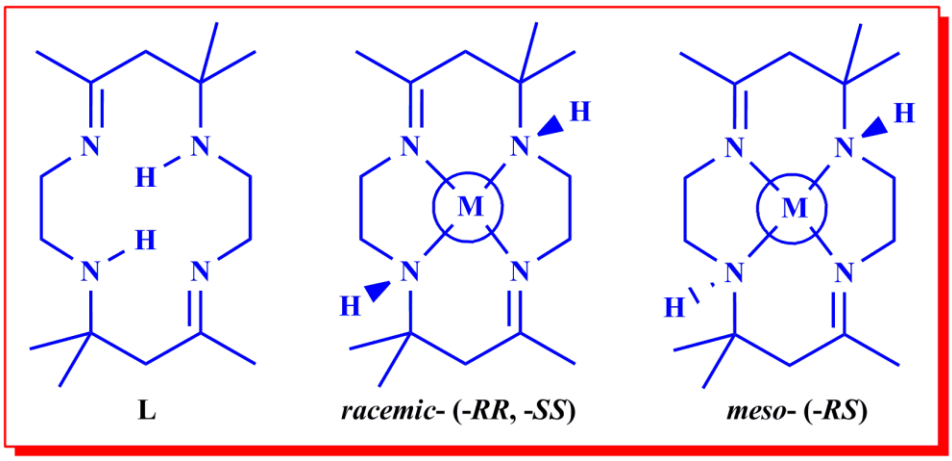

The higher stability of the coordination complexes of L as compared to that of an open chain chelating ligand e.g. ethylenediamine is a direct consequence of the macrocyclic effect. An accepted explanation for this phenomenon is the intricacy in detaching the first donor atom from the metal ion in what is probable to be a stepwise dissociation of the polydentate ligand. A polydentate chelate can be dissociated from a metal ion in the course of successive S_N1 replacement steps, commencing with a terminal donor. However, a macrocyclic ligand cannot be dissociated in a similar way as because there is no end group. Therefore, some sort of ligand rearrangement has to occur so as to weaken one M−L bond prior to its dissociation, thereby eventually impelling the rest of

the ligand to dissociate. Since such type of a rearrangement exacts a cost in energy, hence the dissociation step is found to be very slow. Even though similar problems might be expected to slow the rate of formation reaction as well, experimental database have suggested that the macrocyclic effect arises primarily from the dissociation step, signifying that dissociation is more delayed than is binding. Moreover, the macrocyclic effect is expected to be associated with more favorable entropy of complexation. This is for the reason that upon coordination, a linear ligand tends to lose free rotations around its single bonds to some degree while in a macrocycle, these rotations are already partially lost (although macrocycles possess a considerable degree of conformational flexibility). Thus, the primarily dissociative effect in addition to this highly associative chelate effect leads to a large increase in stabilization for macrocyclic complexes.

Scheme 2. Two synthetic procedures to obtain the macrocycle, L.

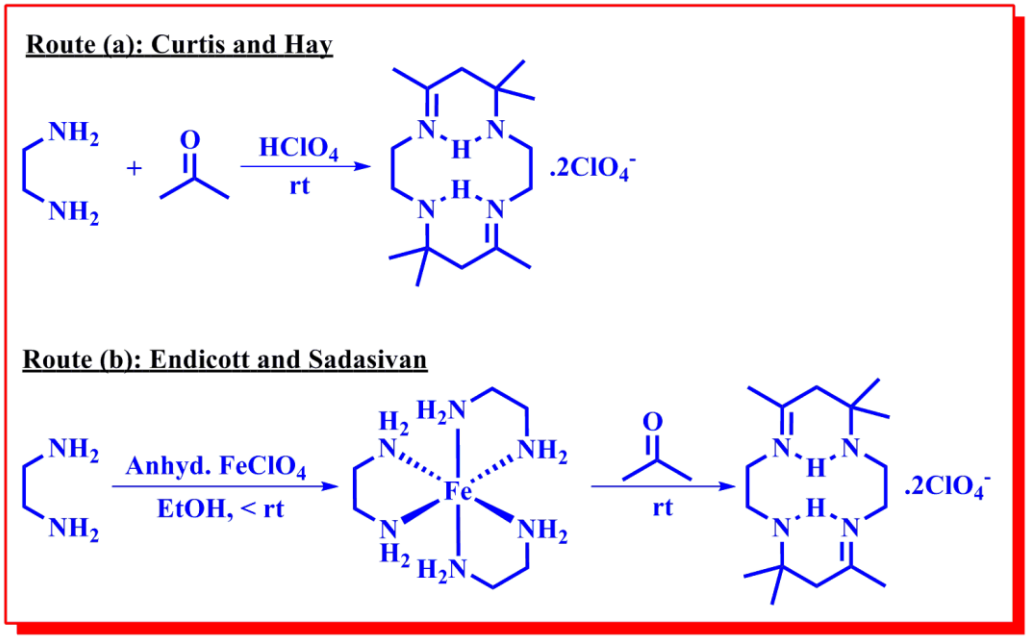

Two different synthetic procedures to obtain the macrocycle have been individually reported by (a) Curtis and Hay,[6f] and (b) Endicott and Sadasivan.[6g] Infact, both the aforementioned routes can be used for the synthesis of the dihydroperchlorate salt of L (see Scheme 2). Curtis and Hay (1966) synthesized the title compound by a simple Schiff condensation between ethylenediamine and acetone in presence of perchloric acid.[6f] In the same year (1966), Endicott and Sadasivan followed metal-template condensation

procedure to synthesize $L{\cdot}2HClO_4$.[6g] The concerned synthetic methodology involved condensation between $Fe(en)_3(ClO_4)_2$ and acetone at room temperature.[6g] Although the same reaction was tested with various other transition metals (copper, nickel, cobalt, zinc etc.), it was finally established that only iron could template the desired compound in good yield. However, the synthetic route (b) has some major drawbacks such as, (i) the synthesis is complex as compared to route (a) and special care has to be taken to avoid moisture, (ii) the desired compound gets contaminated with colored impurities, metal oxides, hydroxides etc., (c) repeated recrystallization of the isolated solid is required for its purification, etc.

Scheme 3. Synthetic routes to obtain some of the $Co(L)X_2$ complexes; L = transdiene, X = axial ligand.

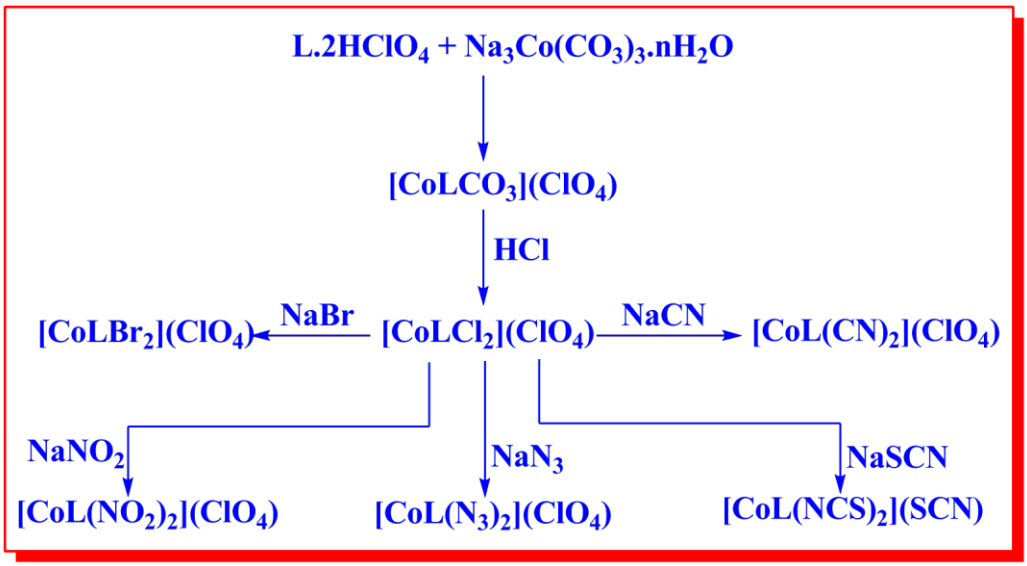

Previously, Endicott and co-workers synthesized a series of cobalt complexes of L and studied their spectral properties.[11] In the pertinent study, the coordination geometry around the metal center in the Co^{III} complexes, was found to be octahedral in which the four nitrogen atoms of the macrocycle provided the basal coordination and two additional ligands (halide, nitro, isothiocyanato etc.) occupied the axial positions. The relevant complexes were formulated as $Co^{III}LX_2$ in which X was the axial ligand. It was shown that a diverse class of macrocyclic compounds could be synthesized through simple wet-syntheses as schematized in Scheme 3. The pertinent compounds were synthesized using $[Co^{III}(L)Cl_2](ClO_4)$ as the starting precursor which was obtained by the reaction between

$L{\cdot}2HClO_4$ and $Na_3[Co(CO_3)_3]{\cdot}3H_2O$, followed by acidification with HCl. Thus, it is quite evident that the lability of the Co−Cl bonds renders the replacement of cobalt bound axial chloride ligands by several other nucleophiles (NO_2^-, N_3^-, SCN^-, CN^- etc.) easy. Infact, all the complexes differ in their color, based on the axial ligands. For example, the precursor complex, $[Co^{III}(L)Cl_2](ClO_4)$ is green in color while replacement of the axial ligands by nitro leads to the isolation of $[Co^{III}(L)(NO_2)_2](ClO_4)$ which is orange-yellow. A simple crystal field model for the relevant cobalt complexes was also established by Endicott *et. al* on the basis of UV-visible spectroscopic data.[11] The absorption spectra of $Co^{III}LX_2$ complexes, in the pertinent study, were found to consist of three low-intensity absorption bands in the visible and near-ultraviolet spectral regions which were assigned to the Bands IA, IB and II based on the convention of Linhard and Weigel.[11] The same convention has also been used to explain the absorption spectra of the cobalt complexes presented in Chapter 2. The structures of the aforementioned $Co^{III}LX_2$ compounds were unambiguously elucidated later after the invention of X-ray diffractometer. At this point, it is interesting to note that the crystal structures of Co^{III}–L and Co^{II}–L complexes were found to be remarkably different. The Co^{III} complexes were found to be low–spin and octahedral in which the macrocycle provided the basal coordination and two auxiliary ligands occupied the apical sites. In contrast, the Co^{II} complexes were found to be tetra–coordinated (square planar).

It has already been mentioned that, transition metal complexes of L have been heavily used for the study of electron transfer reactions. Endicott and co-workers investigated the electron transfer reactions of dihalogen radical anions ($2X_2^- \rightarrow X_2 + 2X^-$) with Co^{III} and Co^{II} complexes of transdiene.[12] The relevant study was very crucial as only few reactions of dihalide radical anions with transition metal substrates were known during that period. It was observed that the tetradentate ligand, L remained coordinated to Co^{II} for long periods in aqueous solutions. As such, radical recombination reactions were expected to be particularly important for charge transfer photochemistry of the $Co^{III}LX_2$ species (X = axial ligand). In addition to this, it was also observed that the Co^{II}–L species was weakly reducing and low–spin, and thus, it was suggested that such systems could act as good model systems for examining the reactivity of low–spin Co^{II} complexes with simple radicals.

Besides, cobalt complexes of the macrocycle, L are also used as model systems of vitamin B_{12}. The octahedral complexes of the type $[Co^{III}LX_2]^-$ (where X is anionic axial ligand) exist as two diastereomers *viz*. *racemic*– and *meso*–. Interestingly, the symmetry of such type of complexes is further reduced when the two axial positions are differently substituted. Creutz and co-workers reported an organo–cobalt complex with the axial positions of the Co^{III} center being occupied by a methyl and an aquo substituent.[13] The general structural feature of the complex is presented in Scheme 4, which reveals the possibility of three isomeric forms of the concerned Co–L complex. The two vertical lines in each of the cartoon representations denote the orientation of the axial methyl groups of the macrocycle. They project to the same face of the macrocycle in case of the *racemic*– isomers while the reverse order is followed in case of the *meso*– diastereomers.

Scheme 4. Molecular structure of the $[Co(L)(CH_3)(OH_2)]^{2+}$ cation along with the cartoon representation showing the three possible isomers of the cobalt complex.

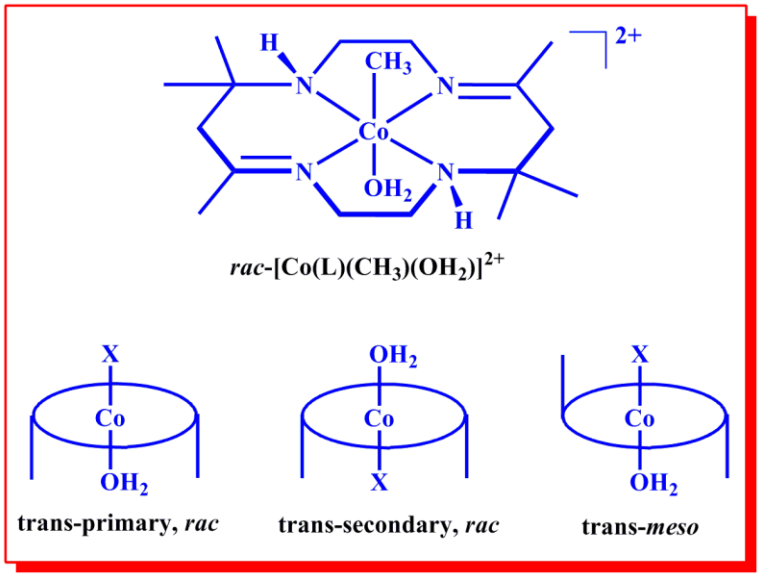

Accordingly, if the open face of the macrocyclic complex is denoted as "primary" and the face toward which the axial methyl groups point is denoted as "secondary", then the two isomers of the *racemic*– diastereomer are termed primary X, aquo and secondary X, aquo. The determination of crystal structure of the compound, $[Co(L)(CH_3)(OH_2)](CF_3SO_3)_2$, in the pertinent study, pointed out that the stereochemistry of the coordination complex was *trans–sec*, *rac*–.[13] The macrocycle in the title crystal structure was found to

be twisted so that the two "axial" methyl groups of the macrocycle were swept back away from the axially coordinated methyl ligand. This configuration was thought to be stabilized by the hydrogen bonding interactions between the macrocycle amine hydrogen atoms and the trifluoromethane sulfonate anions. The system was further stabilized by hydrogen bonds between the axial aquo ligand and the trifluoromethanesulfonate anion. These hydrogen bonding interactions, as well as the methyl–methyl repulsion on the secondary face of the macrocycle, were considered to be responsible for the folding of the macrocycle towards the axial water ligand and away from the axial methyl ligand.[13]

Apart from the cobalt complexes, coordination complexes of transdiene with Ni^{II}, Fe^{III}, Cu^{II}, Zn^{II} etc. as the metal centers, have also been synthesized. Endicott and Sadasivan prepared a series of M–L complexes (M = Ni^{II}, Cu^{II}, Zn^{II}) using dihydroperchlorate salt of L and appropriate transition metal precursors.[6g] However, structures of the synthesized complexes could not be affirmed at that time. It was only after the introduction of X-ray diffractometer in 1970s, that geared up research in structural chemistry. The determination of the crystal structures of the relevant nickel complexes revealed that, unlike the hexa–coordinated Co^{III} complexes, the Ni^{II} center was rather tetra–coordinated and in square planar geometry. Surprisingly, it was also observed in the pertinent study that the square planar Ni^{II} complexes were very robust to coordination enhancement to hexa–coordination even in presence of highly coordinating ligand e.g. CN^{-}. This observation was interpreted by several plausible explanations e.g. (a) strong tendency of the amine protons to hydrogen bond with the counter anions in both the solid and solution state, (b) tendency toward decreased coordination in the axial positions of six–coordinate Ni^{II} complexes containing strong inplane fields, (c) steric crowding of the axial ligating sites etc.[6g] Although, the Ni^{II}–L complexes are mostly tetra–coordinated and square planar, exceptions are also known. For instance, Liao and co-workers reported a penta–coordinate complex, $[Ni(L)(NCS)]ClO_4$ about a decade ago, with a thiocyanate ligand bound to one of the apical sites leading to a square pyramidal geometry around the metal center.[14]

The nickel complexes of L, have also been found to exhibit catalytic oxidation activity, wherein the host-guest nanoscale nickel complex, (Ni^{II}–L) is formed by the encapsulation of the macrocycle into the zeolite matrix. For example, cyclohexene is

catalytically oxidized to 2–cyclohexene–1–ol and 2–cyclohexene–1–one in the presence of O_2 and $[Ni(L)]^{2+}$–NaY in a solvent-free medium at 70 °C.[15]

Till date, several crystal structures associated with the transition metal complexes of L have been reported. All the structures exhibit some general features, for instance, longer M–N(amine) bonds compared to shorter M–N(imine) bonds, the five–membered ring bite angles are 4–8° less than 90° and the six–membered ring bite angles are 4–6° greater than 90° etc. In case of the *racemic*– diastereomers, the two axial methyl groups of the macrocycle project towards the same face of L whereas; they are observed in opposite projection in case of the *meso*– isomers. The stereochemistry of the M–L complexes can therefore, be unambiguously assigned on the basis of projection of the axial methyl groups even if the amine hydrogen atoms are not located from the X-ray diffraction data. Apart from the strong intermolecular non-covalent interactions such as N–H···O, O–H···O, O–H···N etc., the C–H···O hydrogen bonding interaction has been observed in several crystal structures which play a pivotal role in constructing multidimensional supramolecular frameworks. It is nonetheless, important to mention that, the periphery of the M–L complexes comprises many methyl and methylene groups which might participate in intermolecular C–H···O interactions with an exterior hydrogen bond acceptor. The metal oxo–cluster anions or polyoxometalates (POMs) have been used as the hydrogen bond acceptors to the macrocycle donors in the present study. A brief introduction to this supramolecular building block is made at a later stage in this chapter. The key reason behind pairing up of the two important classes of materials *viz.* the transition metal complexes of transdiene and the POMs is described in a separate section (*vide infra*).

● 1.2.2. Cyclen

The tetra-aza crown ether 1,4,7,10–tetraazacyclododecane, commonly named as cyclen, is another important macrocycle, widely known both in the areas of supramolecular and coordination chemistry. Cyclen readily forms complexes with transition metals, lanthanides and actinides. However, only few instances are known where this macrocycle binds alkali and alkaline earth metals. The selectivity of cyclen towards the *d*- and *f*-block elements over the *s*- and *p*- block elements is evidently a consequence of the HSAB principle. The most significant aspect of this macrocycle lies in the fact that the

gadolinium complexes of cyclen and its derivatives are promising contrast agents for Magnetic Resonance Imaging (MRI).[16a–d] A few important derivatives of cyclen are exemplified in Chart 2. It has been found that the attachment of hydrophilic side chains to cyclen noticeably increases the tolerability of the corresponding Gd^{III} complexes.[16a–d]

Chart 2. Some important derivatives of cyclen.

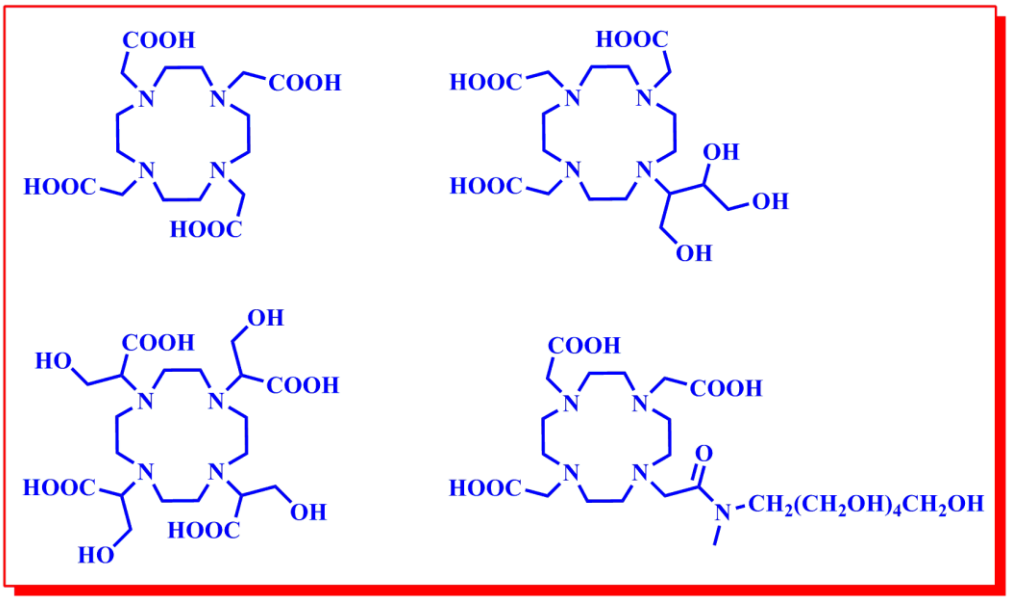

Furthermore, such types of macrocyclic polyamine systems have proven to be extremely valuable as scaffolds for encapsulating metal ions into larger molecular fragments. As a result, derivatized forms of cyclen are becoming increasingly popular as typical building blocks in the applications requiring highly selective metal ion chelation[16e–i]. Thus interestingly, aza-crown macrocycles have the potential to reduce the toxicity of toxic metal environment/surrounding through their strong coordination with concerned metal ions. However, such supramolecular complex species are generally soluble in common laboratory solvents, as a result of which, separation of the concerned metal ions from solution becomes difficult. As such, heavy anions, such as polyoxometalate cluster anions can act as useful candidates in the sense that, they can easily be associated with such soluble supramolecular complex cations (ion–pair association/adduct formation) to form insoluble precipitates. This is a handy way of separating specific metal ions (depending on cavity size of the aza-crown ethers) from an aqueous solution by precipitation method.[16j–k]

● 1.2.3. Crown ethers as supramolecular building blocks

Crown ethers are the paradigms in supramolecular chemistry which have been investigated heavily as a host for various organic and inorganic guests. This important class of macrocycle was serendipitously discovered by C. J. Pedersen.[17] Till date, a large number of crown ethers have been reported, in which the heteroatoms are mostly oxygen, nitrogen, sulfur, mixed oxygen and nitrogen or sulfur atoms, and they are bridged by aliphatic or aromatic carbon spacers. Among the several derivatives of crown macrocycles, the all oxygen, all nitrogen and mixed oxygen–nitrogen heteroatom containing derivatives are mostly used to recognize neutral or ionic organic and inorganic species. The oxygen atom is the predominant heteroatom in the crown ether chemistry. The general structural feature of such macrocyclic hosts, being saturated and repeating glycolic units (–O–CH_2–CH_2–O–), confers structural elasticity or conformational mobility to the crown ethers, whereby the nature of guest incorporation is largely governed by their cavity sizes and the most stable complexes are formed with the closest match between host cavity and cation size. As for example, the ionic radii of the alkali metal cations along with the approximate diameter of complementary crown ethers in idealized binding conformations are shown in Scheme 5. This remarkable selectivity of metal cation binding to macrocycles in fact illustrates the principle of molecular recognition and in a broader sense, the "lock and key" principle and is the basis for many applications. This size fit argument, as a basis for solution selectivity patterns has undergone much revision and addition at a later stage. Though the smaller crown ether, 12–crown–4 has no selectivity towards any metal cation, there are instances where it binds Li^+ or Na^+ cations with the crown being distorted because of the size mismatch.[18] A similar trend of deviation from the hole–size concept has also been observed for the complexes of transition metal cations with azamacrocycles.[19] Thus, it can be concluded that the hole–size concept apparently works better for more rigid systems which exhibit a size–match selectivity for both small and large cations.

The crown ethers possess a hydrophobic ring surrounding a hydrophilic cavity, which enables them to form stable complexes with metal ions and also to be simultaneously incorporated in the lipid fraction of the cell membrane. Natural and synthetic ionophores are capable of forming stable, most often lipophilic complexes with charged hydrophilic

Scheme 5. A comparison of the ionic radii(Å) of alkali metal cations with the cavity diameter(Å) of crown ethers.

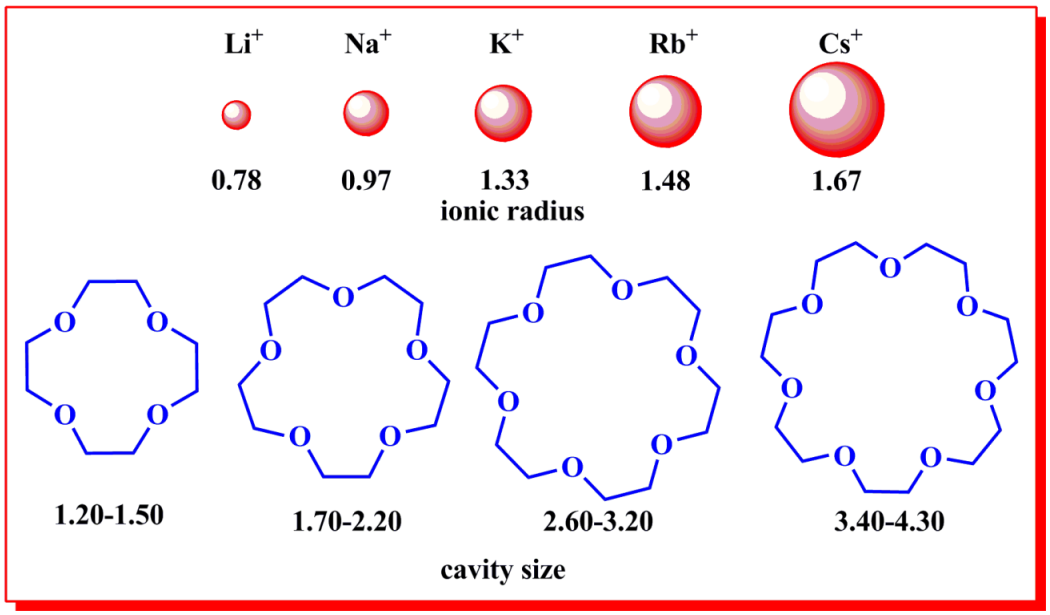

species. They can transfer ions into the lipophilic phases and can therefore, be used as trans-membrane carriers. As a rule, the complexation demands that the process is quite specific and thus, the ionophores get a fair chance to discriminate between metal cations of different charge and different size. Ionophores behave as host molecules for the simplest guests of spherical shape, e.g. alkali and alkaline earth cations, and encapsulate them within their cavities through electrostatic forces.[20] Most often, the majority of ionophores which have been used for elimination of metal ions are neutral crown ethers. Anions generally accompany these macrocyclic complexes to maintain electrical neutrality when these are used to mediate metal cations.

Crown ethers have been extensively used in the area of crystal engineering. In the relevant crystals, these macrocycles play two major roles; (i) act as hydrogen bonding acceptor through the involvement of D–H···O interaction between the guest donor and the electronegative oxygen acceptor of the host and, (ii) act as hydrogen bonding donor through weak C–H···A interaction with another acceptor fragment in the crystal. The excellent review article by Steed in 2001 brings to light a sound overview of the alkali metal–crown ether chemistry. Their complexation with organic ammonium, arenediazonium, guanidinium, tropylium, and pyridinium cations has also been studied.[21-22] Though various research groups including Nangia, Atwood, Zaworotko, Fonari,

Nakamura, Stoddart, Braga, Steed, Rogers,etc., have been working on diverse classes of crown ether based host-guest systems with simple to complicated topologies, research incorporating organic ammonium ions (RNH_3^+, $ArNH_3^+$ etc.) as guests with crown ethers still reigns the field of supramolecular chemistry. The organic ammonium ions generally perch into the oxy–crown ether cavity through the N–H···O hydrogen bonds. Very recently, our group has reported ammonium–crown ether complexes in supramolecular association with metal–oxo cluster anions.[23a] In the pertinent study, it was observed that the crystal packing feature was dependent on the size of the crown ether and shape/symmetry of the anions. The substitution of one of the hydrogen atoms of ammonium ion by a phenyl ring generated an anilinium ion, which resembled the ammonium ion as far as the nature of guest geometry was concerned. In most of the cases, it was observed that this Ar–NH_3^+group (i.e. anilinium) lay in the perching position rather than in the nesting position of the crown ether cavity.[23a] The perching position is usually around 1 Å out of plane from the oxygen atoms of the crown ring. For instance, even the ammonium ion which has a diameter of 1.48 Å perches about 1.19 Å out of plane from the 18–crown–6 cavity.[23b–c]

Another feature of host-guest complexes incorporating the crown ethers is that the size of the crown ether and the nature of the ammonium cation (NH_4^+, RNH_3^+etc.) are responsible for the stoichiometry and stability of such complexes. Though numerous studies on 18–crown–6 (18C6) and its derivatives revealed a 1:1 stoichiometry of the crown ether with both NH_4^+ and RNH_3^+ cations, but with the smaller crown ether, 15–crown–5 (15C5) and its derivatives, a different stoichiometry (2:1) was observed. These complexes of 15–crown–5 were found to exhibit a sandwich structure with the NH_4^+ cation in between two almost parallel 15C5 residues.[20c,24a–c] The same type of coordination was also observed for the oxonium ion in the crown ether complex, $[(H_3O)(B15C5)_2]^+$, the oxonium ion being isoelectronic with RNH_3^+.[24d]

In general, anilium ions are known to lie in perching positions of the crown ether cavity. However, Trueblood and co-workers reported that the ammonium or substituted ammonium ions could move nearly to the center of the ring, if their stabilities in such positions were somewhat enhanced by other interactions. As such, a 1:l crystalline complex, $[(NH_2–NH_3)^+\cdots(18–crown–6)](ClO_4)$, was examined, in which the –NH_3^+group

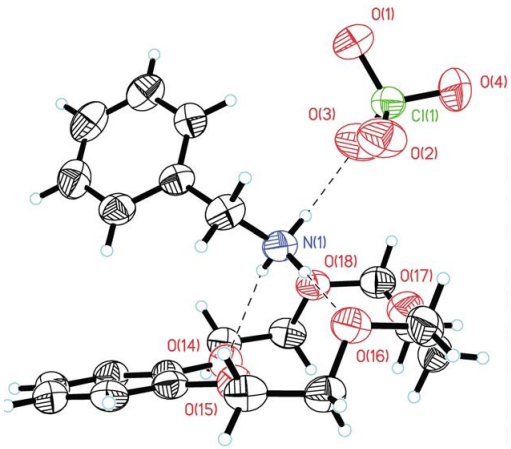

[$PhCH_2NH_3(B15C5)](ClO_4$) (**a**)

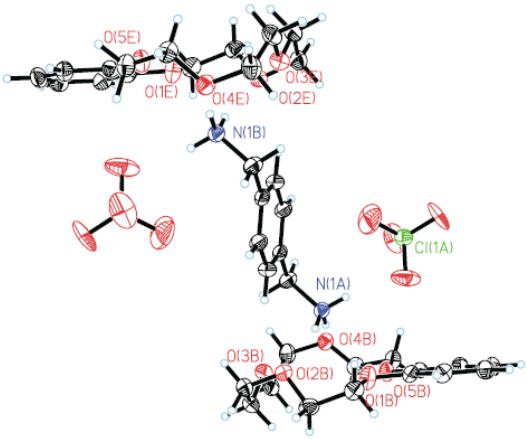

[p-$C_6H_4(CH_2NH_3)_2(B15C5)_2](ClO_4)_2$ (**b**)

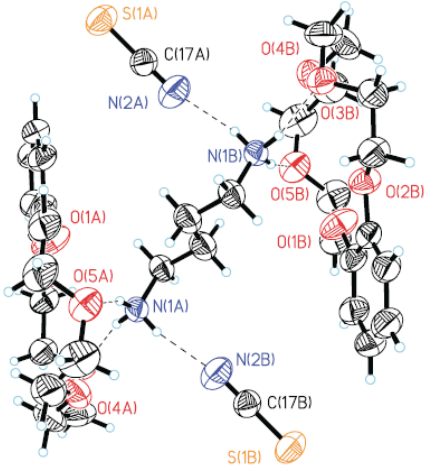

[{$H_3N(CH_2)_4NH_3$}$(B15C5)_2](SCN)_2$ (**c**)

Figure 1. Crystal structures of some of the ammonium···crown ether complexes adopted from reference 25b.

was found to be almost in plane with the crown ring.[25a] In order to investigate this contradiction and the underlaying chemistry, two other complexes, $[(OH–NH_3)^+\cdots(18–crown–6)](ClO_4)$ and $[(CH_3–NH_3)^+\cdots(18–crown–6)](ClO_4)$ were also synthesized. In the latter two complexes, the ammonium nitrogen atoms were in intermediate positions, about 0.68 and 0.83 Å from the oxygen plane. In the pertinent study, it was found that, in all the three structures, the oxygen atoms of the crown were found to be displaced alternately above and below the plane of the ring. Also, the $-NH_3^+$ nitrogen atom in the hydrazinium···crown complex was positioned in between the two three-oxygen planes, with a mean deviation of only 0.11 Å from the plane of all six oxygen atoms, whereas in the other two structures, they were positioned above both the oxygen planes. In the hydrazinium···crown structure, weak hydrogen bonding interactions between the $-NH_2$

group of hydrazinium ion and the crown oxygen atoms were observed, though these bonds were about 0.2 Å longer than the other N−H···O bonds. Moreover, one of these hydrogen bonds was weakly bifurcated and so was also involved in hydrogen bonding with one perchlorate oxygen atom. The $-NH_3^+$ group was however, involved in hydrogen bonding interactions with the oxygen atoms of one plane of the crown ether ring. In contrast, the hydroxylammonium···crown complex was found to encompass interactions of the $-NH_3^+$group with the ring, in addition to the hydrogen bonding interactions from the −OH group to a water molecule and from that water molecule to two perchlorate ions. Both the O−H···O hydrogen bonds in this structure was found to be almost linear and the orientation of the water molecule was such that the line from the hydroxylammonium oxygen atom, to itself was just *ca*. 16° from a tetrahedral direction defined by the positions of the hydrogen atoms of H_2O.

Another study which emphasized alkylammonium···crown ether interactions was reported by Akimova and co-workers in which three complexes of benzo–15–crown–5 (B15C5) with protonated primary amines were synthesized.[25b] It was observed that in all the three complexes studied, $[PhCH_2NH_3(B15C5)](ClO_4)$ (**a**), $[p\text{-}C_6H_4(CH_2NH_3)_2(B15C5)_2]\ (ClO_4)_2$ (**b**), and $[\{H_3N(CH_2)_4NH_3\}(B15C5)_2](SCN)_2$ (**c**), only 1:1 stoichiometry was formed (see Figure 1). The complex (**a**) was formed due to the hydrogen bonding interactions between the protonated amino group of the ammonium fragment and two of the oxygen atoms in the crown residue. Apart from these, the RNH_3^+ cation also formed hydrogen bonding with the perchlorate anion. A skew conformation was adopted by the crown ether and the nitrogen atom of RNH_3^+ group was displaced by *ca*. 1.842(4) Å from the mean plane of the crown ether. It was put forward that such short ammonium···crown separation was typical of unconstrained 1:1 adducts and was in fact, attributed to additional interactions that might be present in the host-guest adducts. An additional instance having such short separation, was observed in the complex $[(H_3O)(B15C5)_2][Me_2NH_2]_2[PMo_{12}O_{40}]\cdot 2(B15C5)$ in which the cations and crown ether molecules were packed in a 1:1 ratio in the voids of the crystal lattice formed by large polyoxometalate anions.[24e] Thus, it was argued that alkylammonium cations typically formed 1:1 adducts with 15C5 derivatives and the formation of sandwich complexes was precluded because the alkyl substituent blocked access to any second crown ether

molecule. This feature was in contrast to the NH_4^+-based sandwiches which are generally formed by the 'sharing' of the singly charged guest and the electronegative regions of two equidistant host molecules. The other two complexes (**b**) and (**c**) crystallized in the centrosymmetric space group, C_i. Each ammonium group in complex (**b**) registered itself with three hydrogen bonds; two with the crown ether and the third with the perchlorate anion. Furthermore, it was observed in the pertinent study that, the geometry and nature of the host-guest interactions was not altered on substituting the p-xylylenediammonium cation with the less bulky tetramethylenediammonium cation in complex (**c**).[25b]

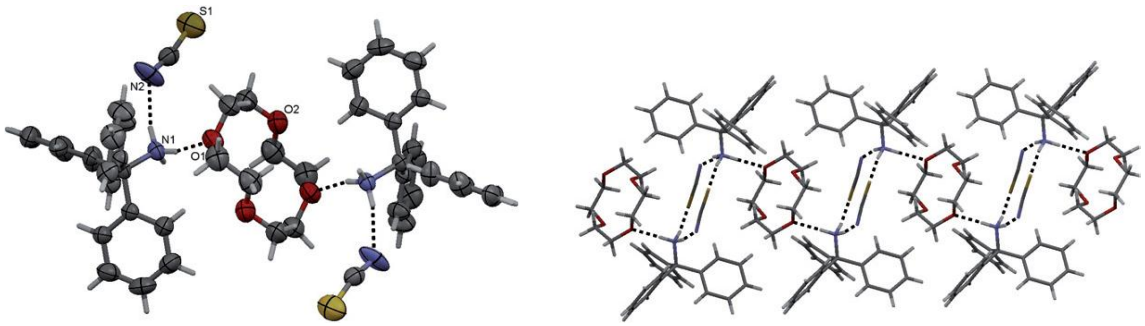

(**a**) (**b**)

Figure 2. (a) Crystal structure of $[Ph_3CNH_3(12C4)](NCS)$ and (b) packing topology of the concerned compound adopted from reference 25d.

Fonari and co-workers reported the selective interactions of some triphenylmethane derivatives with crown ethers, such as triphenylmethanaminium thiocyanate···12C4 (see Figure 2a). In the pertinent study, this compound was found to crystallize in the centrosymmetric space group, $P2_1/c$, with the crown residing at the center of inversion. In It was also portrayed that the $R–NH_3^+$ group participated in three charge assisted hydrogen bonding interactions, *viz.* one with the crown ether and the other two with the two inversion-related NCS^- anions, thereby giving a tape-like topology. The adjacent tapes were found to pack in an anti-parallel arrangement in the aforementioned compound and the packing topology is shown in Figure 2b.[25c]

In order to better understand the host-guest complexation between crown ether derivatives and ammonium cations, simple systems incorporating guest units with hydrogen bonding sites in angular fashion were chosen in the present work. Also, the cavity dimension of the crown ethers was varied from 12C4 to 21C7. The underlaying

supramolecular chemistry in the resulting host-guest systems have been discussed in Chapter 3.

● 1.2.4. Polyoxometalates as a supramolecular entity

Metal–oxo cluster anions or polyoxometalates (POMs) are giant inorganic anions usually formed by the group 5 or group 6 transition metals. The general structural feature of these macro-anions is linking of the metal centers by oxygen atoms.[26] These cluster anions are usually isolated using external cationic counterparts and possess three dimensional structures depending upon the number of metal centers and nature of linkages. The metal atoms which are typically in their higher / highest oxidation states, build the framework and are termed as *addenda atoms*. The electronic configuration of the addenda atoms in these higher oxidation states is d^0 or d^1. Some typical and common instances of addenda atoms include molybdenum (VI), tungsten (VI), vanadium (V) etc. Apart from the ideal ionic radius and charge for favorable combination with oxygen, molybdenum and tungsten, possess empty d–orbitals which render them ideal for participation in metal–oxygen π–bonding. Therefore, even though, other transition metals, like niobium (V), tantalum (V), hexavalent Tc, Re, Ru, Os; pentavalent Cr, Mo, W, Tc, Re, tetravalent Ti, V, Cr, Mo, W etc. are valuable components for cluster formation, molybdenum and tungsten metals take a special note and have become very well-known in the area of POM chemistry.

Based on the constituents, the polyoxoanions are broadly classified into two categories; (a) heteropolyanions and (b) isopolyanions. The popular and major members of the POM family are the heteropolyanions and in these macro-anions, *p*-, *d*- or *f*- block hetero elements are included in addition to the *addenda* atoms. The heteropolyanions are thus, formulated as $[X_xM_mO_y]^{q-}(x \leq m)$ where M is the *addenda* atom and X is the heteroelement. In contrast to heteropolyanions, the isopolyanions are constituted with only *addenda* atoms and oxygen atoms and are formulated as $[M_mO_y]^{p-}$. The structures of the polyoxoanions are conveniently described in terms of assemblages of metal–centered MO_n polyhedra through corner, edge and (rarely) face sharing. However, all the polyoxoanion structures do not include metal atoms lying at the center of the polyhedron of oxide ions; rather they are strongly displaced towards a vertex or edge of its own polyhedron.

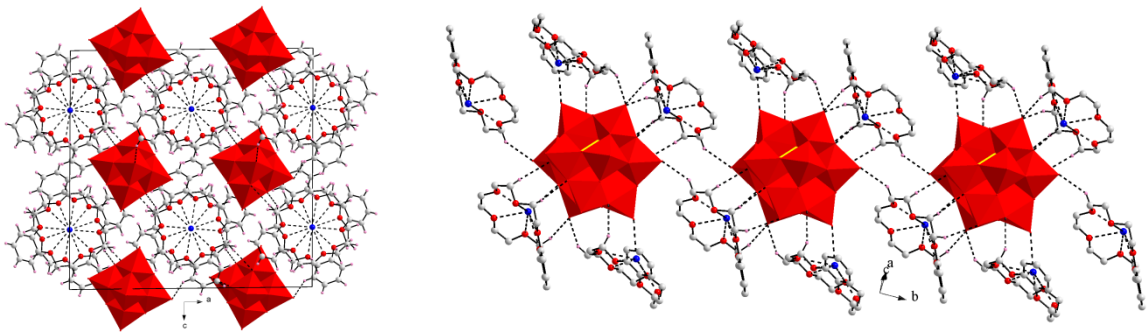

(**a**) (**b**)

Figure 3. Crystal packing feature of (a) $[NH_4(DB18C6)]_2[Mo_6O_{19}]$and (b) $[NH_4(B18C6)]_4[SiW_{12}O_{40}]$ adopted from reference 23a.

The polyoxoanions can be isolated from both aqueous and non-aqueous solutions. There is no rule of thumb that can explain the systematic and designed rational synthesis of polyoxometalates. The synthesis and isolation of these cluster anions are well controlled by many factors, under confined conditions.

These cluster anions are excellent building blocks to construct multidimensional network structures. Very recently, our research group has demonstrated supramolecular association between ammonium···crown ether complexes and polyoxoanions.[23a] It was portrayed that, the surface oxygen atoms of the anions were involved in extensive hydrogen bonding interaction with the appropriate donor functionalities. The topology of the resulting supramolecular complexes was found to vary with the size of the polyanion. Two such examples are pictorially depicted in Figure 3 which clearly show the differing packing features of ammonium-embedded crown ether supramolecular complexes with two different polyoxoanions.

● 1.3. CHEMISTRY OF 2,2'–BIPYRIDINES

● 1.3.1. General features

Since its discovery at the end of nineteenth century, the bipyridine ligand (also known as bipyridyl, dipyridyl and dipyridine ligand) has been extensively used as a building block in supramolecular and coordination chemistry, macromolecular chemistry as well as in nanoscience.[27] These ligands are nitrogen containing hetero–biaryl neutral compounds wherein two pyridine rings are coupled together. The bipyridine ligands, well-known as bidentate chelating ligands in the area of coordination chemistry, represent one of the archetypes of polypyridine ligands and exist as six regioisomers, *viz.* 2,2', 2,3', 2,4', 3,3',

Chart 3. Symmetrical and disymmetrical isomers of the bipyridine ligand.

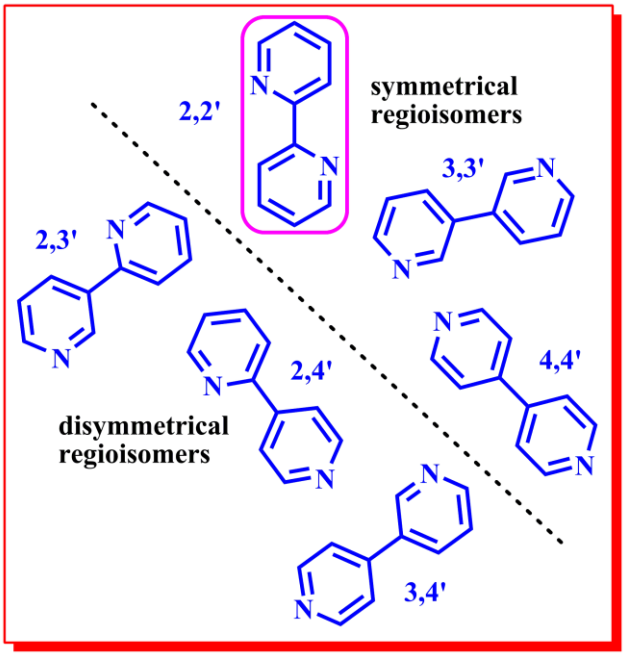

3,4' and 4,4'; the 2,2'–bipyridine ligand being the most common (Chart 3). It is quite feasible to make a distinction between the symmetrical (2,2', 3,3', and 4,4') and the disymmetrical isomers of bipyridine (2,3', 2,4', and 3,4'), with only the 2,3'- and 3,3'-bipyridines being naturally abundant in certain varieties of tobacco.[28]

The major characteristic features of the bipyridine ligand are: (i) it is a neutral ligand and can easily chelate metal cations to form charged complexes, (ii) it can be easily functionalized for custom-tailored applications, (iii) metal–bpy ligands with extended π−conjugated frameworks find applications in material science, including nonlinear optics (NLO),[29] and photovoltaics.[30] As a result, the design and synthesis of new bipyridine ligands featuring extended oligophenylenevinylene π−conjugated backbones (OPV bipyridines) are in great demand in the modern scientific community. As the present work aims at synthesizing new bipyridine derivatives and studying their photophysical properties, a brief introduction to the associated chemistry is made in the following sections.

● 1.3.2. Synthesis of bipyridine based ligands

Though several synthetic strategies have been devised over the years to improve the formation of bipyridine derivatives, the most extensively employed method is the metal-

catalyzed (Ni and Pd/C catalyzed) coupling of pyridine, substituted pyridines, or 2–halopyridines to form the desired 2,2'–bipyridine products. A meticulous investigation on such type of systems reveal that better yields of bipyridines can be obtained under milder conditions by incorporating several improvements to the Ni-catalyzed homo–coupling of aryl halides rather than the traditional Ullmann coupling,[31] Recently, procedures utilizing directed cross-coupling reactions, such as Stille–type and Negishi–type have come to the limelight for the synthesis of symmetrically as well as unsymmetrically functionalized bipyridines in high yields.[32–33]

● 1.3.2.1. Homo-coupling of pyridine

Badger and Sasse used the Raney nickel catalyst to synthesize 2,2′–bipyridine as well as its symmetrically disubstituted derivatives.[34a–c] A key advantage of this coupling procedure is that there is complete recovery of the unchanged starting material and thus, it can be easily recycled. However, in such cases, the conversion is found to be rather poor for each synthetic cycle. In order to exemplify this process, 2,2′–bipyridine was synthesized by simply heating neat pyridine in the presence of active W7 Raney nickel catalyst.[34a] Subsequent pyrolysis yielded the desired bipyridine product with traces of an insoluble organo-nickel compound as a side product.

● 1.3.2.2. Homo-coupling of 2-halopyridines

Recent synthetic methods used for the preparation of symmetrical 2,2′–bipyridine derivatives in high yield involve transition metal-mediated homo–coupling of 2–halopyridines. Though the classic Ullmann reaction can be used to generate 3,3′–dimethyl–2,2′–bipyridine by coupling 2–bromo–3–methylpyridine in high-boiling solvents, utilizing Cu powder, it suffers from some major drawbacks, such as, usage of drastic experimental conditions to procure the desired product and low conversions from reactants to products.[35a] However, such a low conversion was improved by using phase transfer conditions, e.g., 2–bromo–6–picoline with 5% Pd/C afforded pure 6,6′–dimethyl–2,2′–bipyridine in 50–68% yield.[35b–d]

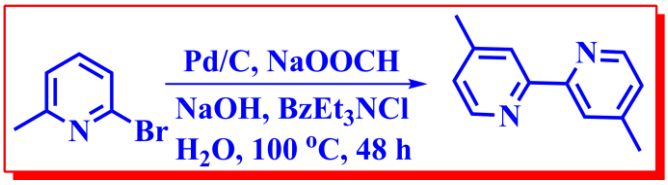

In recent times, the Ni-catalyzed homo–coupling of aryl halides has received substantial consideration due to a number of reasons, such as, it permits the incorporation of a number of functional groups, e.g., an aldehyde or ketone; it utilizes milder conditions relative to the Ullmann reaction and finally, it also results in good yields (*ca.* 75%).[36] Furthermore, Lemaire *et al*. brought in a catalytic alternative to the Ullmann reaction to obtain 2,2′–bipyridines and their symmetrical 5,5′–dimethyl derivatives in very high yields (*ca*. 90%) by employing $Pd(OAc)_2$ as the catalyst with *n*-Bu_4NBr and trialkyl-amine, as a base in 2–propanol. The usage of K_2CO_3 as base instead of trialkylamine, resulted in 70% yield of the 5,5′–dimethyl homo–coupling product.[37]

● 1.3.2.3. Cross-coupling of 2-halopyridines

Fraser *et al*. reported an efficient synthetic strategy for the preparation of 4–, 5–, and 6–methyl–2,2′–bipyridines by a Negishi cross-coupling reaction.[38] For instance, an *in situ* lithium/halogen exchange was carried out by treating 2–bromopyridine with *tert*-butyllithium followed by Li to Zn transmetallation. The desired bipyridine product was obtained in 93–98% yield by the subsequent addition of (methyl)pyridyltriflate and the $Pd(PPh_3)_4$ catalyst generated *in situ*. Due to the halogen/lithium exchange, this reaction is, however, restricted to the bromo- or iodo- functionalized pyridines.

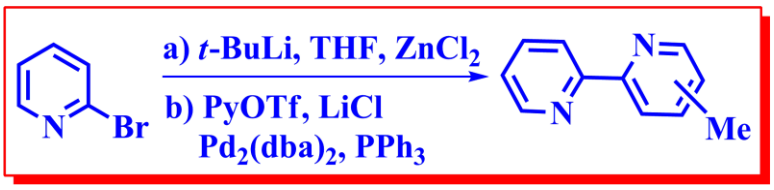

The Stille-type cross-coupling procedure, which involves organotin compounds and palladium catalysts, is the second widely used methodology for the preparation of bipyridines. Initially, (trimethylstannyl)pyridine was cross-coupled with bromopyridines in the presence of a catalytic quantity of $Pd(PPh_3)_4$ to afford the 2,2′–bipyridine product in 77% yield. Later, the same method was extended for the syntheses of symmetrical as well as unsymmetrical methyl-substituted bipyridines, along with bromo-, trimethyltin-,

nitro-, ester-, and hydroxymethyl-functionalized bipyridines.[39] A valuable feature of this method is that different functional groups, such as protected esters and hydroxy groups, are tolerated in this coupling procedure.

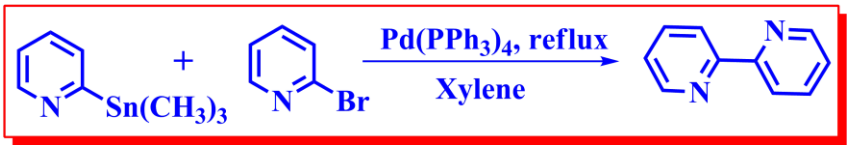

● 1.3.2.4. Monosubstituted bipyridines

Monosubstituted bipyridine ligands can effortlessly be synthesized by the traditional Kröhnke procedure, directed cross-coupling of halopyridine derivatives utilizing Negishi-type or Stille type, monosubstitution on bipyridine or by ligand-coupling methodologies like Suzuki-type reactions.[40a] The functionalization on bipyridines originate from the methyl precursor, which can be oxidized, brominated or halogenated, lithiated and modified under diverse conditions. These mono-functionalized precursors draw increasing interest as building blocks in supramolecular and macromolecular chemistry as well as in nanoscience.

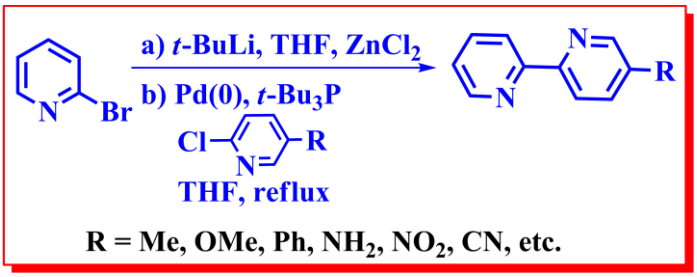

The usage of a modified Negishi cross-coupling procedure yielded 5–monosubstituted 2,2'–bipyridines in high yields.[40b] The initial step involved the formation of the lithiated derivative by adding 2–bromopyridine to a *t*-BuLi solution in THF and subsequent addition of $ZnCl_2$ to obtain the respective organozinc derivatives. Finally, the cross-coupling reactions with the respective mono-derivatized chloropyridine were carried out using a palladium catalyst, the observed yields being dependent on the functional group on the chloropyridine.

● 1.3.2.5. π–Conjugated bipyridines

Apart from simple bipyridine derivatives, interest in synthesizing π–conjugated donor–acceptor bipyridine derivatives has been mounting over the years because of their

potential applications in photonic devices. Although homo-coupling of substituted pyridines is a useful route for synthesizing such molecular systems, they can be effectively synthesized through simpler alternative synthetic protocols. The 4,4'–π–conjugated–2,2'–bipyridine derivatives are very familiar in this aspect and these can be obtained using 4,4'–dimethyl–2,2'–bipyridine as the starting precursor. The olefinic functionalities at the 4,4'– positions of 2,2'–bipyridine can be introduced through various

Scheme 6. Synthesis of halomethyl derivatives of 2,2′–bipyridine

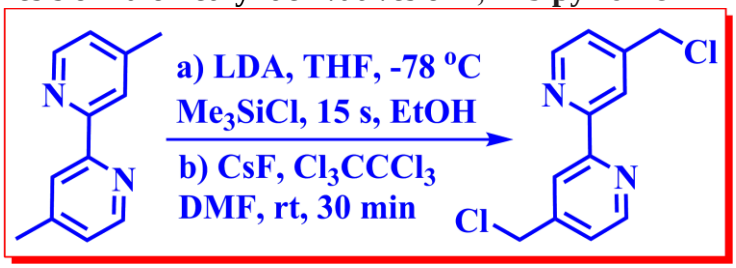

pathways, though the Horner–Wadsworth–Emmons reaction is the most common. The title reaction requires a phosphonate precursor which can easily be synthesized through an Arbuzov reaction with the appropriate halomethyl derivatives. Though the classical method for the synthesis of halomethyl bipyridine precursors includes reaction of dimethyl bipyridine with *N*–halosuccinimide, these reactions offer a major drawback as they render multiply halogenated products which make the isolation of the desired products complicated. An alternate and very efficient protocol to synthesize the halomethyl derivatives of 2,2′–bipyridine was reported by Fraser and co-workers (Scheme 6). The concerned synthetic pathway incorporated lithiation of 4,4′–dimethyl–2,2′–bipyridine with 2 equivalents of lithium diisopropylamide (LDA) followed by trapping of the carbanion with trimethylsilyl chloride (TMSCl). Subsequent reaction between the silylated bipyridine and the commercially available electrophile, hexachloroethane in presence of a dry fluoride source, CsF finally resulted in isolation of the chloromethyl derivative in excellent yield.[27,41] The same procedure can be used for mono-chlorination of 2,2′–bipyridine using controlled amount of the base. The chloromethyl derivatives, formed by the aforementioned method, can then be transformed into their triphenyl phosphonium salts for the conventional Wittig reaction with proper aldehydes so as to introduce the double bonds at the 4– or 4,4'– positions of 2,2'–

bipyridine. Alternatively, they can be treated with trialkylphosphites to result in a phosphonate ester of 2,2′–bipyridine which will then undergo a Horner–Wadsworth–Emmons reaction with the appropriate aldehydes to yield the corresponding 4– or 4,4'–π–conjugated products. The better performance and higher *E*–selectivity of the Horner–Wadsworth–Emmons protocol compared to the conventional Wittig pathway makes it a better choice for synthesizing similar bipyridine derivatives.

Alternatively, the 4– or 4,4'–π–conjugated–2,2'–bipyridine derivatives can be synthesized using the Knoevenagel type reactions between the methyl bipyridine derivatives and appropriate aldehydes in presence of strong bases such as LDA or potassium tertiary butoxide. Both the protocols involve the formation of a carbanion which undergoes addition to the aldehyde electrophiles forming a secondary alcohol. If LDA is used as the base, the corresponding alcohol is isolated from the reaction mixture and is subsequently dehydrated usually, by pyridinium *p*-toluene sulfonate (PPTS) to obtain the desired olefin functionalized bipyridines.[42a] However, in case of potassium tertiary butoxide as the base, the desired product is obtained directly without isolation of the alcohol.[42b]

The above synthetic protocols have been used to synthesize a large number of 2,2′–bipyridine derivatives with diverse end-capping functionalities which exhibit tunable optical properties. Le Bozec and co-workers reported a series of *p*-phenylenevinylene–2,2′–bipyridine in which the π–conjugated backbone varied from styryl, thienylvinyl, phenylimino and phenylazo etc., and the ligands were end-capped with various donor or acceptor functionalities such as $–NBu_2$, –OOct, $–SO_2Oct$, $–NO_2$.[42b] Similarly, hydroxyl alkylamino functionalities were also introduced to the 2,2′–bipyridine core using appropriate alcohol functionalized dialkylamino benzaldehydes.[43a–b]

● 1.3.3. Complexation and applications of π–conjugated–2,2'–bipyridine derivatives

It is worth mentioning that the 4,4'–disubstituted–2,2'–bipyridine ligands with a π–extended skeleton have been grabbing considerable attention of the scientific community due to the very interesting photophysical and photochemical properties exhibited by the ligands as well as their transition metal complexes. When suitable donor end-capping functionalities are introduced into the pyridine rings via π–linkers, then ‘push-pull’ or EDA molecules are formed. These molecules, being synthetically flexible offer easy

tuning of the optical properties (absorption, emission etc.) through simple modification of their π–backbones. A simple compound of such category namely, the 4,4'–*bis*(2,5–dimethoxy)styryl–2,2'–bipyridine (known as **N945L**) is well known as a blue organic light emitting diode (OLED).[44a] Very often, such bipyridine derivatives are highly fluorescent and their photophysical properties are simply tuned through proper selection of the donor termini. It has been observed that absorption due to such ligands shifts to longer wavelength upon increasing the donor strength and the π–conjugation. The lowest energy absorption band due to these ligands appears predominantly due to an intramolecular charge transfer (ICT). The absorption maxima of these ligands also depend upon the π–spacers. Moreover, the variation of fluorescence property of such ligands generally maintains a similar trend as that of the absorption behavior. Bozec and co-workers observed a substantial bathochromic shift of the ICT band upon changing the π–spacers in the order of phenylazo > thienylvinyl > phenylimino > styryl > vinyl, in the case of an invariable donor group. However, the introduction of imine functionality instead of the alkene moiety was found to quench the fluorescence of the samples.[42b]

Transition metal complexes of extended π–conjugated ligands are promising as new molecular materials for photonic and optoelectronic applications and are excellent building blocks for the construction of dipolar or octupolar (either octahedral or pseudo-tetrahedral) complexes. Ruthenium complexes of similar ligands are well-known as sensitizers for dye-sensitized solar cells (DSSC).[30b,44b] Since the present thesis mainly deals with the optical properties of 4,4'–π–conjugated–2,2'–bipyridine derivatives (linear) and their transition metal complexes (linear and nonlinear), therefore a brief introduction to the nonlinear optical properties of such complexes is made in the following section.

Nonlinear optics (NLO) generally deals with the interaction of electromagnetic radiation and matter in which the matter responds nonlinearly to the incident radiation. It has been observed that the most extensively studied nonlinear optical phenomena are the second- and third-order effects e.g., second harmonic generation (SHG) and two-photon absorption (2PA) respectively. Second harmonic generation, which is also called frequency doubling, is a second order nonlinear optical process, in which photons interacting with a nonlinear material are combined to generate new photons with twice the energy or frequency and hence, half the wavelength of the irradiated photons. On the

other hand, two-photon absorption is a third order nonlinear optical process which accounts for the simultaneous absorption of two photons of identical or different frequencies so as to excite a molecule from an initial state to a higher energy electronic state. The two-photon absorption differs from linear absorption in the sense that the strength of absorption in the former case depends on the square of the light intensity and hence is several orders of magnitude weaker than linear absorption.

The nonlinear optical phenomenon is generally related to the polarizability of a molecule. For instance, all materials are considered as charged particles in optics. As such, when a dielectric material is considered, the charged particles are bound together even though the bonds are not fully rigid. When an electromagnetic field, E is applied, the charges on the dielectric material are displaced slightly from their mean positions thereby inducing a polarization. This induced polarization (P) is represented by the equation:

$$\vec{P} = \mu_0 + \alpha\vec{E} + \beta\vec{E}^2 + \gamma\vec{E}^3 + \cdots,$$

where, μ_0 represents the ground state electric dipole moment, α represents dipole (or linear polarizability tensor), β represents quadratic polarizability (or first dipole hyperpolarizability) tensor, γ represents cubic polarizability (or second dipole hyperpolarizability tensor) and so on.

Thus, the value of the first dipole hyperpolarizability tensor, β gives us idea about SHG while the imaginary part of the second dipole hyperpolarizability γ is related to the 2PA cross-section (σ_2). Also, it has been established that apart from excellent octupolar nonlinearities based on extended π–conjugated systems, coordination chemistry can also be a useful tool in building various branched structures including dipolar and octupolar systems by gathering the coordinating ligands in a pre-designed fashion to yield large values of γ and σ_2.[44c]

It is worth mentioning that transition metal coordination complexes of functionalized bipyridine ligands are popular as nonlinear optical materials. The metal ion plays some pivotal roles in this aspect, such as; (i) acting as a powerful template to gather ligands in predetermined octupolar arrangements, (ii) inducing a low-energy metal–ligand charge-transfer transition (MLCT) and, (iii) acting as a Lewis acid to induce a strong intraligand charge-transfer (ILCT) transition; thereby contributing to sizable second- and third-order

NLO activity. It can be aptly said that, more the polarization in a molecule, more will be its NLO activity depending on the strength of the donor and acceptor moieties. A majority of the NLO–phores comprise relatively simple dipolar electronic structures, however, octupolar compounds have also enticed scientists, especially for potential quadratic (second-order) applications. Though octupolar molecules have zero net ground-state dipole moments, intramolecular charge transfer (ICT) excitations can lead to large changes in dipole moment thereby imparting substantial values to the first hyperpolarizability (β) which governs quadratic NLO effects at the molecular level.

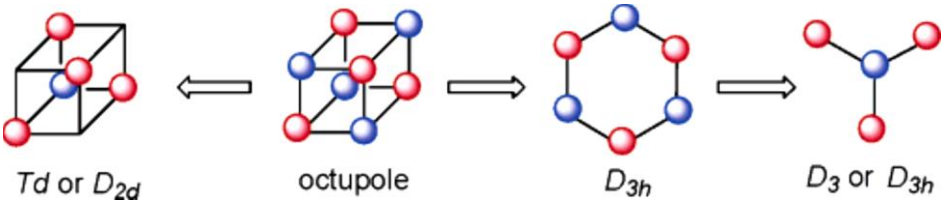

Figure 4. Derivation of octupolar symmetry from a cubic structure (adopted from reference 45d).

Coordination chemistry is a useful tool in developing octupolar nonlinearity at the molecular level and this concept has been developing since the early 1990s based on group theoretical and quantum mechanical calculations. The octupolar nature of D_3 tris-chelate transition metal complexes was first brought to light by Zyss and co-workers to obtain large β values for the salts $[Ru^{II}(bpy)_3]Br_2$ and $[Ru^{II}(phen)_3]Cl_2$, using the hyper-Rayleigh scattering(HRS) measurements and a three-state theoretical model. The octupolar structure can be best described as a cubic structure with alternating donor and acceptor groups at the edges of the cube. Therefore, the pure octupolar symmetries can be derived from this cubic structure either by projection along the 3–fold rotational axis of the cube, resulting in D_3 or D_{3h} symmetry, or by fusion of one type of charge at the barycenter of the cube leading to D_{3h}, D_3, T_d or D_{2d} symmetry (see Figure 4). A large number of NLO–active transition metal complexes of functionalized 2,2'–bipyridine systems have been documented since then in literature, especially from the research group of Bozec.[45a–f] Apart from the octupolar D_3 complexes, the bipyridyl ligands are also used for the design of D_{2d} tetrahedral octupoles by the coordination of two bipyridine ligands to metal ions such as Cu^I, Ag^I, or Zn^{II}. The incorporation of alkyl or aryl

substituents at the 6,6′– positions of the bipyridyl ligand plays a pivotal role in stabilizing the tetrahedral geometry as well as in protecting the central metal ion against oxidation.[45g]

In recent times, apart from the second order NLO, the third-order nonlinear optical properties, such as two-photon absorption properties of complexes of π–conjugated systems, have also come to the limelight. Abbotto and co-workers studied the two–photon absorption properties of Zn^{II} octupolar molecules and found that the obtained experimental result contradicted the theoretical prediction which estimated an enormous enhancement of the TPA cross-section on complexation of the ligand to a Zn^{II} center. The experimental cross-section values were found to be much smaller than those predicted for the same theoretically. The lack of TPA cross-section enhancement in the Zn-complex compared to the free ligand was attributed to the inability of the Zn^{II} center to propagate the intramolecular charge transfer process between the ligands as well as between ligands and the Zn^{II} metal center.[46a] Another such surprising result was observed in case of a Ni^{II}–phenanthroline complex reported by Prasad and co-workers, even though coordinating metal ions were expected to act as strong three-dimensional templates for enhancing the TPA cross-section. In this case, it was reported that nickel complexes of phenanthroline ligands, bearing strong electron-donating groups such as a dialkylamino group decreased the TPA cross-section whereas those bearing weaker electron donors such as alkyloxy or alkylthio groups enhanced the TPA cross-section.[46b] In 2007, Le Bozec and co-workers studied the linear properties and second- and third-order nonlinearities of a series of octupolar *tris*[4,4′–bis[(dialkylamino)styryl]–2,2′–bipyridine]M^{II} complexes (M = Ru, Fe, Zn, Cu, Ni). These compounds exhibited relatively large first hyperpolarizabilities (β) and TPA cross-section values in the range 650 GM < δ_2 (765nm) < 2200 GM. This result pointed out that the role of the metallic core was not only to act as a template, but also to participate in the NLO activity. It was also suggested that the two-photon activity of such metal complexes could be significantly enhanced upon increasing the π–conjugated backbone in the bipyridine unit.[46c]

Very recently, phenylpyridine based iridium complexes have attracted our attention, though this class of compounds has been very less explored in terms of nonlinear optics. Beeby and co-workers studied a series of cyclometalated iridium complexes where it was

suggested that if the conjugation of the pyridyl fragment was increased, then the charge separation of the MLCT state would be greater, resulting in larger TPA cross- sections.[47]

● 1.4. MOTIVATION OF THE PRESENT WORK

The above background information gives a sound overview of the chemistry behind the two important molecular systems of the present work i.e. macrocycles and 2,2'–bipyridines. Based on the information extracted from previous literature reports, we found that a few vital facts have not been addressed yet; (i) chiral resolution of transition metal complexes of transdiene, (b) whether supramolecular complexes of crown ethers with angular shaped guests would lead to helical crystal packing or not and, (c) the difference in photophysical behavior of 2,2'–bipyridines end-capped with hetero-donor functionalities instead of the known homo-donor derivatives.

● 1.4.1. Chiral resolution of M–L complexes (L = transdiene)

The macrocycle, transdiene, readily undergoes complexation with transition metal ions. The coordination complexes of this ligand comprise two stereogenic centers on the two amine nitrogen atoms. In the relevant complexes, based on orientation of the amine hydrogen atoms, two diastereomeric forms are possible i.e. *racemic*– (*RR*– and *SS*–) and *meso*– (*RS*–). Similarly, the racemic diastereomers exist as a mixture of two enantiomorphs, *viz*. *RR*– and *SS*–. The metal complexes are usually isolated as a mixture of all these isomers from which the diastereomers can easily be separated with the aid of differing solubility. The *racemic*– product which is obtained, is a mixture of *RR*– and *SS*–enantiomers in 50:50 statistical ratio. The bulk mixture of these enantiomers is thus achiral but, might be resolved to the individual enantiomorphs and is consequently, the special attraction of the present work. The working strategy is outlined in Scheme 7.

An important and fundamental aspect of structural recognition in this type of supramolecular complexation is chiral recognition, where multidentate organic ligands are mostly used to generate helical structures. In the synthesis of such chiral molecules, two generalized approaches have been established to obtain stacking/packing of the crystallizing substances following a screw symmetry *viz.*, (a) helicity induction through the usage of a chiral substance, and (b) chiral packing motif of the molecular components through spontaneous resolution. The packing of molecular components in chiral space

symmetry is often complicated to predict *a priori* and so, spontaneous resolution through self-assembly without the use of any chiral ligand or chiral auxiliary still remains a challenge and is a growing topic of interest in light of its importance in biology and advanced materials. According to long held views, some sort of well-organized and inevitable asymmetric augmentation process might have operated for generation of enantiomeric excess (*ee*) thereby paving the way for biomolecular homochirality.

Scheme 7. Pictorial representation showing the mixture of isomers.

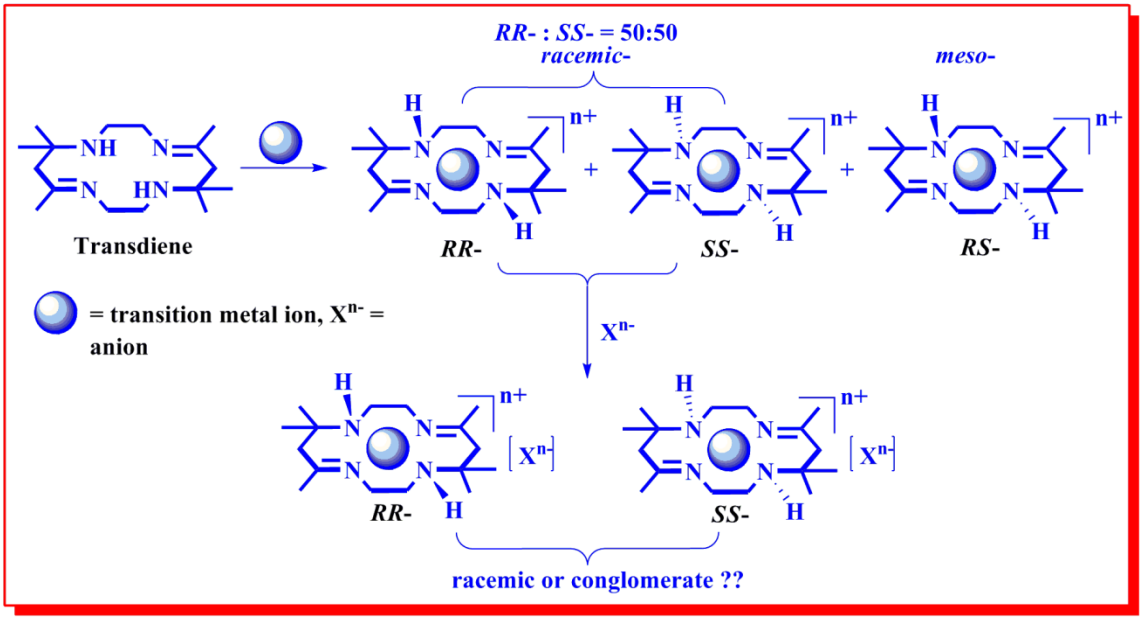

In general, majority of the chiral molecules crystallize as racemic compounds, but for spontaneous resolution of enantiomers to take place, the formation of racemic conglomerates is a prerequisite (individual enantiomorphs crystallize in different crystals). In fact, when nucleation of crystals takes place from dissolved racemic components, three limiting situations might arise: (a) formation of a racemic crystal in which both the enantiomers maintain opposite chirality/helicity in the same crystal thereby nullifying the overall chirality of the individual crystals (and thus bulk sample), (b) formation of a conglomerate in which 50 : 50 distribution of the crystals containing individual enantiomers makes the bulk sample optically inactive and, (c) formation of a *pseudo*-racemate which maintains inhomogeneous distribution of the enantiomers. However, only the conglomerate formation involves spontaneous resolution of the

enantiomers which in turn occurs with just 5–10% of the racemates and hence, a lot of effort has been undertaken to convert racemic compounds into racemic conglomerates. It is thus obvious that induction of heterochirality through the chirality transport among the helical packing motifs of the crystallizing substances is more common than the maintenance of homochirality in a crystal lattice. Among the various intermolecular non-covalent forces that assemble the adjoining molecules in the crystals in an ordered array, hydrogen bonds are more fascinating due to their strong directional nature and are found to be mostly responsible for controlling homochiral aggregation in the metal complexes thereby causing their spontaneous resolution.

It is thus understood that, isolation of chiral crystals is a rare phenomenon as the inversion symmetry often hinders to do so. The transition metal complexes of transdiene were hitherto isolated as perchlorate, thiocyanate, nitrate, halide etc. salts. Several crystal structures of M–L complexes have been reported so far, none of which encounters the phenomenon of spontaneous resolution. However, in this work, we have introduced a special type of counter anion, namely, polyoxometalate which are excellent building blocks in supramolecular chemistry and are known to be good hydrogen bond acceptors. We were thus, keen to know whether the structural difference between the conventional anions and the polyoxometalates would bring about the isolation of individual enantiomorphs of the M–L complexes through spontaneous resolution or not. The overall investigation has been elaborately discussed in Chapter 2.

● 1.4.2. Supramolecular complexes of crown ethers

In contrast to aza-macrocycles which are more prone to transition metal complexation, the crown ethers are mostly known to bind alkali or alkaline earth metals. However, they are also known to encapsulate a large variety of cationic guests such as H_3O^+, NH_4^+, RNH_3^+ etc. The encapsulation of these guests usually takes place through non-covalent D–H···X interactions (D = hydrogen bond donor, X = acceptor heteroatom). In addition to the electronegative heteroatoms which act as hydrogen bond acceptors, the donation capability of the peripheral C–H bonds makes them attractive building blocks for generating new supramolecular networks. Thus, in the crystals of the relevant host-guest complexes, the crown ethers play a double role of hydrogen bond donation as well as acceptance. Among the members of the crown ether family, the 18–crown–6 (18C6) and

its derivatives have mostly been explored as hosts for diverse neutral and cationic guests whereas, the other members are relatively less studied. The ammonium cations are excellent guest species which usually include in the crown ether cavity through three N–H···O supramolecular contacts.

Chart 4. Hydrogen bonding sites of organic ammonium ions in an angular geometrical fashion.

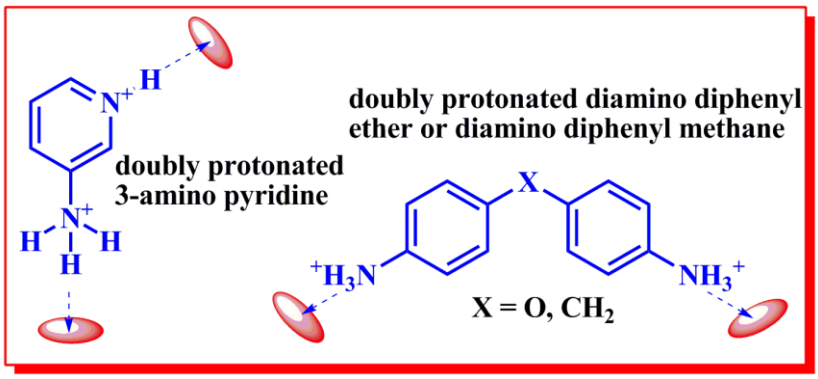

After rigorous literature and crystallographic database survey, we focused our aim at analyzing the crystal structures of crown ether based host-guest complexes in which the guest molecules would possess two hydrogen bonding sites at an angular position. For this purpose, we chose two different types of guest molecules *viz.*, doubly protonated 3–amino pyridine and doubly protonated di-anilines (see Chart 4). The stoichiometry of the host and guests in the resulting supramolecular complexes would depend upon the size of the crown ethers and separation of the hydrogen bonding sites in the guest cations. For example, if the two anilinium sites of a guest are separated by a large distance then, a 1:2 stoichiometry between the guest and the host could be expected and vice versa. The angular geometry of the guest hydrogen bonding sites instead of a linear geometry was chosen so as to comprehend as to whether complexation at an angular fashion would lead to a helical crystal packing or not. The relevant results are portrayed in details in Chapter 3.

● 1.4.3. Hetero-donor functionalized 2,2'–bipyridine ligands and their complexes

The 2,2'–bipyridine based ‘push-pull’ chromophores are important materials in the area of integrated electronics. A variety of functionalities can be introduced with the pyridine rings using proper synthetic strategies. The photophysical properties of the resulting

molecules largely depend upon the strength of the donor functionality, conjugation length and the type of π–spacer. Dipolar and octupolar metal complexes of such conjugated systems are gaining much more recognition because charge transfer transitions play a pivotal role in augmenting the NLO activity of a material. Hence, an increasing effort has been devoted over the past decade to the design of chromophores with large NLO responses whereby, attention is being progressively moved from the well-known push-pull dipolar molecular structures towards more complex molecular architectures. Therefore, it can be aptly said that, the study of new functionalized bipyridine ligands and their transition metal complexes would be an interesting topic of research.

An ample number of bipyridine based donor–acceptor systems are known till date, the most abundantly used donor functionalities being amino and alkoxy type. Amines are stronger electron donors as compared to the alkoxy functionalities and hence, influence the ICT process to a greater extent. As a result, the chromophores with amine functionalities absorb and emit at longer wavelengths than those with alkoxy substituents. As such, we asked ourselves the question as to whether the outcome of introducing two donor functionalities into the same chromophore would be interesting or not. Accordingly, we synthesized a series of bipyridine derivatives with hetero–donor functionalities which were hitherto unknown and subsequently studied their photophysical properties. The complete study has been illustrated in Chapter 4.

Most of the previous studies involved polypyridine complexes of 3d metal ions, Ru^{II} and Os^{II}, though cyclometalated Ir^{III} species have been far less exploited mainly due to difficulties in their synthetic strategies. Two types of complexes, *viz.* homoleptic and heteroleptic complexes can be synthesized, though the latter is the preferred one. For the homoleptic metal complexes, two forms of isomers are known i.e., meridional and facial isomers. It has been observed that *fac*–Ir(C^N)$_3$ (C^N indicates a phenylpyridine derivative) tends to form at high temperature, whereas *mer*–Ir(C^N)$_3$ forms at low temperature. Therefore, *mer*– isomers can be converted to *fac*– isomers under treatment at high temperatures. The heteroleptic synthetic pathway, on the other hand, cuts down the chance of formation of any isomeric form thereby making its synthesis easy. Thus, owing to their relatively high luminescence quantum yields and their aptitude to behave as photoreductants, such cyclometalated Ir^{III} compounds may preferably replace Ru^{II} and

Os^{II} complexes as building blocks for supramolecular systems designed for specific functions. After the synthesis of a series of new bipyridine ligands, we were interested to study the optical nonlinearity of the cyclometalated Ir^{III} complexes bearing the above mentioned synthesized bipyridine ligands. Infact, we were keen to know whether the nature of donor functionalities at the π–skeleton of the bipyridine ligands would affect linear and nonlinear optical properties of the relevant complexes or not. The outcome of the overall investigation has been demonstrated in Chapter 5.

● 1.5. REFERENCES

1. (a) Lehn, J. –M. *Struct. Bonding (Berlin),* **1973**, *16*, 1. (b) Lehn, J. –M. *Pure Appl. Chem.* **1978**, *50*, 871. (c) Lehn, J. –M. *LeGon Inaugurale*, Collège de France, Paris **1980**. (d) Lehn, J. –M. *Acc. Chem. Res*. **1978**, *11*, 49. (e) Lehn, J. –M. in Z. I. Yoshida and N. Ise (Eds.): "*Biomimetic Chemistry*", Kodansha, Tokyo, Elsevier, Amsterdam **1983**, 163. (f) Lehn, J. –M. *Science* **1985**, *227*, 849. (g) Steed, J. W. ; Atwood, J. L. *Supramolecular Chemistry*, John Wiley & Sons Ltd., Chichester, England, **2000**.
2. (a) Leininger, S.; Olenyuk, B.; Stang, P. J. *Chem Rev*. **2000**, *100*, 853. (b) Bouhadir, G.; Bourissou D. *Chem. Soc. Rev*. **2004,** *33*, 210. (c) Cowley, A. H. *J. Org. Chem.* **2004,** *689*, 3866. (d) Baker, R. J.; Jones, C. *J. Chem. Soc. Dalton Trans.* **2005,** 1341. (e) Healey, E. R.; Vickaryous, W. J.; Berryman, O. B.; Johnson, D. W.; Ariga, K.; Nalwa, H. S.; Eds.; American Scientific Publishers: Stevenson Ranch, **2006**.
3. Constable E. C.; Cargill Thompson, A. M. W. *J. Chem. Soc. Chem. Commun.* **1992**, 617.
4. Müller-Dethlefs, K.; Hobza, P. *Chem. Rev*. **2000**, *100*, 143.
5. Weber, P. C. ; Wendoloski, J. J.; Pantoliano, M. W.; Salemme, F. R. *J. Am. Chem. Soc.* **1992**, *114*, 3197.
6. (a) Curtis, N. F. *M.Sc. Thesis*, University of Auckland, New Zealand, **1954**. (b) Curtis, N. F. *J. Chem. Soc.* **1960**, 4409. (c) Curtis, N. F. ; House, D. A. *Chem. Ind. Lond.* **1961**, *42*, 1708. (d) Curtis, N. F.; Curtis, Y. M.; Powel, H. K. J. *J. Chem. Soc. A* **1966**, 1015. (e) Curtis, N. F. *Coord. Chem. Rev.* **1968**, *3*, 3. (f) Curtis, N. F.; Hay, R. W. *J. Chem. Soc. Chem. Commun.* **1966**, 524. (g) Sadasivan, N.; Endicott, J. F.

J. Am. Chem. Soc. **1966**, *88*, 5468. (h) Bailey, M. F.; Maxwell, J. E. *J. Chem. Soc. Chem. Commun.* **1966**, 908. (i) Hay, R. W.; Lawrance, G. A. ; Curtis, N. F. *J. Chem. Soc. Perkin Trans. I* **1975**, 591.

7. (a) Endicott, J. F.; Durham, B.; Glick, M. D.; Anderson, T. J.; Kuszaj, J. M.; Schmonsees, W. G.; Balakrishnan, K. P. *J. Am. Chem. Soc.* **1981**, *103*, 1431. (b) Endicott, J. F.; Wong, C. L.; Ciskowski, J. M.; Balakrishnan, K. P. B. *J. Am. Chem. Soc.* **1980**, *102*, 2100. (c) Endicott, J. F.; Kumar, K.; Ramasami, T.; Rotzinger, F. P. *Prog. Inorg. Chem.* **1983**, *30*, 141.
8. (a) Bresciani–Pahor, N.; Forcolin, M.; Marzilli, L. G.; Randaccio, L.; Summers, M. F.; Toscano, P. J. *Coord. Chem. Rev.* **1985**, *63*, 1. (b) Bacac, A.; Espenson, J. H. *Inorg. Chem.* **1987**, *26*, 4353.
9. (a) Fuzita, E. *Coord. Chem. Rev.* **1999**, *185–186*, 373. (b) Ogata, T.; Yanagida, S.; Brunschwig, B. S.; Fuzita, E. *J. Am. Chem. Soc.* **1995**, *117*, 6708. (c) Fuzita, E.; Creutz, C.; Satin, N.; Brunschwig, B. S. *Inorg. Chem.* **1993**, *32*, 2657. (d) Creutz, C.; Schwarz, H. A.; Wishart, J. F.; Fuzita, E.; Sutin, N. *J. Am. Chem. Soc.* **1991**, *113*, 3361; Fuzita, E.; Creutz, C.; Sutin, N.; Szalda, D. J. *J. Am. Chem. Soc.* **1991**, *113*, 343. (e) Geiger, T.; Anson, F. C. *J. Am. Chem. Soc.* **1981**, *103*, 7489.
10. (a) Warner, J. G.; Rose, N. J.; Busch, D. H. *J. Am. Chem. Soc.* **1968**, *90*, 6938. (b) Szalda, D. J. ; Schwarz, C. L.; Creutz, C. *Inorg. Chem.* **1991**, *30*, 586. (c) Lee, S.; Shih, H. –C.; Su, T. –H.; He, K. –C.; Chen, K. –N. *Inorg. Chim. Acta* **2004**, *357*, 485.
11. Sadasivan, N.; Kersohak, J.; Endicott, J. F. *Inorg. Chem.* **1967**, *6*, 770.
12. Malone, S. D.; Endicott, J. F. *J. Phys. Chem.* **1972**, *76*, 2223.
13. Szalda, D. J.; Schwarz, C. L., Creutz, C. *Inorg. Chem.* **1991**, *30*, 586.
14. Shen, H. –Y.; Liao, D. –Z.; Jiang, Z. –H.; Yan, S. –P. *Transition Met. Chem.* **1999**, *24*, 581.
15. Masoud, S. –N. *J. Mol. Cat. A* **2005**, *229*, 159.
16. (a) Caravan, P.; Ellison, J. J.; McMurry, T. J.; Lauffer, R. B. *Chem. Rev.* **1999**, *99*, 2293. (b) Felix, R.; Heshiki, A.; Hosten, N.; Hricak, H. (Eds.), Magnevist Monograph, Blackwell Scientific Publications, Oxford, **1994**. (c) Oudkerk, M.; Sijens, P. E.; Van Beek, E. J. R.; Kuijpers, T. J. A. *Invest. Radiol*. **1995**, *30*, 75. (d)

Tóth, E.; Király, R.; Platzek, J.; Radüchel, B.; Brücher, E. *Inorg. Chim. Acta* **1996**, *249*, 191. (e) Aoki, S.; Kimura, E. *Chem. Rev.* **2004**, *104*, 769. (f) Kikuta, E.; Aoki, S.; Kimura, E. *J. Am. Chem. Soc.* **2001**, *123*, 7911. (g) Kikuta, E.; Aoki, S.; Kimura, E. *J. Biol. Inorg. Chem*. **2002**, *7*, 473. (h) Kimura, E. *Acc. Chem. Res*. **2001**, *34*, 171. (i) Kumar, K.; Tweedle, M. *Pure Appl. Chem*. **1993**, *65*, 515. (j) Rajec, P.; Švec, V.; Mikulaj, V.; Hanzel, R.; *J. Radioanal. Nucl. Chem.* **1998**, *229*, 9. (k) Fernando, L. A.; Miles, M. L.; Bowen, L. H. *Anal. Chem*. **1980**, *52*, 1115.

17. (a) Pederson, C. J. *J. Am. Chem. Soc*. **1967**, *89*, 7017. (b) Pederson, C. J. *J. Am. Chem. Soc*. **1970**, *92*, 391. (c) Pederson, C. J. *J. Am. Chem. Soc*. **1970**, *92*, 386. (d) Pedersen, C. J. *Science* **1988**, *241*, 536. (e) Pedersen, C. J. *J. Inclusion Phenom. Mol. Recognit. Chem.* **1992**, *12*, 7.
18. (a) Groth, P. *Acta Chem. Scand. A* **1981**, *35*, 463. (b) Liddle, S. T.; Clegg, W. *Polyhedron* **2003**, *22*, 3507.
19. Hancock, R. D. *Progr. Inorg. Chem*. **1989**, *37*, 187.
20. (a) Inoue, Y.; Gokel, G. W. (Eds.) *Cation Binding by Macrocycles*, Marcel Dekker, New York, **1990**. (b) Christensen, J. J.; Eatough, D. J.; Izatt, R. M. *Chem. Rev*. **1974**, *74*, 351. (c) Izatt, R. M.; Bradshaw, J. S.; Nielson, S. A.; Lamb, J. D.; Christensen, J. J. *Chem. Rev*. **1985**, *85*, 271. (d) Izatt, R. M.; Pawlak, K.; Bradshaw, J. S.; Bruening, R. L. *Chem. Rev*. **1991**, *91*, 1721.
21. (a) Steed, J. W. *Coord. Chem. Rev.* **2001**, *215*, 171 and references therein. (b) Méric, R.; Vigneron J. –P.; Lehn, J. –M. *J. Chem. Soc. Chem. Commun*. **1993**, 129. (c) Gokel, G. W.; Cram, D. J. *J. Chem. Soc. Chem. Commun*. **1973**, 481. (d)Izatt, R. M.; Lamb, J. D.; Rossiter, B. E.; Izatt, N. E.; Christensen, J. J. *J. Chem. Soc. Chem. Commun*. **1978**, 386. (e) Kyba, E. P.; Helgeson, R. C.; Madan, K.; Gokel, G. W.; Tarnowski, T. L.; Moore, S. S.; Cram, D. J. *J. Am. Chem. Soc*. **1977**, *99*, 2564.
22. (a) Lehn, J. M.; Vierling, P.; Hayward, R. C. *J. Chem. Soc. Chem. Commun*. **1979**, 296. (b) Uiterwijk, J. W. H. M; Harkema, S.; Geevers, J.; Reinhoudt, D. N. *J. Chem. Soc., Chem. Commun.* **1982**, 200. (c) Uiterwijk, J. W. H. M; Van Staveren, C. J.; Reinhoudt, D. N.; Hertog, H.; Kruise, L.; Harkema, S. *J. Org. Chem*. **1986**, *51*, 1575. (d) Van Staveren, C. J.; Hertog, H. J.; Reinhoudt, D. N.; Uiterwijk, J. W. H. M.; Kruise, L.; Harkema, S. *J. Chem. Soc., Chem. Commun*. **1984**, 1409. (e)

Lämsä , M.; Suorsa, T.; Pursiainen, J.; Huuskonen, J.; Rissanen, K., *J. Chem. Soc. Chem. Commun*. **1996**, 1443. (f) Lämsä, M.; Huuskonen, J.; Rissanen, K.; Pursiainen, J. *Chem. Eur. J*. **1998**, *4* , 84.

23. (a) Chatterjee, T.; Sarma, M.; Das, S. K. *Cryst. Growth Des*. **2010**, *10*, 3149. (b) Newcomb, M.; Moore, S. S.; Cram, D. J. *J. Am. Chem. Soc*. **1977**, *99*, 6405. (c) Dobler, M.; Phizackerley, R. P. *Acta Crystallogr*. **974**, *B30*, 2746.

24. (a) Metzger, A.; Gloe, K.; Stephan, H.; Schmidtchen, F. P. *J. Org. Chem*. **1996**, *61*, 2051. (b) Doxsee, K. M.; Francis, P. E. J.; Weakley, T. J. R. *Tetrahedron* **2000**, *56*, 6683. (c) Owen, J. D. *J. Chem. Soc. Perkin Trans. 2* **1983**, 407. (d) You, W.; Zhu, Z.; Wang, E.; Xu, L.; Hu, C. J. *Chem. Crystallogr*. **2000**, *30*, 577.

25. (a) Trueblood, K. N.; Knobler, C. B.; Lawrence, D. S.; Stevens, R. V. *J. Am. Chem. Soc*. **1982**, *104*, 1355. (b) Kryatova, O. P.; Korendovych, I. V.; Rybak-Akimova, E. V. *Tetrahedron* **2004**, *60*, 4579. (c) Fonari, M. S.; Simonov, Y. A.; Wang, W. –J.; Tang, S. –W.; Ganin, E. V. *CrystEngComm*. **2009**, *11*, 94.

26. Pope, M. T. *Heteropoly and Isopoly Oxometalates*; Springer–Verlag: Berlin, **1983**.

27. Newkome, G. R.; Patri, A. K.; Holder, E.; Schubert, U. S. *Eur. J. Org. Chem*. **2004**, 235.

28. (a) Schumacher, J. N.; Green, C. R.; Best, F. W.; Newell, M. P. *J. Agric. Food Chem*. **1977**, *25*, 310. (b) Foder, G. B.; Colasanti, B. In *Alkaloids*: *Chemical and Biological Perspectives*; Pelletier, S. W. Ed.; Wiley: New York, **1985**; Vol.*3*, Chapter 1. (c) Jacob, P.; Benowitz, N.; Yu, L.; Duan, M. J.; Liang, G. *Addiction* **1997**, *92*, 626.

29. a) *Molecular Nonlinear Optics* (Ed.: J. Zyss), Academic Press, New York, **1994**. b) Burland, D. M. *Chem. Rev*. **1994**, *94*, 1. c) Prasad, P. N.; Williamsin, D. J. *Introduction to Nonlinear Optical Effects in Moleculesand Polymers*, Wiley, New York, **1991**.

30. a) Grätzel, M. *Nature* **2001**, *414*, 338. b) O′Regan, B.; Grätzel, M. *Nature* **1991**, *353*, 737. c) Polo, A. S.; Itokazu, M. K.; Murakami Iha, N. Y. *Coord. Chem. Rev*. **2004**, *248*, 1343.

31. Fanta, P. E. *Synthesis* **1974**, 9.

32. (a) Stille, J. K. *Angew. Chem. Int. Ed. Engl.* **1986**, *25*, 508; *Angew. Chem.* **1986**, *98*, 504. (b) Echavarren, A. M.; Stille, J. K. *J. Am. Chem. Soc.* **1987**, *109*, 5478.

33. (a) Negishi, E.; King, A. O.; Okukado, N. *J. Org. Chem.* **1977**, *42*, 1821. (b) Schubert, U. S.; Eschbaumer, C.; Hochwimmer, G. *Tetrahedron Lett.* **1998**, *39*, 8643. (c) Schubert, U. S.; Eschbaumer, C.; Heller, M. *Org. Lett.* **2000**, *2*, 3373. (d) Savage, S. A.; Smith, A. P.; Fraser, C. L. *J. Org. Chem.* **1998**, *63*, 10048. (e) Loren, J. C.; Siegel, J. S. *Angew. Chem. Int. Ed.* **2001**, *40*, 754; *Angew. Chem.* **2001**, *113*, 776. (f) Mongin, F.; Trecourt, F.; Mongin, O.; Queguiner, G. *Tetrahedron* **2002**, *58*, 309.

34. (a) Badger, G. M.; Sasse, W. H. F. *J. Chem. Soc.* **1956**, 616. (b) Sasse, W. H. F.; Whittle, C. P. *J. Chem. Soc.* **1961**, 1347. (c) Newkome, G. R.; Weis, C. D. *Org. Prep. Proced. Int.* **1996**, *28*, 485.

35. (a) Nakamaru, K. *Bull. Chem. Soc. Jpn.* **1982**, *55*, 2697. (b) Newkome, G. R.; Puckett, W. E.; Kiefer, G. E.; Gupta, V. K.; Xia,Y.; Coreil, M.; Hackney, M. A. *J. Org. Chem.* **1982**, *47*, 4116. (c) Wang, Z.; Reibenspies, J.; Motekaitis, R. J.; Martell, A. E. *J. Chem. Soc., Dalton Trans.* **1995**, 1511. (d) Eisenbach, C. D.; Goeldel, A.; Terskan-Reinold, M.; Schubert, U. S. *Macromol. Chem. Phys.* **1995**, *196*, 1077.

36. (a) Leadbeater, N. E.; Resouly, S. M. *Tetrahedron Lett.* **1999**, *40*, 4243. (b) Jolly, P. W.; Wilke, G. *The Organic Chemistry of Nickel*, Academic Press, New York, **1975**. (c) Jolly, P. W. *Nickel Catalyzed Coupling of Organic Halides and Related Reactions*, Pergamon Press, New York, **1982**. (d) Tiecco, M.; Testaferri, L.; Tingoli, M.; Chianelli, D.; Montanucci, M. *Synthesis* **1984**, 736. (e) Iyoda,M.; Otsuka, H.; Sato, K.; Nisato, N.; Oda, M. *Bull. Chem .Soc. Jpn.* **1990**, *63*, 80.

37. (a) Hassan, J.; Penalva, V.; Lavenot, L.; Gozzi, C.; Lemaire, M. *Tetrahedron* **1998**, *54*, 13793. (b) Naka, K.; Uemura, T.; Chujo, Y. *J. Polym. Sci. Part A: Polym.Chem.* **2001**, *39*, 4083.

38. Savage, S. A.; Smith, A. P.; Fraser, C. L. *J. Org. Chem.* **1998**, *63*, 10048.

39. (a) Yamamoto, Y.; Azuma, Y.; Mitoh, H. *Synthesis* **1986**, 564. (b) Schubert, U. S.; Eschbaumer, C.; Hochwimmer, G. *Synthesis*, **1999**, 779. (c) Cárdenas, D. J.; Sauvage, J. –P. *Synlett* **1996**, 916. (d) Hanan, G. S.; Schubert, U. S.; Volkmer, D.;

Rivière, E.; Lehn, J. –M.; Kyritsakas, N.; Fischer, J. *Can. J. Chem.* **1997**, *75*, 169. (e) Schubert, U. S.; Eschbaumer, C. *Org. Lett.* **1999**, *1*, 1027. (f) Ulrich, G.; Bedel, S.; Picard, C.; Tisnes, P. *Tetrahedron Lett.* **2001**, *42*, 6113. (g) Schubert, U. S.; Weidl, C. H.; Lehn, J. M. *Des. Monomers Polym.* **1999**, *2*, 1.

40. (a) Miyaura, N.; Suzuki, A. *Chem. Rev.* **1995**, *95*, 2457. (b) Lützen, A.; Hapke, M. *Eur. J. Org. Chem.* **2002**, 2292.

41. Quici, S.; Cavazzini, M.; Ceragioli, S.; Montanari, F.; Pozzi, G. *Tetrahedron Lett.* **1999**, *40*, 3647.

42. (a) Kocian, O.; Mortimer, R. J.; Beer, P. D. *J. Chem. Soc. Perkin Trans. 1* **1990**, 3203. (b) Maury, O.; Guégan, J. –P.; Renouard, T.; Hilton, A.; Dupau, P.; Sandon, N.; Toupet, L.; Bozec, H. L. *New J. Chem.* **2001**, *25*, 1553.

43. (a) Bouder, T. L.; Viau, L.; Guégan, J. –P.; Maury, O.; Bozec, H. L. *Eur. J. Org. Chem.* **2002**, 3024. (b) Viau, L.; Maury, O.; Bozec, H. L. *Tetrahedron Lett.* **2004**, *45*, 125.

44. Berner, D.; Klein, C.; Nazeeruddin, Md. K.; Angelis, F. D.; Castellani, M.; Bugnon, Ph.; Scopelliti, R.; Zuppiroli, L.; Grätzel, M. *J. Mater. Chem.* **2006**, *16*, 4468. (b) Campbell, W. M.; Burrell, A. K.; Officer, D. L.; Jolley, K. W. *Coord. Chem. Rev.* **2004**, *248*, 363. (c) Coe, B. J.; Fielden, J.; Foxon, S. P.; Brunschwig, B. S.; Asselberghs, I.; Clays, K.; Samoc, A.; Samoc, M. *J. Am. Chem. Soc.* **2010**, *132*, 10498 and the references therein.

45. (a) Zyss, J.; Dhenaut, C.; Chauvan, T.; Ledoux, I. *Chem. Phys. Lett.* **1993**, *206*, 409. (b) Bozec, H. L.; Renouard, T. *Eur. J. Inorg. Chem.* **2000**, 229. (c) Sénéchal, K.; Maury, O.; Bozec, H. L.; Ledoux, I.; Zyss, J. *J. Am. Chem.. Soc.* **2002**, *124*, 4560. (d) Maury, O.; Bozec, H. L. *Acc. Chem. Res.* **2005**, *38*, 691. (e) Maury, O.; Viau, L.; Sénéchal, K.; Corre, B.; Guégan, J. –P.; Renouard, T.; Ledoux, I.; Zyss, J.; Bozec, H. L. *Chem. Eur. J.* **2004**, *10*, 4454. (f) Aubert, V.; Guerchais, V.; Ishow, E.; Hoang–Thi, K.; Ledoux, I.; Nakatani, K.; Bozec, H. L. *Angew. Chem. Int. Ed.* **2008**, *47*, 577. (g) Renouard, T.; Bozec, H. L.; Brasselet, S.; Ledoux, I.; Zyss, J. *Chem. Commun*. **1999**, 871.

46. (a) Mazzucato, S.; Fortunati, I.; Scolaro, S.; Zerbetto, M.; Ferrante, C.; Signorini, R.; Pedron, D.; Bozio, R.; Locatelli, D.; Righetto, S.; Roberto, D.; Ugo, R.;

Abbotto, A.; Archetti, G.; Beverina, L.; Ghezzi, S. *Phys. Chem. Chem. Phys*. **2007**, *9*, 2999. (b) Zheng, Q.; He, G. S.; Prasad, P. N. J. *Mater. Chem*. **2005**, *15*, 579. (c) Feuvrie, C.; Maury, O.; Bozec, H. L.; Ledoux, I.; Morrall, J. P.; Dalton, G. T.; Samoc, M.; Humphrey, M. G. *J. Phys. Chem. A* **2007,** *111*, 8980.

47. Edkins, R. M.; Bettington, S. L.; Goeta, A. E.; Beeby, A. *Dalton Trans*. **2011**, *40*, 12765.

••••

Chapter-2

Transition Metal Complexes of Tetra-aza Macrocycles in Polyoxometalate Association: Racemization or Conglomeration?

ABSTRACT: Intermolecular non-covalent association between transition metal complexes of two tetra-aza macrocyclic systems and Lindqvist type polyoxometalate (POM) cluster anions has been demonstrated. Eight new ion-pair complexes were synthesized through simple ionic metathesis reaction and fully characterized. The infrared and UV-visible spectroscopic behavior of the obtained compounds corresponds to both the macrocyclic systems and the POM cluster anions. The analyses of the crystal structures of the resulting compounds reveal that the polyoxometalate cluster anions not only serve as the counter anions but are also involved in extensive non-covalent interactions with the macrocyclic cationic complexes in their respective crystals. The most important finding of the present work is the occurrence of spontaneous resolution of the copper complex of one of the macrocyclic systems with the POM anions during crystallization whereas the other six compounds crystallize in centrosymmetric space groups. A thorough scrutiny of the crystal structures of all the systems clearly manifests the reason behind these differing behaviors and has been outlined in this chapter.

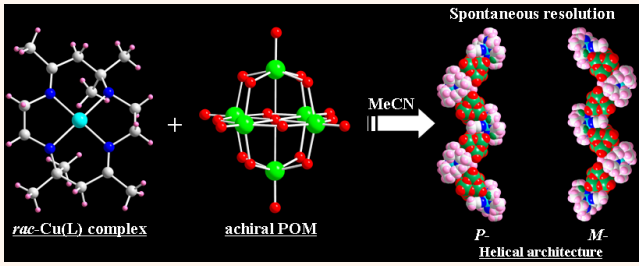

• 2.1. INTRODUCTION

Since the manufacture of the X-ray diffractometer, and with the rapid progress in information processing through high speed digital devices, research in polyoxometalate (POM) chemistry has achieved an elevated profile due to the excellent structural and chemical miscellany of these vast classes of cluster anions and their applications in multiple areas.[1–4] The generalized structural feature of these cluster anions is their oxy-surface which plays a key role in the crystals containing the POMs. The surface oxygen atoms of the POMs can either form a coordinate covalent linkage with external metal atoms (thus the POMs acting as a ligand) or can act as a hydrogen bond acceptor to interact with a donor species present in the lattice. Till-date, the research in POM chemistry has mainly been dominated by the inorganic-organic hybrid materials in which the POM anion not only serves as a counter anion or as a ligand, but also as a supramolecular entity to form a range of discrete to extended structures.[5–6]

Crystallization of the coordination complexes of macrocyclic systems with the POMs results in the isolation of a new kind of inorganic-organic hybrid solid in which both the electrostatic (coulombic) as well as the intermolecular non-covalent forces play a pivotal role in the union of the components.[7–9] The aza-macrocycles are superior candidates over the oxy-macrocycles for binding / encapsulating transition metal ions. The incorporation of POMs as a counter anion in the relevant compounds reduces solubility of the metal-ligand systems and this concept was initially introduced to separate toxic metal ions using both macrocycles (receptor) and POMs (separator).[10]

The two component systems depicted in his chapter contains transition metal complexes of 5,7,7,12,14,14-hexamethyl-1,4,8,11-tetraazacyclotetra-deca-4,11-diene (commonly known as **Transdiene**, henceforth L) and 1,4,7,10-tetraazacyclododecane (commonly known as **cyclen**) as the cationic counter parts and the $[Bu_4N]_2[M_6O_{19}]$ (M = Mo, W) as the counter anions (see Figure 1). Transdiene and cyclen are prominent in the area of coordination chemistry owing to their affinity towards forming stable complexes with transition metals.

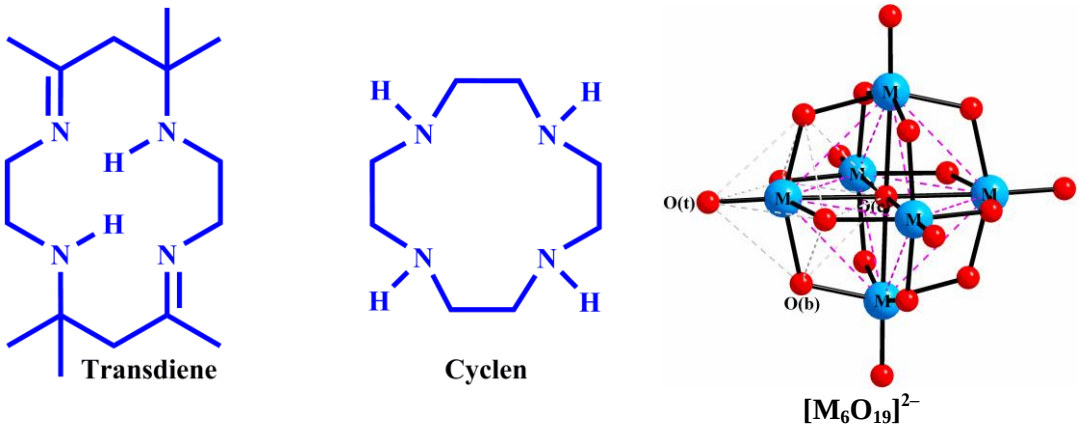

Figure 1. Molecular structure of Transdiene (L), Cyclen and the $[M_6O_{19}]^{2-}$ anion. Coordination geometry of the central oxygen atom and one of the metal centers of the $[M_6O_{19}]^{2-}$ anion is shown.

The Schiff condensed macrocycle, L was first synthesized by N. F. Curtis.[11–13] Later, coordination complexes of the same were extensively investigated in terms of electron transfer reactions,[14] as model systems for understanding the active sites of some biologically active metallo-proteins (e.g. Vitamin B_{12})[15] and in terms of catalysis (e.g.

H_2O and CO_2 reduction).[16] The macrocycle (L) was chosen as the major component in the present work because (i) it is easily synthesizable, (ii) it owes high stability toward air/moisture or acidic reaction conditions contrast to the Schiff bases (imines) derived from the aliphatic primary amines which are susceptible to hydrolysis in acid catalyzed medium and most importantly, (iii) coordination complexes of L comprise two stereogenic NH(*sec*) centers (Scheme 1). The complexes of L are usually isolated as perchlorate salts, the counter anions of which can be exchanged with other anionic species.[17] Thus, the relevant coordination complexes exist as two diastereomers *viz.* *racemic*– (*RR*– or *SS*–) if both the NH(*sec*) atoms are on the same face of the macrocycle and *meso*– (*RS*–) if they project to different faces.[18] Hence, such complexes might be useful as model systems for studying the phenomenon of spontaneous resolution which is defined as the segregation of enantiomers without the necessity of a chiral auxiliary.[19]

Scheme 1. Schematic representation showing the molecular structures of L (left), *trans–racemic*– (middle) and *trans–meso*– (right) stereoisomers of M–L complexes (metal geometry being four or six coordinate). Wedged bonds = axial atoms, hashed wedged bonds = equatorial atoms.

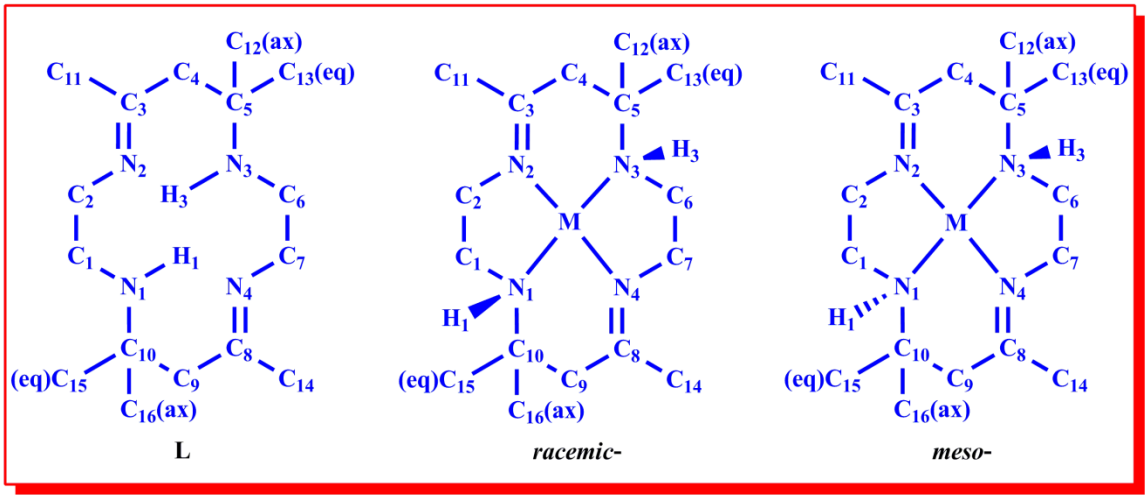

Although the question arises as to whether the M–L complexes could be used as a chiral probe or not, it cannot be answered in a straightforward manner as the overall chirality of a crystalline solid is often serendipitous. The packing of molecular components in chiral space symmetry is often complicated to predict a priori and depends on several factors such as solvent, crystallization conditions, counter anion (if the chiral

species is cationic) etc. Most often, the isolation of chiral crystals is thwarted by racemization and conglomeration, the foremost problem in this context. In chiral synthesis, two generalized approaches have been established to obtain stacking/packing of the crystallizing substances following a screw symmetry *viz.*, (a) helicity induction through the usage of a chiral substance,[20] and (b) chiral packing motif of the molecular components through spontaneous resolution.[21] During the nucleation of crystals from dissolved racemic components, three limiting situations might arise: (a) formation of a racemic crystal in which both the enantiomers maintain opposite chirality/helicity in the same crystal thereby nullifying the overall chirality of the individual crystals (and thus bulk sample), (b) formation of a conglomerate in which 50 : 50 distribution of the crystals containing individual enantiomers makes the bulk sample optically inactive and (c) formation of a *pseudo*-racemate which maintains inhomogeneous distribution of the enantiomers. Only the conglomerate formation involves spontaneous resolution of the enantiomers which in turn occurs with 5–10% of the racemates only. It is thus obvious that induction of heterochirality through the chirality transport among the helical packing motifs of the crystallizing substances is more common than the maintenance of homochirality in a crystal lattice. Among the various intermolecular non-covalent forces that assemble the adjoining molecules in the crystals in an ordered array, hydrogen bonds are more appealing due to their strong directional nature. Since the past few decades, the scientific community has been witnessing a number of homochiral metal-organic frameworks and their versatile applications in the areas of optical materials, chiral separation, enantioselective catalysis, nonlinear optical materials, and porous materials, etc.[22]

The symmetry-breaking approach to obtain enantiopure crystals of the POM-associated hybrid solids is generally hindered by the frequent intrusion of the inversion symmetry which imposes centric twining, thereby leading to the isolation of racemic crystals. The multimetallic archetype of the POM in itself is a racemization hazard because of the possibilities of partial hydrolysis or fluxional behavior, etc. Alternatively, it can be said that the isolation of POM-based chiral superstructures is still of considerable interest to polyoxometalate chemists and this is in fact manifested by a good number of examples which deal with chirality induction in the POM-based hybrid

solids.[23] In an endeavor to comprehend the phenomenon of spontaneous resolution of POM-associated M–L complexes, we synthesized seven ion-pair compounds namely, $[Co^{III}(L)(Cl)_2]_2[Mo_6O_{19}]$ (**1**), $[Co^{III}(L)(NO_2)_2]_2[Mo_6O_{19}]$ (**2**), $[Co^{III}(L)(NCS)_2]_2[W_6O_{19}]\cdot 2CH_3CN$ (**3**), $[Ni^{II}(L)][W_6O_{19}]\cdot DMSO\cdot DCM$ (**4**), $[Cu^{II}(L)(CH_3CN)][Mo_6O_{19}]$ (**5**), $[Cu(L)(CH_3CN)][W_6O_{19}]$ (**6**) and $[Zn^{II}(L)(Cl)]_2[W_6O_{19}]$ (**7**). Among all the compounds synthesized, interestingly, only the copper compounds **5** and **6** crystallize in the chiral space group $P2_12_12_1$. The occurrence of spontaneous resolution for these two compounds during crystallization was revealed through crystallographic analyses. In order to further comprehend whether the macrocycle or the POM played the major role in the occurrence of spontaneous resolution, we also synthesized the compound [Cu(cyclen)(MeCN)][W_6O_{19}] (**8**). The coordination complexes of cyclen have versatile applications, for example, in the areas of medical science,[24–26] biology,[27–29] photochemistry and sensor materials[30–33] etc. Till date, several transition metal complexes of simple or functionalized cyclen have been reported.[24–33]

● 2.2. RESULTS AND DISCUSSION

● 2.2.1. Synthesis

(a) Transdiene (L) related compounds, 1–7. Condensation of acetone with $Fe(en)_3^{2+}$ (en = ethylenediamine) usually results in the formation of the dihydroperchlorate salt of L ($L\cdot 2HClO_4$),[13a] which is the key precursor in synthesizing several metal complexes.[34–36] An alternate method by Curtis' described the synthesis of $L\cdot 2HClO_4$ by a simple Schiff condensation between acetone and ethylenediamine in the presence of perchloric acid.[13b] The second protocol, being more facile and effortless, was followed in the present study. At this juncture, it is important to mention that, although the macrocyclic Schiff base ligand, L is closely related to the aliphatic Schiff bases, the dihydrogen perchlorate salt of L is a stable compound in contrast to the aliphatic Schiff bases which are immensely prone to hydrolysis in acid catalyzed medium.[13a] The reaction of $L\cdot 2HClO_4$ with $Na_3[Co(CO_3)_3]\cdot 3H_2O$ in water formed the *cis*-carbonato complex which was isolated as dark red solid (see Scheme 2). Subsequent acidification of this compound with HCl resulted in the formation of the dichloro complex $[Co^{III}(L)(Cl)_2](ClO_4)$ (**1a**) that was isolated as green crystalline blocks.[13a,34a] Thereafter, the axial chloride ions were replaced from $[Co^{III}(L)(Cl)_2]^+$ by V-shaped NO_2^- and linear shaped NCS^- ligands to yield comp-

Scheme 2. Synthetic protocol to obtain the ion-pair solids 1–7.

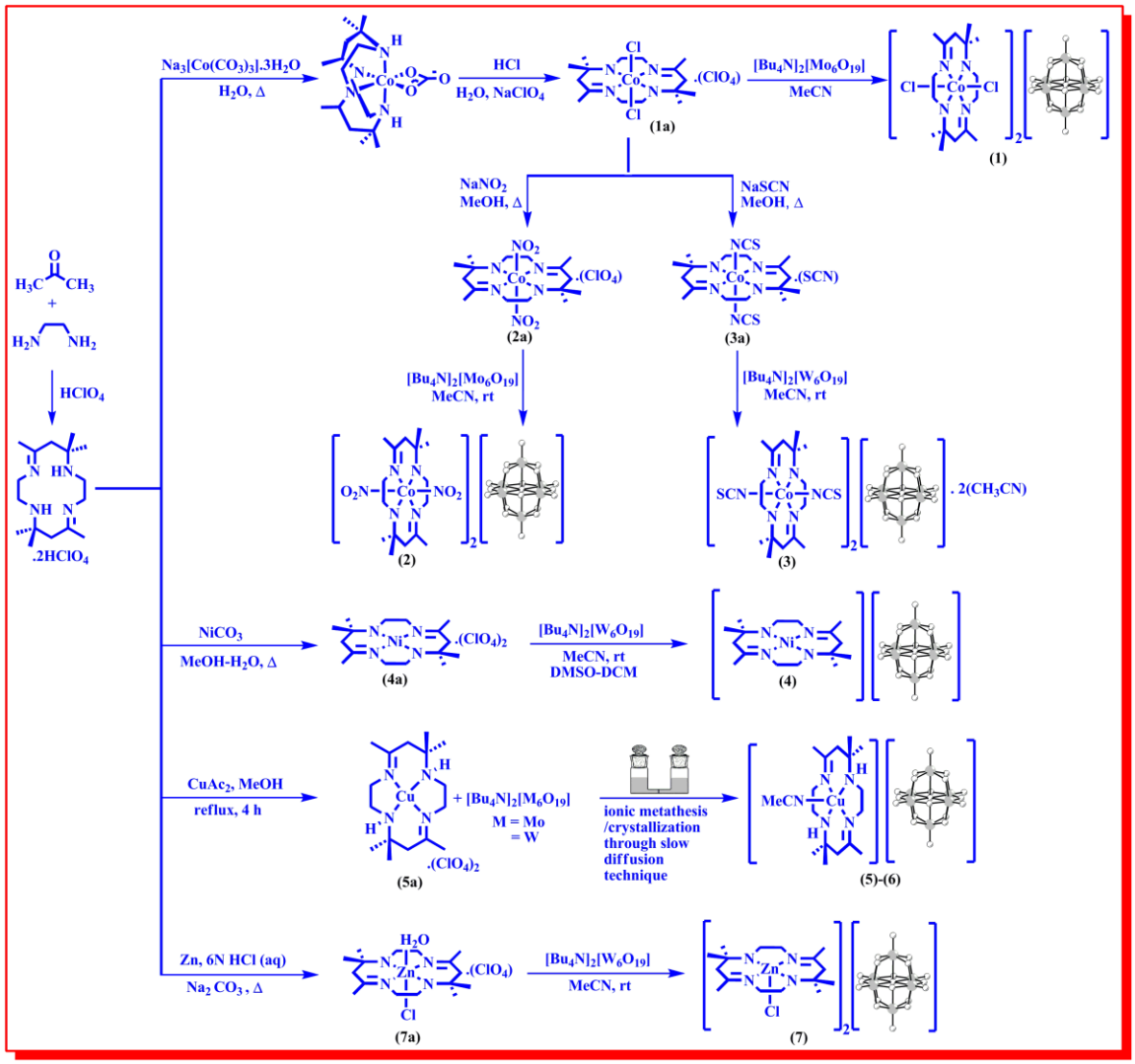

-lexes **2a** and **3a** respectively. On the other hand, reaction between Ni^{II} and Zn^{II} salts with $L{\cdot}2HClO_4$ led to the formation of the perchlorate salts $[Ni(L)](ClO_4)_2$ (**4a**) and $[Zn(L)(Cl)(H_2O)](ClO_4)$ (**7a**) respectively (see Scheme 2).[13a] In addition, treatment of the dihydroperchlorate salt of L with cupric acetate in refluxing methanol resulted in the formation of the copper complex $[Cu(L)](ClO_4)_2$ (**5a**). In all the cases, the starting precursors were purified *via* repeated recrystallization and used in the succeeding step to trim down any unwanted deposition/contamination of the *meso*– diastereomer with the *racemic*– isomer.[37]

The compounds **1**–**7** are the result of ionic-metatheses between the *rac*–perchlorate / isothiocyanate salts of the M–L complexes and tetrabutylammonium salts of the

hexamolybdate (compounds **1, 2, 5**) or hexatungstate anions (compounds **3, 4, 6, 7**). The compound $[Cu(L)(MeCN)][W_6O_{19}]$ (**6**) was isolated as red crystals by the metathesis reaction between *rac*–$[Cu(L)](ClO_4)_2$ and $[Bu_4N]_2[W_6O_{19}]$ in acetonitrile in dilute condition (Scheme 2). However, a similar ion-exchange reaction with the molybdenum analogue $[Bu_4N]_2[Mo_6O_{19}]$ immediately formed a precipitate. As such, X-ray diffraction quality single crystals of the compound $[Cu(L)(MeCN)][Mo_6O_{19}]$ (**5**) were grown by trimming down the rate of ionic metathesis in acetonitrile *via* the slow diffusion in a U-shaped cell. The overall synthetic route is presented in Scheme 2.

Scheme 3. Synthetic route used to obtain the macrocycle, cyclen.

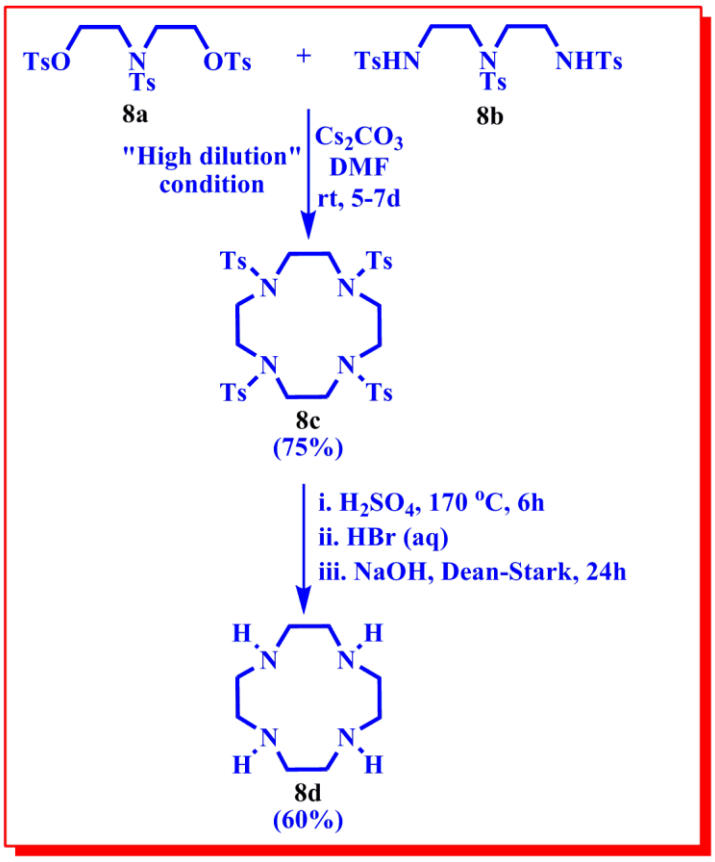

(b) Cyclen related compound (8). Cyclen was synthesized in gram quantities adopting a procedure published elsewhere.[38] The synthetic strategy involved tosylation of diethanolamine and diethylenetriamine to yield **8a** and **8b** respectively followed by base mediated cyclization under "high dilution condition" to obtain the cyclic product **8c** which was finally detosylated to cyclen (**8d**) as shown in Scheme 3. The direct mixing of

a solution (MeCN, MeOH etc.) containing a Cu^{II} salt and cyclen (i.e. Cu–cyclen coordination complex) with $[Bu_4N]_2[W_6O_{19}]$ resulted in the immediate formation of a blue precipitate, which could not be characterized unambiguously. Thus, single crystals of the compound $[Cu(cyclen)(CH_3CN)][W_6O_{19}]$ (**8**), suitable for X-ray crystallography, were grown by a slow diffusion technique, more specifically, in a U-tube set-up as shown in Figure 2.

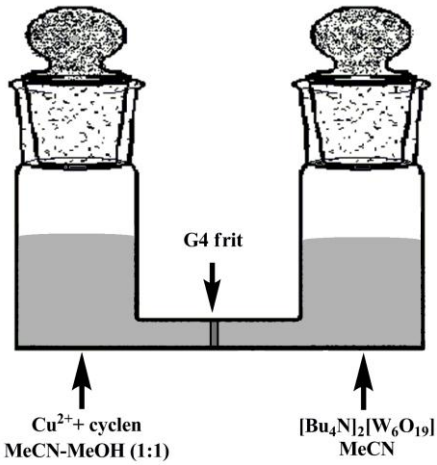

Figure 2. Slow diffusion between two components in a U-shaped cell for the growth of good quality crystals suitable for single crystal XRD analysis.

All the compounds **1–8** were isolated as crystalline solids and characterized by spectroscopy (IR, ESR (wherever active), UV-visible) including elemental analysis and their structures were unambiguously determined by single crystal X-ray crystallography.

● 2.2.2. Infrared spectroscopy

The vibrational spectra of the Co–L complexes, **1–3** exhibit characteristic features concerning the macrocycle, the axially coordinated ligands to cobalt and the hexametalate cluster anions. These spectra have been compared with their respective parent molecules *viz.*$[Co^{III}(L)(Cl)_2](ClO_4)$ (**1a**), $[Co^{III}(L)(NO_2)_2](ClO_4)$ (**2a**) and $[Co^{III}(L)(NCS)_2](SCN)$ (**3a**) and are summarized in Table 1. The highest energy band at 3190, 3124 and 3190 cm^{-1} in the FT-IR spectra of the compounds **1**, **2** and **3** respectively is due to the N–H stretching vibration. The stretching absorption due to the imine functionality (C=N) in the compounds **1a** (1651 cm^{-1}) and **1** (1651 cm^{-1}), **2a** (1649 cm^{-1}) and **2** (1647 cm^{-1}) occurs in (almost) same energy region. But in the case of compound **3**, a considerable negative

Table 1. Selected IR stretching frequencies (solid state, KBr, cm^{-1}) and absorption wavelengths for compounds 1–7 in comparison with 1a–7a.

Compound	υ_{max} / cm^{-1}			λ_{abs} / nm
	$\upsilon(N–H_{str})$	υ $(C–H_{str})$	υ $(C=N_{str})$	
1a	3190 (s)	2980 (m)	1651 (s)	280, 338, 634
1	3204 (m)	2970 (m)	1651 (s)	275, 335, 630
2a	3232	2979	1649	
2	3124	2970	1647	270, 364, 450
3a	3196	2973	1628	
3	3190	2964	1651	265, 365, 540
4a	3173 (s)	2982 (m)	1660 (s)	282, 439
4	3123 (m)	2970 (m)	1658 (s)	280, 435
5a	3213	2984	1674	281, 520
5	3242	2934	1666	275, 330, 516
6	3244	2972	1664	275, 517
7a	3244 (s)	2980 (s)	1678 (s)	270
7	3263 (m) 3211 (m)	2974 (m)	1658 (s)	280

shift of the band, associated with the C=N vibration, is observed (23 cm^{-1}) when the SCN^- counter anion is displaced from **3a** ($\upsilon_{C=N}$ = 1628 cm^{-1}) by the hexatungstate cluster anion resulting in the formation of **3** ($\upsilon_{C=N}$ = 1651 cm^{-1}). A very strong absorption band at 2065 cm^{-1} in the vibrational spectrum of compound **3** is attributed to the cobalt coordinated NCS^- ligand. Two strong and sharp bands at 1390 and 1311 cm^{-1} in the IR spectrum of compound **2** are due to the stretching absorption of the NO_2^- ligand. These two distinctive bands for the concerned functionality appear nearly at the same energy (1398 and 1311 cm^{-1}) in the spectrum of the perchlorate salt **2a**. A comparison between the IR spectra of compounds **2** and **3** is pictorially represented in Figure 3. The absorption due to the N–H stretching vibrational motion in the nickel compound **4** ($\upsilon_{N–H}$ = 3123 cm^{-1}) is significantly shifted to the lower energy region compared to that of the corresponding perchlorate salt, **4a** ($\upsilon_{N–H}$ = 3173 cm^{-1}). This denotes that the NH(*sec*) pro-

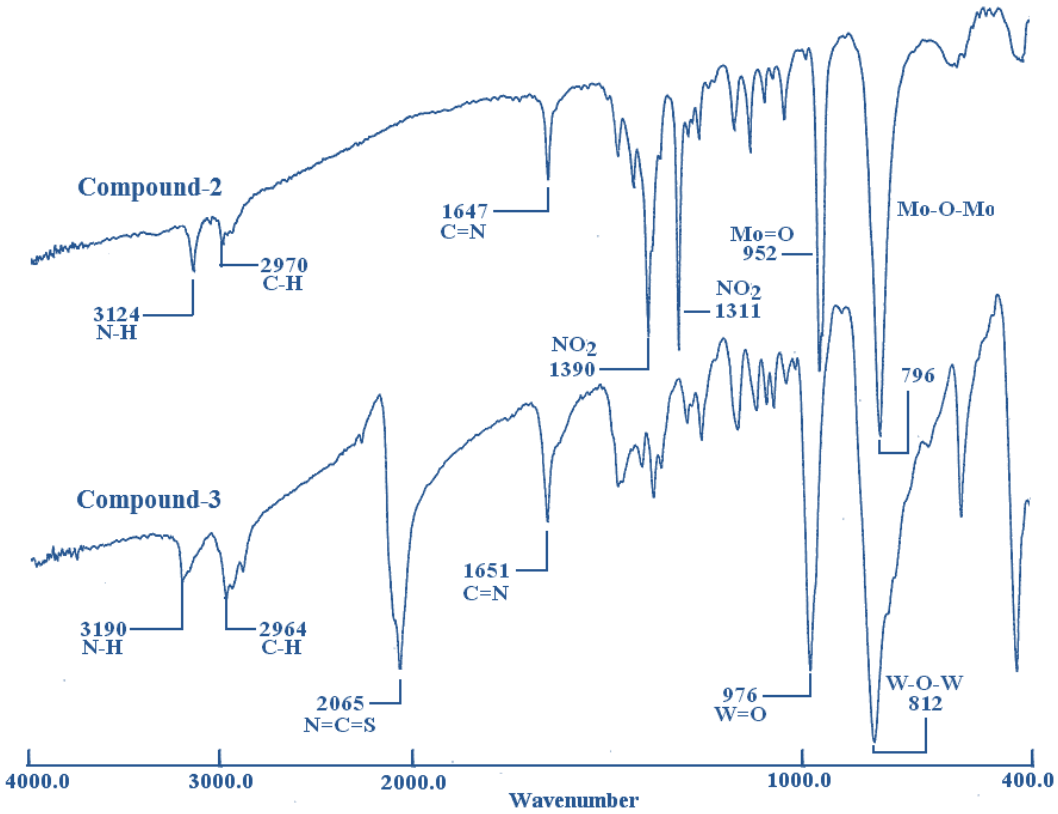

Figure 3. A comparison between the IR spectra of compounds **2** and **3**.

-tons in compound **4** are in a stronger hydrogen bonding environment compared to **4a**. It is in fact known that NH(*sec*) protons in the Ni–L complexes have a general propensity to be involved in stronger hydrogen bonding interactions with the counter anions and thus, these complexes are very inert towards coordination expansion even in the presence of a strong ligating nucleophile like CN^-.[39] The medium intensity sharp band at around 3240 cm^{-1} in the IR spectra of the compounds, **5** and **6** corresponds to the N–H stretching vibration of the amine functionalities in the Cu–L complexes, whereas the corresponding C=N stretching of the imine functionalities in these compounds appear at 1666 and 1649 cm^{-1} respectively as a strong band.

The appearance of a single N–H stretching band in the IR spectra of compounds **1**–**6** reveals that the NH(*sec*) protons are in a similar environment in the pertinent solids. The scenario is a little different in the IR spectrum of compound **7** which shows the existence of two N–H stretching absorptions separated by 52 cm^{-1} (see Table 1) whereas, the perchlorate salt **7a** shows only a single absorption at 3244 cm^{-1} due to the aforementioned vibrational motion. The presence of two N–H stretching bands for compound **7** compared

to the single band for compound **7a** might be due to different local environments around the two NH(*sec*) protons in compound **7**.

The presence of the hexametalate cluster anions in a solid matrix is usually characterized by the occurrence of two strong absorption bands at the low frequency region of the vibrational spectra. Thus, the intense infrared absorption bands near 950 and 795 cm^{-1} in the IR spectra of the molybdate based compounds are denoted as the Mo=O stretching and Mo–O_b–Mo bending motions respectively of the $[Mo_6O_{19}]^{2-}$ cluster anion. The hexatungstate cluster anion exhibits IR bands near 975 (W=O) and 810 (W–O_b–W) cm^{-1}. Thus, it is clearly evident from the vibrational spectroscopy of the title compounds that both the macrocyclic and polyoxometalate cluster units are present in the synthesized compounds.

The infrared spectrum of compound **8** shows the characteristic features for the tetra-aza-crown ether and the POM anion. The strong IR band at 3250 cm^{-1} is assigned to the asymmetric and symmetric N–H stretching vibrations of cyclen whereas, the band for C (sp^3)–H stretching at 2949 cm^{-1} is weakly intense. The medium intensity and sharp IR band at 2310 cm^{-1} might be attributed to Cu coordinated MeCN molecule. The characteristic IR absorptions of the hexatungstate POM anion appear as strong bands centered at 983 cm^{-1} and 808 cm^{-1} that correspond to the W=O stretching and W–O_b–W bending motions of the cluster anion respectively.

● 2.2.3. UV-visible spectroscopy

The electronic absorption properties of the title compounds **1**−**8** were examined both in solution state as well as in the solid state. The absorption spectra of the compounds **1**–**7** are displayed in Figure 4 and that of compound **8** in Figure 5. All the spectra of the cobalt complexes (compounds **1**–**3**) elucidate typical feature of the *trans*-$[Co^{III}(L)X_2]^+$ complexes (X = Co bound axial ligands e.g. halogen, H_2O, NH_2, NO_2^-, NCS^- etc.).[34b] The crystal field for the octahedral $[Co^{III}(L)X_2]^+$ complexes has already been modelled in previous literature, which effectively explains the origination of various absorption bands in their electronic spectra.[34b, 40] For example, both the solid state and the solution state absorption spectra of compound **1** exhibit weak intensity bands in the visible region 630–632 nm which is assigned to the metal centered $^1A_{1g} \rightarrow {}^1T_{1g}$ transition (see Figure 4a–b) and designated as band–I according to the convention of Linhard and Weigel.[40] This band

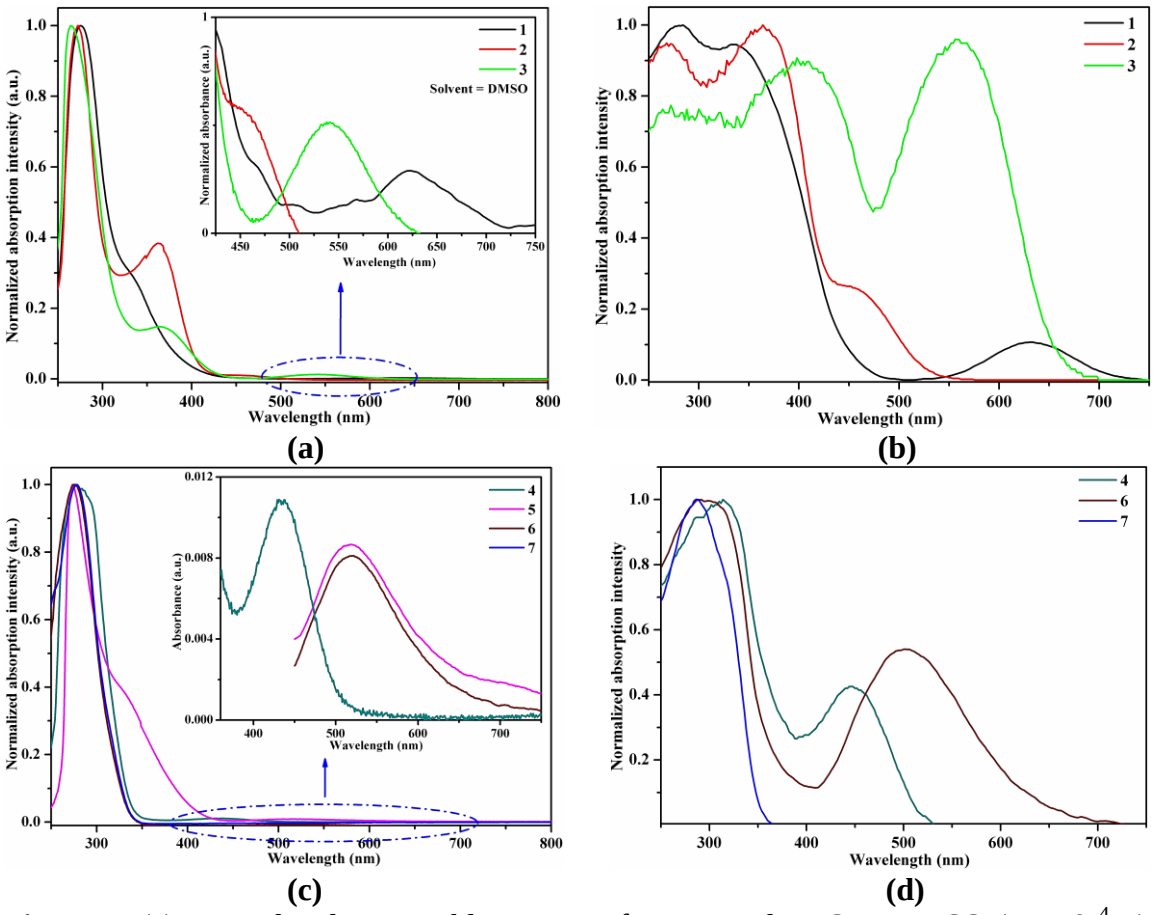

Figure 4. (a) Normalized UV-visible spectra of compounds **1**–**3** in DMSO (*ca*. 10^{-4}M). Spectra at the inset correspond to the weak d–d absorptions. (b) Normalized diffuse reflectance spectra of compounds **1**–**3** ($BaSO_4$). (c) Normalized UV-visible spectra of compounds **4**–**7** in DMSO (*ca*. 10^{-4} M). Spectra at the inset correspond to the weak d–d absorptions. (d) Normalized diffuse reflectance spectra of compounds **4**–7. All spectra were recorded at 298K.

for compounds **2** and **3** is observed at 450 nm (shoulder) and 540 nm respectively in DMSO solution. The large blue shift in case of compound **2** might be due to the presence of strongly electron withdrawing NO_2^- group. It is known that, for the *trans*-$[Co^{III}(L)X_2]^+$ complexes, the corresponding absorption (band–I) does not split into multiple components and appear as a broad absorption band in the electronic spectrum.[37b] The absorption spectrum of compound **1** is further characterized either by the appearance of a shoulder (solution) or an intense band (solid state) at ~335 nm which is assigned to band–II (metal centered) following the same convention.[40] This band for compound **2** is observed at ~364 nm in both solid and solution states. The solution state as well as the solid phase absorption spectra of compound **2** has not shown any disparity as far as the

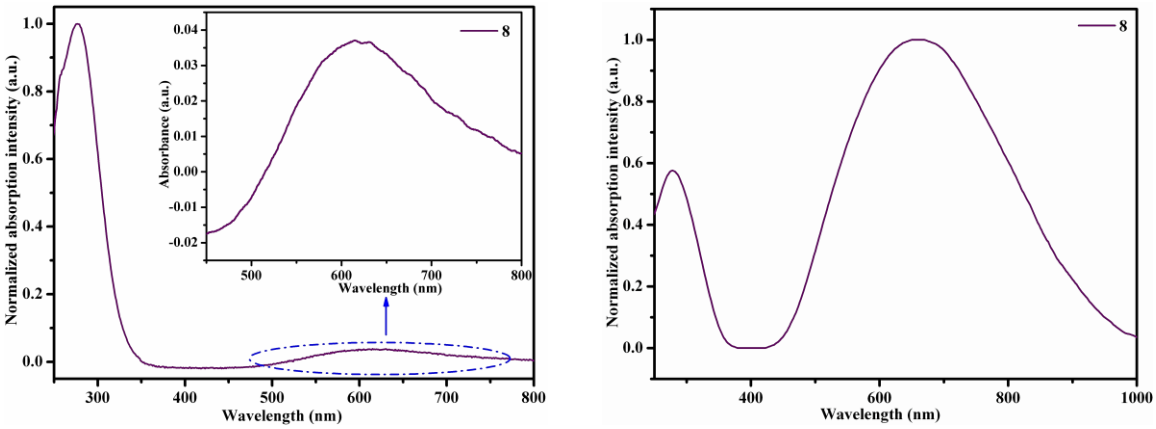

Figure 5. (a) Normalized UV-visible spectra of compound **8** (DMSO, *ca*. 10^{-4} M). The inset corresponds to the zoomed section of the absorption spectrum showing the Cu^{2+} centered d–d transition. (b) Diffuse reflectance spectrum of compound **8** (spread over $BaSO_4$).

position of the various bands is concerned (Figures 4a–b). However, a minor divergence in the electronic spectral behavior of compound **3** is observed from the solid to the solution state. For example, band–I and band–II appear at 540 and 365 nm respectively in DMSO solution of compound **3** but at 560 and 402 nm in the relevant solid state spectrum. In other words, it can be said that, there is a considerable hypsochromic shift of the metal centered (Co^{III}) transition energies of compound **3** when it is brought into its solution state.

The lowest energy band at 435 nm in solution state and at 445 nm in the solid state absorption spectra of compound **4** is assigned to the d–d transitions of the Ni^{II} metal center. The relevant transition in the copper complexes **5** and **6** appear as a weakly intense band at *ca.* 520 nm (Figure 4c) in DMSO solution but as an intense band at ~500 nm in solid state (Figure 4d).

The absorption spectra (solution and solid) of compound **7** is devoid of any band in the visible region and show only an intense absorption band near 270–280 nm (see Figures 4c and 4d). This is inevitably due to the absence of any d–d transition in the zinc complex (compound **7**) in contrast to the Co^{III}, Ni^{II} and Cu^{II} complexes discussed in the previous sections (compounds **1**–**6**).

All the spectra of compounds **1**–**7** consist of a very intense absorption at the high energy region of the spectra (270–280 nm) which can be assigned to the combined

absorptions due to the M–L coordination complex (charge transfer, C=N etc.[11b, 41–42]) and Ö→M charge transfer in the POM anion. The escalation of these bands in presence of the POM anions alludes to the fact that origination of these bands is due to the combined absorption of the M–L complexes and the POM anions. From the optical data provided in Table 1, it is evident that the variation of the counter ion from perchlorate to the POM cluster anion has not affected the absorption properties of the M–L complexes considerably, apart from intensification of the highest energy absorption band.

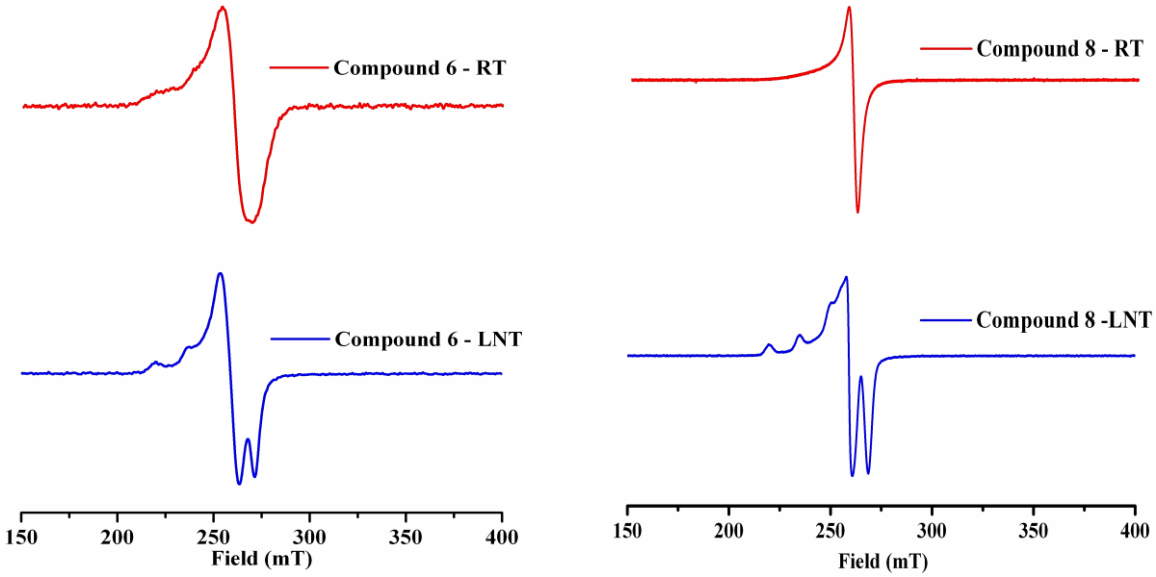

Figure 6. ESR spectra of compounds **6** and **8** recorded at room temperature (red trace) and at –140ºC (blue trace, frozen DMSO).

A broad band in the visible region is observed at *ca.* 610 nm in the electronic absorption spectrum of compound **8**, which is assigned to the d–d transition in a Cu^{II} (d^9) system. The solution state and diffuse reflectance spectra of compound **8** is shown in Figure 5.

● 2.2.4. Electronic Spin Resonance (ESR) spectroscopy

The ESR spectra of all the compounds were recorded both in DMSO solution and in solid powdery form at room temperature as well as at –140 ºC. The compounds **1**, **2** and **3** do not resonate with the X–band microwave radiation in the ESR spectrophotometer which confers to $t_{2g}^6e_g^0$ electronic configuration to the octahedral Co^{III} metal center ($t_{2g}^6e_g^0$) in the respective solids. Also, the ESR spectra of the nickel and zinc compounds

(compounds **4** and **7** respectively) delineate their diamagnetic nature (low–spin), bestowing the d_{xy}^2 d_{x2-y2}^0 (Sq. Pl., Ni^{II}, compound **4**) and d^{10} (Zn^{II}, compound **7**) electronic configuration to the concerned metal centers in the respective compounds. The compounds **6** and **8** containing the Cu^{II} metal center are ESR active. The ESR spectra of these compounds are shown in Figure 6. The four-component hyperfine ESR spectra of these compounds with $g_{\|}$= 2.26 ($A_{\|}$= 210.7 G) and $g_{\perp}$ = 2.03 (for compound **6**) and $g_{\|}$ = 2.28 ($A_{\|}$ = 179–198 G) and $g_{\perp}$ = 2.07 (for compound **8**), suggests the tetragonally elongated environment around the Cu^{II} (d^9) ion with $g_{\|} > g_{\perp}$ (Figure 6).[43–44]

● 2.2.5. Description of crystal structures

Most of the previously reported M–L complexes are collected from the Cambridge Structural Database (CSD) and compiled in Table 2 which reveals the variation of space symmetry of the crystals with the metal bound axial ligands and the counter anion. For example, the *rac*–dichloro cobalt complex crystallizes under $P2_1$ space symmetry with tetrahedral perchlorate counter anion,[16] but under $P\bar{1}$ space symmetry with more symmetrical $[Sb_2Cl_8]^{2-}$,[16] or $[Mo_6O_{19}]^{2-}$ counter anions.[42a] A thorough analysis of the crystal structures of compounds **1**–**8** containing bulky POM counter anions indeed reveals an alteration of the geometrical and structural parameters of the M–L complexes from the earlier reported complexes encompassing smaller anions.

Compound $[Co^{III}(L)(Cl)_2]_2[Mo_6O_{19}]$ (1). The crystal structures of both the *trans*–*rac*– and *trans*–*meso*– diastereomers of $[Co(L)(Cl)_2](ClO_4)$ (**1a**) i.e. the macrocycle precursor in synthesizing compound **1,** were previously reported.[34a,34e] The structure of the *trans*–*rac*– stereoisomer reported by House and co-workers[34a] (CSD depository code QANXOS) has a two-fold screw symmetry (space group $P2_1$) whereas, the *trans*–*meso*–isomer crystallizes with an inversion symmetry site at the metal center (CSD depository code QANXUY, space group $P2_1/c$).[34a] Compound $[Co^{III}(L)(Cl)_2]_2[Mo_6O_{19}]$ (**1**) is composed of two $[Co(L)(Cl)_2]^+$ cations and one octahedral symmetrical (O_h) $[Mo_6O_{19}]^{2-}$ isopolyanion for charge compensation. It crystallizes in $P\bar{1}$ space symmetry placing the center of inversion at O(6) central oxygen atom of the hexamolybdate anion (0.5, 0.5, 0.5) with respect to which the two $[Co(L)(Cl)_2]^+$ cations are related. Thus, the ion-pair complex **1** is centrosymmetric, the inversion center being the central oxygen atom of the isopolyanion. The asymmetric unit of the crystal structure consists of one Co^{III}–L cation

Table 2. Some of the previously reported M–L complexes entered in CSD.

Compound	CSD code [a]	Sp. Gr.	Geometry [b]	Ref
rac–$[Co^{III}L(H_2O)(Me)](ClO_4)_2$	BADFIV	$P2_1/n$	Octahedral	35b
meso–$[Co^{III}L(OAc)_2](I_3)$	BEVHUG	$P2_1/c$	Octahedral	35f
meso–$[Co^{II}L(H_2O)_2](BF_4)_2$	DNCOBF10	$P2_1/c$	Octahedral	35g
meso–$[Co^{III}L(NH_3)_2](ClO_4)_3$	DNCOPC10	$A2/a$	Octahedral	13a
meso–$[Co^{III}L(H_2O)(CH_2OH)](ClO_4)_2$	FEDHOM	$P2_1$	Octahedral	40c
rac–$[Co^{II}L(H_2O)](ClO_4)_2$	JASKUJ	$Pbcn$	Sq. py.	45a
rac–$[Co^{II}L(ClO_4)](ClO_4)$	JASLEU	$P2_1/c$	Sq. py.	45a
rac–$[Co^{III}L(H_2O)(CH_2Cl)](ClO_4)_2$	JETSIK	$P2_1/c$	Octahedral	45b
rac–$[Co^{III}L(H_2O)(Me)](CF_3SO_3)_2$	JIMJEU	$P2_1/c$	Octahedral	45c
rac–$[Co^{III}L(H_2O)(H_2SO_3)](ClO_4)$	KEGSAQ	$P2_12_12_1$	Octahedral	35e
meso–$[Co^{III}L(N_3)_2](ClO_4)$	MELZIN	$P2_1/n$	Octahedral	45d
rac–$[Co^{III}(PhCH(OH)COO)](ClO_4)$	QANXEI	$R3$	Octahedral	16
rac–$[Co^{III}L(Cl)_2](ClO_4)$	QANXOS	$P2_1$	Octahedral	16
rac–$[Co^{III}L(Cl)_2]_2(Sb_2Cl_8)$	QANYAF	$P\bar{1}$	Octahedral	16
rac–$[Co^{III}L(NCS)_2](SCN)$	TEKZEO	$P2_12_12_1$	Octahedral	45e
rac–$[Co^{I}L(CO)](ClO_4)$	VAKTIK	$C2$	Sq. Py.	34e
rac–$[Ni(L)](ClO_4)_2$	MAZTNI02	$Pbca$	Sq.Pl.	36a
meso–$[Ni(L)](ClO_4)_2$	KUGNEF	$P2_1/c$	Sq.Pl.	36a
meso–$[Ni(L)](I)_2$	CIXQUW	$P\bar{1}$	Sq.Pl.	36b
meso–$[Cu(L)](ClO_4)_2$	CEJNMG	$P2_1/c$	Sq.Pl.	45f
meso–$[Cu(L)(H_2O)](ClO_4)_2$	CUCJOY	C_2/c	Sq. py.	45g
rac–$[Cu(L)(NO_3)](ClO_4)$	CERFUA	$P2_1/c$	Sq. py.	45h
rac–$[Cu(L)](ClO_4)_2$	BAPPUD	$P2_1/c$	Sq.Pl.	45i
meso–$[Zn(L)](ClO_4)_2$	TAQRIN	$P2_1/c$	Sq.Pl.	45j
rac–$[Co^{III}L(Cl)_2]_2[Mo_6O_{19}]$	present study	$P\bar{1}$	Octahedral	42a
rac–$[Co^{III}L(NO_2)_2]_2[Mo_6O_{19}]$	present study	$P\bar{1}$	Octahedral	42b
rac–$[Co^{III}L(NCS)_2]_2[W_6O_{19}]$	present study	$P2_1/c$	Octahedral	42b
rac–$[Ni(L)][W_6O_{19}]$	present study	$P2_1/c$	Sq.Pl.	42a
rac–$[Cu(L)(MeCN)][M_6O_{19}]$	present study	$P2_12_12_1$	Sq. py.	42c
rac–$[Zn(L)(Cl)][W_6O_{19}]$	present study	$P2_1/c$	Sq. py.	42a

[a] Based on CSD version 5.32, November 2010 at University of Hyderabad, [b] coordination geometry around the metal center

and half of the POM anion (Z' = ½) (see Figure 7a). The macrocycle in compound **1** has *trans*– conformation (as in the perchlorate salt **1a**), in which, the four nitrogen atoms of the macrocycle N(1), N(2), N(3) and N(4) define the equatorial coordination to the metal center, Co(1), and two Cl^- anions occupy the apical sites leaving the metal center in an axially elongated octahedral coordinating territory. N(1), N(2), N(3) and N(4) ligating sites of the macrocycle are almost coplanar and the metal center is shifted by 0.032(2) Å from the mean macrocycle {N4} plane i.e. the Co^{3+} cation is almost completely encapsul-

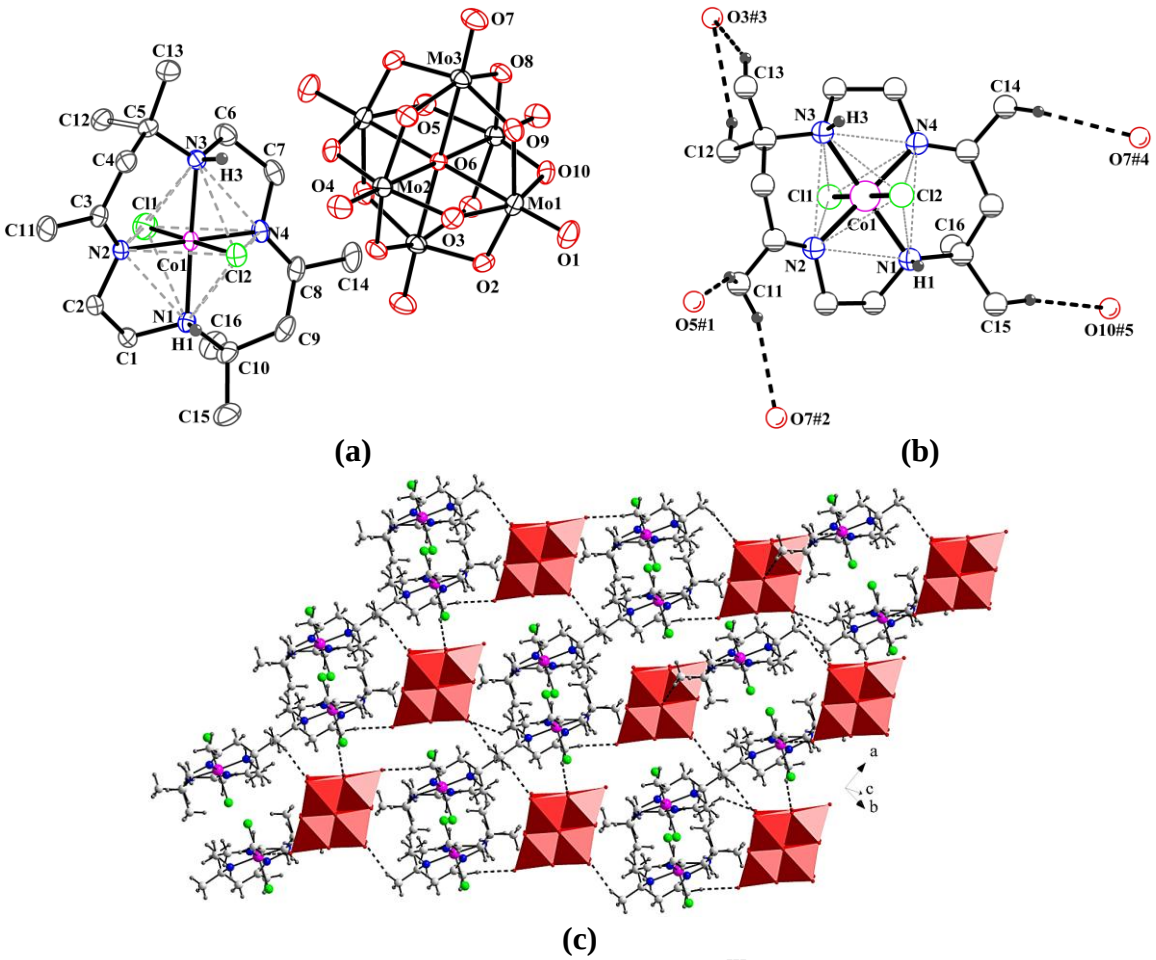

Figure 7. (a) The crystal structure of compound $[Co^{III}(L)(Cl)_2]_2[Mo_6O_{19}]$ (**1**) in 30% thermal probability levels. Only one macrocyclic cationic complex is shown and hydrogen atoms have been excluded for a clearer view. (b) Hydrogen bonding environment surrounding the $[Co^{III}(L)(Cl)_2]^+$ cation. Atoms labelled with additional numbers (#) are related to each other by the symmetry operations as appeared in Table 4. (c) A fragment of packing of the molecules in the crystal. Hydrogen bonds are shown in black dotted lines. Color code: C, light grey, H, medium grey; N, blue; Cl, green; Co, pink; $[Mo_6O_{19}]^{2-}$ anion, red polyhedra. The same color convention is used throughout the chapter.

-ated in the cavity of the macrocycle (see Figure 7a). In the Co^{III}–L complex cation, the metal–ligand bond lengths are observed to be Co(1)–N(amine) 1.965(3)–1.973(3) Å, Co(1)–N(imine) 1.921(3)–1.923(3) Å and Co(1)–Cl 2.276(2)–2.280(4) Å (see Table 3 for various observed bond distances). Thus, it follows the conventional trend: Co(1)–N(amine) > Co(1)–N(imine). This shows a feature of shorter M–N lengths in the crystal structure of compound **1**. As shown in Figure 7b, one face of the $\{CoN_4\}$ plane consists of the NH(*sec*) atoms H(1) and H(3); on the other face, both axial methyl groups C(12)

Table 3. Selected bond lengths for the crystal structure of compounds 1–4.

Bond	**1**	**2**	**3**	**4**
C1–C2	1.524(6)	1.459(17)	1.512(15)	1.498(12)
C3–C4	1.493(6)	1.524(18)	1.535(14)	1.485(12)
C4–C5	1.524(6)	1.495(19)	1.496(16)	1.542(12)
C6–C7	1.512(6)	1.48(2)	1.513(15)	1.490(12)
C8–C9	1.496(7)	1.48(2)	1.506(15)	1.492(12)
C9–C10	1.529(7)	1.541(19)	1.540(16)	1.518(12)
C3–C11	1.494(5)	1.498(16)	1.503(16)	1.503(12)
C5–C12(ax)	1.524(6)	1.555(19)	1.533(17)	1.529(12)
C5–C13(eq)	1.532(6)	1.589(19)	1.517(14)	1.513(12)
C8–C14	1.498(6)	1.520(17)	1.515(15)	1.507(12)
C10–C15(eq)	1.526(7)	1.519(19)	1.544(16)	1.532(13)
C10–C16(ax)	1.522(7)	1.54(2)	1.507(17)	1.533(13)
C1–N1amine	1.474(5)	1.499(15)	1.488(13)	1.494(10)
C10–N1(amine)	1.506(5)	1.529(17)	1.527(14)	1.492(11)
C2–N2(imine)	1.480(5)	1.495(15)	1.477(12)	1.460(11)
C3–N2(imine)	1.277(5)	1.258(16)	1.288(13)	1.285(11)
C5–N3(amine)	1.509(5)	1.467(18)	1.511(14)	1.512(11)
C6–N3(amine)	1.475(5)	1.484(17)	1.468(14)	1.476(11)
C7–N4(imine)	1.469(6)	1.483(17)	1.492(13)	1.470(11)
C8–N4(imine)	1.277(5)	1.258(18)	1.280(12)	1.284(11)
M–N1(amine)	1.965(3)	1.956(11)	1.995(8)	1.920(7)
M–N3(amine)	1.973(3)	1.979(11)	1.987(7)	1.930(7)
M–N2(imine)	1.921(3)	1.945(11)	1.925(9)	1.900(7)
M–N4(imine)	1.923(3)	1.925(11)	1.922(10)	1.891(7)

and C(16) are projected; thus the stereoisomer of the macrocycle in compound **1** is characterized as *racemic*. The relatively shorter C–N lengths of C(3)–N(2) 1.277(5) and C(8)–N(4) 1.277(5) Å compared to the longer lengths of C(5)–N(3) 1.509(5) and C(10)–N(1) 1.506(5) Å confirm the position of the imine C=N bonds in the macrocycle. In the distorted octahedral coordination geometry of the Co^{III}–L cation in the crystal structure of compound **1**, the bite angles for the five and six membered rings are observed to be N(1)–Co(1)–N(2) 83.94º, N(3)–Co(1)–N(4) 83.86º and N(2)–Co(1)–N(3) 95.91º, N(1)–Co(1)–N(4) 96.28º respectively. On the other hand, the isopolyanion $[Mo_6O_{19}]^{2-}$ anion (known as Lindqvist type POM anion) is characterized as an almost spherical shaped cluster anion. Each Mo atom resides in a distorted octahedral environment coordinating to one terminal (O(t)), four μ_2–bridging (O(b)) and the μ_6–central oxygen (O(c)) atoms, making

the overall symmetry of the cluster to approach octahedral (O_h). The Mo–O bonds in this POM anion is generally grouped into three categories based on molybdenum–oxygen distances and these lengths are observed to be M=O(t) 1.676(3)–1.686(3) Å, M–O(b) 1.896(3)–1.956(3) Å and M–O(c) 2.313(3)–2.320(3) Å in the crystal structure of compound **1**. Apart from the Coulombic association between the ionic counterparts, supramolecular weak interactions (C–H···O) between the various peripheral methyl groups of the macrocycle and the oxide surface of the POM anion are registered in the crystal structure of compound **1** as shown in Figure 7b (see Table 4 for the geometrical parameters for these interactions). Interestingly, the NH(*sec*) hydrogen atoms H(1) and H(3) are not found to be involved in hydrogen bonding interactions. These polar interactions (electrostatic, C–H···O hydrogen bonding etc.) along with other non–polar forces in the crystal lattice of compound **1** assemble the molecules to pack in an intricate fashion as shown in Figure 7c.

Compound $[Co(L)(NO_2)_2]_2[Mo_6O_{19}]$ (2). The crystal structure of the compound $[Co^{III}(L)(NO_2)_2]_2[Mo_6O_{19}]$ (**2**) shows the presence of two *trans*–$[Co(L)(NO_2)_2]^+$ cations and one $[Mo_6O_{19}]^{2-}$ isopolyanion for elctro-neutrality. The counter parts of this molecule prefer to stack with each other using $P\bar{1}$ (triclinic) space symmetry in which the center of inversion resides on O(6), central oxygen atom of the hexamolybdate anion (0.5, 0.5, 0.5). The asymmetric unit of the concerned crystal comprises half of the ion-pair compound (Z' = ½), i.e. one $[Co(L)(NO_2)_2]^+$ cation and half of the hexamolybdate cluster anion. The two cobalt macrocyclic complexes are related to each other via the inversion symmetry located at O6. As a result, the ion–pair complex **2** is centrosymmetric, with the central oxygen atom of the isopolyanion occupying the inversion center. The crystal structure of compound **2** is shown in Figure 8a. The NH(*sec*) atoms could be located from the relevant difference Fourier map and their co-facial orientation in the relevant crystal evidently registers the stereochemistry of Co–L complex cation as the *rac*– one. Similarly, the axial methyl carbon atoms i.e., C12 and C16 are projected towards the same face of the macrocycle (opposite to the face in which the two NH(*sec*) atoms are directed) as required for the *rac*– enantiomer (see Figure 8a). The Co1 metal center is almost completely encapsulated by the macrocycle and resides in an octahedral coordination environment, in which the basal tetra-coordination of $\{CoN_6\}$ octahedron is

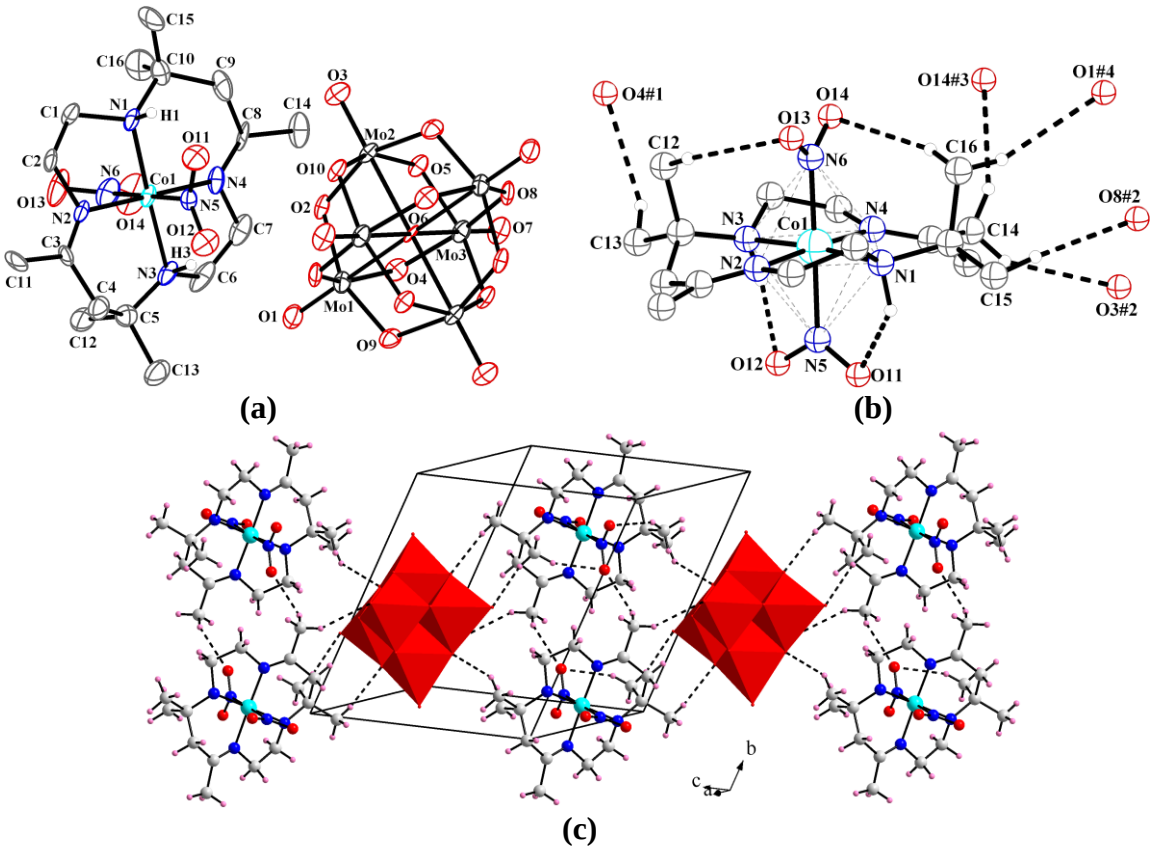

Figure 8. (a) Thermal ellipsoidal plot (40%) of compound $[Co(L)(NO_2)_2]_2[Mo_6O_{19}]$ (**2**). The atom C5 is isotropic. Only one cationic complex has been shown for clarity. (b) Hydrogen bonding environment surrounding the $[Co^{III}(L)(NO_2)_2]^+$ cation. (c) Fraction of crystal packing featuring the various intermolecular non-covalent interactions. The C–H···O interactions are shown in black dashed lines.

provided by the macrocycle through the N1 to N4 ligating sites. The two $–NO_2$ groups occupy the apical coordination sites of Co1 and flank with each other in perpendicular fashion. The mean Co–N bond lengths in the concerned crystal are found to be: Co1–N(amine) 1.966 Å, Co1–N(imine) 1.935 Å, Co1–N(nitro) 1.974 Å. These values clearly indicate an axially elongated octahedral coordination geometry around the metal center and are in accord with the regular trend i.e. Co(1)–N(amine) > Co(1)–N(imine). A similar trend is also observed with the mean C–N bond lengths, C–N(amine) 1.497 Å > C–N(imine) 1.373 Å. Thus, the relatively shorter C–N(imine) lengths compared to the longer C–N(amine) bonds confirm the position of the imine C=N bonds in the macrocycle. The Co–L cationic complex consists of two six membered and two five membered chelate rings. The mean bite angles for the six and five membered rings are measured as 94.56º and 85.31º respectively. The packing of the molecular fragments in

Table 4. Geometrical parameters for the hydrogen bonding interactions in the crystal structures of compounds 1–4.

	d(D–H)	*d*(H···A)	*d*(D···A)	<(D–H···A)	Symmetry
Compound–1					
C11–H11B···O5#1	0.96	2.50	3.391(5)	154.8	–x+1,–y+1,–z+2
C11–H11C···O7#2	0.96	2.55	3.467(6)	159.6	x+1, y, z+1
C12–H12A···O3#3	0.96	2.69	3.498(6)	142.6	x, y–1, z
C13–H13C···O3#3	0.96	2.63	3.491(6)	149.9	x, y–1, z
C14–H14B···O7#4	0.96	2.61	3.460(7)	148.2	x+1, y, z
C15–H15B···O10#5	0.96	2.53	3.463(6)	164.1	–x+2, –y+1, –z+1
Compound–2					
C12–H12A···O13	0.96	2.47	3.34(2)	149.4	Intramolecular
C14–H14B···O14	0.96	2.58	3.404(18)	144.2	2–x, 1–y, –z
C14–H14A···O3	0.96	2.54	3.395(19)	147.8	2–x, 1–y, 1–z
C15–H15B···O8	0.96	2.43	3.363(16)	163.6	2–x, 1–y, 1–z
C16–H16A···O14	0.96	2.43	3.34(2)	158.4	Intramolecular
N3–H3···O12	0.95(19)	1.8(2)	2.706(14)	153(17)	Intramolecular
Compound–3					
C7–H7A···O1	0.97	2.54	3.388(13)	146.2	1–x,–0.5+y,1.5–z
C14–H14A···O1	0.96	2.54	3.344(14)	141.7	x, 0.5–y, 0.5+z
C11–H11A···O1	0.96	2.62	3.442(15)	143.9	1–x, 1–y, 1–z
Compound–4					
C1–H1A···O15#1	0.97	2.44	3.302(10)	147.8	x, –y+0.5, z–0.5
C6–H6B···O10	0.97	2.32	3.235(11)	156.7	Intramolecular
C9–H9B···O12	0.97	2.48	3.422(10)	162.5	Intramolecular
C13–H13B···O16#2	0.96	2.52	3.475(11)	173.3	–x+2, –y+1, –z+1
C14–H14B···O9#3	0.96	2.65	3.558(11)	158.2	–x+1, –y+1, –z+1

the crystal structure of compound **2** is governed by several intra– and intermolecular non-covalent weak interactions. It is evident from Figure 8a that the NH(*sec*) atoms and the axial methyl groups C12 and C16 are projected on opposite faces of the macrocycle. The nitro groups are involved in hydrogen bonding interactions with both of these groups (see Table 4 for the various geometrical parameters). Apart from these intramolecular interactions, intermolecular C–H···O interactions are also depicted in the crystal structure of the compound **2**. These interactions lead to a chain like topology for arranging the macrocyclic complexes with the POM cluster anions as shown in Figure 8c. Lastly, it is

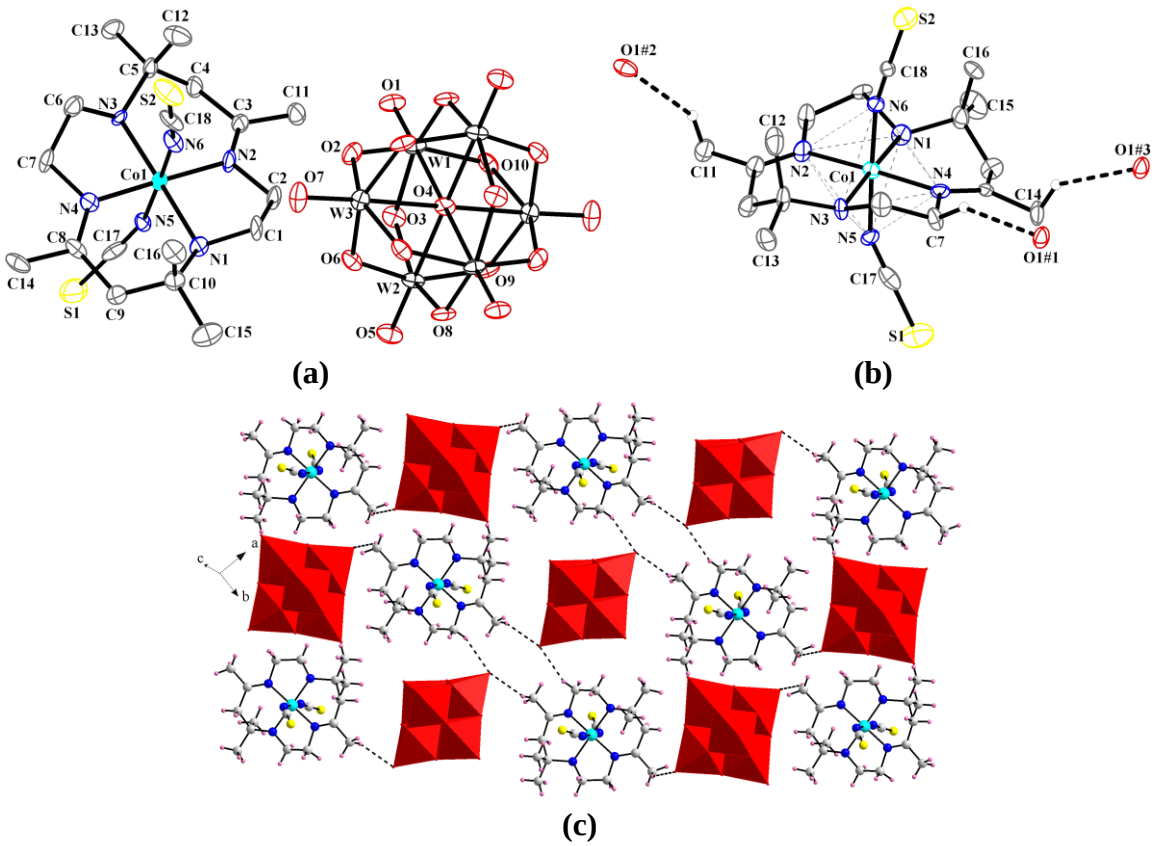

Figure 9. (a) Crystal structure of the compound $[Co(L)(NCS)_2]_2[W_6O_{19}]\cdot 2CH_3CN$ (**3**). The thermal ellipsoids are drawn at 40% distribution levels. Only one Co–L cation is shown and the solvent molecules have been omitted for a clearer view. (b) Hydrogen bonding environment surrounding the $[Co^{III}(L)(NCS)_2]^+$ cation. (c) Picture displaying a portion of packing of the Co–L cations with the hexatungstate cluster anions. The C–H···O interactions are shown in black dashed lines.

observed that both the compounds *rac*–$[Co^{III}L(Cl)_2]_2[Mo_6O_{19}]$[42a] and *rac*–$[Co^{III}L(NO_2)_2]_2[Mo_6O_{19}]$[42b] crystallize under same space symmetry ($P\bar{1}$). Thus, the symmetry of the crystal is not altered on replacing the spherical shaped chlorine atoms from the Co–L complex by the V–shaped nitro ligand, the anion being the same i.e., the hexamolybdate cluster anion.

Compound $[Co(L)(NCS)_2]_2[W_6O_{19}]$ (3). Similar to compound **2**, compound **3** also comprises two monocationic Co–L complexes and a dianionic POM cluster anion (hexatungstate) in both its molecular and crystal structures. Interestingly, the compound $[Co(L)(NCS)_2]_2[W_6O_{19}]$ (**3**) adopts higher space symmetry than the crystal of compound **2** but, reduced symmetry than its precursor $[Co(L)(NCS)_2](SCN)$ (**3a**) which crystallize in $P2_12_12_1$ space group. Alternatively, it can be said that, although the $[Co(L)(NCS)_2]^+$

complex crystallizes in a chiral manner with the SCN^- counter anion which has a linear geometry, presence of the spherically shaped and centrosymmetric hexatungstate cluster anion presumably results in arrangement of the molecules in a centrosymmetric fashion. Analogous to compound **2**, the compound **3** crystallizes as an acetonitrile solvate with one $[Co(L)(NCS)_2]^+$ cation and half of the $[W_6O_{19}]^{2-}$ anion in its asymmetric unit (Z' = ½). The central oxygen atom of the POM cluster i.e. O4 is positioned at the inversion site (0.0, 0.5, 0.5) with respect to which the two Co–L complexes are related to each other. The crystal structure of compound **3** is shown in Figure 9a which clearly depicts octahedral coordination geometry around the metal center. The metal center is almost coplanar with the macrocycle $\{N_4\}$ plane which provides the basal coordination to Co1. The apical sites are occupied by two NCS^- ligands. The NH(*sec*) atoms of the macrocycle could not be located from the diffraction data of this crystal. But the projection of the axial methyl groups (C12 and C16) on the same face of the macrocycle essentially proves its *rac–trans*– conformation. The axial NCS^- ligands project in the same direction and binds the metal center in an angular fashion, <Co1–N5–C17 = 151.2º, < Co1–N6–C18 = 166.3º. The geometrical parameters for Co coordination are observed as follows: Co–N(amine) 1.991 Å, Co–N(imine) 1.923 Å and Co–N(NCS) 1.911 Å (see Table 3). These values indicate an axially compressed octahedral coordination environment around the concerned metal center. Similarly, the C–N lengths are observed as C–N(amine) 1.499 Å and C–N(imine) 1.384 Å, hence obeying the regular practice i.e. Co–N(amine) > Co–N(imine) and C–N(amine) > C–N(imine). The mean bite angles for the five and six membered chelate rings of the Co–L complex are calculated as 84.95º and 94.99º respectively. Thus, these bite angles in the crystal structure of both the compounds **2** and **3** are in the range of 90±5º. Supramolecular C–H···O contacts between the macrocycle and the POM anion are also observed in this crystal. The macrocycle meets three different symmetry related POM anions through hydrogen bonding: C7–H7A···O1 (rotation), C14–H14A···O1 (reflection) and C11–H11A···O1 (inversion) (see Table 4 for the geometrical parameters of these interactions). A view of packing of the inversion symmetry related Co–L complexes with the POM anions are displayed in Figure 9c.

Compound $[Ni^{II}(L)][W_6O_{19}]\cdot DMSO\cdot DCM$ (4). The EXAFS analysis as well as the single crystal X–ray structure of compound $[Ni^{II}(L)](ClO_4)_2$ (**4a**), the starting precursor of

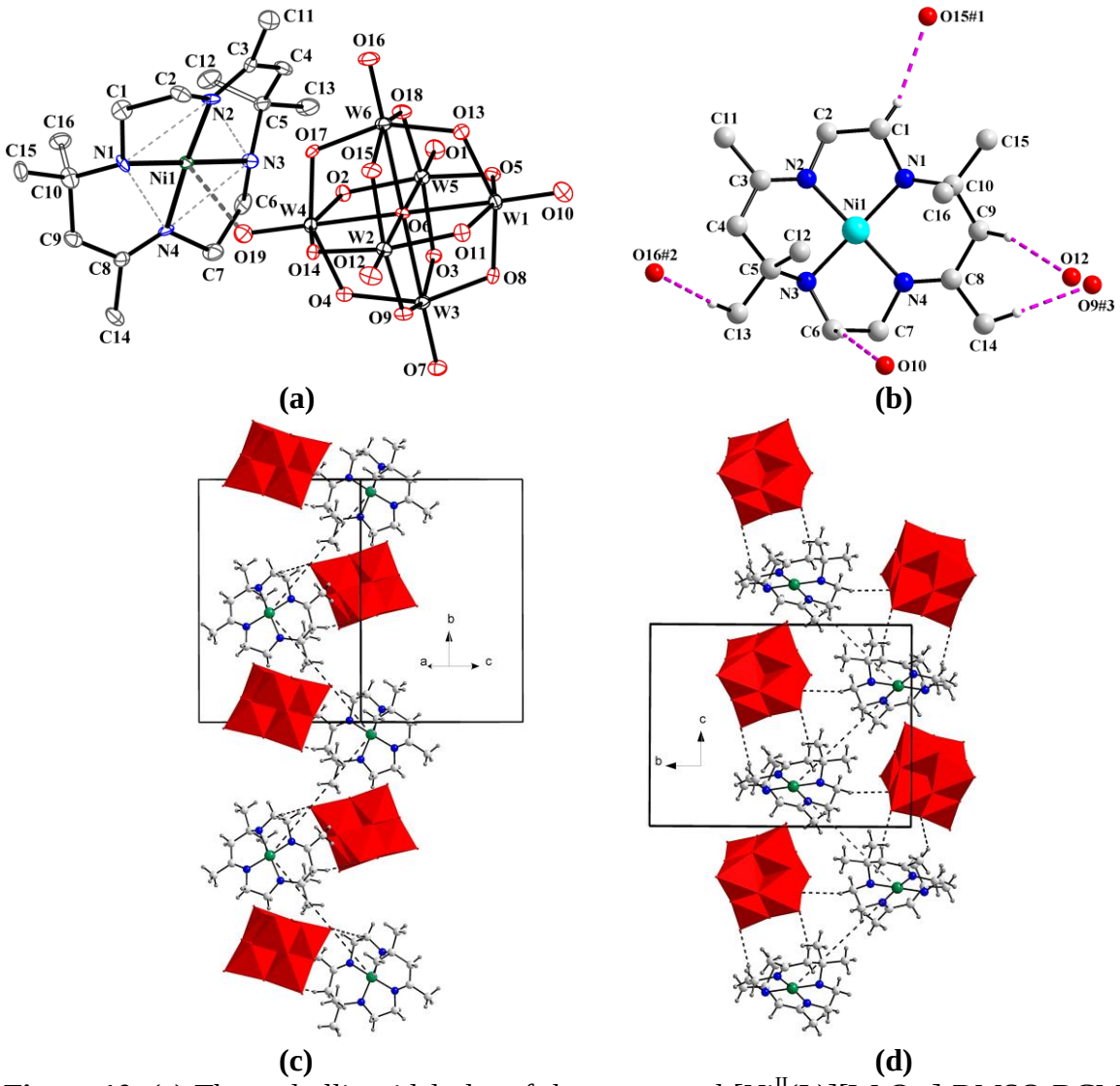

Figure 10. (a) Thermal ellipsoidal plot of the compound $[Ni^{II}(L)][W_6O_{19}]\cdot DMSO\cdot DCM$ (**4**) in 50% confidence levels. The short Ni···O interaction are shown in grey dotted lines. Hydrogen atoms and the solvent molecules have been excluded for a lucid view. (b) Hydrogen bonding environment surrounding the $[Ni^{II}(L)]^{2+}$ cation. (c) Packing of the 2_1 symmetry related molecules parallel to the crystallographic *b*–axis. (d) Molecular array of the *c*–glide related molecules through non-covalent interactions viewed down the crystallographic *c*–axis. C–H···O interactions between the macrocycles and POMs are shown by black dotted lines.

compound **4**, were previously reported in literature.[36] In contrast to compounds **1**, **2** and **3**, that contains two mono-cationic species along with a dianionic POM cluster, compound **4** comprises a dicationic Ni–L complex and $[W_6O_{19}]^{2-}$ as the anion for charge balance. The compound $[Ni^{II}(L)][W_6O_{19}]\cdot DMSO\cdot DCM$ (**4**) was isolated as yellow blocks and the crystal structure is characterized as a solvate with one DCM and one DMSO

molecule in its asymmetric unit. This compound crystallizes in $P2_1/c$ space symmetry with a square planar $[Ni^{II}–L]^{2+}$ cation and a charge complementary hexatungstate anion $[W_6O_{19}]^{2-}$ (Z' = 1) in the asymmetric unit. The thermal ellipsoidal plot of compound **4** is shown in Figure 10a. Although the NH(*sec*) hydrogen atoms could not be located in the relevant crystal structure, stereoisomerism of the macrocycle is unambiguously designated as *rac*– *trans*– because both the axial methyl groups C(12) and C(16) project on the same face of the $\{NiN_4\}$ plane in contrast to the opposite projection of these groups as required in the *meso*– stereoisomer. All the metal coordinating sp^3 and sp^2 nitrogen atoms of the macrocycles are almost coplanar and the Ni^{2+} cation is located at 0.051(4) Å from the mean macrocycle plane. The mean Ni–N bond lengths for the square planar coordination geometry around Ni^{2+} are observed as Ni–N(amine) = 1.925(7) and Ni–N(imine) = 1.896(7) Å respectively and thus, Ni–N(amine) > Ni–N(imine) in accordance with expectation and earlier literature reports (see Table 3). Similarly, the knowledge of longer C(5)–N(3) 1.512(11) and C(10)–N(1) 1.492(11) Å lengths with respect to the shorter C(3)–N(2) 1.285(11) and C(8)–N(4) 1.284(11) Å distances and corresponding angles C(9)–C(8)–C(14) 114.6(7)º, C(4)–C(3)–C(11) 114.5(7)º unequivocally determine the position of the C=N bonds within the macrocycle (C(3)=N(2), C(8)=N(4)) (see Table 3 for selected lengths). Similarly, the bite angles of the six membered rings N(1)–Ni(1)–N(4) 92.9(3)º, N(2)–Ni(1)–N(3) 92.4(3)º and those of the five membered rings N(1)–Ni(1)–N(2) 87.2(3)º, N(3)–Ni(1)–N(4) 87.5(3)º clearly illustrate almost perfect square planar geometry around Ni(1). There is an unusual short contact between the Ni^{2+} center and one terminal oxygen atom of the POM anion Ni(1)···O(19) 2.762(6) Å in the crystal structure of compound **4** (Figure 10a) indicating a strong interaction between the nickel coordination complex cation and POM cluster anion. The square planar geometry around nickel ion (instead of square pyramidal or octahedral) in compound **4** can be justified by the presence of two axial methyl groups C(12) and C(16) of the macrocycle (that are projected on same side) and the close proximity between the macrocycle and the POM anion (unusual short contact of Ni(1)···O(19) 2.762 (6) Å) on the other side / face of the macrocycle. In other words, if two axial methyl groups C(12) and C(16) block the fifth coordination, then the POM anion prevents the sixth coordination on the nickel ion. In addition to the strong

Ni(1)···O(19) interaction between the Ni^{II}–L cation and the POM anion, intermolecular non-covalent interactions (C–H···O) between the macrocycle and the POM anions are also observed in the crystal lattice of compound **4** (see Table 4). These interactions keep the macrocyclic cation in an environment surrounded by four POM anions (including one glide and two inversion symmetry related POMs). Two views for packing of the molecules in the crystal of compound **4** are shown in Figures 10c and 10d respectively.

Table 5. Selected bond lengths for the crystal structure of compounds 5–7.

Bond	**5**	**6P**	**6M**	**7**
C1–C2	1.522(5)	1.499(14)	1.512(13)	1.526(10)
C3–C4	1.504(5)	1.492(14)	1.490(12)	1.481(11)
C4–C5	1.532(5)	1.521(14)	1.522(13)	1.546(12)
C6–C7	1.518(5)	1.448(15)	1.504(14)	1.502(10)
C8–C9	1.516(5)	1.503(16)	1.503(15)	1.497(10)
C9–C10	1.534(5)	1.534(16)	1.536(14)	1.524(10)
C3–C11	1.512(4)	1.495(14)	1.486(12)	1.507(10)
C5–C12(ax)	1.525(5)	1.530(14)	1.552(13)	1.525(11)
C5–C13(eq)	1.542(4)	1.546(13)	1.516(13)	1.553(10)
C8–C14	1.499(5)	1.499(16)	1.525(13)	1.498(10)
C10–C15(eq)	1.528(5)	1.524(15)	1.517(13)	1.547(10)
C10–C16(ax)	1.536(5)	1.534(15)	1.515(14)	1.541(10)
C1–N1amine	1.481(4)	1.477(14)	1.481(12)	1.462(9)
C10–N1(amine)	1.505(4)	1.493(13)	1.494(12)	1.498(9)
C2–N2(imine)	1.472(4)	1.468(12)	1.455(11)	1.474(9)
C3–N2(imine)	1.279(4)	1.272(13)	1.265(11)	1.273(8)
C5–N3(amine)	1.507(4)	1.477(14)	1.502(12)	1.476(9)
C6–N3(amine)	1.485(4)	1.539(13)	1.487(11)	1.485(9)
C7–N4(imine)	1.472(4)	1.515(13)	1.485(12)	1.483(9)
C8–N4(imine)	1.276(4)	1.256(13)	1.260(12)	1.264(8)
M–N1(amine)	2.008(3)	2.023(8)	2.015(7)	2.150(6)
M–N3(amine)	2.016(3)	2.015(8)	2.013(7)	2.151(6)
M–N2(imine)	1.971(3)	1.977(8)	1.976(7)	2.086(6)
M–N4(imine)	1.973(3)	1.964(9)	1.972(7)	2.070(6)

Compound [Cu(L)(MeCN)][Mo_6O_{19}] (5). The crystal structures described hitherto (compounds **1**–**4**) in this chapter, contain a chiral *rac*–(M–L) complex as one of the components, but interference of the inversion symmetry in all the crystals lead to the transmission of opposite chirality or helicity to the adjoining partners thereby nullifying

the overall chirality. The individual crystals fall under the category of racemic crystals as stated in the introduction section. There is an alteration in the situation for the compounds [Cu(L)(MeCN)][Mo_6O_{19}] (**5**) and [Cu(L)(MeCN)][W_6O_{19}] (**6**) which exhibit spontaneous resolution during crystallization. Both these crystals are isostructural as indicated by their unit cell parameters (see experimental section) and crystallize in $P2_12_12_1$ space group.

The structural elucidation of compound **5** through single crystal X-ray diffraction technique reveals formulation of the concerned solid as [Cu(L)(MeCN)][Mo_6O_{19}] in which an acetonitrile solvent molecule is coordinated to the copper center. The cationic entity of compound **5** is a Cu^{II}–L complex with an axially bound MeCN solvent molecule, that is, square pyramidal coordination environment around the metal center. Unfortunately, the crystals of compound **5** were found to be weakly diffracting which constrained us to separate the two enantiomorphs of the relevant compound from its mixture (data collection through randomly mounted crystals). Also, the optical resolution of the pertinent crystals was affected by twining, as revealed by the distribution of Flack parameters in the range 0.1–0.4 in a few tested crystals. However, replacement of the $[Mo_6O_{19}]^{2-}$ cluster anion (compound **5**) by the $[W_6O_{19}]^{2-}$ anion (compound **6**) improved the scenario. The crystals of compound **6** were found to be strongly diffracting and we finally succeeded in separating the two enantiomorphs of the relevant compound and structurally characterize them. Although, similar chiral behavior was expected for both the compounds **5** and **6**, the probable reason behind the poorer spontaneous resolution of compound **5** could not be comprehended at this level. Hence, compound **6,** for which both enantiomers could be fully resolved, was extensively studied in this work and the relevant crystallographic analysis is presented below.

Compound [Cu(L)(MeCN)][W_6O_{19}] (6). Analogous to compound **5**, this solid is formulated as [Cu(L)(MeCN)][W_6O_{19}] in which an acetonitrile solvent molecule is coordinated to the copper center, based on single crystal X-ray diffraction data. The ion-pair complex **6** crystallizes in a chiral space group $P2_12_12_1$ belonging to the orthorhombic crystal system. Most interestingly, we were able to structurally characterize both the enantiomers of compound **6**, *P*– or right-handed (**6P**) and *M*– or left-handed (**6M**) helical structural motifs (see Figure 11) from the bulk crystalline sample obtained from the same crystallization batch. The near-zero absolute structure parameter (Flack parameter) of the

Table 6. Geometrical parameters for the hydrogen bonding interactions in the crystal structures of compounds 6–8.

	d(D–H)	*d*(H···A)	*d*(D···A)	<(D–H···A)	Symmetry
Compound–6					
C2–H2B···O4#1	0.97	2.39	3.195(13)	139.9	1.5–x, 1–y, 0.5+z
C4–H4A···O10	0.97	2.62	3.502(12)	151.5	Intramolecular
C7–H7B···O15#2	0.97	2.51	3.411(14)	153.7	–1+x, y, z
C7–H7A···O9	0.97	2.53	3.370(13)	144.3	Intramolecular
C9–H9A···O18#1	0.97	2.58	3.424(13)	145.8	1.5–x, 1–y, 0.5+z
C13−H13A···O7	0.96	2.57	3.428(13)	149.4	Intramolecular
Compound–7					
C9–H9B···O1#1	0.97	2.67	3.569(9)	154.5	–x+2, –y+1, –z+1
C16–H16B···O5#2	0.96	2.69	3.613(9)	162.2	x, –y+0.5, z+0.5
N3–H3···Cl1#3	0.83(5)	2.61(5)	3.397(7)	157(4)	–x+1, –y+1, –z+1
Compound–8					
C1–H1A···O5#1	0.97	2.68	3.601(15)	159.4	–x+0.5, y+0.5, –z+0.5
C2–H2A···O3#2	0.97	2.50	3.315(14)	141.4	–x+1, y, –z+0.5
N1–H1N···O7#3	0.88(11)	2.44(11)	3.301(13)	169(10)	x, –y, z+0.5
N2–H2N···O4	0.79(11)	2.46(12)	3.175(14)	151(11)	Intramolecular

relevant crystals (–0.002(13) for **6P** and –0.016(12) for **6M**) indicates proper evaluation of the absolute structures in the studied crystals.[46] The Cu^{II} center in the crystal structure of compound **6** is described by a square pyramidal coordination geometry in which the acetonitrile solvent molecule occupies the axial coordination (Cu(1)–N(5) = 2.407 Å) and the basal coordination of the metal center are satisfied by the four nitrogen atoms of the macrocycle. The Cu(1)–N(amine) and the Cu(1)–N(imine) bond lengths are observed to be in the range 2.014–2.023 and 1.965–1.977 Å respectively which are in accord with the general trend of longer metal–N(amine) coordination lengths than the shorter metal–N(imine) bond distances in the related complexes of L.[42] The copper center is almost coplanar with the mean plane, defined by the four ligating N sites of L and the N(amine)–Cu(1)–N(imine) bite angles of the five and six membered chelated rings are observed to be in the range 90±4°. Although the H(1) and H(3) atoms of the stereogenic amine centers could not be detected crystallographically, the diastereomer of the Cu(L) complex in the pertinent solids is unambiguously set as *rac*– on the basis of projection of the two

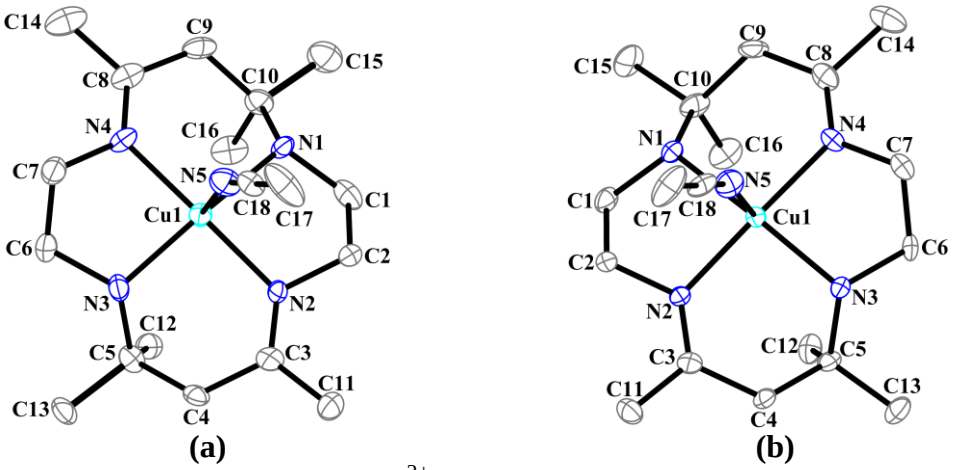

Figure 11. Crystal structures of the Cu^{2+}(L) cationic fragment in (a) **6P** (*SS*–) and (b) **6M** (*RR*–). The displacement ellipsoids are drawn at 30% thermal distribution level and the hydrogen atoms have been excluded for clarity.

axial methyl groups C(12) and C(16) on the same face of the macrocycle. For a *meso*–isomer, the two concerned groups project to the opposite faces of L. The various W–O bond lengths of the relevant POM cluster anion in the crystal structure of compound **6** are observed as follows: W–O(t) 1.688–1.722, W–O(b) 1.903–1.949 and W–O(c) 2.315–2.348 Å. The selected bond distances for the **6P** and **6M** enantiomers are almost identical and are tabularized in Table 5.

The fascinating feature of compound **6** is the supramolecular interaction of its cationic and anionic counterparts through screw symmetry and the phenomenon of spontaneous resolution during crystallization. The supramolecular helical chains in the lattices of **6P** and **6M** are formed by the C–H···O hydrogen bonding interactions. The macrocyclic fragment in the crystal of compound **6** acts as a weak hydrogen bond donor (C–H) and the POM cluster anion serves the role of hydrogen bond acceptor through its peripheral oxygen atoms. The packing of homochiral helical motifs in the lattice of **6P** and **6M** are shown in Figure 12 which clearly shows the single strand right– and left–handed helical chains when viewed down the crystallographic *b* axis. The Cu–L complex is associated with two screw related POM cluster anions through C–H···O supramolecular interactions parallel to the crystallographic *c*-axis. The C2···O4 ($d_{C\cdots O}$ = 3.195(13) Å), C4···O10 ($d_{C\cdots O}$ = 3.502(12) Å), C7···O9 ($d_{C\cdots O}$ = 3.370(13) Å), C9···O18 ($d_{C\cdots O}$ = 3.424(13) Å) and C13···O7 ($d_{C\cdots O}$ = 3.428(13) Å) weak non-covalent interactions between the Cu–L complex and the screw related POM cluster anions along with their

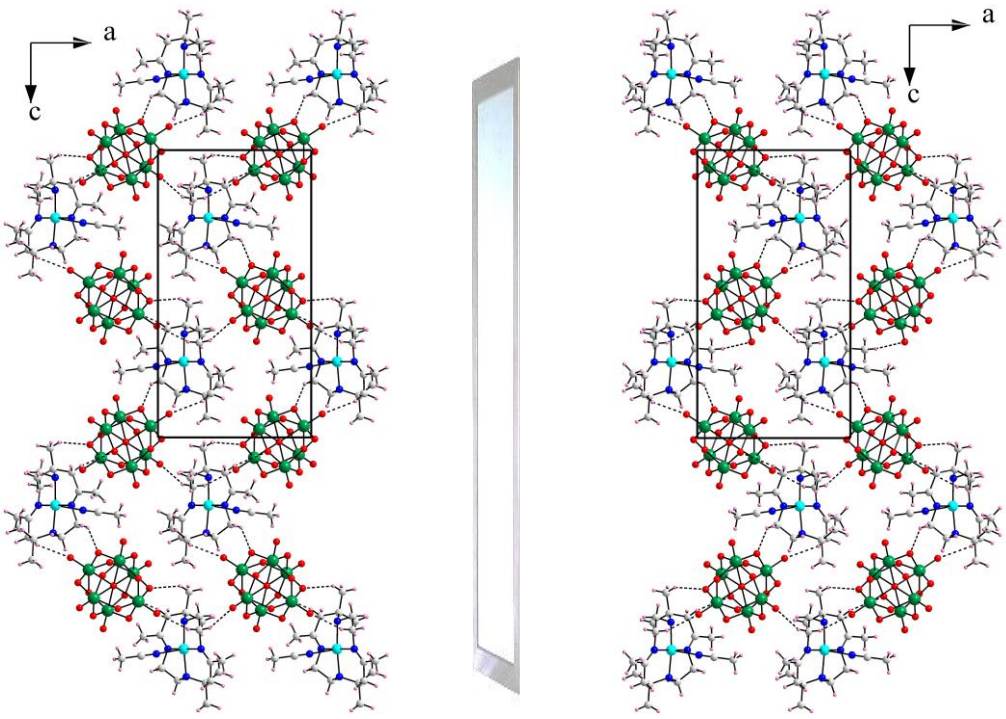

Figure 12. Hydrogen bonded homochiral helical chains in the crystal structures of **6P** (left) and **6M** (right) viewed down the crystallographic *b*–axis showing the *intra*– and *inter*–strand connections.

symmetry equivalent partners form infinite homochiral helical chains propagating parallel to the crystallographic *c*-axis (see Figure 12). Each helical pitch comprises four Cu–L complexes and three POM cluster anions, the pitch lengths being 20.737 and 20.732 Å for **6P** and **6M** respectively which are nearly identical to the length of the *c* unit cell vectors (20.7375(17) for **6P** and 20.7320(18) for **6M**). Each helical chain is further connected to the adjacent chain through C–H···O interactions in a zipper-like fashion which, in turn, transmits the same chirality to the adjoining helical chain. Each Cu^{II}–L macrocyclic unit, therefore, acts as the bridge between two homochiral helical chains and thus assists to form an infinite 2D framework (see Figure 12).

Compound $[Zn(L)(Cl)]_2[W_6O_{19}]$ (7). A recent CSD search shows that only one structurally characterized Zn^{II}–L complex has been reported so far.[45j] The crystal structure of the complex *meso–trans*–$[Zn(L)](ClO_4)_2$ reported by Y. –M. Yang (CSD depository code TAQRIN, space group $P2_1/c$) is a square planar Zn^{II}–L complex. Crystallographic investigation on the compound $[Zn(L)(Cl)]_2[W_6O_{19}]$ (**7**) reveals remarkable structural divergence from its precursor perchlorate salt $[Zn(L)(Cl)(H_2O)]$

(ClO_4) (**7a**) in terms of molecular formulae of the M–L coordination complexes. The complex precursor for compound **7** i.e. $[Zn(L)(Cl)(H_2O)](ClO_4)$ (**7a**), reported by Endicott and co-workers,[12a] possess one axially coordinated water molecule to Zn^{II} metal

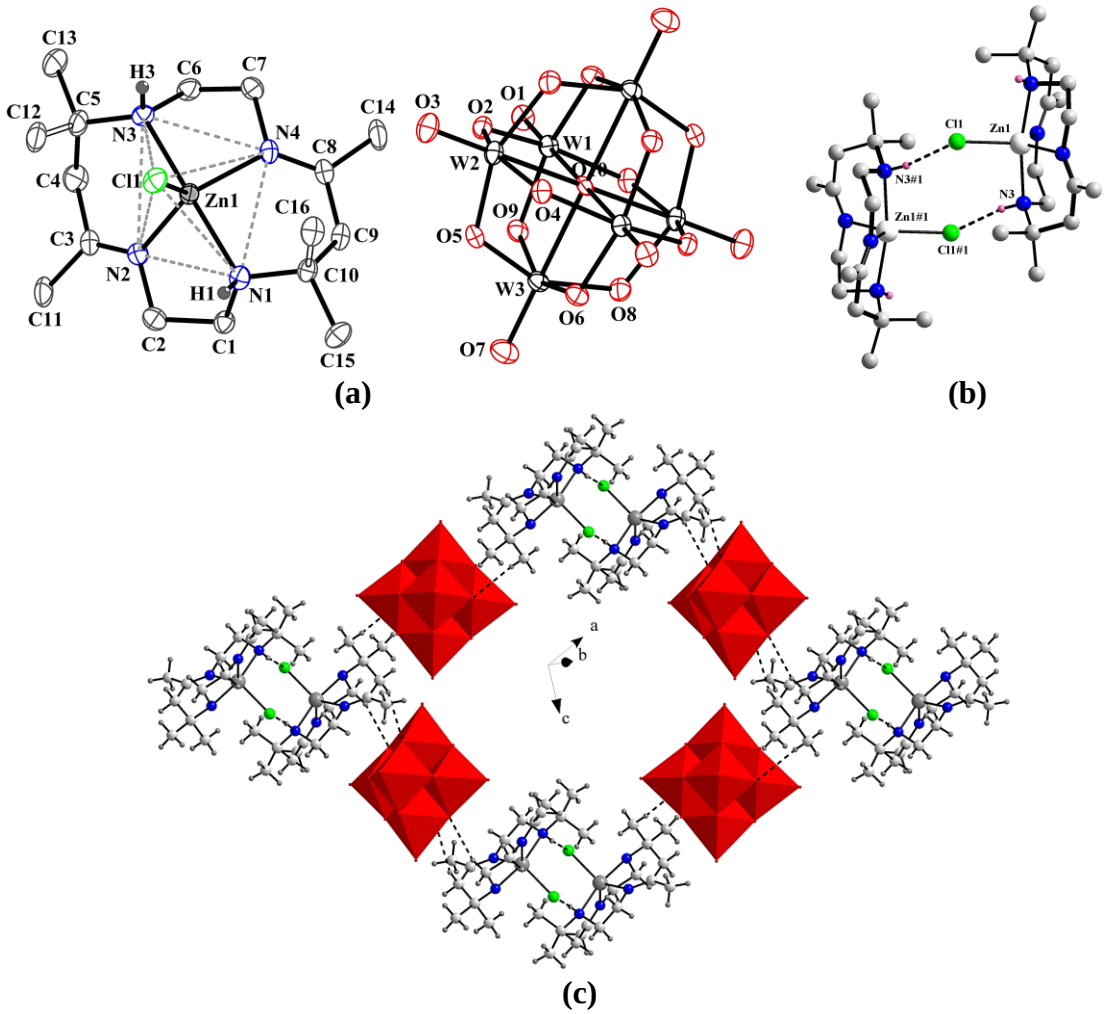

Figure 13. (a) Crystal structure of the compound $[Zn(L)(Cl)]_2[W_6O_{19}]$ (**7**). The thermal ellipsoids are drawn in 20% distribution levels. (b) Formation of supramolecular dimer in the crystal structure of compound **7** through hydrogen bonding interactions. Atoms labelled with additional symmetry operations are in accord with that mentioned in Table 6. (c) Arrangement of the structural motifs through intermolecular non-covalent interactions.

center which is absent in the crystal structure of the POM based compound $[Zn(L)(Cl)]_2[W_6O_{19}]$ (**7**). It has already been mentioned in the spectroscopic discussion section (*vide supra*) that the O–H stretching absorption, due to the metal bound water molecule found in **7a**, is not observed in the IR spectrum of compound **7**. Thus, the

crystallographic structure determination of compound **7** is in full concurrence with the IR spectrum of compound **7**. Compound **7** was isolated as colorless blocks and the relevant crystal structure is characterized by an assembly of the molecules obeying $P2_1/c$ space symmetry. The concerned asymmetric unit comprises one $[Zn(L)(Cl)]^+$ cation and half of the $[W_6O_{19}]^{2-}$ POM cluster anion (Z' = ½). The crystal structure of compound **7** is shown in Figure 13a. The metal center is found to reside in a distorted square pyramidal geometry (octahedral in its perchlorate salt) where, the equatorial coordination to the Zn^{II} metal center is defined by four nitrogen atoms of the macrocycle L. Neither the metal center nor the nitrogen atoms of the macrocycle are coplanar in the corresponding crystal structure and they are found to deviate significantly from the mean {N4} plane of the macrocycle. The H(1) and H(3) NH(*sec*) protons could be located in the crystal of compound **7** and they are found to project on the same face of the macrocycle along with the axial methyl groups C(12) and C(16) thereby indicating that the stereoisomer of the macrocycle present in the crystal structure of compound **7** is *rac*– (Figure 13a). In the macrocyclic cationic complex, the metal–ligand mean lengths are observed as Zn–N(amine) 2.150(6) Å, Zn–N(imine) 2.078(6) Å and Zn–Cl 2.302(4) Å which represent an axially elongated tetragonal coordination environment around Zn(1) in the relevant crystal structure (see Table 5 for various bond lengths). The macrocycle is found to be folded along N(1)–N(3) and the dihedral angle between N(1)–N(2)–N(3) and N(1)–N(4)–N(3) is measured as 32.79 (0.24)º. The N(3)–H(3)···Cl(1) supramolecular interactions between the inversion symmetry related macrocycle cationic complexes result in the formation of a supramolecular dimer (see Figure 13b), that remains as a counter cation $[Zn(L)(Cl)]_2^{2+}$ associated with one POM cluster anion $[W_6O_{19}]^{2-}$. The H(1) atom is found to be inert towards any supramolecular interaction and so, the two NH(*sec*) protons in the crystalline solid **7** have different local environments. This is a further corroboration between IR spectroscopy and the crystal structure determination of compound **7** (appearance of two different energy N–H stretching bands). The inversion symmetry site of the molecule lies at the centroid of the eight membered chair–like cyclooctane ring formed by Cl(1), Zn(1), N(3), H(3) and their symmetry equivalent atoms through N–H···Cl interactions. The resulting dimeric cations are further associated with the POM anions via C–H···O interactions as shown in Figure 13c.

Compound [Cu(cyclen)(MeCN)][W_6O_{19}] (8). It has already been depicted that the Cu–L systems i.e. compounds **5** and **6** exhibit spontaneous resolution during crystallization. Crystal structures of these two compounds differ from compounds **1**–**4** and compound **7** in the sense that, imposition of the centric twining in the crystals of the latter group leads to the formation of racemic condensates in which each helical structural motifs bear opposite chirality. However, in case of the compounds **5** and **6**, each of the helices transmits its chirality to the adjoining strands maintaining the same chirality. A 50:50 deposition of the enantiomers results in the formation of a conglomerate bulk material from which individual enantiomers can be manually separated. Initially it was believed that, coordination of the acetonitrile solvent molecule to the copper center was responsible for the occurrence of spontaneous resolution during crystallization of compounds **5** and **6** as no solvent molecule coordination could be traced in the crystal structures of the compounds **1**–**4** and compound **7**. However, whether the macrocycle cationic system or the POM cluster anion played the major role for the occurrence of spontaneous resolution in compounds **5** and **6** remained uncertain. To better unveil the matter, a copper complex of another tetra-aza macrocycle, cylen, was synthesized *in situ*, and was crystallized as its hexatungstate salt (compound **8**).

Single crystal X-ray structural determination of compound [Cu(cyclen)(CH_3CN)] [W_6O_{19}] (**8**) is elucidated by the assembly of molecules obeying *C2/c* space symmetry (unlike compounds **5** and **6**, having $P2_12_12_1$ space symmetry) with half of the $[Cu(cyclen)(MeCN)]^{2+}$ cation and half of the $[W_6O_{19}]^{2-}$ isopolyanion in its asymmetric unit (Z' = ½, see Figure 14a). The coordination geometry around copper in the crystal structure of compound **8** is square pyramidal in which the four nitrogen atoms of cyclen provide the basal coordination and a solvent acetonitrile molecule defines the axial coordination of the square pyramid. The POM anion is positioned at the center of the crystallographic [100] axis. O(10) i.e. the central oxygen atom of the hexatungstate anion is located at the crystallographic inversion center (0.5, 0.0, 0.0) with half occupancy in the asymmetric unit. Cu(1)–N(3)–C(5)–C(6) axis of the square pyramid projects parallel to the two–fold rotational axis of a monoclinic crystal system, as a result of which, these atoms are found to have half occupancies in the asymmetric unit of the concerned crystal structure. The cavity size of the tetra–aza crown ether cyclen is not large enough for com-

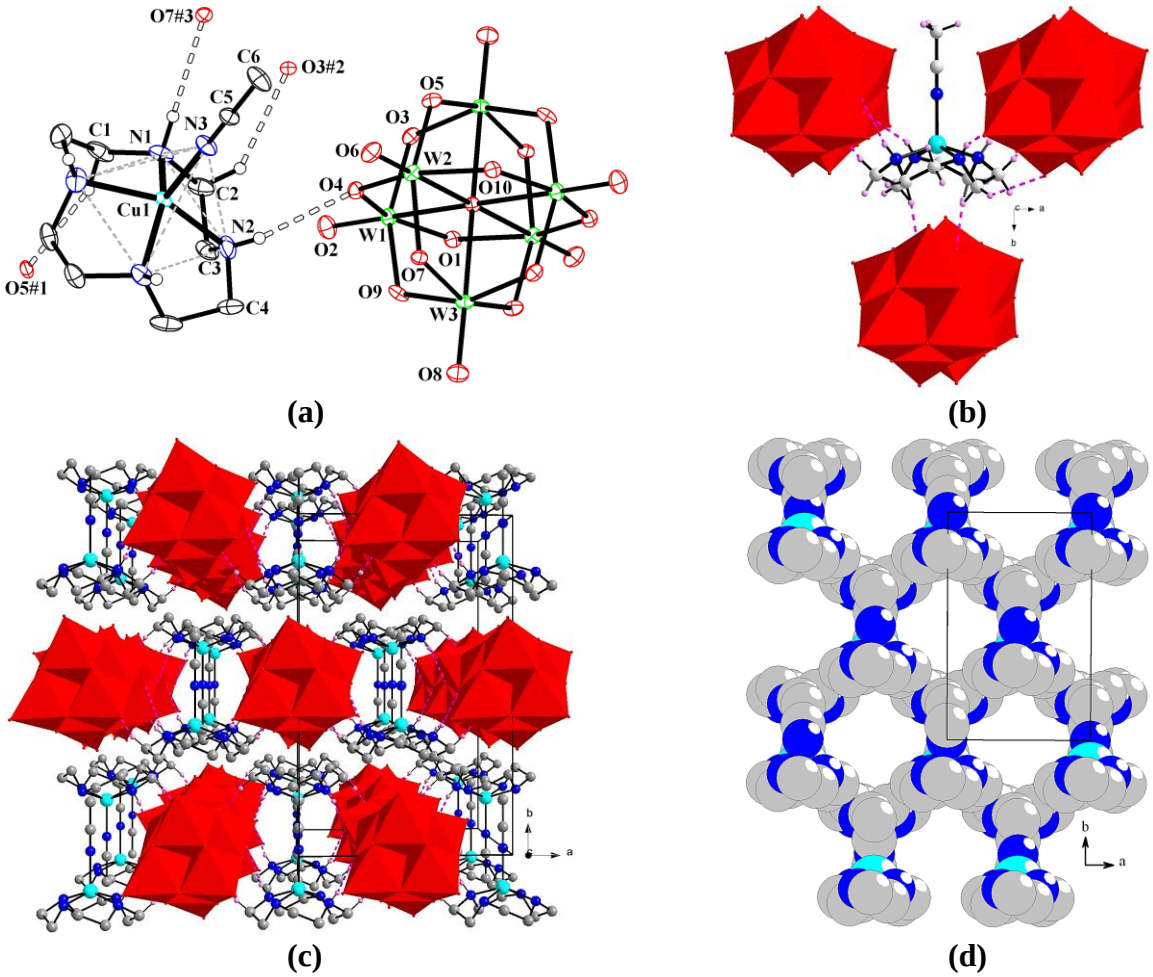

Figure 14. (a) ORTEP drawing of [Cu(cyclen)(MeCN)][W_6O_{19}] (**8**) in 20% probability level with the possible hydrogen bonding interactions in the asymmetric unit. Only symmetry independent atoms are labelled and the hydrogen atoms have been omitted for clarity. (b) Hydrogen bonding environment around the Cu–cyclen coordination complex. (c) Perspective view for packing of the molecules in the crystal. Note the channel–like arrangement of the Cu–cyclen complexes down [001] axis. (d) space–filling model for the arrangement of the complex cations in the crystal of compound **8**.

-plete encapsulation of Cu^{II} due to large size of the cation. Thus, in the crystal structure of compound **8**, the Cu^{II} ion is located 0.564(8) Å away from the basal {N4} plane of the macrocycle (Figure 14b) and the macrocycle is found to be bent outwards from Cu^{II} ion for facile Cu–N coordination. In the relevant crystal structure, the bond lengths of cyclen are observed as an average C–C 1.512(20) Å and average C–N 1.431–1.507(19) Å. The average Cu–N bond length for the $[Cu(cyclen)(MeCN)]^{2+}$ complex cation is found to be 2.019(12) Å for cyclen coordination whereas, the apical MeCN molecule is located at a distance of 2.071(14) Å from Cu(1). Extensive C–H···O and N–H···O supramolecular

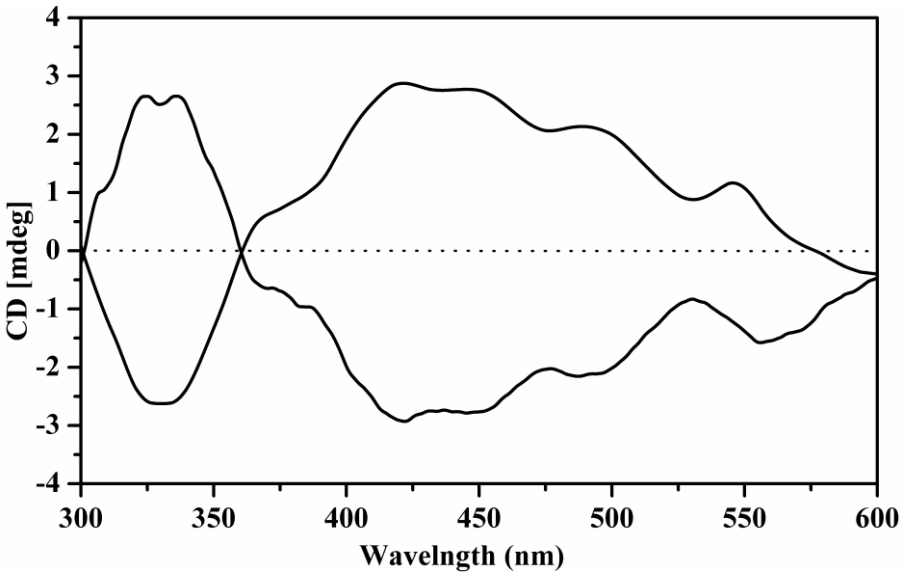

Figure 15. CD spectra of the two enantiomorphs of compound **6** (**6P** and **6M**). The spectra were recorded by grinding the enantiopure crystals with KBr and finally pressed to make a disc.

hydrogen bonding interactions between $[Cu(cyclen)(MeCN)]^{2+}$ counter cation and the POM anion is observed in the crystal lattice of compound **8** (see Figure 14b). Along with the coulombic interactions between the cationic and anionic counterparts of compound **8**, the supramolecular C–H···O and N–H···O hydrogen bonding interactions between them assemble six POM cluster anions around the cationic complex (see Figure 14b and Table 6 for the geometrical parameters for the relevant supramolecular interactions). The Cu–cyclen complexes pack in such a way that a channel–like arrangement is formed in the crystal lattice of **8** (Figure 14c, 14d) in which the POM cluster anions fill up the voids through coulombic and H–bonding interactions.

● 2.2.6. Circular Dichroism spectroscopy

The occurrence of spontaneous resolution in compound **6** was further scrutinized through the Circular Dichroism (CD) spectroscopy. The spectra for the ground crystals of **6P** and **6M** were obtained by the diffused reflectance technique over KBr matrix and are shown in Figure 15. As can be seen from the relevant picture, the Cotton effects at ~330 and ~450 nm bear an almost mirror image relationship for the two enantiomorphs, the intensity of the relevant bands, however, being very weak. Unfortunately, we were unable to separate the two enantiomorphs of compound **5** thereby restraining us to measure the CD spectra of the individual enantiomers of the pertinent compound.

Table 7. Summary of the electrochemical data (*vs* Ag/AgCl, solvent = DMSO, scan rate = 100 mV s^{-1}, electrolyte = tetrabutylammonium perchlorate.

Compound	$E_{1/2}$ /V	ΔE_p /V	Assignment
$[Bu_4N]_2[Mo_6O_{19}]$	–0.38[a]	0.46	$[Mo_6O_{19}]^{2-}$ reduction
	–1.05[a]	0.37	$[Mo_6O_{19}]^{2-}$ reduction
$[Bu_4N]_2[W_6O_{19}]$	–0.70[a]	0.14	$[W_6O_{19}]^{2-}$ reduction
$[Co^{III}(L)(Cl)_2](ClO_4)$ (**1a**)	–0.52[b]	—	$Co^{III} \rightarrow Co^{II}$
	–1.40[b]	—	$Co^{II} \rightarrow Co^{I}$
$[Co^{III}(L)(Cl)_2]_2[Mo_6O_{19}]$ (**1**)	–0.30[c]	0.08	$[Mo_6O_{19}]^{2-}$ reduction
	–1.33[b]	—	$Co^{III} \rightarrow Co^{II}$
	–1.70[b]	—	$[Mo_6O_{19}]^{2-}$ reduction
	–1.85[b]	—	$Co^{II} \rightarrow Co^{I}$
$[Ni^{II}(L)](ClO_4)_2$ (**4a**)	–0.90[a]	0.3	$Ni^{II} \rightarrow Ni^{I}$
	–1.70[b] (w)	—	—
$[Ni^{II}(L)][W_6O_{19}]$ (**4**)	–0.71[c]	0.07	$[W_6O_{19}]^{2-}$ reduction
	–1.20[b]	—	$Ni^{II} \rightarrow Ni^{I}$
	–1.73[b] (w)	—	—
$[Zn(L)(Cl)(H_2O)](ClO_4)$ (**7a**)	–1.63[b] (vw)	—	—
$[Zn^{II}(L)(Cl)]_2[W_6O_{19}]$ (**7**)	–0.70[c]	0.06	$[W_6O_{19}]^{2-}$ reduction
	–1.68[c] (vw)	0.08	—

[a] quasi–reversible, [b] irreversible, [c] reversible, w = weak, vw = very weak

● 2.2.7. Electrochemistry

To investigate any influence of the POM anion on the redox behavior of the M–L complexes, electrochemical studies on the compounds, **1** (Co–L complex), **4** (Ni–L complex) and **7** (Zn–L complex) were carried out in DMSO solution. For the purpose of ready comparison and peak assignment, cyclic voltammetry was also executed on all the starting precursors *viz.* $[Co^{III}(L)(Cl)_2](ClO_4)$ (**1a**), $[Ni^{II}(L)](ClO_4)_2$ (**4a**), $[Zn(L)(Cl)(H_2O)](ClO_4)$ (**7a**), $[Bu_4N]_2[Mo_6O_{19}]$ and $[Bu_4N]_2[W_6O_{19}]$. The relevant experiments were carried out using the three electrode assembly consisting of the Pt electrode as the working electrode, Ag/AgCl as the reference electrode (unless mentioned elsewhere) and a Pt gauge as the auxiliary (counter) electrode. Ultra high pure nitrogen was purged for ~20–30 minutes into the electrochemical vessel prior to each measurement in order to eliminate any perturbation from dissolved oxygen. It was also verified that no electro-active species was present in the blank solvent in the potential range of –2.0 V to 2.0 V *vs* Ag/AgCl and all the experiments were repeated twice. A summary of the electrochemical

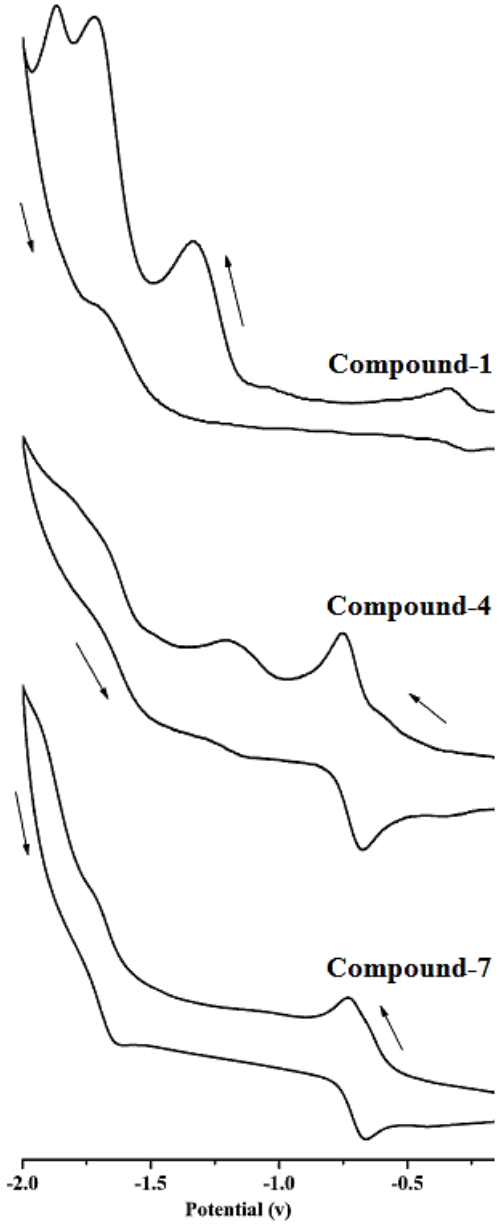

Figure 16. Cyclic voltammograms of the compounds **1**, **4** and **7** in DMSO solution at 25 ºC (concentration of the samples are 10^{-3} M) with a scan rate of 100mVs^{-1} using tetrabutylammonium perchlorate as the supporting electrolyte.

data is composed in Table 7 and cyclic voltammograms of the title compounds are shown in Figure 16. The cyclic voltammetric data of the perchlorate salts of the macrocyclic precursors (**1a**, **4a** and **7a**) are reported in literature, which clearly demonstrated the reversible nature of the concerned redox couples (Co, Ni, Zn) in acetonitrile.[47] However, due to poorer solubility of the POM based M–L compounds in common organic solvents (e.g. dichloromethane, acetonitrile etc.); we were constrained to perform the

electrochemical experiments in DMSO only. Although, an oxidative response corresponding to the $[Ni^{III}(L)]^{3+}/ [Ni^{II}(L)]^{2+}$ was observed for **4a** in other solvents (e.g., MeCN),[47] no such response has been observed in the cyclic voltammogram of both compounds **4a** and **4** in DMSO under the present experimental condition.

The cyclic voltammogram of $[Bu_4N]_2[Mo_6O_{19}]$ in DMSO is characterized by two reductive signals at $E_{1/2}$ = –0.38 and –1.05 V due to reduction of the molybdenum cluster. This cluster shows only one reductive response in MeCN and two in DCM.[48a-c] However, the $[Bu_4N]_2[W_6O_{19}]$ cluster exhibits only one reductive signal at $E_{1/2}$ = –0.70 V in DMSO in the potential range of –2.0 to +2.0 V *vs* Ag/AgCl. The reductive response of the hexatungstate cluster ($E_{1/2}$ = –0.70 V) occurs at a more negative potential compared to the first reductive signal of the hexamolybdate cluster ($E_{1/2}$ = –0.38 V) because of the lesser tendency of the former to get reduced (see Table 7).

Electrochemical analysis on $[Co^{III}(L)(Cl)_2](ClO_4)$ (**1a**) reveals the presence of two irreversible reductive signals at $E_{1/2}$ = –0.52 V and –1.40 V due to the redox couples, $[Co^{III}(L)(Cl)_2]^{1+}/[Co^{II}(L)(Cl)_2]^0$ and $[Co^{II}(L)(Cl)_2]^0/[Co^{I}(L)(Cl)_2]^{-1}$ respectively (in DMSO, present case). In acetonitrile, the concerned peaks were reported to appear at $E_{1/2}$ = –0.18 V and –1.51 V (*vs* SCE) respectively.[47] Therefore, four electrochemical responses would be expected in the cyclic voltammogram of the POM based ion-pair complex $[Co^{III}(L)(Cl)_2]_2[Mo_6O_{19}]$ (**1**): two for the molybdenum cluster reduction and two for the metal–macrocycle coordination system. The relevant cyclic voltamogram of compound **1**, indeed, features four reductive signals: one reversible reductive response at $E_{1/2}$ = –0.30 V and one irreversible reductive peak at $E_{1/2}$ = –1.70 V due to reduction of the $[Mo_6O_{19}]^{2-}$ cluster and the other two irreversible responses at $E_{1/2}$ = –1.33 V and –1.85 V are assigned to the $[Co^{III}(L)(Cl)_2]^{1+}/[Co^{II}(L)(Cl)_2]^0$ and the $[Co^{II}(L)(Cl)_2]^0/ [Co^{I}(L)(Cl)_2]^{-1}$ redox couples respectively (Table 7). The compound $[Ni^{II}(L)](ClO_4)_2$ (**4a**) shows a reductive response at $E_{1/2}$ = –0.90 V (DMSO) due to $[Ni^{II}(L)]^{2+}/ [Ni^{I}(L)]^{1+}$ redox couple while a weak reductive response near $E_{1/2}$ = –1.70 V might be due to the $[Ni^{I}(L)]^{+}/ [Ni^{0}(L)]^{0}$ redox system. Thus, in the cyclic voltammogram of the compound $[Ni^{II}(L)] [W_6O_{19}]\cdot$DMSO·DCM (**4**), the reversible reductive peak at $E_{1/2}$ = –0.71 V *vs* Ag/AgCl with a separation of 0.07 V between the cathodic and anodic peaks (see Figure 16) should correspond to the reduction of the $[W_6O_{19}]^{2-}$ cluster anion (in the range of –2.0 V

to +2.0 V). The other two irreversible reductive signals at $E_{1/2}$ = –1.20 V and –1.73 V (weak) in the cyclic voltammogram of compound **4** should represent the $[Ni^{II}(L)]^{2+}$/ $[Ni^{I}(L)]^{1+}$ and $[Ni^{I}(L)]^{+}$ / $[Ni^{0}(L)]^{0}$ redox couples respectively.

The zinc precursor $[Zn(L)(Cl)(H_2O)](ClO_4)$ (**7a**) shows a very weak reductive response at $E_{1/2}$ = –1.63 V *vs* Ag/AgCl (in DMSO) thereby revealing almost electrochemical silence of zinc. Thus, for the compound $[Zn^{II}(L)(Cl)]_2[W_6O_{19}]$ (**7**), the reversible reductive peak at $E_{1/2}$ = –0.70 V (*vs* Ag/AgCl) with a separation of 0.06 V between the cathodic and anodic peaks (see Figure 16), can be assigned to the reduction of the $[W_6O_{19}]^{2-}$ cluster (in the range of –2.0 V to +2.0 V). The cyclic voltammogram of the relevant compound is also characterized by a very weak reductive signal at $E_{1/2}$ = –1.68 V which might be due to reduction of zinc.

At this point it is worth mentioning that, the co-existence of POM cluster anions with the macrocyclic cationic complexes in solution, induces a significant negative shift of the redox potentials of Co^{III} and Ni^{II}. The $Co^{III}\rightarrow Co^{II}$ reduction is the most affected among the two, and a considerable shift of the concerned redox potential by 0.81 V is noticed as the counter anion of the Co–L complex is replaced from perchlorate (**1a**) to $[Mo_6O_{19}]^{2-}$ (**1**). Again, the redox potential of the Ni^{II}/Ni^{I} system is altered by 0.30 V in presence of the hexatungstate POM anion. Therefore, in the present scenario, the POM cluster anions can be said to have imposed a strong restriction on the reduction of the Co^{III}–L and Ni^{II}–L coordination systems upon their coexistence with the former in solution. However, due to insufficient proofs, a strong conclusion about the plausible reason for this phenomenon cannot be firmly established at the present moment.

● 2.3. SUMMARY AND CONCLUSION

In summary, a series of transition metal complexes of two tetra-aza macrocycles *viz.* transdiene and cyclen, were synthesized as their hexametalate salts (compounds **1**–**8**) and their spectroscopic and crystallographic analyses have been put forward in this chapter. The crystallographic investigation on **1**–**7** emphasizes the characteristic features of a typical M–L complex, such as, (a) the M–N(amine) lengths are longer than M–N(imine) bonds; (b) in all the compounds, the macrocycle is found to be in the *racemic*– form; and (c) bite angles for the five and six membered rings in all the crystal structures are in the

range 90±5º etc. The present work aims at the spontaneous resolution of M–L complexes (L = transdiene) which has not hitherto been reported. The M–L complexes exist as two diastereomers namely, *racemic*– and *meso*– out of which only the *racemic*– isomers were used in the present study for synthesizing the POM based compounds. The *racemic*– isomers essentially have a 50:50 distribution of the *RR*– and *SS*– enantiomers which are generally known to form racemic condensates. The reason behind this is the intervention of inversion symmetry which relates the adjoining *P*– and *M*– helices in the same crystal thereby nullifying the overall crystal chirality. This is in fact the case with compounds **1**–**4** (Co and Ni complexes) and compound **7** (Zn complex) in the present study which form racemic crystals. Although the relevant macrocyclic coordination complexes have well–defined chiral centers, incorporation of the symmetrical shaped / centrosymmetric POM cluster anions might be responsible for this phenomenon.

However, crystallographic analyses on the copper complexes **5** and **6** have shown astounding results. The title compounds crystallize in a chiral space group $P2_12_12_1$ and in case of the hexatungstate analogue (compound **6**), the two enantiomorphs could be manually separated indicating the occurrence of spontaneous resolution in this case. Although, the same behaviour was expected for the hexamolybdate analogue (compound **5**), the reason behind the poorer resolution (indicated by the distribution of Flack parameter) of this compound is not fully understood at this level. The observation with the compound **6** clearly manifests that the two enantiomorphs of the M–L complexes *viz*. *RR*– and *SS*– can be spontaneously resolved to form a conglomerate bulk. It is very interesting to note that the *rac*– diastereomer of $[Cu(L)](ClO_4)_2$ (**5a**) from methanol crystallizes as a racemate (space group = $P2_1/c$) in which the perchlorate counter anion acts as a mediator for transferring opposite chirality between two opposite handed Cu^{II}–L helical chains.[45i] The same result is also obtained upon crystallization of **5a** from acetonitrile. On the contrary, replacement of the perchlorate counter anion from **5a** by the hexatungstate anion (compound **6**) in acetonitrile solvent leads to the occurrence of spontaneous resolution during crystallization of compound **6**. It is believed that both POM anion participation and acetonitrile coordination to the copper center play an important role in this phenomenon. The structural elucidation of both the enantiomorphs of compound **6** (**6P** and **6M**) reveals that interstrand chirality is transmitted through

hydrogen bonding interactions throughout the network in order to bring about spontaneous resolution in the title solid. This incidence has further been confirmed on the basis of CD spectra of the compounds **6P** and **6M** which exhibit opposite Cotton effects. To the best of our knowledge, this is a unique example, where a *racemic*– transition metal coordination complex has been resolved through spontaneous resolution assisted by a POM anion.

● 2.4. EXPERIMENTAL SECTION

● 2.4.1. Materials and methods

All the reactions were performed in open reaction vessels at ambient conditions unless mentioned elsewhere. All the chemicals were procured from commercial sources and used as received. HPLC grade DMSO solvent, used for UV-visible, ESR spectroscopy and cyclic voltammetry, were received from Acros organics and used without further purification. $[Bu_4N]_2[Mo_6O_{19}]$,[41a] $[Bu_4N]_2[W_6O_{19}]$,[41b] L·2HClO$_4$,[22a,b] $[Co^{III}(L)(Cl)_2](ClO_4)$ (**1a**),[22a] $[Co^{III}(L)(NO_2)_2](ClO_4)$ (**2a**),[37] $[Co^{III}(L)(NCS)_2](SCN)$ (**3a**),[37] $[Ni^{II}(L)](ClO_4)_2$ (**4a**),[22a] $[Cu(L)](ClO_4)_2$ (**5a**),[38] and $[Zn^{II}(L)(H_2O)(Cl)](ClO_4)$ (**7a**),[22a] were prepared according to methods reported elsewhere. Fourier transformed Infrared spectra (FT-IR) of the solid samples were recorded as KBr pellets on a JASCO–5300 FT-IR spectrophotometer at room temperature. Microanalytical data of the compounds were obtained using a FLASH EA series 1112 CHNS analyzer. ESR spectra were recorded using a JEOL JES–FA200 spectrometer in powdery form at room temperature and in frozen DMSO at –140ºC. Electronic absorption studies were carried out using a Cary 100 Bio UV-visible spectrophotometer at room temperature. Diffuse reflectance spectra of the compounds were recorded by a Shimadzu UV-PC 3600 spectrophotometer (spread over barium sulfate) at 298±2 K. The CD spectra were measured with a JASCO J-810 spectropolarimeter. A CH–Instruments Model 620A electrochemical analyzer was used for cyclic voltammetric experiment.

● 2.4.2. Synthesis and characterization data

$[Co^{III}(L)(Cl)_2]_2[Mo_6O_{19}]$ (1). 0.136 g of $[Co^{III}(L)(Cl)_2](ClO_4)$ (**1a**) (0.25 mmol) and 0.17g of $[Bu_4N]_2[Mo_6O_{19}]$ (0.125 mmol) were separately dissolved in 150 ml of acetonitrile and slowly mixed in a 500 ml conical flask. Dark green crystalline blocks of

compound **1** were isolated by filtration after one day. Yield ≈ 32% (based on molybdenum).

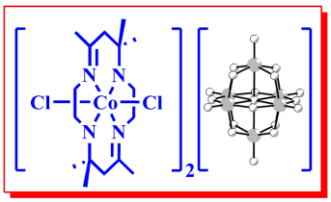

IR (KBr, cm^{-1}): 3204 (N–H), 2970 (C–H), 2924, 1651 (C=N), 1450, 1408, 1375, 1288, 1249, 1161, 1111, 1012, 952 (Mo=O), 796 (Mo–O–Mo), 603, 426.

Anal. calcd. for $C_{32}H_{64}Cl_4Co_2Mo_6N_8O_{19}$ (1700.21): C, 22.59; H, 3.76; N, 6.59. Found: C, 22.45; H, 3.71; N, 6.68.

$[Co^{III}(L)(NO_2)_2]_2[Mo_6O_{19}]$ (2). 0.250 mmol of $[Co(L)(NO_2)_2](ClO_4)$ (**2a**) and 0.125 mmol of $[Bu_4N]_2[Mo_6O_{19}]$ were dissolved separately in 50 mL of acetonitrile. The two solutions were then mixed carefully in a 250 mL Erlenmeyer flask and left undisturbed at room temperature. Yellow needles of compound **2** were isolated by filtration after few days. Yield ≈ 26% (based on molybdenum).

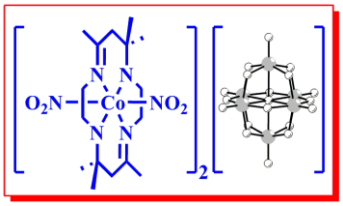

IR (KBr, cm^{-1}): 3124 (N–H), 2970 (C–H), 1647 (C=N), 1467, 1427, 1390 (NO_2), 1311 (NO_2), 1168, 1128, 1039, 952 (Mo=O), 796 (Mo–O–Mo), 430.

Anal. calcd. for $C_{32}H_{64}Co_2Mo_6N_{12}O_{27}$ (1742.45): C, 22.06; H, 3.70; N, 9.65. Found: C, 22.12; H, 3.61; N, 9.45.

$[Co^{III}(L)(NCS)_2]_2[W_6O_{19}]$ (3). This compound was synthesized following the analogous procedure as described for compound **2**. 0.125 mmol of $[Bu_4N]_2[W_6O_{19}]$ was used instead of $[Bu_4N]_2[Mo_6O_{19}]$. Burgundy blocks of compound **3** were isolated after few days. Yield ≈ 38% (based on tungsten).

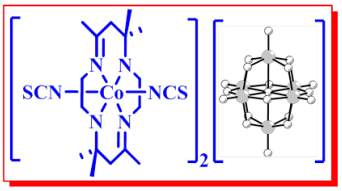

IR (KBr, cm^{-1}): 3190 (N–H), 2964 (C–H), 2092, 2065 (N=C=S), 1651 (C=N), 1469–1111 (multiple bands), 976 (W=O), 812 (W–O–W), 584, 443.

Anal. calcd. for $C_{40}H_{70}Co_2N_{14}O_{19}S_4W_6$ (2400.30): C, 20.02; H, 2.94; N, 8.17. Found: C, 19.85; H, 2.87; N, 8.32.

$[Ni^{II}(L)][W_6O_{19}]\cdot DMSO\cdot DCM$ (4). $[Ni^{II}(L)](ClO_4)_2$ (**4a**) (0.134g, 0.25 mmol) was dissolved in 10 ml of acetonitrile. A separate solution was prepared by dissolving 0.473 g of $[Bu_4N]_2[W_6O_{19}]$ (0.25 mmol) in 30 ml of acetonitrile. These two solutions were then

mixed and stirred at room temperature for 30 minutes. The yellow precipitate that appeared by this time was filtered and dissolved in a minimum volume of DMSO. Slow diffusion of dichloromethane in the DMSO solution rendered yellow blocks after two days that were isolated by filtration. Yield ≈ 20% (based on molybdenum).

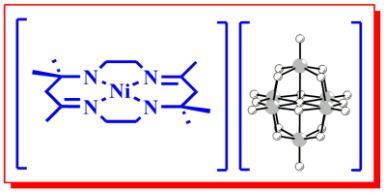

IR (KBr, cm^{-1}): 3645 (O–H), 3123 (N–H), 2970 (C–H), 2881, 1658 (C=N), 1460, 1439, 1408, 1375, 1275, 1170, 1128, 1113, 1066, 976 (W=O), 808 (W–O–W), 584, 443.

Anal. calcd. for $C_{19}H_{40}Cl_2N_4NiO_{20}SW_6$ (1909.32): C, 11.94; H, 2.10; N, 2.93. Found: C, 12.12; H, 2.10; N, 2.85.

[Cu(L)(MeCN)][Mo_6O_{19}] (5). 0.025 mmol of $[Bu_4N]_2[Mo_6O_{19}]$ and 0.025 mmol of $[Cu(L)](ClO_4)_2$ (**5a**) were separately dissolved in 15 mL of MeCN. These two solutions were allowed to slowly mix with each other in a U-shaped cell. Red blocks of compound **5** were isolated by filtration after *ca.* four weeks. Yield ≈ 40% (based on molybdenum).

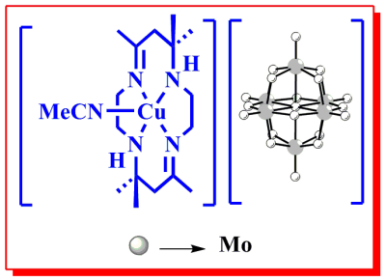

IR (KBr, cm^{-1}): 3242 (N–H), 2976 (C–H), 2934, 1666 (C=N), 1462, 1373, 1159, 960 (Mo=O), 792 (Mo–O–Mo), 584.

Anal. calcd. for $C_{18}H_{35}CuN_5O_{19}Mo_6$: C, 17.09; H, 2.79; N, 5.54. Found: C, 16.85; H, 2.86; N, 5.39.

[Cu(L)(MeCN)][W_6O_{19}] (6). 0.25 mmol of $[Bu_4N]_2[W_6O_{19}]$ and 0.25 mmol of $[Cu(L)](ClO_4)_2$ (**5a**) were separately dissolved in 100 mL of MeCN. These two solutions were slowly mixed with each other in a 500 mL conical flask. Burgundy colored crystals of compound **6** were isolated by filtration after two days. Yield ≈ 60% based on tungsten.

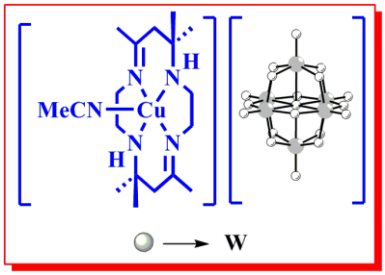

IR (KBr, cm^{-1}): 3240 (N–H), 2974 (C–H), 2934, 2878, 1666 (C=N), 1460, 1404, 1373, 1161, 979 (W=O), 810 (W–O–W), 584, 439.

Anal. calcd. for $C_{18}H_{35}CuN_5O_{19}W_6$: C, 12.06; H, 1.97; N, 3.91. Found: C, 12.18; H, 1.89; N, 3.85.

[Zn(L)(Cl)]$_2$(W_6O_{19}) (7). A 75 ml acetonitrile solution containing 0.124 g of [Zn(L)(H_2O)(Cl)](ClO_4) (**7a**) (0.25 mmol) was slowly added to a 75 ml acetonitrile solution of [Bu_4N]$_2$[W_6O_{19}] (0.237g, 0.125 mmol) and was left undisturbed for two days. Colorless crystalline blocks of compound **7** were isolated by filtration after this period. Yield ≈ 41% (based on tungsten).

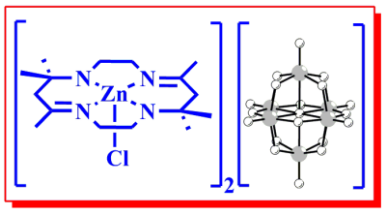

IR (KBr, cm^{-1}): 3263 (N–H), 3211 (N–H), 2964 (C–H), 2874, 1938, 1707, 1647 (C=N), 1469, 1381, 1172, 974 (W=O), 812 (W–O–W), 584, 443.

Anal. calcd. for $C_{32}H_{64}Cl_2N_8O_{19}W_6Zn_2$ (2169.65): C, 17.70; H, 2.95; N, 5.16. Found: C, 18.12; H, 2.86; N, 5.23.

[Cu(cyclen)(MeCN)][W_6O_{19}] (8). To a 10 ml (1:1 mixture of CH_3CN and CH_3OH) solution of cyclen (51.6 mg, 0.3 mmol) was added $Cu(NO_3)_2$ (69.8 mg, 0.3 mmol) and the reaction mixture was stirred overnight at room temperature. A solution of [Bu_4N]$_2$[W_6O_{19}] (567mg, 0.3 mmol) in CH_3CN was prepared separately. These two solutions were then charged onto two different arms of a U-tube set-up (see Figure 2) and allowed to mix slowly through a G4 frit that joins two arms of the U-tube. Deep blue needles of **8** were isolated after few days. Yield ≈ 27% (based on tungsten).

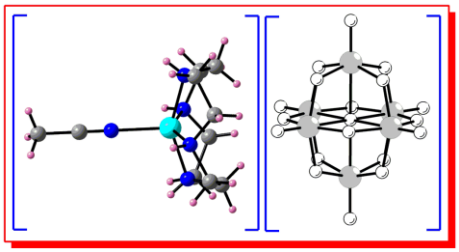

IR (KBr, cm^{-1}): 3250 (N–H), 2949 (C–H), 2883, 2310 (M–N≡C), 983.78 (W=O), 808 (W–O–W).

Anal. calcd. for $C_{10}H_{23}CuN_5O_{19}W_6$ (1683.97): C, 7.12; H, 1.37; N, 4.16. Found: C, 7.21; H, 1.31; N, 4.32.

● 2.4.3. X-ray data collection and structure determination

Single crystals of compounds **1**–**8** suitable for X-ray analysis were picked up from the mother liquors and mounted on a Bruker SMART APEX three circle diffractometer equipped with CCD area detector system. Data collection was performed under Mo–Kα (λ=0.71073 Å) graphite monochromatic X-ray beam, crystal to detector distance 60 mm, collimator 0.5 mm. The scans were recorded at 298 K with an ω scan width of 0.3º each. 2400 frames were collected each with 8 sec. exposure. Data reduction was performed by

Table 8. Crystal data and structure refinement parameters for the compounds 1–4.

	1	2	3	4
Formula	$C_{32}H_{64}Cl_4Co_2Mo_6N_8O_{19}$	$C_{32}H_{64}Co_2Mo_6N_{12}O_{27}$	$C_{40}H_{70}Co_2N_{14}O_{19}S_4W_6$	$C_{19}H_{40}Cl_2N_4NiO_{20}SW_6$
FW	1700.21	1742.45	2400.30	1909.32
T (K)	298(2)	298 (2)	298 (2)	298(2)
Crystal system	triclinic	triclinic	monoclinic	monoclinic
Space group	$P\bar{1}$	$P\bar{1}$	$P2_1/c$	$P2_1/c$
a (Å)	10.7302(8)	10.0480(17)	11.3545(12)	18.1285(13)
b (Å)	11.3642(8)	11.924(2)	16.521(2)	16.4933(12)
c (Å)	11.7568(9)	12.159(2	17.215(2)	12.8503(9)
α (°)	107.9180(10)	107.886(3)	90.00	90.00
β (°)	101.7540(10)	94.921(3)	100.282(11)	96.5540(10)
γ (°)	95.4500(10)	102.865(3)	90.00	90.00
V (Å^3)	1316.22(17)	1332.8(4)	3177.4(7)	3817.1(5)
Z	1	1	2	4
D_{calcd} (Mg/m^3)	2.145	2.171	2.505	3.322
μ (mm^{-1})	2.273	2.066	11.528	18.761
F(000)	838	862	2244	3456
GooF on F^2	1.046	1.290	0.934	1.184
R_1, wR_2 [$I>2\sigma(I)$]	0.0326, 0.0763	0.0994, 0.1680	0.0431, 0.0809	0.0337, 0.0607
R_1, wR_2 [all data]	0.0400, 0.0796	0.1225, 0.1765	0.0795, 0.0896	0.0380, 0.0621
Largest diff. peak, hole (e.Å^{-3})	1.142, –1.557	2.478, –1.131	2.478, –1.131	1.314, –0.836

SAINTPLUS (Software for the CCD Detector System, Bruker Analytical X-ray Systems Inc., Madison, WI, 1998), an empirical absorption correction using equivalent reflections was performed with the program SADABS,[49a] structure solution using SHELXS–97[49b] and full–matrix least square refinement using SHELXL–97.[49c] The electron density corresponding to all non–hydrogen scatterers were assigned in the relevant difference Fourier maps and correctness of the assignment was affirmed by the lowering of the printed value of *R* indices during refinement of the model structures by the weighted full–matrix least square method on F^2 using SHELXL–97 program.[49d] The hydrogen atoms attached to the various methyl and/or methylene carbon atoms of the macrocycles (or solvent molecules) were introduced on the calculated positions using suitable AFIX card of SHELXL–97 and included as riding atoms with appropriate U_{iso} values in the succeeding refinement cycles. The amine hydrogen atoms H(1) and H(3) of L for the

Table 9. Crystal data and structure refinement parameters for the compounds 5–8.

	5	**6**		**7**	**8**
		6P	**6M**		
Formula	$C_{18}H_{35}Cu\ N_5\ Mo_6O_{19}$	$C_{18}H_{35}Cu\ N_5\ W_6O_{19}$	$C_{18}H_{35}Cu\ N_5\ W_6O_{19}$	$C_{32}H_{64}Cl_2N_8\ O_{19}W_6Zn_2$	$C_{10}H_{26}CuN_5\ W_6O_{19}$
FW	1264.69	1792.13	1792.15	2169.65	1687.00
T (K)	100(2)	298 (2)	298 (2)	298(2)	298(2)
Crystal system	orthorhombic	orthorhombic	orthorhombic	monoclinic	monoclinic
Space group	$P2_12_12_1$	$P2_12_12_1$	$P2_12_12_1$	$P2_1/c$	$C2/c$
a (Å)	10.9162(7)	11.0430(9)	11.0347(10)	14.799(3)	10.827(4)
b (Å)	14.9446(10)	15.0977(12)	15.0878(13)	11.888(2)	17.180(6)
c (Å)	20.5098(13)	20.7375(17)	20.7320(18)	18.130(3)	15.006(5)
α (°)	90.00	90.00	90.00	90.00	90.00
β (°)	90.00	90.00	90.00	111.842(3)	94.008(6)
γ (°)	90.00	90.00	90.00	90.00	90.00
V (Å^3)	3345.9(4)	3457.4(5)	3451.7(5)	2960.6(9)	2784.4(17)
Z	4	4	4	2	4
D_{calcd} (Mg/m^3)	2.511	3.439	3.449	2.434	4.024
μ (mm^{-1})	2.884	20.561	20.596	12.555	25.517
F(000)	2444	3204	3212	2004	2984
GooF on F^2	1.043	1.016	1.076	1.070	1.158
R_1, wR_2 [$I>2\sigma(I)$]	0.0165, 0.0368	0.0285, 0.0533	0.0238, 0.0559	0.0327, 0.0653	0.0372, 0.0671
R_1, wR_2 [all data]	0.0172, 0.0370	0.0331, 0.0547	0.0250, 0.0564	0.0417, 0.0686	0.0455, 0.0703
Flack param.	0.464(11)	–0.002(13)	–0.016(12)	–	–
Largest diff. peak, hole (e.Å^{-3})	0.333,–0.418	0.849,–0.948	0.919,–1.545	0.598,–0.926	1.222,–0.978

compounds **1**, **2** and **7** were located from the difference Fourier map and refined isotropically. These atoms for the crystal structures of **3**, **4**, **5** and **6** remained unallocated, although they were included with the molecular formula and molecular mass. All attempts to crystallize compound **2** ended up with tiny yellow needles, out of which one crystal with dimension 0.20 x 0.04 x 0.04 mm^3 was selected for data collection. Calculation of the ADPs for C5 atom in this structure remained unsuccessful and this atom was refined isotropically for convergence of the refinement. The scenario could not be altered even after repeated trials to improve the quality of the crystals of this compound. Similarly, the larger ghost residual electron density near C6 and C7 (2.48

e.Å^{-3}) in the structure of compound **3** could not be resolved. However, in both the cases good convergence of the data was achieved. In case of compound **8**, hydrogen atoms on the C atoms of cyclen and Cu-bound acetonitrile were introduced on calculated positions and were included in the refinement riding on their respective parent atoms, while the amine hydrogen atoms (H(1N) and H(2N)) of cyclen were located from the difference Fourier map and refined isotropically. Hydrogen atoms for the MeCN molecules were found to be symmetrically disordered over two places (2-fold rotational axis passes through Cu-MeCN axis). Therefore, these hydrogen atoms were refined using AFIX 133 after constraining their occupancies to 0.5. The U_{eq} values of the amine protons (H(1N) and H(2N)) were set to –1.2 for refinement stability. A summary of the crystal data and structure refinement parameters for the compounds **1–8** are tabularized in Tables 8 and 9.

● 2.5. REFERENCES

1. (a) Pope, M. T. In *Heteropoly and Isopoly Oxometalates*; Springer–Verlag: Berlin, **1983**. (b) Pope, M.T.; Müller, A. *Polyoxometalate Chemistry*, Kluwer, Dordrecht, **2001**.
2. (a) Hagrman, D.; Hagrman, P. J.; Zubieta, J. *Angew. Chem. Int. Ed.* **1999**, *38*, 2638. (b) Long, D. L.; Burkholder, E.; Cronin, L. *Chem. Soc. Rev*. **2007**, *36*, 105. (c) Proust, A., Thouvenot, R., Gouzerh, P. *Chem. Commun*. **2008**, 1837.
3. Hill, C. L. *Topical issue on polyoxometalates*; Guest Ed. *Chem. Rev*. **1998**, *98*, 1 and the references therein.
4. (a) Desiraju, G. R. *The Crystal as a Supramolecular Entity, Wiley*, **1996**. (b) Desiraju, G. R. *Organic Solid State Chemistry*, Elsevier, **1987**.
5. (a) Khan, M. I.; Nome, R. C.; Deb, S.; McNeely, J. H.; Cage, B.; Doedens, R. J. *Cryst. Growth Des.* **2009**, *9*, 2848. (b) Khan, M. I.; Yohannes, E.; Golub, V. O.; O'Connor, C. J.; Doedens, R. J. *Chem. Mater*. **2007**, *19*, 4890. (c) Khan, M. I.; Deb, S.; Doedens, R. J. *Inorg. Chem. Commun.* **2006**, *9*, 25. (d) Khan, M. I.; Ayesh, S.; Doedens, R. J.; Yu, M.; O'Connor, C. J. *Chem. Commun.* **2005**, 4658. (e) Khan, M. I.; Yohannes, E.; Nome, R. C.; Ayesh, S.; Golub, V. O.; O'Connor, C. J.; Doedens, R. J. *Chem. Mater*. **2004**, *16*, 5273.
6. (a) Thomas, J.; Ramanan, A. *Cryst. Growth Des.* **2008**, *8*, 3390. (b) Pavani, K.; Lofland, S. E.; Ramanujachary, K. V.; Ramanan, A. *Eur. J. Inorg. Chem.* **2007**,

568. (c) Upreti, S.; Ramanan, A. *Crystal Growth Des.* **2006**, *6*, 2066. (d) Upreti, S.; Ramanan, A. *Crystal Growth Des.* **2005**, *5*, 1837. (e) Pavani, K.; Ramanan, A. *Eur. J. Inorg. Chem.* **2005**, 3080. (f) Asnani, M.; Sharma, S.; Lofland, S. E.; Ramanujachary, K. V.; Buffat, P. A.; Ramanan, A. *Eur. J. Inorg. Chem.* **2005**, 401. (g) Chakrabarti, S.; Natarajan, S. *Crystal Growth Des.* **2002**, *2*, 333. (h) Natarajan, S. *Inorg. Chim. Acta.* **2003**, *348*, 233.

7. (a) Shivaiah,V.; Das, S. K. *Angew. Chem. Int. Ed.* **2006**, *45*, 245. (b) Shivaiah,V. Das, S. K. *Inorg. Chem*. **2005**, *44*, 7313. (c) Chatterjee, T.; Sarma, M.; Das, S. K. *Cryst. Growth Des.* **2010**, *10*, 3149. (d) Chatterjee, T.; Sarma, M.; Das, S. K. *J. Mol. Struct.* **2010**, *981*, 34. (e) Chatterjee, T.; Sarma, M.; Das, S. K. *Inorg. Chem. Commun.* **2010**, *13*, 1114.

8. (a) Li, Y.; Hao, N.; Wang, E.; Yuan, M.; Hu, C.; Hu, N.; Jia, H. *Inorg. Chem.* **2003**, *42*, 2729. (b) You, W.; Wang, E.; Xu, Y.; Li, Y.; Xu, L.; Hu, C. *Inorg. Chem.* **2001,** *40*, 5468. (c) You, W. S.; Wang, E.; Zhang, H.; Xu, L.; Wang, Y. B. *J. Mol. Struct.* **2000**, *554*, 141. (d) You, W. S.; Wang, E.; Xu, L.; Zhu, Z. M.; Gu, Y. P. *J. Mol. Struct.* **2002**, *605*, 41. (e) You, W. S.; Wang, E.; He, Q. L.; Xu, L.; Xing, Y.; Jia, H. Q. *J. Mol. Struct.* **2000**, *524*, 133. (f) Li, Y. G.; Wang, E.; Wang, S. T.; Lu, Y.; Hu, C. W.; Hu, N. H.; Jia, H. Q. *J. Mol. Struct.* **2001**, *607*, 133. (g) Soares–Santos, P. C. R.; Silva, L. C.; Sousa, F. L.; Nogueira, H. I. S. *J. Mol. Struct.* **2008**, *888*, 99. (h) Streb, C.; McGlone, T.; Brücher, O.; Long, D. –L.; Cronin, L. *Chem. Eur. J.* **2008**, *14*, 8861. (j) Zhao, Y.; Shi, Z.; Ding, S.; Bai, N.; Liu, W.; Zou, Y.; Zhu, G.; Zhang, P.; Mai, Z.; Pang, W. *Chem. Mater.* **2000**, *12*, 2550. (k) Akutagawa, T.; Endo, D.; Kudo, F.; Noro, S.–I.; Takeda, S.; Cronin, L.; Nakamura, T. *Cryst. Growth Des.* **2008**, *8*, 812.

9. (a) Bazzan, G.; Smith, W.; Francesconi, L. C.; Drain, C. M. *Langmuir* **2008**, *24*, 3244. (b) Falber, A.; Burton–Pye, B. P.; Radivojevic, I.; Todaro, L.; Saleh, R.; Francesconi, L.C.; Drain, C. M. *Eur. J. Inorg. Chem.* **2009**, 2459. (c) Yokoyama, A.; Kojima, T.; Ohkubo, K.; Fukuzumi, S. *Chem. Commun.* **2007**, 3997.

10. (a) Rajec, P.; Švec, V.; Mikulaj, V.; Hanzel, R. *J. Radioanal. Nucl. Chem*. **1998**, 2299. (b) Sheen, S. –R.; Shih, J. –S. *Analyst* **1992**, *117*, 1691. (c) Fernando, L. A.; Miles, M. L.; Bowen, L. H. *Anal. Chem*. **1980**, *52*, 1115.

11. (a) Curtis, N. F. *M. Sc. Thesis*, University of Auckland, New Zealand, **1954** (b) Curtis, N. F. *J. Chem. Soc*. **1960**, 4409.

12. (a) Curtis, N. F.; House, D. A. *Chem. Ind. Lond*. **1961**, *42*, 1708. (b) Curtis, N. F.; Curtis, Y. M.; Powel, H. K. J. *J. Chem. Soc. A* **1966**, 1015. (c) Curtis, N. F. *Coord. Chem. Rev*. **1968**, *3*, 3. (d) Bailey, M. F.; Maxwell, J. E. *J. Chem. Soc. Chem. Commun*. **1966**, 908.

13. (a) Sadasivan, N.; Endicott, J. F. *J. Am. Chem. Soc.* **1966**, *88*, 5468. (b) Curtis, N. F.; Hay, R. W. *J. Chem. Soc. Chem. Commun.* **1966**, 524. (c) Hay, R. W.; Lawrance, G. A.; Curtis, N. F. *J. Chem. Soc. Perkin Trans. 1*. **1975**, 591.

14. (a) Endicott, J. F.; Durham, B.; Glick, M. D.; Anderson, T. J.; Kuszaj, J. M.; Schmonsees, W. G.; Balakrishnan, K. P. *J. Am. Chem. Soc.* **1981**, *103*, 1431. (b) Endicott, J. F.; Wong, C. L.; Ciskowski, J. M.; Balakrishnan, K. P. B.; *J. Am. Chem. Soc.* **1980**, *102*, 2100. (c) Endicott, J. F.; Kumar, K.; Ramasami, T.; Rotzinger, F. P. *Prog. Inorg. Chem.* **1983**, *30*, 141.

15. (a) Bresciani-Pahor, N.; Forcolin, M.; Marzilli, L. G.; Randaccio, L.; Summers, M. F.; Toscano, P. J. *Coord. Chem. Rev.* **1985**, *63*, 1. (b) Bacac, A.; Espenson, J. H. *Inorg. Chem*. **1987**, *26*, 4353.

16. (a) Fuzita, E. *Coord. Chem. Rev.* **1999**, *185–186*, 373. (b) Ogata, T.; Yanagida, S.; Brunschwig, B. S.; Fuzita, E. *J. Am. Chem. Soc.* **1995**, *117*, 6708. (c) Fuzita, E.; Creutz, C.; Satin, N.; Brunschwig, B. S. *Inorg. Chem*. **1993**, *32*, 2657. (d) Creutz, C.; Schwarz, H. A.; Wishart, J. F.; Fuzita, E.; Sutin, N. *J. Am. Chem. Soc.* **1991**, *113*, 3361. (e) Fuzita, E.; Creutz, C.; Sutin, N.; Szalda, D. J. *J. Am. Chem. Soc*. **1991**, *113*, 343. (f) Geiger, T.; Anson, F. C. *J. Am. Chem. Soc.* **1981**, *103*, 7489.

17. House, D. A.; Browning, J.; Pipal, J. R.; Robinson, W. T. *Inorg. Chim. Acta.* **1999**, *292*, 73.

18. (a) Warner, J. G.; Rose, N. J.; Busch, D. H. *J. Am. Chem. Soc.* **1968**, *90*, 6938. (b) Szalda, D. J.; Schwarz, C. L.; Creutz, C. *Inorg. Chem.* **1991**, *30*, 586. (c) Lee, S.; Shih, H. –C.; Su, T. –H.; He, K. –C.; Chen, K. –N. *Inorg. Chim. Acta* **2004**, *357*, 485.

19. (a) Jacques, J.; Collet, A.; Wilen, S. H. *Enantiomers, Racemates and Resolutions*, Krieger Publishing, Malabar, Florida, **1994**. (b) García, L. P.; Amabilino, D. B. *Chem. Soc. Rev*. **2002**, *31*, 342.

20. (a) Anthony, S. P.; Basavaiah, K.; Radhakrishnan, T. P. *Cryst. Growth Des*. **2005**, *5*, 1663. (b) Zhou, P.; Li, H. *Dalton Trans*. **2011**, *40*, 4834. (c) Pradeep, C. P.; Zacharias, P. S.; Das, S. K. *Eur. J. Inorg. Chem*. **2005**, 3405. (d) Prabhakar, M.; Zacharias, P. S.; Das, S. K. *Inorg. Chem.* **2005**, *44*, 2585.

21. (a) Khatua, S.; Harada, T.; Kuroda, R.; Bhattacharjee, M. *Chem. Commun.* **2007**, 3927. (b) Khatua, S.; Stoeckli- Evans, H.; Harada, T.; Kuroda, R.; Bhattacharjee, M. *Inorg. Chem*. **2006**, *45*, 9619. (c) Jayanti, S.; Radhakrishnan, T. P. *Chem. Eur. J*. **2004**, *10*, 2661. (d) Jiang, L.; Feng, X. L.; Su, C. Y.; Chen, X. M.; Lu, T. B. *Inorg. Chem*. **2007**, *46*, 2637. (e) Zhang, W.; Sun, H. L.; Sato, O. *CrystEngComm* **2010**, *12*, 4045. (f) Kendrick, J.; Gourlay, M. D.; Neumannb, M. A.; Leusen, F. J. J. *CrystEngComm* **2009**, *11*, 2391. (g) Enamullah, M.; Sharmin, A.; Hasegawa, M.; Hoshi, T.; Chamayou, A. C.; Janiak, C. *Eur. J. Inorg. Chem*. **2006**, 2146. (h) Tunyogi, T.; Deák, A.; Tárkányi, G.; Király, P.; Pálinkás, G. *Inorg. Chem*. **2008**, *47*, 2049. (i) Makino, T.; Masu, H.; Katagiri, K.; Yamasaki, R.; Azumaya, I.; Saito, S. *Eur. J. Inorg. Chem*. **2008**, 4861. (j) Bhuvan Kumar, N. N.; Kumara Swamy, K. C. *Tetrahedron Lett*. **2008**, *49*, 7135. (k) Supriya, S.; Das, S. K. *Chem. Commun*. **2011**, 2062. (l) Imai, Y.; Kawaguchi, K.; Tajima, N.; Sato, O.; Kuroda, R.; Matsubara, Y. *Chem. Commun*. **2008**, 362.

22. (a) Jaya, M.; Prakash, Radhakrishnan, T. P. *Cryst. Growth Des.* **2005**, *5*, 721. (b) Dang, D.; Wu, P.; He, C.; Xie, Z.; Duan, C. *J. Am. Chem. Soc*. **2010**, *132*, 14321. (c) Mastai, Y.; Sedlák, M.; Cölfen, H.; Antonietti, M. *Chem. –Eur. J*. **2002**, *8*, 2430.

23. (a) Hou, Y.; Fang, X.; Hill, C. L. *Chem. –Eur. J*. **2007**, *13*, 9442. (b) Hasenknopf, B.; Micoine, K.; Lacôte, E.; Thorimbert, S.; Malacria, M.; Thouvenot, R. *Eur. J. Inorg. Chem.* **2008**, 5001 and references therein. (c) Lan, Y. −Q.; Li, S. −L.; Wang, X. −L.; Shao, K. −Z.; Du, D. −Y.; Su, Z. −M.; Wang, E. *Chem. –Eur. J*. **2008**, *14*, 9999. (d) An, H. −Y.; Wang, E.; Xiao, D. −R.; Li, Y. −G.; Su, Z. −M.; Xu, L. *Angew. Chem. Int. Ed*. **2006**, *45*, 904. (e) Xiao, F.; Hao, J.; Zhang, J.; Lv, C.; Yin, P.; Wang, L.; Wei, Y. *J. Am. Chem. Soc.* **2010**, *132*, 5956. (f) Zhang, Y.; Zhang, L.;

Hao, Z.; Luo, F. *Dalton Trans*. **2010**, *39*, 7012. (g) Micoine, K.; Hasenknopf, B.; Thorimbert, S.; Lacôte, E.; Malacria, M.; *Angew. Chem. Int. Ed.* **2009**, *48*, 3466. (h) Yan, L.; López, X.; Carbó, J. J.; Sniatynsky, R.; Duncan, D. C.; Poblet, J. M. *J. Am. Chem. Soc.* **2008**, *130*, 8223. (i) Fang, X.; Anderson, T. M.; Hill, C. L. *Angew. Chem. Int. Ed*. **2005**, *44*, 3540. (j) Naruke, H.; Iijima, J.; Sanji, T. *Inorg. Chem*. **2011**, *50*, 7535. (k) Tan, H.; Li, Y.; Chen, W.; Liu, D.; Su, Z.; Lu, Y.; Wang, E. *Chem. –Eur. J*. **2009**, *15*, 10940.

24. Villaraza, A. J. L.; Bumb, A.; Brechbiel, M. W. *Chem. Rev*. **2010**, *110*, 2921 and the references therein.
25. Lauffer, R. B. *Chem. Rev*. **1987**, *87*, 901 and the references therein.
26. Caravan, P.; Ellison, J. J.; McMurry, T. J.; Lauffer, R. B. *Chem. Rev*. **1999,** *99*, 2293 and the references therein.
27. Aoki, S.; Kimura, E. *Chem. Rev*. **2004**, *104*, 769 and the references therein.
28. Haas, K. L.; Franz, K. J. *Chem. Rev*. **2009**, *109*, 4921 and the references therein.
29. Mukhopadhyay, S.; Mandal, S. K.; Bhaduri, S.; Armstrong, W. H. *Chem. Rev*. **2004**, *104*, 3981 and the references therein.
30. Svoboda, J.; König, B. *Chem. Rev*. **2006**, *106*, 5413 and the references therein.
31. Binnemans, K. *Chem. Rev*. **2009**, *109*, 4283 and the references therein.
32. Martínez-Máñez, R.; Sancenón, F. *Chem. Rev*. **2003**, *103*, 4419 and the references therein.
33. de Silva, A. P.; Gunaratne, H. Q. N.; Gunnlaugsson, T.; Huxley, A. J. M.; McCoy, C. P.; Rademacher, J. T.; Rice, T. E. *Chem. Rev*. **1997**, *97*, 1515 and the references therein.
34. (a) House, D. A.; Browning, J.; Pipal, J. R.; Robinson, W. T. *Inorg. Chim. Acta*, **1999**, *292*, 73. (b) Sadasivan, N.; Kernohan, J. A.; Endicott, J. F. *Inorg. Chem.* **1967**, *6*, 770. (c) Gainsford, G. J.; Curtis, N. F. *Aust. J. Chem.* **1984**, *37*, 1799. (d) Kolinski, R. A.; Korybut-Daszkiewicz, B. *Inorg. Chim. Acta*, **1975**, *14*, 237. (e) Szalda, D. J.; Fuzita, E.; Creutz, C. *Inorg. Chem.* **1989**, *28*, 1446. (f) Curtis, N. F.; Flood, K.; Robinson, W. T. *Polyhedron*, **2006**, *25*, 1579. (g) Furenlid, L. R.; Renner, M. W.; Szalda, D. J.; Fujita, E. *J. Am. Chem. Soc.* **1991**, *113*, 883.

35. (a) Lu, T. −H.; Tahirov, T. H.; Chen, B. −H.; Lai, C. −Y.; Chung, C. −S. *Acta Crystallogr*. **1996**, *C52*, 2684. (b) Heeg, M. J.; Endicott, J. F.; Glick, M. D. *Inorg. Chem.* **1981**, *20*, 1196. (c) Creutz, C.; Chou, M. H.; Fujita, E.; Szalda, D. J. *Coord. Chem. Rev.* **2005**, *249*, 375. (d) Lee, S.; Espenson, J. H.; Bakac, A. *Inorg. Chem.* **1990**, 29, 3442. (e) Gibney, S. C.; Ferraudi, G.; Shang, M. *Inorg. Chem.* **1999**, *38*, 2898. (f) Zhang, S. –S.; Niu, S. –Y.; Jie, G. –F.; Li, X. –M.; Jiao, K.; *Acta Crystallogr*. **2004**, *E60*, m966. (g) Endicott, J. F.; Lilie, J.; Kuszaj, J. M.; Ramaswamy, B. S.; Schmonsees, W. G.; Simic, M. G.; Glick, M. D.; Rillema, D. P. *J.Am.Chem.Soc*. **1977**, *99*, 429.

36. (a) Szalda, D. J.; Fujita, E. *Acta Crystallogr.* **1992**, *C48*, 1767. (b) Wang, W. −B.; Yang, L. −X.; Yu, L. −C.; Song, C. −X.; Wu, S. −Y.; *J. Coord. Chem.* **2008**, *61*, 528. (c) Curtis, N. F.; Pawley, R.; Robinson, W. T. *Acta Crystallogr.* **2006**, *E62*, m80. (d) Ballester, L.; Gutierrez, A.; Perpinan, M. F.; Sanchez, A. E.; Azcondo, M. T.; Gonzalez, M. J. *Inorg. Chim. Acta*. **2004**, *357*, 1054. (e) Bienko, A.; Klak, J.; Mrozinski, J.; Boca, R.; Brudgam, I.; Hartl, H. *Dalton Trans.* **2007**, 2681. (f) Jian, F.; Jiao, K.; Liu, F.; Wang, Q. *Anal. Sci.* **2003**, *19*, 643. (g) Shen, H. −Y.; Liao, D. −Z.; Jiang, Z. −H.; Yan, S. −P. *Transition Met. Chem.* **1999**, *24*, 581.

37. Palmer, J. M.; Papaconstantinou, E.; Endicott, J. F. *Inorg. Chem.* **1969**, *8*, 1516.

38. (a) Wilson, J. M.; Giordani, F.; Farrugia, L. J.; Barrett, M. P.; Robins, D. J.; Sutherland, A. *Org.Bimol. Chem*. **2007**, *5* 3651. (b) Hervé, G. ; Bernard, H. ; Bris, N. L. ; Yaouanc, J. –J. ; Handel, H. ; Toupet, L. *Tetrahedron Lett.* **1998**, *39*, 6861. (c) Reed, D. P.; Weisman, G. R.; *Org. Synth*. **2004**, *10*, 667. (d) Atkins, T. J.; Richman, J. E.; Oettle, W. F. *Org. Synth*. **1998**, *6*, 652.

39. Warner, J. G.; Rose, N. J.; Busch, D. H. *J. Am. Chem. Soc.* **1968**, *90*, 6938.

40. (a) Linhard, M.; Weigel, M.; *Z. Anorg. Allgem. Chem.* **1951**, *321*, 264. (b) Linhard, M.; Weigel, M. *Z. Anorg. Allgem. Chem.* **1951**, *267*, 113. (c) Linhard, M.; Weigel, M. *Z. Anorg. Allgem. Chem*. **1951**, *267*, 121. (d) Wentworth, R. A**.** D.; Piper, T. S.; *Inorg. Chem*. **1965**, *4*, 709.

41. (a) Hur, N. H.; Klemperer, W. G.; Wang, R. –C. *Inorg. Synth.* **1990**, *27*, 77. (b) Fournier, M.; *Inorg. Synth.* **1990**, *27*, 80. (c) Linhard, M.; Weigel, M.; *ibid*. **1951**, *267*, 121.

42. (a) Sarma, M.; Chatterjee, T.; Das, S. K. *Dalton Trans.* **2011**, *40*, 2954. (b) Sarma, M.; Chatterjee, T.; Das, S. K. *J. Mol. Struct.* **2011**, *1004*, 31. (c) Sarma, M.; Chatterjee, T.; Das, S. K. *Dalton Trans.* **2012**, *41*, 1862.

43. (a) Styka, M. C.; Smierciak, R. C.; Blinn, E. L.; Desimone, R. E.; Passariello, J. V. *Inorg. Chem.* **1978**, *17*, 82. (b) Shivaiah, V.; Das, S. K. *Inorg. Chem.* **2005**, *44*, 8846. (c) Costes, J. –P.; Dahan, F.; Novitchi, G.; Arion, V.; Shova, S.; Lipkowski, J. *Eur. J. Inorg. Chem.* **2004**, 1530.

44. Sarma, M.; Chatterjee, T.; Das, S. K. *Inorg. Chem. Commun.* **2010**, *13*, 1114.

45. (a) Szalda, D. J.; Schwarz, C. L.; Endicott, J. F.; Fujita, E.; Creutz, C. *Inorg.Chem.* **1989**, *28*, 3214. (b) Lee, S.; Espenson, J. H.; Bakac, A. *Inorg. Chem.* **1990**, *29*, 3442. (c) Szalda, D. J.; Schwarz, C. L.; Creutz, C. *Inorg. Chem.* **1991**, *30*, 586. (d) Zhou, H. –B.; Liao, D. –Z.; Deng, L. –X.; Yu, J. –Z.; Gao, Y. –P.; Yang, X. –F.; Jiang, Z. –H.; Yan, S. –P.; Cheng, P. *Struct. Chem.* **2006**, *17*, 43. (e) Lu, T. –H.; Tahirov, T. H.; Chen, B. –H.; Lai, C. –Y.; Chung, C. –S. *Acta Crystallogr.* **1996**, *C52*, 2684. (f) Lee, T. J.; Lu, T. H.; Chung, C. –S.; Lee, T. Y. *Acta Crystallogr.* **1984**, *C40*, 70. (g) Lu, T. –H.; Liang, W. –C.; Wu, D. –T.; Chung, C. –S. *Acta Crystallogr.* **1986**, *C42*, 801. (h) Lee, T. –J.; Lee, H. Y. J.; Lee, C. –S.; Chung, C. –S. *Acta Crystallogr.* **1984**, *C40*, 641. (i) Lu, T. H.; Lee, T. J.; Liang, B. F.; Chung, C. S. *J. Inorg. Nucl. Chem.* **1981**, *43*, 2333. (j) Yang, Y. –M. *Acta Crystallogr.* **2005**, *E61*, m1618.

46. Flack, H. D. *Acta Crystallogr.* **1983**, *A39*, 876.

47. Rillema, D. P.; Endicott, J. F.; Papaconstantinou, E. *Inorg. Chem.* **1971**, *10*, 1739.

48. (a) Strong, J. B.; Yap, G. P. A.; Ostrander, R.; Liable–Sands, L. M.; Rheingold, A. L.; Thouvenot, R.; Gouzerh, P.; Maatta, E. A. *J. Am. Chem. Soc.* **2000**, *122*, 639. (b) Niu, Y.; Ren, X.; Yin, B.; Wang, D.; Xue, G.; Hu, H.; Fu, F.; Wang, J. *J. Organomet. Chem.* **2010**, *695*, 1863. (c) Bank, S.; Liu, S.; Shaikh, S. N.; Sun, X.; Zubieta, J.; Ellis, P. D. *Inorg. Chem.* **1988**, *27*, 3535.

49. (a) SAINT: *Software for the CCD Detector System*; Bruker Analytical X-ray Systems, Inc.: Madison, WI, **1998**. (b) SADABS: *Program for absorption correction*; Sheldrick, G. M. University of Göttingen: Göttingen, Germany, **1997**. (c) SHELXS–97: *Program for structure solution*; Sheldrick, G. M. University of

Göttingen: Göttingen, Germany, **1997**. (*d*) SHELXL–97: *Program for Crystal Structure Analysis*; Sheldrick, G. M. University of Göttingen: Göttingen, Germany, **1997**.

••••

Chapter-3

Ammonium–Crown Ether Based Host-guest Systems: N–H···O Hydrogen Bond Directed Guest Inclusion Featuring N–H Donor Functionalities in Angular Geometry

ABSTRACT: This chapter demonstrates crown ether based host-guest adduct formation in a series of crystalline solids **1**–**7**, in which ammonium–type cationic guests are integrated with various crown ethers. The addition of more than two equivalents of perchloric acid to an acetonitrile solution of 3–aminopyridine (3AmPy) or 4,4'–diamino diphenylmethane (DADPM) or 4,4'–diaminodiphenylether (DADPE) generates the doubly protonated anilinium (or ammonium) cationic species (written as $3AmPyH_2$, $DADPMH_2$ and $DADPEH_2$ respectively) which act as the guests to the various crown ether hosts present in solution. The relevant compounds crystallize as their perchlorate salts and the structural characterization through X-ray diffraction technique reveals formulation of the relevant solids to be $[3AmPyH_2(12C4)_2](ClO_4)_2$ (**1**), $[3AmPyH_2(B15C5)]_2(ClO_4)_4\cdot 2H_2O$ (**2**), $[3AmPyH_2(DB21C7)]_3(ClO_4)_6\cdot 5H_2O\cdot 0.5CH_3CN$ (**3**), $[DADPMH_2(12C4)]_2(ClO_4)_4\cdot H_2O$ (**4**), $[DADPMH_2(15C5)_2](ClO_4)_2$ (**5**), $[DADPMH_2(18C6)_2]_2(ClO_4)_4\cdot 6.75H_2O\cdot CH_3CN$ (**6**) and $[DADPEH_2(18C6)_2](ClO_4)_2\cdot 2CH_3CN$ (**7**) where, 12C4 = 12–crown–4, B15C5 = benzo–15–crown–5, 15C5 = 15–crown–5, DB21C7 = dibenzo–21–crown–7 and 18C6 = 18–crown–6. The N–H···O hydrogen bond interactions between the aforementioned guests and the crown ether hosts are found to be responsible for host-guest complexation in the compounds **1**–**7**. The solid–state stoichiometry between the host and the guest is found to vary with the cavity size of the crown ether.

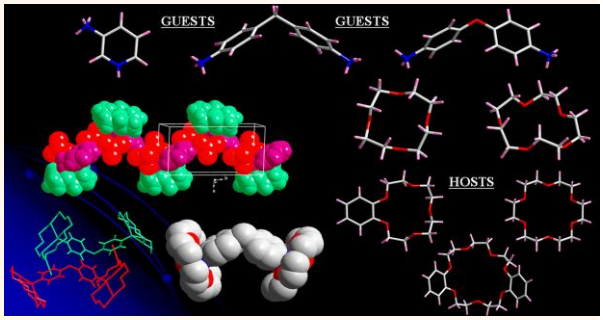

● 3.1. INTRODUCTION

Since the discovery of crown ethers, they have been extensively used as hosts for the recognition of a diverse class of guest species.[1–2] Till date, plenty of such systems have been reported, in which the heteroatoms are mostly oxygen, nitrogen, sulfur, mixed oxygen and nitrogen or sulfur atoms, and they are bridged by aliphatic or aromatic carbon spacers. Among the several derivatives of crown macrocycles, the all oxygen, all nitrogen and mixed oxygen–nitrogen heteroatom containing derivatives are frequently used to recognize neutral or ionic organic and inorganic species.[3] The oxygen atom is the predominant heteroatom in the crown ether chemistry. The general structural feature of such macrocyclic hosts, being saturated and repeating glycolic units (–O–CH_2–CH_2–O–),

confers structural elasticity or conformational mobility to the crown ethers, whereby the nature of guest incorporation is largely governed by their cavity sizes. The stoichiometry of the resulting host-guest complexes is usually administered by the structure of the host and the size of the guest, although violation of the straightforward structural prediction is sometimes registered. The most characteristic feature of the crown ethers is their lipophobic / hydrophilic cavity surrounded by a lipophilic / hydrophobic ring unit and very often, selective binding of guest is achieved by alteration of the heteroatoms. For instance, the all–oxygen macrocycles are better choices for encapsulating/sensing alkali metal ions than the all–nitrogen or mixed–oxygen–nitrogen containing crown ethers, which on the contrary, exhibit more selectivity towards binding soft transition metal ions. Apart from being well-known in the research area of sensing of metal ions, these macrocyclic hosts have also been explored in the area of crystal engineering, as they can be extensively used for building simple to complex supramolecular / supermolecular architectures. The preferential treatment, meted out by the crown ethers to the cationic guests, is superior to that of the neutral guests. The metal ions which possess a spherical geometry, are usually bound through the X:→M dative (coordinate covalent) linkages (X = heteroatom) whereas, D–H···X interactions (D = H–bond donor) between the cations (e.g. H_3O^+, NH_4^+, RNH_3^+ etc.) and the crown ethers (X = acceptor heteroatom, O and N being the most common) are mainly responsible for the guest encapsulation via non-covalent molecular recognition process. The excellent review article by Steed in 2001 brings to light a sound overview of the alkali metal – crown ether chemistry.[4a] During 1990–early 2000, various research groups, mainly Atwood, Steed, Junk and others were actively involved in studying the binding of oxonium ions by several small to large cavity sized crown ether derivatives; the topic being mostly covered in the perspective "Crown ethers as stabilizing ligands for oxonium ions" by Junk in 2008.[4b] A diverse class of crown ether based host-guest systems with simple to complicated topologies have already been reported by several groups including Nangia, Atwood, Zaworotko, Fonari, Nakamura, Stoddart, Braga, Steed, Rogers and others.[5–10]

The tetrahedral guest cation, ammonium ion (NH_4^+), or organic ammonium ion (RNH_3^+, $ArNH_3^+$ etc.) is generally perched into the oxy–crown ether cavity through the N–H···O hydrogen bond. Selected database entries (CSD version 5.32, November 2010)

Table 1. Selected CSD dataset for ammonium–crown ether host-guest systems.

Crown	Guest	Sp. Gr.	Counter anion	CSD code	Ref
12C4	1,4–$Cy(CH_2NH_3^+)_2$	$P\bar{1}$	Ni(II) dithiolato complex	AJUPUQ	6a
12C4	NH_4^+	$P2/n$	Ni(II) dithiolato complex	HUFHAR	6b
12C4	$Ph_3CNH_3^+$	$P2_1/c$	thiocyanate	WOPCOU	6c
B15C5	$PhCH_2NH_3^+$	$P\bar{1}$	perchlorate	AWUYEW	6d
B15C5	1,4–$Ph(CH_2NH_3^+)_2$	$P\bar{1}$	perchlorate	AWUYIA	6d
B15C5	$H_3N^+(CH_2)_4NH_3^+$	$P\bar{1}$	thiocyanate	AWUYOG	6d
B15C5	NH_4^+	$P2_1/c$	*bis*((μ_2–iodo)–diodo–Cd)	NASTAC	6e
B15C5	NH_4^+	$P2_1/c$	nitrate	QOBJIA	6f
18C6	1,4–$Cy(NH_3^+)_2$	$P\bar{1}$	Ni(II) dithiolato complex	AJUPIE	6a
18C6	1,4–$Cy(CH_2NH_3^+)_2$	$P\bar{1}$	Ni(II) dithiolato complex	AJUQAX	6a
18C6	NH_4^+	$F2dd$	dihydrogenphosphate	BOLKUJ	6g
18C6	$CH_3NH_3^+$	$P2_1/c$	triflate	BUHBOV	6h
18C6	BF_3NH_3	$P2_12_12_1$	—	CEDZAM	6i
18C6	$PhCOCH_2NH_3^+$	$P2_1/n$	hexafluorophosphate	COVXAM	6j
18C6	$NH_2NH_3^+$	$Pn2_1$	perchlorate	CRAMCA10	7a
18C6	$OHNH_3^+$	$C2/c$	perchlorate	CRAMCB10	7a
18C6	$CH_3NH_3^+$	$C2/c$	perchlorate	CRAMCC10	7a
18C6	$PHCH_2NH_3^+$	$P\bar{1}$	thiocyanate	CRBZCN	7b
18C6	NH_4^+	R–3	hexachlorouranium	GICLIN	7c
18C6	NH_4^+	Fd–3	tetraiodothallate	HOVQAK01	7d
18C6	$OHNH_3^+$	$P2_1/c$	cis,cis–3,5–Dicarboxy–cyclohexane–1–carboxylate	JEDPEO	5a
18C6	NH_4^+	$Pna2_1$	cis,cis–3,5–Dicarboxy–cyclohexane–1–carboxylate	JEDPUE	5a
18C6	adamantylammonium	$P\bar{1}$	Ni(II) dithiolato complex	JEXVIS	7e
18C6	4–Fluoroanilinium	$P\bar{1}$	Ni(II) dithiolato complex	LEBROA	7f
18C6	4–Methylanilinium	$P\bar{1}$	Ni(II) dithiolato complex	LEBRUG	7f
18C6	$PhNH_3^+$	$P\bar{1}$	Ni(II) dithiolato complex	MIGSUQ	7g–i
18C6	1,4–$Ph(NH_3^+)_2$	$P\bar{1}$	Ni(II) dithiolato complex	MIGTAX	7g
18C6	NH_4^+	$P2_1/c$	tetrachloromanganese	MOYNET	7j
18C6	NH_4^+	$C2/c$	hexafluorosilicate	ODAGIJ	8a
18C6	NH_4^+	$P2_12_12_1$	nitrate	QOBJAS	6f
18C6	$[PhCH(NH_3^+)]_2$	$P\bar{1}$	Ni(II) dithiolato complex	RAQPUV	8b
18C6	(Ammine–bis (benzenethiolato)–pyridyl–beryllium)	$P\bar{1}$	—	SIZNAQ	8c
18C6	1,4–$Ph(NH_3^+)_2$	$P\bar{1}$	phosphomolybdate	TEQFOL	8d
18C6	NH_4^+	$C2/c$	hydrogensulfate	WIGMUV	8e,f
18C6	Ammonia–(cyclotriborane)	$P2_1/n$	—	XOWCOC	8g
18C6	3–Fluoroanilinium	$P\bar{1}$	Ni(II) dithiolato complex	KUNCAY	8h
DB21C7	η^4–(1,5–COD) – $Rh(NH_3)_2$	$P2_1/c$	hexafluorophosphate	DUDSUQ	8i

associated with ammonium–crown supramolecular complexes are collected in Table 1.

The binding of this guest system has mostly been studied with the 18–crown–6 (18C6) derivatives, whereas associated entries with other crown ether systems e.g. 12–crown–4 (12C4), 15–crown–5 (15C5) or 21–crown–7 (21C7) or their derivatives are relatively less. We have recently reported a series of NH_4^+/$ArNH_3^+$–crown ether supramolecular adducts in association with the isopoly– and heteropoly– anions and demonstrated, how the symmetry and/or cavity size of the crown ethers and the symmetry of the polyanions govern the crystal packing feature.[11] Crown ethers generally serve two roles while they pack in their crystal lattice *viz.*, (i) act as hydrogen bonding acceptor through the involvement of D–H···O interaction between the guest donor and the electronegative oxygen acceptor of the host and (ii) act as hydrogen bonding donor through weak C–H···A interaction with another acceptor fragment in the crystal.[9g]

Scheme 1. Probable binding modes between the studied guests with the crown ether hosts, (a) protonated 3–aminopyridine, (b) protonated DADPE and (c) protonated DADPM. The arrows indicate the direction of the hydrogen bonding interactions.

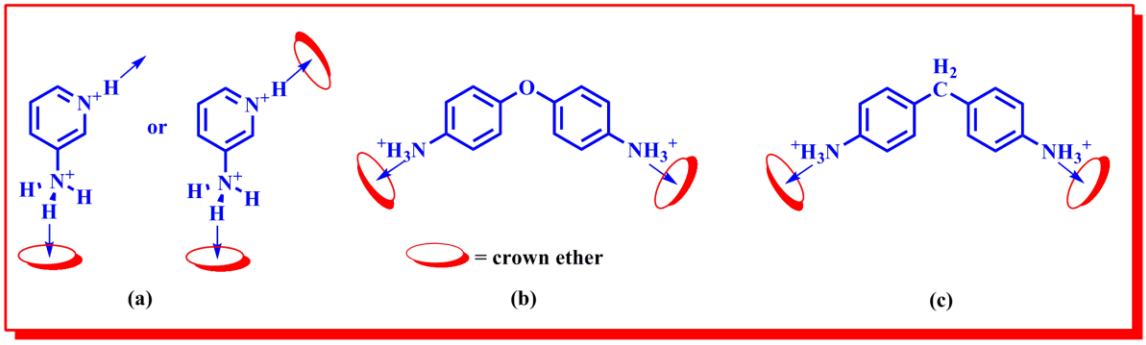

In continuation with our endeavor towards achieving diverse topologies based on molecular recognition processes by the macrocyclic hosts,[11] we were interested to gain more insight into the molecular packing of crown ether inclusion complexes incorporating guest units that bear hydrogen bonding sites in an angular geometrical fashion. In the present work, we chose doubly protonated 3–amino pyridine (hereafter $3AmPyH_2$), diamino diphenyl ether (hereafter $DADPEH_2$) and diamino diphenyl methane (hereafter $DADPMH_2$) that would serve the role of anchoring units to the crown ethers (see Scheme 1). It is worth mentioning that 3–Amino pyridine has biomedicinal implications, while the two angular diamines, DADPE and DADPM, are important precursors in the polymer industry.[12] $3AmPyH_2$ has two hydrogen bonding sites, *viz.* the

pyridinium N–H bond and the anilinium N–H bonds separated by 120º angular span which can interact with either two crown ethers or with one crown ether and another acceptor species (e.g., counter anion) in the relevant crystal lattice (see Scheme 1). The geometrical situation for the H–bonding interactions of this dication resembles non–protonated or protonated 1,3–phenylenediamine for which 1:2 stoichiometry between the guest and the hosts (crown ethers) in the solid state has recently been reported.[8d] The cocrystallization of DADPE and DADPM with the *bis*–phenol systems was reported in earlier literature.[13] The ammonium systems has mostly been studied with the 18C6 derivatives, but the supramolecular chemistry associated with the host-guest complexes between smaller crown ethers (12C4, 15C5 etc.) and ammonium guests having angular geometry is relatively less explored. This incited us to select the present topic and examine if the angular geometry of the guest would lead to a helical crystal packing. To the best of our knowledge, there are no reports so far that portray hydrogen bonded complexes of DADPM and DADPE with crown ether systems.[14] In this chapter, we have described the syntheses, crystal structures and supramolecular chemistry of seven host-guest complexes formulated as $[3AmPyH_2(12C4)_2](ClO_4)_2$ (**1**), $[3AmPyH_2(B15C5)]_2(ClO_4)_4\cdot 2H_2O$ (**2**), $[3AmPyH_2(DB21C7)]_3(ClO_4)_6\cdot 5H_2O\cdot 0.5CH_3CN$ (**3**), $[DADPMH_2(12C4)]_2(ClO_4)_4\cdot H_2O$ (**4**), $[DADPMH_2(15C5)_2](ClO_4)_2$ (**5**), $[DADPMH_2(18C6)_2]_2(ClO_4)_4\cdot 6.75H_2O\cdot CH_3CN$ (**6**) and $[DADPEH_2(18C6)_2](ClO_4)_2\cdot 2CH_3CN$ (**7**).

The solid–state stoichiometry between the host and the guest is found to vary with the cavity size of the crown ether. For example, $3AmPyH_2$ undergoes adduct formation in 1:2 ratio with the smaller crown ether 12C4 in compound **1** but with larger crown ethers, B15C5 and DB21C7 in compounds **2** and **3** respectively, it maintains 1:1 stoichiometry. Extensive non-covalent interactions i.e. hydrogen–bonding, π–stacking etc. play a major role in space association of the various molecular counterparts in the relevant crystals, the extent of these supramolecular cements being governed by the type of host and guest molecules. In the series of host-guest complexes described in the present work, the small macrocycle 12C4 renders unusual results. Only the $3AmPyH_2\cdots$12C4 adduct exhibits a two–fold screw symmetrical packing of the components ($P2_1$), whereas the other $3AmPyH_2\cdots$(crown ether) adducts crystallize in the centric space groups. Similarly, only 12C4 maintains a 1:1 stoichiometry with $DADPMH_2$ guest dication but a 2:1

stoichiometry is maintained between the crown ethers and the guest in compounds **5**–**6**.

● 3.2. RESULTS AND DISCUSSION

● 3.2.1. Synthesis and characterization

In situ protonation of 3AmPy, DADPM and DADPE generated the relevant cationic (ammonium) guests which on integration with the crown ethers present in solution precipitated out as the perchlorate salts of the supramolecular complexes in crystalline form. The usage of more than two equivalents of perchloric acid ensured the complete protonation of the neutral guest molecules. Apart from compound **1**, which was isolated as a stable colorless solid, all the other compounds (**2**–**7**) were moisture sensitive and formed a gummy mass after evaporation of the solvent (mother liquor). Several attempts to obtain stable solids for these compounds by means of alteration of the crystallization conditions ended up without much success. In addition to mechanochemical grinding methods, the extent of endeavor for procuring stable solids included the variation of solvents, using mixed solvents and usage of the separately synthesized diperchlorate salts of the neutral guests rather than *in situ* protonation. The infrared spectra of the compounds **2-7** exhibit a broad feature in the region of 3500–3100 cm^{-1} indicating the presence of moisture in the compounds. In the IR spectrum of compound **1**, the medium intensity bands at 3368 and 3219 cm^{-1} might be attributable to the N–H(str) vibrational motion of the $3AmPyH_2$ guest whereas, in all the other compounds, clarity of this pertinent absorption mode is masked by the absorption due to the high moisture content, present in the solids in this region. However, two IR bands near 1600 and 1500 cm^{-1} in the spectra of the compounds **1**–**7** might be due to asymmetric and symmetric N–H (def) vibrational mode of the guest ammonium cations which indicates the presence of the guest moiety in the relevant solids. The existence of crown ether hosts in the compounds **1**–**7** is elucidated by the presence of weak intensity C–H(str) bands near 3000 cm^{-1} and strong to medium intensity IR bands in the region of 1300–1050 cm^{-1} due to the C–C and C–O vibrational modes of the ethereal hosts.

● 3.2.2. Description of crystal structures

Compound $[3AmPyH_2(12C4)_2](ClO_4)_2$ (1). Single crystal X-ray diffraction analysis of the isolated perchlorate salt of $3AmPyH_2\cdots12C4$ supramolecular complex (compound **1**)

reveals 1:2 stoichiometry between the $3AmPyH_2$ guest and the ethereal host rendering the formulation of the relevant compound to be $[3AmPyH_2(12C4)_2](ClO_4)_2$. Among the series of supramolecular complexes demonstrated in this chapter, the compound **1** crystallizes in chiral space symmetry ($P2_1$), the asymmetric unit of which is characterized by the presence of a host-guest complex and two perchlorate counter anions. The small crown ether 12C4, which itself holds less room to act as a guest molecule, does not possess enough room for complete encapsulation of a tetrahedral $R/ArNH_3^+$ guest i.e. the geometry of the crown ether does not support three N–H···O hydrogen bonds from the trigonal base of the ammonium tetrahedron. The $3AmPyH_2$ guest dication possesses two types of N–H bonds *viz*. the anilinium N–H and the pyridinium N–H bonds. In the crystal structure of compound **1**, the tetrahedral anilinium moiety of the guest interacts with the host unit through N2···O1 ($d_{N\cdots O}$ = 2.911(5) Å) and N2···O3 (d_{N-O} = 2.815(6) Å) non-covalent interactions and the pyridinium N–H bond of the guest is projected towards the cavity of another host molecule ($d_{N\cdots O}$ = 2.913(4)–3.051(4) Å). The two crown ethers are connected by C13···O7 ($d_{C\cdots O}$ = 3.454(5) Å) interaction. The third N–H bond of the tetrahedral anilinium moiety of the guest dication is involved in N–H···O interaction with a perchlorate counter anion (d_{N-O} = 2.875(4) Å).

The V–shaped guest molecules e.g. H_2O, $R/ArNH_2$ etc., which possess only two D–H bonds for hydrogen bonding interaction, have matching geometrical criterion for 12C4 and can form host-guest complexes through D–H···O hydrogen bonds with the two alternate oxygen atoms of 12C4. On the other hand, this crown ether uses only two oxygen acceptor atoms for hydrogen bonding with the guest molecules having a trigonal base e.g. H_3O^+, NH_3, $R/ArNH_3^+$ etc., and the involvement of another acceptor fragment becomes necessary for completion of the hydrogen bonding sphere around the guest. This is a common custom in the lattice of host-guest complexes concerning $R/ArNH_3^+$ guests in association with the 12C4 hosts. Nakamura group reported the complexation between dicyclohexyldimethanaminium cation and 12C4 electroneutralized with a Ni(II)–dithiolato complex (CSD code AJUPUQ) in which weak N–H···S contacts between the ammonium guests and the dithiolato complexes completed the hydrogen bonding sphere around the ammonium cations.[6a] The 2009 *CrystEngComm* article by Fonari and co-workers demonstrated supramolecular complexes of triphenylmethanaminium cation with

12C4 (CSD code WOPCOU) in which the crown ether interacted with the guest ammonium cation through only one N–H···O interaction, the two other N–H bonds of the

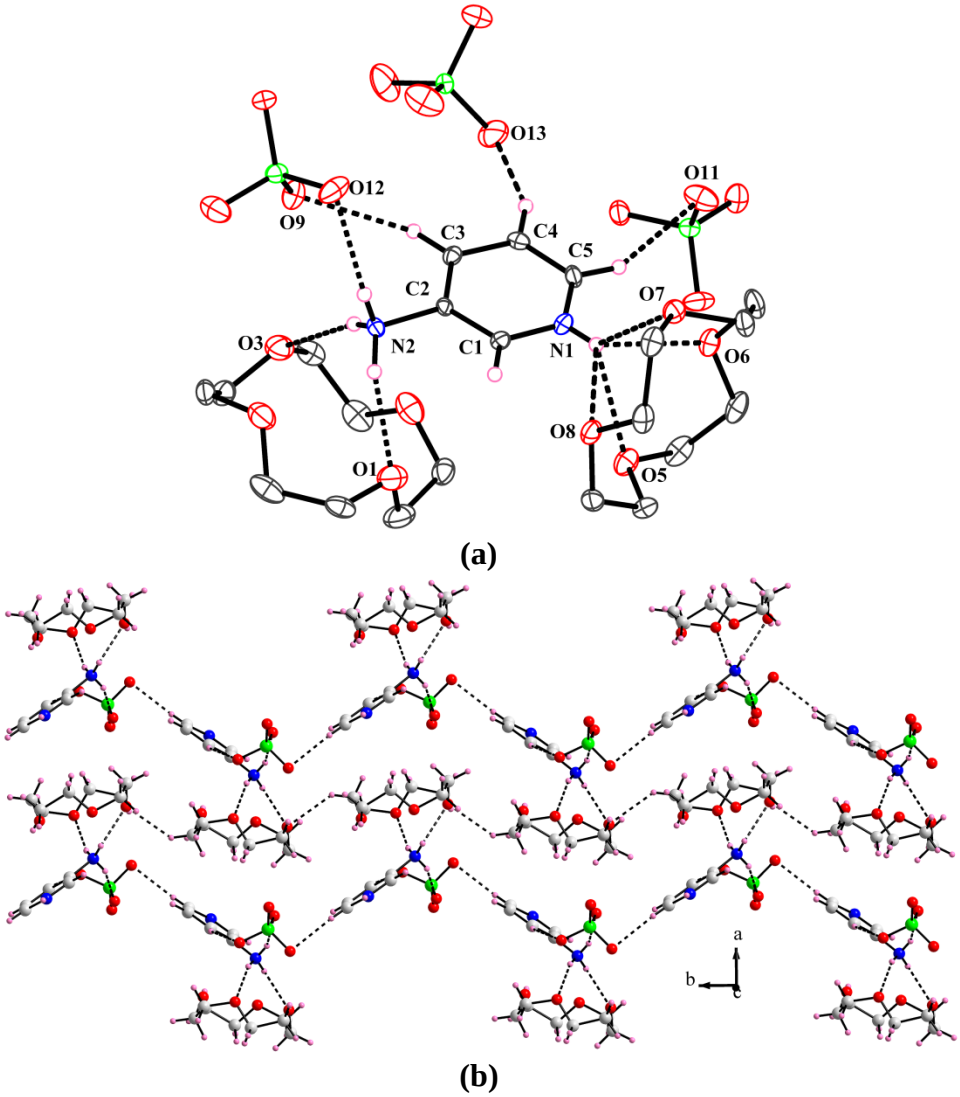

(a)

(b)

Figure 1. (a) Thermal ellipsoidal representation of the $3AmPyH_2$–12C4 host-guest adduct in compound **1** along with the most relevant hydrogen bonding interactions. The ellipsoids are set to 40% thermal distribution level. Symmetry operations for the equivalent acceptor atoms are described in Table 2. (b) Zig-zag chain-like packing in compound **1**. Only one crown ether has been shown for clarity.

tetrahedral guest is involved in N–H···S contact with two thiocyanate counter anions.[6b] Another report by Nakamura group registered N–H···O hydrogen bond between the doubly protonated 1,4–phenylenediamine and phosphomolybdate counter anion in the 1:2 supramolecular complex of the protonated diamine with 12C4 (CSD code TEQFUR).[8d] In

addition, the single crystal structure of the macrocycle 12C4 reported earlier, depicted the deviation of the four oxygen atoms of the crown ether from planarity.[15] However, in the crystal structure of compound **1**, the oxygen atoms of both the crown ether units are essentially almost coplanar as revealed by the deviation of the concerned atoms from the mean planes defined by the four oxygen atoms: O1, 0.0004 (2) Å; O2, –0.0004 (2) Å; O3, 0.0004 (2) Å and O4, –0.0004 (2) Å versus O5, –0.0120 (1) Å; O6, 0.0124 (1) Å; O7, –0.0123 (1) Å and O8, 0.0119 (1) Å respectively in the crown ethers bearing O1–O4 and O5–O8 atoms. This observation is in accord with the cases that reported involvement of two oxygen atoms of the crown ether for hydrogen bonding interaction with the ammonium guests,[6a–b] but not with the free crown ether[15] or the instances where the crown ether involved only one oxygen atom for the aforementioned purpose.[6c]

The O–C–C–O dihedral angles in both the 12C4 host units in the crystal structure of compound **1** are in the range of 60±3º (gauche) and the crowns adopt "– – – –" i.e. all–down conformation. The packing topology in the crystal of compound **1** is shown in Figure 1 which reveals a zig-zag chain-like assembly of the host-guest complexes mediated by the C–H···O hydrogen bonds between the $3AmPyH_2$ guests and the perchlorate counter anions, most notably, the C5···O11 ($d_{C\cdots O}$ = 3.266(5) Å) supramolecular contact (see Table 2).

Compound $[3AmPyH_2(B15C5)]_2(ClO_4)_4\cdot 2H_2O$ (2). Compounds **1** and **2**, comprising 12C4 and B15C5 respectively as the host molecules, include the same guest cation $3AmPyH_2$ in their respective crystals. π–stacking interactions involving the phenyl ring of B15C5 might arise in case of this crown ether and such a picture is indeed observed in the crystal lattice of compound **2**. Even though there are some reports describing complex formation between B15C5 and simple ammonium (NH_4^+) or organic ammonium $R/ArNH_3^+$ guests (see Table 1), the structural database pertaining to host-guest complexation between ammonium ion and B15C5 is relatively meager. Bond and Weakley separately reported two NH_4^+–B15C5 adducts which were crystallized with *bis*((μ_2–iodo)–diodo–Cd) (CSD code NASTAC) and nitrate (CSD code QOBJIA) counter anions respectively (see Table 1). In both cases, the crystals exhibited $P2_1/c$ space symmetrical arrangement of the counterparts, in which NH_4^+ was sandwiched (as a guest) between the two skew shaped crown ether hosts. In addition to NH_4^+ ion, organic ammo-

Table 2. Geometrical parameters for the hydrogen bonding interactions in 1–3.

D–H···A	*d*(D–H)	*d*(H···A)	*d*(D···A)	<(DHA)	Symmetry of A
		[3AmpyH$_2$(12C4)$_2$](ClO$_4$)$_2$ (1)			
C3–H3···O9	0.95	2.45	3.293(4)	148	x,–1+y,–1+z
C4–H4···O13	0.95	2.61	3.490(6)	155	1–x,–0.5+y,–z
C5–H5···O11	0.95	2.40	3.266(5)	152	1–x,–0.5+y,1–z
C18–H18A···O16	0.99	2.52	3.417(5)	150	x, –1+y,z
C20–H20B···O10	0.99	2.58	3.448(5)	147	1+x, –1+y, z
N2–H1NC···O1	0.92(5)	2.09(5)	2.911(5)	147(4)	1+x, y, z
N2–H1NB···O3	0.73(7)	2.12(7)	2.815(5)	161(7)	1+x, y, z
N2–H1NA···O12	0.85(6)	2.11(5)	2.875(5)	149(4)	x, –1+y, –1+z
		[3AmPyH$_2$(B15C5)]$_2$(ClO$_4$)$_4$·2H$_2$O (2)			
C32–H32···O22	0.95	2.23	3.125(7)	157	0.5x,0.5+y,0.5–z
C35–H35···O24	0.95	2.49	3.287(6)	142	0.5+x,0.5–y,0.5+z
C37–H37···O15	0.95	2.43	3.258(5)	146	0.5–x,–0.5+y,1.5–z
N1–H1NB···O8	0.83(5)	2.19(5)	2.980(6)	160(5)	–0.5+x, 0.5–y, –0.5+z
N1–H1NA···O10	0.95(7)	1.84(7)	2.780(6)	177(6)	–0.5+x, 0.5–y, –0.5+z
N1–H1NC···O22	0.86(9)	2.24(9)	2.959(6)	141(7)	Intramolecular
N1–H1NC···O23	0.86(9)	2.20(9)	2.845(7)	131(7)	Intramolecular
N2···O28	2.812(9)				0.5–x, –0.5+y, 0.5–z
N3–H3NB···O3	0.89(5)	2.11(5)	2.936(5)	153(4)	1–x, 1–y, 1–z
N3–H3NA···O5	0.83(5)	1.95(5)	2.770(4)	166(4)	1–x, 1–y, 1–z
N3–H3NC···O11	0.85(5)	2.10(5)	2.893(5)	155(4)	0.5–x, 0.5+y, 1.5–z
N4–H4N···O27	0.90(5)	1.84(5)	2.687(5)	155(4)	Intramolecular
		[3AmPyH$_2$(DB21C7)]$_3$(ClO$_4$)$_6$·5H$_2$O (3)			
C4–H4···O49	0.93	1.81	2.740(5)	173	x, 1+y, z
C14–H14···O33	0.93	2.40	3.258(5)	153	1–x, 1–y, 1–z
C15–H15···O21	0.93	2.57	3.277(4)	133	1–x, 1–y, 1–z
C15–H15···O32	0.93	2.60	3.293(5)	132	1–x, 1–y, 1–z
C39–H39···O27	0.93	2.57	3.381(5)	146	1–x, 1–y, 1–z
C41–H41···O41	0.93	2.56	3.426(4)	155	x, –1+y, z
C47–H47B···O22	0.97	2.65	3.562(4)	157	x, –1+y, 1+z
C47–H47A···O43	0.97	2.58	3.498(4)	157	1–x, 1–y, 2–z
C54–H54A···O23	0.97	2.60	3.551(4)	168	1–x, 1–y, 1–z
C58–H58B···O33	0.97	2.39	3.292(6)	155	1–x, 1–y, 1–z
C68–H68A···O40	0.97	2.51	3.460(5)	167	–x, 1–y, 1–z
C71–H71A···O29	0.97	2.60	3.430(4)	144	x, –1+y, z
C75–H75···O40	0.93	2.50	3.378(4)	158	1–x, 1–y, 1–z
C78–H78A···O32	0.97	2.41	3.354(5)	163	Intramolecular
N1–H1NA···O1	0.80(6)	2.45(6)	3.082(5)	137(5)	Intramolecular
N1–H1NC···O3	1.01(6)	1.87(6)	2.867(4)	168(5)	Intramolecular
N1–H1NB···O5	0.86(7)	2.33(7)	2.999(5)	135(5)	Intramolecular
N1–H1NA···O7	0.80(6)	2.40(6)	3.030(5)	137(5)	Intramolecular
N3–H3NA···O10	0.97(4)	1.90(4)	2.829(4)	162(3)	Intramolecular
N3–H3NB···O12	0.94(6)	2.13(6)	2.948(4)	144(4)	Intramolecular
N3–H3NC···O14	0.98(5)	1.87(5)	2.832(4)	166(4)	Intramolecular
N4–H4N···O26	0.99(5)	1.94(5)	2.852(4)	153(4)	1–x, 1–y, 1–z

Table 2. Continued...

N5–H5NB···O17	0.88(4)	2.03(4)	2.889(4)	165(4)	1–x, 1–y, 1–z
N5–H5NC···O19	0.96(5)	2.17(5)	2.946(4)	138(4)	1–x, 1–y, 1–z
N5–H5NA···O21	0.97(4)	1.82(5)	2.775(4)	169(4)	1–x, 1–y, 1–z
N6–H6N···O44	0.82(4)	2.11(4)	2.870(4)	154(3)	Intramolecular

-nium ions were also integrated with B15C5. Kryatova *et al.* reported the adduct formation of B15C5 with phenylmethanaminium (CSD code AWUYEW) and 1,4–phenylenedimethanaminium (CSD code AWUYIA) cations (see Table 1) in which the ammonium group interacted with the host using two N–H bonds and the ethereal host adopted a skewed geometry. A very similar structural feature is observed in the crystal of compound **2** which crystallizes as a hydrate and its X-ray structural analysis reveals the formulation to be $[3AmPyH_2(B15C5)]_2(ClO_4)_4\cdot 2H_2O$ i.e. 1:1 complexation between the guest and the host. Two symmetry independent supramolecular complexes are found in the asymmetric unit of compound **2** with one water molecule per formula unit. Analogous to compound **1**, the guest in compound **2,** is integrated with the crown ether cavity through two N–H···O contacts ($d_{N\cdots O}$ = 2.769(6)–2.980(5) Å) using the Ar–NH_3^+ functionality and the third N–H bond interacts with the counter anion ($d_{N\cdots O}$ = 2.892(4)–2.960(8) Å). The lattice water molecules are also found to be involved in non-covalent interactions and are bonded with the guest dications (N–H···O) through the pyridinium fragment ($d_{N\cdots O}$ = 2.687(5)–2.813(9) Å) and with two perchlorate counter anions ($d_{O\cdots O}$ = 2.821(6)–2.936(4) Å) through the O(water)–H···O(perchlorate) hydrogen bonds (see Table 2). The guest dication is further connected to a perchlorate counter anion through C–H···O interaction ($d_{C\cdots O}$ = 3.125(6)–3.289(5) Å). For a convenient and handy structural description, the two crown polyethers have been tagged A and B in Figure 2. In contrast to 12C4, in which all the acceptor heteroatoms are bonded with sp^3 carbon atoms, the host B15C5 comprises two types of oxygen atoms *viz*. the catechol oxygen atoms (bonded with the phenyl ring) and the glycolic oxygen atoms (bonded with the sp^3 carbon atoms). The C(Ar)–O, C(sp^3)–O, C(Ar)–C(Ar) and C(sp^3)–C(sp^3) bond lengths of the two crown ether units A and B in the crystal structure of compound **2** are observed to be in the range 1.362–1.381 Å, 1.423–1.441 Å, 1.363–1.402 Å and 1.481–1.508 Å respectively. The macrocycles A and B are significantly puckered to different extents as exemplified by the disparate degrees of deviation of the acceptor heteroatoms from the

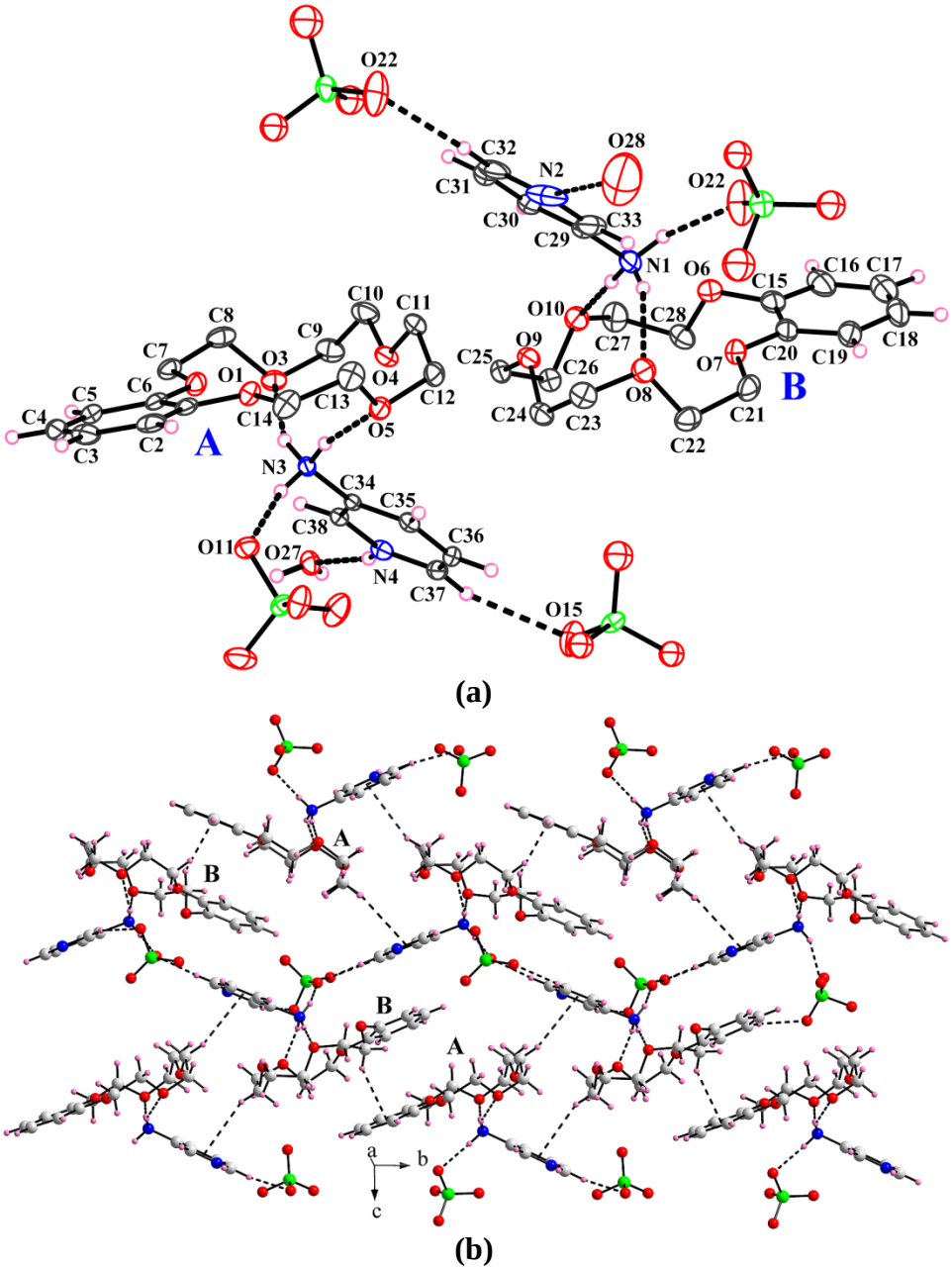

Figure 2. (a) ORTEP (40%) view of the two symmetry independent host-guest adducts in the crystal structure of compound **2** showing the hydrogen bonding environment around the $3AmPyH_2$ guest dication. Symmetry codes for the acceptor atoms are presented in Table 2. Hydrogen atoms on the aliphatic carbon atoms of the crown ethers have been excluded for clarity. (b) A portion of crystal packing featuring diverse supramolecular contacts in the lattice viewed perpendicular to the *bc* plane of the unit cell. Hydrogen bonding and the C–H···π stacking interactions are shown by black dashed lines. The lattice water molecules have been omitted for clarity.

mean plane defined by them. For the crown ether A, these values are observed to be O1, –0.1492(2) Å; O2, –0.0631(2) Å; O3, 0.2631(2) Å; O4, –0.3635(2) Å and O5, 0.3127(2)

Å and for the polyether B as O6, –0.2317(2) Å; O7, 0.2510(3) Å; O8, –0.1395(3) Å; O9, –0.0153(2) Å and O10, 0.1356(2) Å. In addition, dissimilar perching distance of the anilinium groups from the mean macrocycle planes has been observed in the two host-guest adducts, 1.7392(4) Å concerning crown ether A *vs* 1.6752(4) Å in case of the adduct involving unit B. As can be seen in Figure 2, the packing feature of compound **2** bears a two dimensional sheet-like topology.

Compound $[3AmPyH_2(DB21C7)]_3(ClO_4)_6\cdot5H_2O\cdot0.5CH_3CN$ (3). The small crown ethers *viz.* 12C4, 15C5 or related derivatives cannot completely accommodate a guest ammonium cation within their cavities because of room paucity factor whereas the higher homologues e.g. 18C6, 21C7, 24C8 or related derivatives having profuse space can accomplish so. To gain insight into the structural outcome upon altering the cavity dimension of the host from a small to a larger and flexible one, we made use of DB21C7 to be the host for $3AmPyH_2$ dication. Supramolecular chemistry of the macrocycle DB21C7 has relatively been less explored and to the best of our knowledge, there are only a few structural entries associated with the coordination or hydrogen bonded complexes of the concerned crown ether.[8i,16] Under ideal circumstances, this crown polyether possesses a mirror symmetry passing through the oxygen atom in between two catechol units and the opposite $C(sp^3)$–$C(sp^3)$ bond. The complexation with tetrahedral guest systems (e.g. ammonium etc.) occurs through three alternate O heteroatoms of the host, which typically adopts a bowl shape after the molecular recognition process. Stoddart and co-workers reported the second–sphere coordination of this crown ether to the η^4–(1,5–COD) complex of rhodium through the recognition of coordinated ammonia (NH_3) in its cavity.[8i] Pursiainen and co-workers demonstrated chiral architecture in packing of the supramolecular adduct of DB21C7 and protonated imidazole.[16c] Replacing the planar five membered imidazolium cation with the six memberd planar guest cation $3AmPyH_2$ having a perching $–NH_3^+$ group gives compound **3**. Crystallographic analysis on this compound shows the formation of a hydrate and the formulation of the relevant solid as $[3AmPyH_2(DB21C7)]_3(ClO_4)_6\cdot5H_2O\cdot0.5\ CH_3CN$ (**3**). The structure is found to be rather complicated and consists of three symmetry independent host-guest adducts, all the three maintaining 1:1 stoichiometry. The crown ether essentially houses the anilinium moiety through N–H···O hydrogen bonds ($d_{N\cdots O}$ =

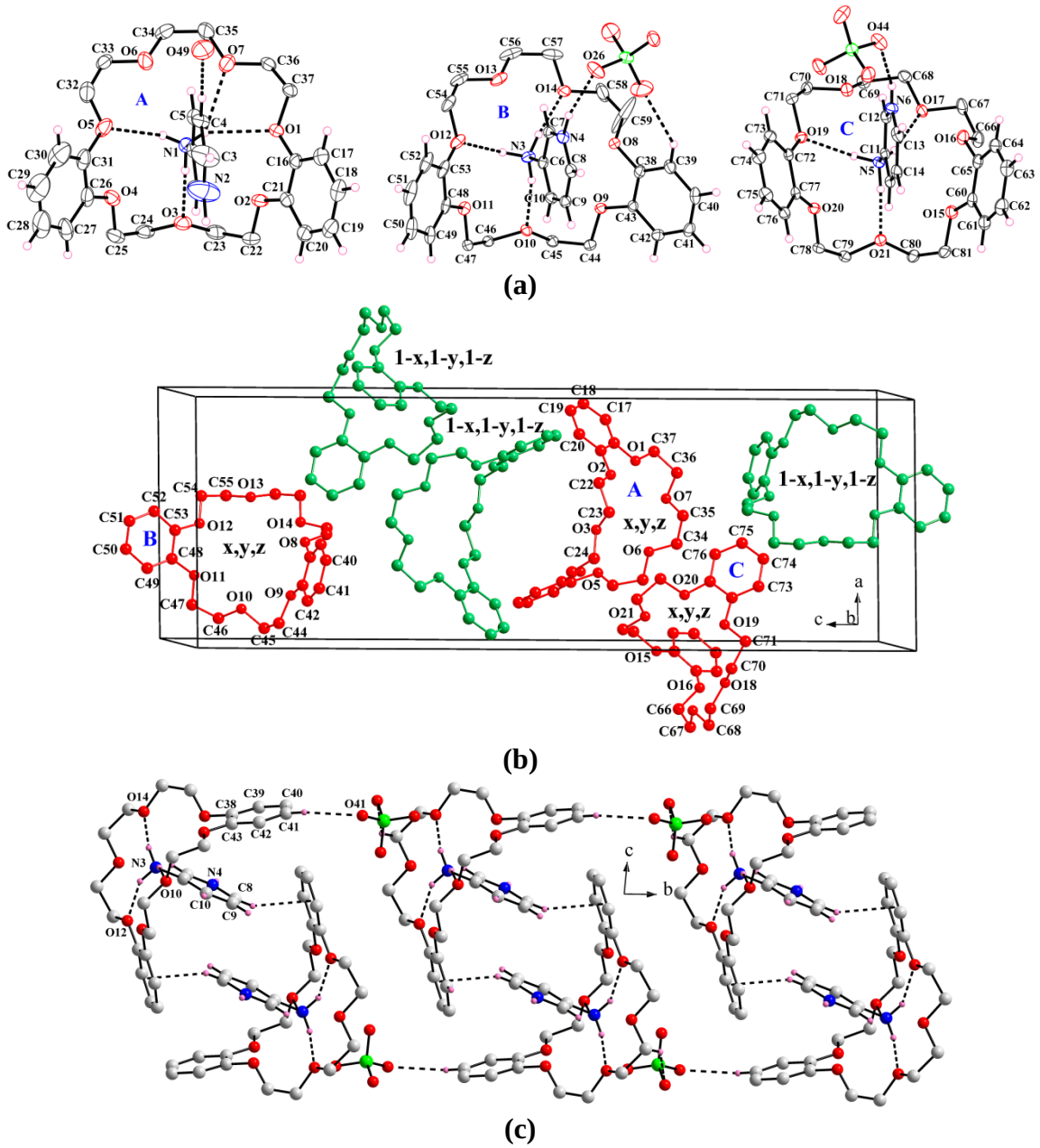

Figure 3. (a) Structure of the three symmetry independent 3AmPyH$_2$–DB21C7 host-guest adducts in the crystal structure of compound **3** in 40% thermal ellipsoidal level. Table 2 describes the symmetry operations for generating the equivalent acceptor atoms. The aliphatic hydrogen atoms of the crown ethers have been omitted to gain viewing lucidity. (b) Orientation of the three host units named as A-C and their inversion partners in the unit cell. The x,y,z equivalents are colored as red and the –x,–y,–z equivalents are colored as green. Chain-like packing topology in compound **3** viewed parallel to the crystallographic 011 plane.

2.775(4)–2.948(4) Å) involving all the three available anilinium N–H bonds of the guest. Geometrical parameters for these supramolecular contacts are presented in Table 2. The

involvement of perchlorate counter anion to saturate the N–H···O hydrogen–bonding possibilities around the guest anilinium moiety, as described for the crystal structures of compounds **1**–**2**, is therefore irrelevant in the structure of compound **3**. The structure of the three symmetry independent $3AmPyH_2$–DB21C7 adducts, as located in the asymmetric unit of compound **3**, is shown in Figure 3, in which the three crown ether units are named as A (O1–O7), B (O8–O14) and C (O15–O21). In contrast to the previous two structures (compounds **1**–**2**), compound **3** crystallizes rather with an elongated unit cell vector (*c* =34.277(2) Å). The cell filling pattern of the three crown ether units together with their inversion partners along this long axis is shown in Figure 3b. The guest dication interacts with the crown ether unit A through two direct N–H···O interactions (N1–O3 and N1–O5) and one bifurcating N–H···O interaction whereas the perching of the guest into the cavity of the crown ether units B and C takes place through three direct N–H···O contacts (see Table 2). As described for B15C5 in the crystal structure of compound **2**, the DB21C7 host in the crystal structure of compound **3** bears two different types of acceptor heteroatoms *viz.* the catechol and the glycolic oxygen atoms. The C(Ar)–C(Ar) bond distances in the three symmetry independent crown ether units A, B and C are observed to be in the range 1.350–1.397, 1.379–1.404 and 1.379–1.392 Å respectively and the $C(sp^3)$–$C(sp^3)$ bond lengths to be in the range 1.455–1.495, 1.474–1.495 and 1.488–1.509 Å respectively for the host units A, B and C. The various C(Ar)–O and $C(sp^3)$–O bond lengths of the three crown ether units in the crystal structure of compound **3** are found to be in the range 1.365–1.382 and 1.378–1.431 Å, 1.366–1.375 and 1.415–1.442 Å, and 1.373–1.383 and 1.422–1.444 Å for A, B and C respectively. In all the three symmetry independent adducts, the guest cation orients almost parallel to the mirror symmetry of the crown ether, which in turn attains a *quasi*–C_s conformation. Similarly, the bending of the crown ether towards the pyridine ring makes the host bowl shaped, the extent of bending being different in the three adducts. The involvement of the lattice water molecules in the hydrogen bonding interactions along with the presence of three symmetry independent host-guest adducts attribute a very complicated three dimensional crystal packing feature. However, a view of the chain-like assembly in the relevant crystal is shown in Figure 3c. Two inversion symmetry related host-guest complexes form a supramolecular dimer through C–H···π stacking interactions between

the pyridine rings and the phenyl rings of the crown ethers ($d_{C\cdots Cg}$ = 3.304(4), <C–H···Cg = 142 °). These dimers are further connected with the perchlorate anions by the C–H···O interactions ($d_{C\cdots O}$ = 3.426(5) Å) parallel to the crystallographic *b*-axis (see Figure 3).

Compound $[DADPMH_2(12C4)]_2(ClO_4)_4\cdot H_2O$ (4). The crown ether based host-guest complexes, discussed so far (compounds **1**–**3**), consist of the planar guest molecule $3AmPyH_2$ in which the two hydrogen bond donor sites i.e. the anilium and pyridinium functionalities are at 120° angular separation. It has been observed that the anilinium moiety of the guest interacts with the crown ether cavity, whereas the pyridinium moiety is involved in N–H···O hydrogen bonding interaction with other acceptor species in the crystal. As such, we were interested in examining the structural scenario of the crown ether based host-guest systems incorporating guests having two ammonium functionalities in an angular and non-planar orientation. Therefore, the next four compounds to be discussed, consist of doubly protonated DADPE and DADPM i.e. $DADPEH_2$ and $DADPMH_2$ as the guests in which the two anilinium functionalities are connected by an ethereal and a methylene spacer respectively. The cocrystal formation by the relevant neutral diamines with the *bis*–phenol coformers was demonstrated by Desiraju, Howard and co-workers (the concerned authors had shown their preference to use the term 'molecular complex' over 'cocrystal').[13] Both DADPE and DADPM and the Schiff bases derived from them were used as coordinating ligands for transition metals.[17] However, associated structural entries in the realm of supramolecular non-covalent interactions are meager [13,18] and to the best of our knowledge, there is no report, which demonstrates host-guest complexation between the crown ethers and these diamines.[14] Several attempts to cocrystallize the neutral diamines *viz*. DADPE and DADPM with the crown ethers failed. Thus, the doubly protonated diamines i.e. $DADPMH_2$ and $DADPEH_2$ have been used as the guest molecular cations to the crown ether hosts in the present work.

The structural characterization of compound **4** reveals a 1:1 stoichiometry between the diammonium guest and the crown ether host (12C4) irrespective of the amount of the reactants used in the synthesis. Although, 1:2 stoichiometric ratio between the guest and the host was anticipated, the solid state characterization sets the formulation of compound **4** as $[DADPMH_2(12C4)]_2(ClO_4)_4\cdot H_2O$ which crystallizes as a hydrate in $P2_1/c$ space sy-

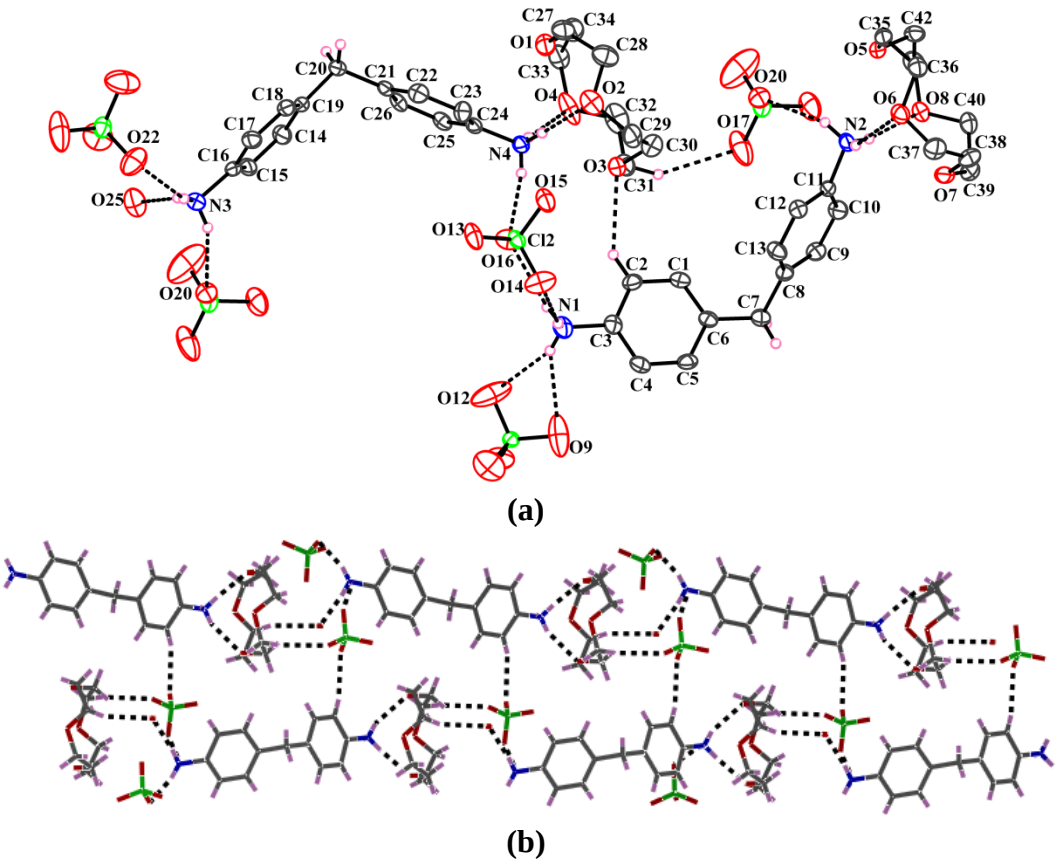

(a)

(b)

Figure 4. (a) ORTEP representation (40%) of the two symmetry independent $DADPMH_2$ –(12C4) supramolecular complexes in the crystal structure of compound **4** with the hydrogen bonding ambience of the ammonium cations. (b) Formation of supramolecular chains through several non-covalent interactions in the lattice of compound **4**.

-mmetry. Two symmetry independent host-guest complexes are located in the relevant crystal in which the two guests adopt different conformations as far as the orientation of the two phenyl rings is concerned. The guest cations interact with the crown ethers using two N–H bonds ($d_{N\cdots O}$ = 2.835(5)–2.880(6) Å). These distances are shorter than the N(ammonium)···O(perchlorate) distances ($d_{N\cdots O}$ = 2.941(6)–3.016(6) Å) between the ammonium ions and the perchlorate counter anions which fulfill the hydrogen bonding surrounding of the ammonium cations. Similarly, the other ammonium end of the guests also interact with the counter anions or with the lattice water molecule ($d_{N\cdots O}$ = 2.693(6)–3.099(6) Å). The geometrical parameters of these interactions are summarized in Table 3. Thus, the ammonium–crown ether interaction scenario is very similar to those involving 12C4 as the host unit in the sense that a perchlorate counter anion is required to saturate the hydrogen bonding ambience of the $-NH_3^+$ functionality. The oxygen atoms of both

the crown ether units are almost in the mean plane defined by the four oxygen atoms indicating almost coplanar arrangement of the four oxygen heteroatoms in the crown ethers. Both the crown ether units in the crystal structure of compound **4** adopt gauche "– – – –" conformation with the O–C–C–O dihedral angles in the range of 60±6º for the macrocycle consisting of O1–O4 heteroatoms and 60±1º for the crown ether unit comprising O5–O8 heteroatoms. A chain-like packing topology is observed in the crystal lattice as shown in Figure 4.

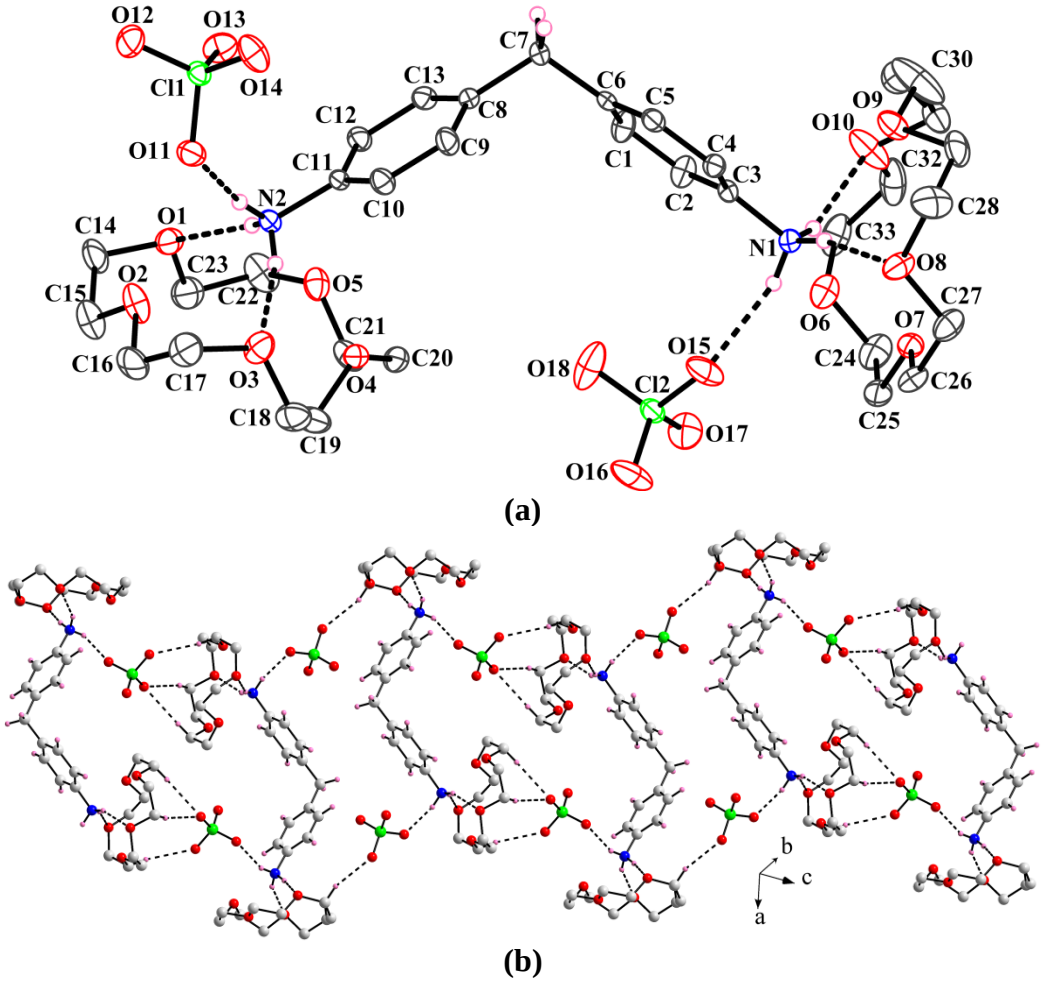

Figure 5. (a) Crystal structure of compound **5** in 40% thermal ellipsoidal representation. The hydrogen atoms have been omitted for clarity. (b) A portion of crystal packing showing various supramolecular interactions in the lattice.

Compound $[DADPMH_2(15C5)_2](ClO_4)_2$ (5). The macrocycle 15C5 is the next higher homologue of 12C4 in the crown ether family. The smaller guests like amine ($–NH_2$) and H_2O, possessing V–shaped geometry are very good partners for 15C5. However, the

cavity dimension of the concerned crown ether is not large enough for complete encapsulation of a tetrahedral guest cation, i.e. the ammonium ion. As a result, longer N(ammonium)···O(crown ether) separation is usually observed in the crystal structures based on host-guest complexes of 15C5 with ammonium cations. An interesting example reported by Rogers and co-workers, demonstrated an NH_4^+ ion sandwiched by two 15C5 hosts, each of the two ethereal units forming two O···H–N bridges with two N–H bonds of the guest cation (CSD code GARLUG).[10l] Three other R/Ar–NH_3^+···15C5 supramolecular systems are also known, in which all the three N–H bonds of the guest cation are hydrogen bonded (N–H···O) with the 15C5 host (CSD code AJUPEA,[6a] TOLRES and TEQFIF01[8d]) and thus involvement of any other counter species (as described in compound **1**) to saturate the hydrogen bonding possibilities of the guest is precluded. However, in the crystal structure of compound **5,** a different type of binding mode has been observed between the ammonium guest and the 15C5 host. An alteration of the crown ethers from the smaller 12C4 to the larger 15C5 reveals a 1:2 stoichiometry between the $DADPMH_2$ guest and the crown ether hosts in compound **5**. The crystal structure of compound **5** exhibits the formulation of the concerned solid as [$DADPMH_2$ $(15C5)_2$]$(ClO_4)_2$ i.e. two hydrogen bonded crown ether hosts per formula unit. The compound **5** crystallizes in triclinic centrosymmetric space group i.e. $P\bar{1}$ with one gross diperchlorate salt of the host-guest complex in the asymmetric unit. The guest dication, in compound **5**, has two crown ether anchoring ammonium ends in its structure, unlike that of compound **4**, and this attachment originates from N–H···O interactions. Each of the two macrocyclic host units in the pertinent solid uses two alternate oxygen acceptor heteroatoms to interact with the ammonium guest moieties and the corresponding donor to acceptor separations (N···O) are found to be in the range 2.855–2.948 Å and 2.906–2.972 Å. The geometrical parameters for the pertinent hydrogen bridges in the crystal structure of compound **5** are collected in Table 3. As the 15C5 host units in the crystal structure of compound **5** is hydrogen bonded with only two N–H bonds of the guest functionalities, involvement of the perchlorate counter anions is required in order to saturate the hydrogen bonding ambience around the guest ammonium cation. The corresponding N(ammonium)···O(perchlorate) distances are found to be in the range 2.831–2.881 Å which are shorter than the relevant N(ammonium)···O(crown ether) dista-

Table 3. Geometrical parameters for the hydrogen bonding interactions in 4–7.

D–H···A	*d*(D–H)	*d*(H···A)	*d*(D···A)	<(DHA)	Symmetry of A
		[DADPMH$_2$(12C4)]$_2$(ClO$_4$)$_4$·H$_2$O (4)			
C18–H18···O19	0.95	2.40	3.300(5)	157	1–x, 1–y, –z
C25–H25···O18	0.95	2.43	3.241(6)	143	–1+x, y, z
C31–H31A···O17	0.99	2.49	3.359(6)	146	1–x, –0.5+y, 0.5–z
C31–H31B···O21	0.99	2.55	3.384(6)	142	x, 0.5–y, –0.5+z
C34–H34A···O25	0.99	2.46	3.338(7)	147	Intramolecular
C36–H36A···O13	0.99	2.54	3.511(5)	167	Intramolecular
C37–H37A···O15	0.99	2.64	3.621(6)	171	1–x,0.5+y,0.5–z
C38–H38B···O9	0.99	2.58	3.409(7)	142	1–x,0.5+y,0.5–z
C41–H41B···O23	0.99	2.53	3.502(7)	167	x, 0.5–y, –0.5+z
N1–H1NA···O9	0.83(7)	2.52(7)	3.245(8)	147(5)	x,1.5–y,0.5+z
N1–H1NA···O12	0.83(7)	2.25(7)	3.023(7)	157(6)	x,1.5–y,0.5+z
N1–H1NB···O14	0.90(6)	2.03(6)	2.842(5)	150(5)	Intramolecular
N2–H2NA···O6	0.81(4)	2.15(5)	2.835(5)	142(4)	x, –1+y, z
N2–H2NB···O8	0.81(5)	2.04(6)	2.835(5)	165(5)	x, –1+y, z
N2–H2NC···O20	0.86(5)	2.22(6)	3.016(6)	155(4)	1–x,–0.5+y,0.5–z
N3–H3NB···O20	0.81(7)	2.25(7)	2.952(5)	145(6)	1–x,0.5+y,0.5–z
N3–H3NC···O22	0.83(8)	2.25(9)	2.997(6)	150(7)	x,1+y,–1+z
N3–H3NA···O25	0.84(4)	1.86(4)	2.693(6)	168(3)	x,1+y,z
N4–H4NB···O2	0.86(6)	1.99(6)	2.850(5)	175(5)	Intramolecular
N4–H4NC···O4	0.78(5)	2.13(5)	2.879(5)	160(5)	Intramolecular
		[DADPMH$_2$(15C5)$_2$](ClO$_4$)$_2$ (5)			
C16–H16B···O5	0.99	2.60	3.516(4)	154	–1+x, y, z
C16–H16A···O17	0.99	2.59	3.555(5)	166	1–x, 1–y, 1–z
C21–H21B···O16	0.99	2.58	3.560(4)	172	1–x, 1–y, 1–z
C33–H33B···O18	0.99	2.63	3.494	146	1+x, –1+y, z
N1–H1NB···O8	0.90(4)	1.99	2.855	167	Intramolecular
N1–H1NA···O10	0.89(5)	2.14	2.948	152	Intramolecular
N1–H1NC···O15	0.82(4)	2.05	2.831	157	x, –1+y, z
N2–H2NB···O1	0.88(4)	2.15	2.972	158	–1+x, y, –1+z
N2–H2NA···O3	0.90(4)	2.08	2.906	159	–1+x, y, –1+z
N2–H2NC···O11	0.83(4)	2.04	2.881	165	–1+x, y, z
		[DADPMH$_2$(18C6)$_2$]$_2$(ClO$_4$)$_4$·6H$_2$O·MeCN (6)			
C18–H18···O41	0.95	2.59	3.536(4)	174	Intramolecular
C28–H28B···O38	0.99	2.49	3.412(5)	155	1–x, 1–y, 1–z
C32–H32A···O32	0.99	2.64	3.590(5)	161	1–x, 1–y, 1–z
C41–H41A···O30	0.99	2.48	3.322(5)	142	1.5–x,–0.5+y,0.5–z
C61–H61A···O36	0.99	2.58	3.453(5)	147	1+x, y, z
C67–H67B···O38	0.99	2.54	3.430(5)	150	Intramolecular
N1–H1NA···O1	0.89(5)	2.02(5)	2.912(4)	173(4)	Intramolecular
N1–H1NB···O3	0.76(5)	2.13(5)	2.886(5)	171(5)	Intramolecular
N1–H1NC···O5	0.85(5)	1.99(5)	2.838(4)	173(4)	Intramolecular
N2–H2NB···O19	0.75(5)	2.11(5)	2.859(4)	175(5)	1+x, y, 1+z
N2–H2NA···O21	0.90(5)	2.02(5)	2.916(4)	174(4)	1+x, y, 1+z
N2–H2NC···O23	0.85(5)	2.04(5)	2.829(4)	156(4)	1+x, y, 1+z

Table 3. Continued...

N3–H3NB···O7	0.71(5)	2.17(6)	2.870(5)	174(5)	Intramolecular
N3–H3NA···O9	0.68(5)	2.15(6)	2.826(4)	174(6)	Intramolecular
N3–H3NC···O11	0.98(6)	1.95(6)	2.930(4)	176(5)	Intramolecular
N4–H4NB···O14	0.74(5)	2.14(5)	2.840(5)	160(5)	–1+x, y, z
N4–H4NC···O16	0.82(6)	2.07(6)	2.875(4)	167(5)	–1+x, y, z
N4–H4NA···O18	0.81(4)	2.06(5)	2.863(4)	171(4)	–1+x, y, z
$[DADPEH_2(18C6)_2](ClO_4)_2 \cdot 2MeCN$ (7)					
C5–H5···O20	0.95	2.53	3.404(3)	153	Intramolecular
C16–H16A···O14	0.99	2.62	3.575(3)	161	x, 1+y, z
C17–H17A···O21	0.99	2.58	3.517(3)	157	x, 1+y, z
C29–H29A···O18	0.99	2.50	3.335(3)	142	–x, 1–y, 1–z
C33–H33A···O16	0.99	2.35	3.237(3)	148	1–x, –y, 1–z
N1–H1NA···O3	0.88(3)	2.01(3)	2.893(2)	178(3)	x, –1+y, z
N1–H1NB···O5	0.89(3)	1.97(3)	2.827(2)	164(2)	x, –1+y, z
N1–H1NC···O7	0.92(3)	1.96(3)	2.873(2)	170(2)	x, –1+y, z
N2–H2NA···O8	0.91(3)	1.94(3)	2.839(2)	172(2)	Intramolecular
N2–H2NC···O10	0.93(3)	1.92(3)	2.848(2)	175(3)	Intramolecular
N2–H2NB···O12	0.90(3)	2.03(3)	2.925(2)	172(2)	Intramolecular

-nces. The two host units in the crystal structure of compound **5** are found to be puckered to different extents as indicated by the deviation of the five oxygen atoms of the crown ethers from the mean plane defined by them. For the crown ether containing O1–O5 oxygen atoms, these values are found to be O1, 0.1174 Å; O2, –0.1963 Å; O3, 0.1987 Å; O4, –0.1286 Å and O5, 0.0089 Å while the N2 ammonium ion is located 1.7109 Å away of this mean plane. Similarly, the deviation of the oxygen heteroatoms from the mean {O5} plane in the crown ether consisting of O6–O10 oxygen atoms are found to be O6, –0.4512; O7, 0.4927; O8, –0.2901; O9, –0.0089 and O10, 0.2575 Å while the N1 ammonium functionality is located 1.6849 Å away from this mean plane. The C–C and C–O bond lengths for the two crown ether units are found to be in the range 1.449–1.511, 1.463–1.498 and 1.401–1.489, 1.414–1.457 Å respectively. The O–C–C–O torsion angles in both the crown ether units are found to be gauche 60±6º and the conformation of the crown ethers are observed to be "+ + + + –" for the O1–O5 host and as "+ + + – –" for the O6–O10 host. The dihedral angle between two phenyl rings of the $DADPMH_2$ guest is +77º and the various bond lengths of the guest are observed as follows: C(Ar)–C(Ar) 1.370–1.391 Å, C(Ar)–C(methylene) 1.512–1.517 Å and C(Ar)–N(ammonium) 1.461–1.462 Å. The basic supramolecular interactions and the packing topology of compound **5**

are pictorially presented in Figure 5b which clearly portrays the differences in hydrogen bonding environment at the two opposite faces of the host polyethers. As demonstrated in the previously described structures (compounds **1**–**4**), the general supramolecular interactions of the crown ether hosts with the guests involve D–H···O (D = donor) interaction using the electronegative oxygen heteroatoms of the macrocycle which in turn acts as the hydrogen bonding acceptor and C–H···A (A = acceptor) interaction with another acceptor moiety in the lattice, the macrocycle acting as a weak hydrogen bonding donor. The involvement of the various C–H···O and N–H···O contacts in the crystal lattice leads to a chain-like arrangement as shown in Figure 5.

Compound $[DADPMH_2(18C6)_2]_2(ClO_4)_4\cdot 6.75H_2O\cdot CH_3CN$ (6). 18C6 is the most studied and popular host among the known crown ethers and the direct consequence of this fact is the large number of structural entries in CSD. Till date, a diverse class of guest systems have been incorporated into the 18C6 cavity and the chemistry associated with this crown ether includes first and second–sphere coordination of the macrocycle to the alkali or transition metals,[19–20] host-guest complexation with R/Ar–NH_2 systems, ammonium compounds etc.[21] The crystal structure of the free crown ether is also reported.[22]

$DADPMH_2$ undergoes complexation with 18C6 in a 1:2 stoichiometric ratio between the guest and the host in compound **6** which crystallizes as a mixed water–acetonitrile solvate in monoclinic centric $P2_1/n$ space symmetry. The concerned asymmetric unit consists of two $DADPMH_2(18C6)_2$ supramolecular complexes, four perchlorate counter anions, six water molecules and an acetonitrile solvent molecule. The ammonium ends of the guest dications incorporate in the crown ether cavity through three N–H···O interactions involving three alternate oxygen acceptor heteroatoms of the host ($d_{N\cdots O}$ = 2.826(4)–2.930(4) Å). The donor (ammonium) to acceptor (crown ether) distances for these hydrogen bridges are summarized in Table 3. The various bond lengths of both the symmetry independent guest dications are found to be almost similar and are observed as follows: C(Ar)–C(Ar) 1.378–1.405 Å, C(Ar)–C(methylene) 1.503–1.523 Å and C(Ar)–N(ammonium) 1.463–1.466 Å. The four crown ether units in the crystal structure of compound **6** adopt *quasi–*D_{3d} "+ – + – + –" conformation as revealed by the O–C–C–O torsion of 60±6–7º (gauche) and C–O–C–C dihedral angle of *ca*. 180±3–5º. The C–C and

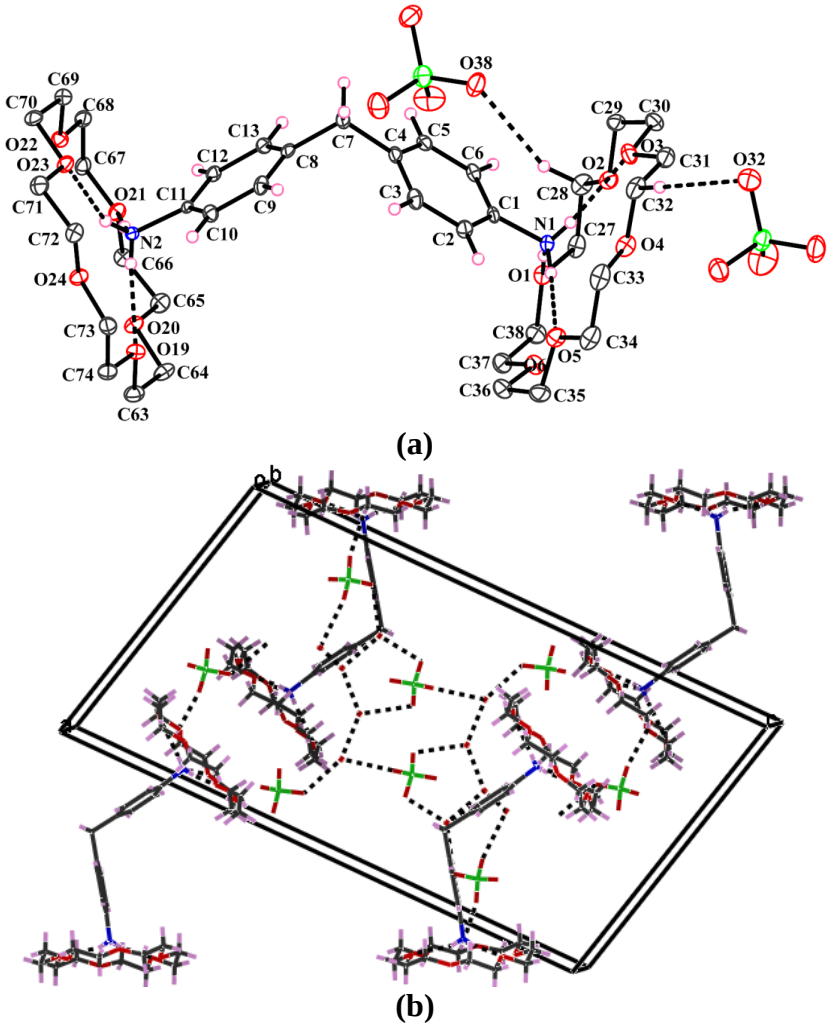

Figure 6. (a) Thermal ellipsoidal representation (40%) of one of the symmetry independent $DADPMH_2$–(18C6) supramolecular complexes in the crystal structure of compound **6**. (b) Hydrogen bonded assembly in compound **6**.

C–O bond lengths of the four crown ethers are almost similar and observed in the range 1.48–1.50 and 1.41–1.43 Å respectively. The N1, N2 and N3, N4 ammonium functionalities of the guest dications are displaced by 0.940, 0.848 and 0.938, 0.604 Å respectively from the mean plane defined by the six oxygen atoms of the crown ethers with which they are hydrogen bonded. Apart from the N–H···O interactions between the ammonium cations and the crown ethers, the C–H···O interactions between the crown ethers and the perchlorate counter anions are also prevalent in the crystal (see Table 3). The lattice water molecules are found to be involved in extensive supramolecular interactions with the various counterparts. A view of packing of the host-guest complexes in compound **6** is shown in Figure 6.

Compound $[DADPEH_2(18C6)_2](ClO_4)_2\cdot 2CH_3CN$ (7). In compound **7**, the guest is $DADPEH_2$, which is similar to $DADPMH_2$, possessing an angular geometry, the only difference being the sp^3 ethereal (–O–) spacer between the two phenyl rings in the former dication as compared to the methylene ($–CH_2–$) spacer in the latter. As a result, analogous to compound **6**, a similar type of host-guest complexation was expected in case of compound **7**, which actually is the case as observed through X-ray diffraction. Our failure to grow single crystal X-ray diffraction quality solids with smaller crown ethers *viz.* 12C4 and 15C5 as the hosts and $DADPEH_2$ as the guest restrained us from drawing a complete structural comparison with the two different sets of data. However, with 18C6, $DADPEH_2$ forms a supramolecular complex (compound **7**) with a 2:1 stoichiometry between the host and the guest. Compound **7** crystallizes as an acetonitrile solvate and the crystal structure of the relevant perchlorate salt evaluates the formulation of compound **7** as $[DADPEH_2(18C6)_2](ClO_4)_2\cdot 2CH_3CN$. This compound maintains packing of the pertinent formula units in triclinic centrosymmetric space group i.e. $P\bar{1}$ and the asymmetric unit of the crystal structure comprises one gross formula unit and two acetonitrile solvent molecules. Both the ammonium ends of the guest dication perch into the crown ether cavity through three N–H···O hydrogen bonds with the three alternate oxygen atoms of the crown ether. The corresponding N1(ammonium)···O(crown ether) and N2(ammonium)···O(crown ether) distances are observed to be in the range 2.827–2.893 and 2.839–2.925 Å respectively (see Table 3). The C–C and C–O bond distances of the two crown ether hosts containing the O2–O7 and O8–O13 oxygen heteroatoms are observed in the range 1.489–1.496, 1.421–1.433 and 1.495–1.503, 1.419–1.441 Å respectively. Similarly, both the crown ethers in the crystal structure of compound **7** adopt very symmetrical "+ – + – + –" conformation with O–C–C–O and C–O–C–C torsions of about 60±8º and 180±9º respectively. The various geometrical parameters of the guest dication are observed as follows: C(Ar)–C(Ar) 1.380–1.389, C(Ar)–O 1.386–1.399 and C(Ar)–N(ammonium) 1.465–1.471 Å. Therefore, the basic host-guest scenario in both the crystal structures of compound **6** and **7** is almost identical. Although varying the guest leads to alteration of space symmetry, the issue is not very straightforward as the relevant host-guest complexes (compounds **6** and **7**) are isolated as solvates in different extents. The role of solvent molecules (water or acetonitrile) is not only found to

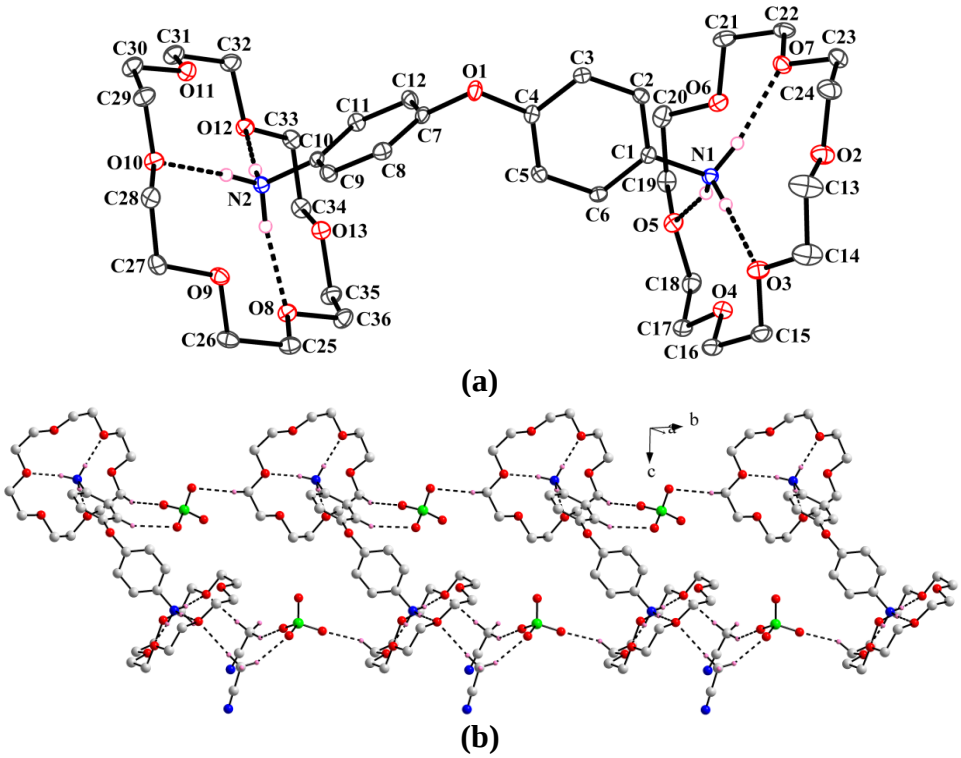

Figure 7. (a) Structure of the $DADPEH_2$–(18C6) adduct in the crystal of compound **7**. Perchlorate counter anions and the hydrogen atoms have been omitted for clarity. The thermal ellipsoids are drawn to 40% distribution level. (b) Chain-like packing topology in compound **7**.

fill up the voids but also to be involved in extensive hydrogen bonding interactions in the lattice. With the intention of getting rid of the solvent molecules to obtain the solvent free X-ray data for compounds **6** and **7**, crystals of the relevant solids were heated in an inert atomosphere (or under vacuum) which resulted in the loss of crystallinity of the samples. A chain-like packing topology has been observed in the lattice of compound **7** (Figure 7).

● 3.2.3. Thermal analysis

The thermal durability of the synthesized solids was checked by heating them in the temperature range 30–500 ºC under nitrogen atomosphere in a thermogravimmetric analyzer. However, among the seven compounds described in this chapter, only compound **1** exhibits excellent thermal stability. The thermal behavior of compound **1** is shown in Figure 8, which illustrates almost no weight loss up to 230 ºC. The 5 and 10% weight loss of this compound occurs only at 290 and 315 ºC respectively and the corresponding DTA graph (not shown in the picture) shows a sharp melting point at 162 ºC.

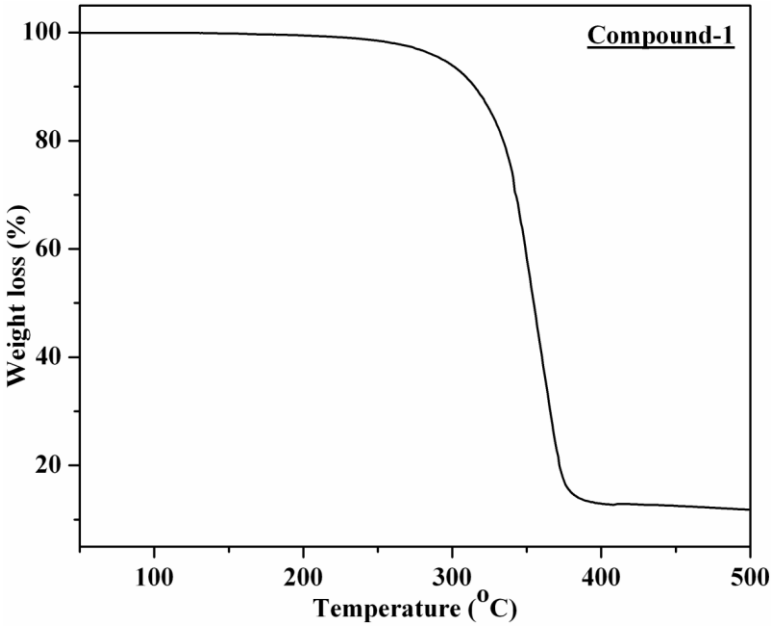

Figure 8. Thermal analysis of compound **1**.

● 3.3. SUMMARY AND CONCLUSION

In summary, a series of crown ether based host-guest systems were structurally characterized and the underlaying supramolecular chemistry has been presented in this chapter. Crown ethers are paradigms of supramolecular chemistry and hitherto a diverse class of crystallographically characterized supramolecular complexes featuring the crown ethers as hosts are reported. Attempts to cocrystallize 3–aminopyridine or the neutral amines (DADPM and DADPE) with the crown ethers i.e. to isolate the host-guest systems utilizing the pertinent amine compounds in lieu of the ammonium functionalities as the guests remained unsuccessful although, there are some reports illustrating amine–(crown ether) supramolecular systems. The compounds **1**–**7** were thus, isolated as their perchlorate salts, the crystallographic analysis of which resembles an established principle i.e. the hydrogen bonding acceptance as well as the donation propensity of crown ethers. While the N–H···O hydrogen bridges between the ammonium functionalities and the oxygen acceptor heteroatoms of the crown ethers are responsible for the guest integration within the host cavity, the weak C–H···O interaction between the crown ethers and the perchlorate counter anions in the crystal lattice of compounds **1**–**7** concomitantly play an important role in packing the host-guest complexes. The differing behavior of 12C4 in compounds **1** (chiral packing) and **4** (1:1 stoichiometry) is not very

clear to us at this level of investigation. Similarly, due to failure of crystallization attempts, the complete set of crystal data regarding complexation of the same crown ether with all the three ammonium systems is unavailable and therefore, drawing a straightforward structure–packing correlation is beyond the scope of the present work.

● 3.4. EXPERIMENTAL SECTION

● 3.4.1. Materials and methods

All the reactions were carried out under aerobic condition. All the chemicals were procured from commercial sources and used as received. The infrared spectra were recorded as KBr pellets on a JASCO–5300 FT-IR spectrophotometer at 298K. The relevant IR bands are represented as follows: s = strong, m = medium, w = weak, sh = sharp and br = broad.

● 3.4.2. Synthesis and characterization data

Appropriate crown ethers (2.5 equivalents) were added to an acetonitrile solution containing 3–aminopyridine or the angular diamines (DADPE or DADPM) (1 equivalent) and 60% perchloric acid (2.5 equivalents). Colorless single crystals suitable for X-ray diffraction were grown through slow evaporation of the solvent in cold condition over a period of 1–3 weeks. Apart from compound **1**, the solids **2**–**7** get moistened within minutes after they are removed from the solution which precluded optimization of the yield of the relevant compounds. The scrutiny of the phase homogeneity of the compounds **2**–**7** was not possible because of lack of powdery sample as required for the PXRD instrumentation.

The characterization data for the relevant compounds are presented below. Only the most prominent and characteristic IR bands are listed.

[3AmPyH$_2$(12C4)$_2$](ClO$_4$)$_2$ (1). IR (KBr, cm^{-1}): ν_{max} 3368 (m, br), 3219 (m, br), 3067 (m), 2922 (m), 1657 (m), 1595 (s, sh), 1510 (s, sh), 1454 (s, sh), 1238 (s, br), 1130 (s, br), 985 (s, sh).

[3AmPyH$_2$(B15C5)]$_2$(ClO$_4$)$_4$·2H$_2$O (2). IR (KBr, cm^{-1}): ν_{max} 3582 (s, br), 3090 (s), 2928 (s), 1502 (m, sh), 1257 (s, sh), 1093 (s, br), 935 (m, sh).

[3AmPyH$_2$(DB21C7)]$_3$(ClO$_4$)$_6$·5H$_2$O·0.5CH$_3$CN (3). IR (KBr, cm^{-1}): ν_{max} 3402 (s, br), 3043 (w), 2928 (m), 1635 (w), 1595 (w), 1504 (s, sh), 1454 (m), 1255 (s, sh), 1213 (m, sh), 1118 (s, br), 945 (s, br).

Table 4. Crystal data and structure refinement parameters for the compounds 1–4.

	1	**2**	**3**	**4**
Formula	$C_{21}H_{40}Cl_2N_2O_{16}$	$C_{38}H_{60}Cl_4N_4O_{28}$	$C_{82}H_{119.5}Cl_6N_{6.5}O_{50}$	$C_{42}H_{66}Cl_4N_4O_{25}$
FW	647.45	1162.70	2209.04	1168.79
T (K)	100(2)	100(2)	298 (2)	100(2)
Crystal system	monoclinic	monoclinic	triclinic	monoclinic
Space group	$P2_1$	$P2_1/n$	$P\bar{1}$	$P2_1/c$
a (Å)	8.3389(4)	17.7353(14)	11.9802(8)	17.190(3)
b (Å)	14.6212(7)	15.4444(12)	12.7041(9)	16.4933(12)
c (Å)	12.1621(6)	19.7642(16)	34.277(2)	12.8503(9)
α (°)	90.00	90.00	85.190(1)	90.00
β (°)	104.483(1)	112.756(1)	89.215(1)	92.640(2)
γ (°)	90.00	90.00	89.297(1)	90.00
V (Å^3)	1435.74(12)	4992.2(7)	5197.7(6)	5210.7(13)
Z	2	4	2	4
D_{calcd} (Mg/m^3)	2.145	2.171	2.505	3.322
μ (mm^{-1})	2.273	2.066	11.528	18.761
F(000)	838	862	2244	3456
GooF on F^2	1.060	1.062	1.029	1.106
R_1, wR_2 [$I>2\sigma(I)$]	0.0500, 0.1279	0.0647, 0.1502	0.0659, 0.1578	0.0828, 0.1978
R_1, wR_2 [all data]	0.0512, 0.1291	0.0732, 0.1559	0.0799, 0.1668	0.0863, 0.2006
Largest diff. peak, hole (e.Å^{-3})	1.142, –1.557	2.478, –1.131	2.478, –1.131	1.314, –0.836

[DADPMH$_2$(12C4)]$_2$(ClO$_4$)$_4$·H$_2$O (4). IR (KBr, cm^{-1}): ν_{max} 3431 (s, br), 3128 (s, br), 2918 (m), 1593 (m, br), 1510 (s, sh), 1452 (m), 1365 (m, sh), 1248 (s, sh), 1095 (s, br), 1024 (s, sh), 914 (s, sh), 846 (m, sh).

[DADPMH$_2$(15C5)$_2$](ClO$_4$)$_2$ (5). IR (KBr, cm^{-1}): ν_{max} 3414 (s, br), 2920 (s), 1628 (m), 1510 (m, sh), 1464 (w), 1356 (s, sh), 1251 (s), 1089 (s, br), 941 (s, sh), 856 (s, sh).

[DADPMH$_2$(18C6)$_2$]$_2$(ClO$_4$)$_4$·6.75H$_2$O·CH$_3$CN (6). IR (KBr, cm^{-1}): ν_{max} 3414 (s, br), 2962 (m), 1630 (w), 1498 (m, sh), 1365 (m, sh), 1257 (s), 1143 (s, br), 1095 (s, br), 1024 (s), 912 (s, sh), 844 (m, sh).

[DADPEH$_2$(18C6)$_2$](ClO$_4$)$_2$·2CH$_3$CN (7). IR (KBr, cm^{-1}): ν_{max} 3414 (s, br), 2914 (s, br), 1635 (m), 1498 (s, sh), 1352 (s, sh), 1257 (s, sh), 1105 (s, br), 960 (s, sh), 829 (s, sh).

Table 5. Crystal data and structure refinement parameters for the compounds 5–7.

	5	6	7
Formula	$C_{33}H_{56}Cl_2N_2O_{18}$	$C_{76}H_{144.5}Cl_4N_5O_{46.75}$	$C_{40}H_{68}Cl_2N_4O_{21}$
FW	839.70	2018.27	1011.88
T (K)	100(2)	100(2)	100(2)
Crystal system	triclinic	monoclinic	triclinic
Space group	$P\bar{1}$	$P2_1/n$	$P\bar{1}$
a (Å)	8.8552(6)	16.1814(9)	12.2134(7)
b (Å)	14.2350(9)	21.7220(12)	13.2564(8)
c (Å)	16.8384(11)	29.3019(17)	17.0677(10)
α (°)	110.236(1)	90.00	75.025(1)
β (°)	95.478(1)	103.233(1)	71.730(1)
γ (°)	90.002(1)	90.00	72.189(1)
V (Å^3)	1981.2(2)	10025.9(10)	2457.6(3)
Z	2	4	2
D_{calcd} (Mg/m^3)	2.145	2.171	3.322
μ (mm^{-1})	2.273	2.066	18.761
GooF on F^2	1.020	1.115	1.030
R_1, wR_2 [$I>2\sigma(I)$]	0.0638, 0.1490	0.0759, 0.1842	0.0447, 0.1118
R_1, wR_2 [all data]	0.0743, 0.1567	0.0919, 0.1931	0.0551, 0.1187
Largest diff. peak, hole(e.Å^{-3})	1.142, –1.557	2.478, –1.131	2.478, –0.836

● 3.4.3. X-ray data collection and structure determination

Crystals suitable for X-ray diffraction were picked up from the mother solution and mounted on a Bruker SMART–APEX three–circle platform diffractometer equipped with a CCD area detector system and a collimator of 0.5 mm. Data were collected at 100 K using the graphite monochromated Mo–Kα radiation through the φ and ω scan strategy with 0.3º frame width, crystal to detector distance of 60 mm. The collected raw data were corrected over background noise and integrated with the aid of Bruker–SAINT program. Semi empirical absorption correction on the equivalent reflections were performed by Bruker–SADABS, structure solution by direct method as implemented in the program SHELXS–97 and full–matrix least–square refinement by SHELXL–97.[23] All the non–hydrogen atoms were refined anisotropically after their successful location in the difference Fourier map. Hydrogen atoms attached to the carbon atoms were introduced at the calculated positions to ride on their respective parents and refined freely. The ammonium, pyridinium and in some cases, water hydrogen atoms were located from the difference Fourier map and their positions were refined. No attempts were made in order

to fix their positions by applying suitable restraints. In some cases, hydrogen atoms of lattice water molecules could not be located although they are included in the molecular formulae and mass. The disordered components of the crown ethers, where observed, were refined isotropically. Tables 4 and 5 summarize the structural data and refinement parameters of the studied crystals. The crystal structure of compound **3** contains one acetonitrile solvent molecule per unit cell and the crystal structure of compound **6** contains three solvent water molecules per unit cell which were considered as diffused contribution to the overall scattering without specific atom positions by SQUEEZE/PLATON.[24]

● 3.5. REFERENCES

1 (a) Pedersen, C. J. *J. Am. Chem. Soc.* **1967**, *89*, 7017. (b) Pedersen, C. J. *J. Am. Chem. Soc.* **1970**, *92*, 391. (c) Pedersen, C. J. *J. Am. Chem. Soc.* **1970**, *92*, 386. (d) Pedersen, C. J. *Science* **1988**, *241*, 536. (e) Pedersen, C. J. *J. Inclusion Phenom. Mol. Recognit. Chem.* **1992**, *12*, 7.

2 (a) Lehn, J. M. In *Comprehensive Supramolecular Chemistry*; Elsevier: Armsterdam **1996**. (b) Dietrich, B.; Viout, P.; Lehn, J. M. In *Macrocyclic Chemistry: Aspects of Organic and Inorganic Supramolecular Chemistry*; VCH: New York, **1993**. (c) Lehn, J. M. In *Nobel Lectures in Chemistry (1981–1990)*; World Scientific Publishing Co. Pte. Ltd.: Singapore, **1992**, 444. (d) Lehn, J. M. In *Supramolecular Chemistry: Concepts and Perspectives*; VCH: Weinheim, **1995**. (e) Atwood, J. L.; Steed, J. W. In *Encyclopaedia of Supramolecular Chemistry*; Taylor & Francis: New York, **2004**.

3 (a) Liu, L.; Dong, X.; Xiao, Y.; Lian, W.; Liu, Z. *Analyst* **2011**, *136*, 2139. (b) Guerchais, V.; Fillaut, J. –L. *Coord. Chem. Rev.* **2011**, *255*, 2448 and references therein. (c) Stephenson, G. R.; Anson, C. E.; Creaser, C. S.; Daul, C. A. *Eur. J. Inorg. Chem.* **2011**, 2086. (d) Piatek, P. *Chem. Commun.* **2011**, *47*, 4745. (e) Cho, E. N. R.; Li, Y.; Kim, H. J.; Hyun, M. H. *Chirality* **2011**, *23*, 349. (f) Kondo, S. –I.; Takahashi, T.; Takiguchi, Y.; Unno, M. *Tetrahedron Lett.* **2011**, *52*, 453.

4 (a) Steed, J. W. *Coord. Chem. Rev.* **2001**, *215*, 171 and references therein. (b) Junk, P. C. *New. J. Chem.* **2008**, *32*, 762 and references therein.

5 (a) Bhogala, B. R.; Nangia, A. *Cryst. Growth Des.* **2006**, *6*, 32. (b) Atwood, J. L.; Bott, S. G.; Coleman, A. W.; Robinson, K. D.; Whetstone, S. B.; Means, C. M. *J. Am. Chem. Soc.* **1987**, *109*, 8100. (c) Atwood, J. L.; Bott, S. G.; Means, C. M.; Coleman, A. W.; Zhang, H.; May, M. T. *Inorg. Chem.* **1990**, *29*, 467. (d) Junk, P. C.; Atwood, J. L. *J. Chem. Crystallogr.* **1994**, *24*, 247. (e) Atwood, J. L.; Junk, P. C.; May, M. T.; Robinson, K. D. *J. Chem. Crystallogr.* **1994**, *24*, 243. (f) Atwood, J. L.; Junk, P. C.; May, M. T.; Robinson, K. D. *J. Coord. Chem.* **1996**, *40*, 247. (g) Atwood, J. L.; Bott, S. G.; Junk, P. C.; May, M. T. *J. Coord Chem.* **1996**, *37*, 89. (h) Junk, P. C.; Atwood, J. L. *J. Chem. Soc., Dalton Trans.* **1997**, 4393. (i) Zaworotko, M. J.; Kerr, C. R.; Atwood, J. L. *Organometallics* **1985**, *4*, 238. (j) Kravtsov, V. C.; Fonari, M. S.; Zaworotko, M. J.; Lipkowski, J. *Acta. Crystallogr.* **2002**, *C58*, 683.

6 (a) Akutagawa, T.; Hashimoto, A.; Nishihara, S.; Hasegawa, T.; Nakamura, T. *J. Supramol. Chem.* **2002**, *2*, 175. (b) Akutagawa, T.; Hasegawa, T.; Nakamura, T.; Takeda, S.; Inabe, T.; Sugiura, K.; Sakata, Y.; Underhil, A. E. *Inorg. Chem.* **2000**, *39*, 2645. (c) Fonari, M. S.; Simonov, Y. A.; Wang, W. –J.; Tang, S. –W.; Ganin, E. V. *CrystEngComm* **2009**, *11*, 94. (d) Kryatova, O. P.; Korendovych, I. V.; Rybak–Akimova, E. V. *Tetrahedron* **2004**, *60*, 4579. (e) Rogers, R. D.; Bond, A. H. *Inorg. Chim. Acta* **1996**, *250*, 105. (f) Doxsee, K. M.; Francis P. E. Jr.; Weakley, T. J. R. *Tetrahedron* **2000**, *56*, 6683. (g) Braga, D.; Modena, E.; Polito, M.; Rubini, K.; Grepioni, F. *New J. Chem.* **2008**, *32*, 1718. (h) Spek, A. L.; Roelofsen, G.; Noltes, J. G.; Alberts A. H. *Cryst. Struct. Commun.* **1982**, *11*, 1863. (i) Colquhoun, H. M.; Jones, G.; Maud, J. M.; Stoddart, J. F.; Williams, D. J. *J. Chem. Soc., Dalton Trans.* **1984**, *105*, 63. (j) Maud, J. M.; Stoddart, J. F.; Williams, D. J. *Acta Crystallogr.* **1985**, *C41*, 137.

7 (a) Trueblood, K. N.; Knobler, C. B.; Lawrence, D. S.; Stevens, R. V. *J. Am. Chem. Soc.* **1982**, *104*, 1355. (b) Bovill, M. J.; Chadwick, D. J.; Sutherland, I. O.; Watkin, D. *J. Chem. Soc., Perkin Trans. 2* **1980**, *105*, 1529. (c) Rogers, R. D.; Benning, M. M.; *Acta Crystallogr.* **1988**, *C44*, 1397. (d) Clemente, D. A. *Inorg. Chim. Acta* **2005**, *358*, 1725. (e) Sato, D.; Akutagawa, T.; Takeda, S.; Noro, S.; Nakamura, T. *Inorg. Chem.* **2007**, *46*, 363. (f) Nishihara, S.; Ren, X. M.; Akutagawa, T.;

Nakamura, T. *Polyhedron* **2005**, *24*, 2844. (g) Nishihara, S.; Akutagawa, T.; Hasegawa, T.; Nakamura, T. *Chem. Commun.* **2002**, *30*, 408. (h) Nishihara, S.; Akutagawa, T.; Hasegawa, T.; Fujiyama, S.; Nakamura, T.; Nakamura, T. *J. Solid State Chem.* **2002**, *168*, 661 (i) Nishihara, S.; Akutagawa, T.; Sato, D.; Takeda, S.; Noro, S.; Nakamura, T. *Chem. –Asian J.* **2007**, *2*, 1083 (j) Fender, N. S.; Kahwa, I. A.; Fronczek, F. R. *J. Solid State Chem.* **2002**, *163*, 286.

8 (a) Fonari, M. S.; Kravtsov, V. Ch.; Simonov, Y. A.; Ganin, E. V.; Gelmboldt, V. O.; Lipkowski, J. *J. Inclusion Phenom. Macrocyclic Chem.* **2001**, *39*, 85. (b) Akutagawa, T.; Matsuura, K.; Hashimoto, A.; Nakamura, T. *Inorg. Chem.* **2005**, *44*, 4454. (c) Chadwick, S.; Englich, U.; Ruhlandt–Senge, K.; *Angew. Chem., Int. Ed.* **1998**, *37*, 3007. (d) Akutagawa, T.; Endo, D.; Imai, H.; Noro, S.; Cronin, L.; Nakamura, T. *Inorg. Chem.* **2006**, *45*, 8628. (e) Braga, D.; Gandolfi, M.; Lusi, M.; Paolucci, D.; Polito, M.; Rubini, K.; Grepioni, F. *Chem. –Eur. J.* **2007**, *13*, 5249. (f) Braga, D.; Curzi, M.; Lusi, M.; Grepioni, F. *CrystEngComm* **2005**, *7*, 276. (g) Yoon, C. W.; Carroll, P. J.; Sneddon, L. G. *J. Am. Chem. Soc.* **2009**, *131*, 855. (h) Akutagawa, T.; Sato, D.; Ye, Q.; Noro, S.; Nakamura, T. *Dalton Trans.* **2010**, *39*, 2191. (i) Colquhoun, H. M.; Doughty, S. M.; Stoddart, J. F.; Slawin, A. M. Z.; Williams, D. J. *J. Chem. Soc., Dalton Trans.* **1986**, 1639. (j) Fonari, M. S.; Ganin, E. V.; Basok, S. S.; Lyssenko, K. A.; Zaworotko, M. J.; Kravtsov, V. Ch. *Cryst. Growth Des.* **2010**, *10*, 5210.

9 (a) Braga, D.; D'Agostino, S.; Grepioni, F.; Gandolfi, M.; Rubini, K. *Dalton Trans.* **2011**, *40*, 4765 and references therein. (b) Braga, D.; D'Agostino, S.; Polito, M.; Rubini, K.; Grepioni, F. *CrystEngComm* **2009**, *11*, 1994. (c) Ganin, E. V.; Basok, S. S.; Yavolovskii, A. A.; Botoshanskyc, M. M.; Fonari, M. S. *CrystEngComm* **2011**, *13*, 674. (c) Calleja, M.; Mason, S. A.; Prince, P. D.; Steed, J. W.; Wilkinson, C. *New J. Chem.* **2003**, *27*, 28. (d) Junk, P. C.; Steed, J. W. *J. Coord. Chem.* **2007**, *60*, 1017. (e) Braga, D.; Polito, M.; Dichiarante, E.; Rubini, K.; Grepioni, F. *Chem. Commun.* **2007**, 1594. (f) Braga, D.; Gandolfi, M.; Lusi, M.; Polito, M.; Rubini, K.; Grepioni, F. *Cryst. Growth. Des.* **2007**, *7*, 919. (g) Steed, J. W.; Sakellariou, E.; Junk, P. C.; Smith, M. K. *Chem. –Eur. J.* **2001**, *7*, 1240. (h) Akutagawa, T.; Hasegawa, T.; Nakamura, T.; Inabe, T. *J. Am. Chem. Soc.* **2002**, *124*, 8903. (i)

Fuller, A. –M.; Mountford, A. J.; Coles, S. J.; Horton, P. N.; Hughes, D. L.; Hursthouse, M. B.; Male, L.; Lancaster, S. J. *Dalton Trans.* **2008**, 6381. (j) Junk, P. C.; McCool, B. J.; Moubaraki, B.; Murray, K. S.; Spiccia, L.; Cashion, J. D.; Steed, J. W. *J. Chem. Soc., Dalton Trans.* **2002**, 1024.

10 (a) Rogers, R. D.; Rollins, A. N. *J. Chem. Cryst.* **1994**, *24*, 531. (b) Rogers, R. D.; Rollins, A. N.; Henry, R. F.; Murdoch, J. S.; Etzenhouser, R. D.; Huggins, S. E.; Nunez, L. *Inorg. Chem.* **1991**, *30*, 4946. (c) Rogers, R. D.; Bond, A. H.; Hipple, W. G.; Rollins, A. N.; Henry, R. F. *Inorg. Chem.* **1991**, *30*, 2671. (d) Hassaballa, H.; Steed, J. W.; Junk, P. C.; Elsegood, M. R. J. *Inorg. Chem.* **1998**, *37*, 4666. (e) Hassaballa, H.; Steed, J. W.; Junk, P. C. *Chem. Commun.* **1998**, 577. (f) Ji, Z. P.; Rogers, R. D. *J. Chem. Cryst.* **1994**, *24*, 415. (g) Rogers, R. D.; Bond, A. H.; Aguinaga, S.; Reyes, A. *J. Am. Chem. Soc.* **1992**, *114*, 2967. (h) Calleja, M.; Mason, S. A.; Prince, P. D.; Steed, J. W.; Wilkinson, C. *New J. Chem.* **2001**, *25*, 1475. (i) Johnson, K.; Steed, J. W. *Chem. Commun.* **1998**, 1479. (j) Junk, P. C.; Steed, J. W. *J. Chem. Soc., Dalton Trans.* **1999**, 407. (k) Luboradzki, R.; Lipkowski, J.; Simonov, Y. A.; Fonari, M. S.; Ganin, E. V.; Yavolovskii, A. A. *J. Inclusion Phenom. Macrocyclic Chem.* **2001**, *40*, 59. (l) Rogers, R. D.; Kurihara, L. K.; Benning, M. M. *Inorg. Chem.* **1987**, *26*, 4346.

11 (a) Chatterjee, T.; Sarma, M.; Das, S. K. *Cryst. Growth Des.* **2010**, *10*, 3149. (b) Chatterjee, T.; Sarma, M.; Das, S. K. *J. Mol. Struct.* **2010**, *981*, 34. (c) Sarma, M.; Chatterjee, T.; Das, S. K. *Dalton Trans.* **2011**, *40*, 2954. (d) Sarma, M.; Chatterjee, T.; Das, S. K. *Inorg. Chem. Commun.* **2010**, *13*, 1114. (e) Shivaiah, V.; Das, S. K. *Angew. Chem. Int. Ed.* **2006**, *45*, 245. (f) Shivaiah, V.; Das, S. K. *Inorg. Chem.* **2005**, *44*, 7313.

12 3–aminopyridine is the core unit of 3–aminopyridine–2–carboxaldehyde thiosemicarbazone, which is found to have anticancer activity.

13 (a) Vangala, V. R.; Mondal, R.; Broder, C. K.; Howard, J. A. K.; Desiraju, G. R. *Cryst. Growth Des.* **2005**, *5*, 99. (b) Dey, A.; Desiraju, G. R.; Mondal, R.; Howard, J. A. K. *Chem. Commun.* **2004**, 2528.

14 Based on Cambridge Structural Database (CSD) version 5.32, November 2010 at University of Hyderabad.

15 Groth, P. *Acta Chem. Scand. A* **1978**, *32*, 279 (CSD code TOXCDP).

16 (a) Wen, M.; Maekawa, M.; Munakata, M.; Suenaga, Y.; Kuroda–Sowa, T. *Inorg. Chim. Acta* **2002**, *338*, 111. (b) Burns, J. H.; Bryan, J. C.; Davis, M. C.; Sachleben, R. A. *J. Inclusion Phenom. Mol. Recognit. Chem.* **1996**, *26*, 197. (c) Kiviniemi, S.; Nissinen, M.; Lamsa, M. T.; Jalonen, J.; Rissanen, K.; Pursiainen, J. *New J. Chem.* **2000**, *24*, 47.

17 (a) Wang, R. –H.; Hong, M. –C.; Luo, J. –H.; Cao, R.; Weng, J. –B. *Eur. J. Inorg. Chem.* **2002**, 3097. (b) Castro–Castro, L. M.; Guloy, A. M. *Inorg. Chem.* **2004**, *43*, 4537. (c) Luo, J.; Hong, M.; Wang, R.; Cao, R.; Shi, Q.; Weng, J. *Eur. J. Inorg. Chem.* **2003**, 1778. (d) Zhi, X. –L.; Zhang, W. –H.; Zhang, Y.; Lang, J. –P. *Acta Crystallogr.* **2004**, *C60*, m554. (e) Wang, R.; Hong, M.; Weng, J.; Cao, R.; Liang, Y.; Zhao, Y. *Acta Crystallogr.* **2001**, *E57*, m344. (f) Zhang, H. –X.; Chen, Z. –N.; Yu, K. –B.; Kang, B. –S. *Inorg. Chem. Commun.* **1999**, *2*, 223. (g) Zhang, Y.; Nishiura, M.; Jianmin, L.; Wei, D.; Imamoto, T. *Inorg. Chem.* **1999**, *38*, 825. (h) Carlucci, L.; Ciani, G.; Proserpio, D. M.; Porta, F. *CrystEngComm* **2006**, *8*, 696. (i) Wu, M.; Wei, W.; Gao, Q.; Yuan, D.; Huang, Y.; Jaing, F.; Hong, M. *Cryst. Growth Des.* **2009**, *9*, 1584. (j) Chen, H. –J.; Chen, X. –M.; Zhou, D. –Y.; Zhou, Y. –C. *Supramol. Chem.* **2002**, *14*, 21.

18 (a) Han, Q. *Acta Crystallogr.* **2007**, *E63*, o4456. (b) Du, G.; Liu, Z.; Chu, Q.; Li, Z.; Zhang, S. *Acta Crystallogr.* **2008**, *E64*, o1947. (c) Wei, L. –H. *Acta Crystallogr.* **2008**, *E64*, o734. (d) Li, J. *Acta Crystallogr.* **2007**, *E63*, o4303, (e) Nahouane, R.; Soumhi, E. H.; Saadoune, I.; Driss, A. *Acta Crystallogr.* **2005**, *E61*, o2850, (f) Wang, Z. –L.; Wei, L. –H.; Li, M. –X.; Wang, J. –P. *J. Mol. Struct.* **2008**, *879*, 150.

19 (a) Kumara Swamy, K. C.; Kumaraswamy, S.; Kommana, P. *J. Am. Chem. Soc.* **2001**, *123*, 12642. (b) Goicoechea, J. M.; Hull, M. W.; Sevov, S. C. *J. Am. Chem. Soc.* **2007**, *129*, 7885. (c) Zheng, B. N.; Miranda, M. O.; DiPasquale, A. G.; Golen, J. A.; Rheingold, A. L.; Doerrer, L. H. *Inorg. Chem.* **2009**, *48*, 4274. (d) Yamashita, M.; Mita, Y.; Yamamoto, Y.; Akiba, K. *Chem. –Eur. J.* **2003**, *9*, 3655. (e) Zi, G.; Li, H. –W.; Xie, Z. *Organometallics* **2002**, *21*, 5415. (f) Ugrinov, A.; Sevov, S. C. *J. Am. Chem. Soc.* **2003**, *125*, 14059. (g) Hernandez–Arganis, M.; Hernandez–Ortega, S.; Toscano, R. A.; Garcia–Montalvo, V.; Cea–Olivares, R. *Chem.*

Commun. **2004**, 310. (h) Rosokha, S. V.; Lu, J.; Han, B.; Kochi, J. K. *New J. Chem.* **2009**, *33*, 545. (i) Kraus, F.; Aschenbrenner, J. C.; Klamroth, T.; Korber, N. *Inorg. Chem.* **2009**, *48*, 1911. (j) He, X.; Allan, J. F.; Noll, B. C.; Kennedy, A. R.; Henderson, K. W. *J. Am. Chem. Soc.* **2005**, *127*, 6920.

20 (a) Cameron, T. S.; Decken, A.; Ilyin, E. G.; Nikiforov, G. B.; Passmore, J. *Eur. J. Inorg. Chem.* **2004**, 3865. (b) Ochiai, M.; Miyamoto, K.; Yokota, Y.; Suefuji, T.; Shiro, M. *Angew. Chem., Int. Ed.* **2005**, *44*, 75. (c) Beard, C. D.; Carr, L.; Davis, M. F.; Evans, J.; Levason, W.; Norman, L. D.; Reid, G.; Webster, M. *Eur. J. Inorg. Chem.* **2006**, 4399. (d) Steed, J. W.; McCool, B. J.; Junk, P. C. *J. Chem. Soc., Dalton Trans.* **1998**, 3417. (e) Doxsee, K. M.; Hagadorn, J. R.; Weakley, T. J. R. *Inorg. Chem.* **1994**, *33*, 2600. (f) Deshayes, L.; Keller, N.; Lance, M.; Nierlich, M.; Vigner, J. –D. *Acta Crystallogr.* **1994**, *C50*, 1541.

21 (a) Fonari, M. S.; Simonov, Y. A.; Kravtsov, V. Ch.; Lipkowski, J.; Ganin, E. V.; Yavolovskii, A. A. *J. Mol. Struct.* **2003**, *647*, 129. (b) Koritsanszky, T.; Buschmann, J.; Denner, L.; Luger, P.; Knochel, A.; Haarich, M.; Patz, M. *J. Am. Chem. Soc.* **1991**, *113*, 8388. (c) Fonari, M. S.; Simonov, Y. A.; Bocelli, G.; Botoshansky, M. M.; Ganin, E. V. *J. Mol. Struct.* **2005**, *738*, 85. (d) Caira, R.; Mohamed, R. *Acta Crystallogr.* **1993**, *B49*, 760. (e) Knochel, A.; Kopf, J.; Oehler, J.; Rudolf, G. *Chem. Commun.* **1978**, 595. (f) Simonov, Y. A.; Fonari, M. S.; Lipkowski, J.; Ganin, E. V.; Yavolovskii, A. A. *J. Supramol. Chem.* **2002**, *2*, 415. (g) Simonov, Y. A.; Fonari, M. S.; Duca, G. G.; Gonta, M. V.; Ganin, E. V.; Yavolovskii, A. A.; Gdaniec, M.; Lipkowski, J. *Tetrahedron* **2005**, *61*, 6596. (h) Nastopoulos, V.; Germain, G.; Weiler, J. *Acta Crystallogr.* **1991**, *C47*, 1546. (i) Fonari, M. S.; Ganin, E. V.; Tang, S. –W.; Wang, W. –J.; Simonov, Y. A. *J. Mol. Struct.* **2007**, *826*, 89. (j) Johnson, K.; Steed, J. W. *J. Chem. Soc., Dalton Trans.* **1998**, 2601.

22 (a) Dunitz, J. D.; Seiler, P. *Acta Crystallogr.* **1974**, *B30*, 2739. (b) Maverick, E.; Seiler, P.; Schweizer, W. B.; Dunitz, J. D. *Acta Crystallogr.* **1980**, *B36*, 615.

23 (a) SAINT: *Software for the CCD Detector System*; Bruker Analytical X-ray Systems, Inc.: Madison, WI, **1998**. (b) SADABS: *Program for absorption correction*; Sheldrick, G. M. University of Göttingen: Göttingen, Germany, 1997.

(c) SHELXS–97: *Program for structure solution*; Sheldrick, G. M. University of Göttingen: Göttingen, Germany, **1997**. (d) SHELXL–97: *Program for Crystal Structure Analysis*; Sheldrick, G. M. University of Göttingen: Göttingen, Germany, **1997**.

24 Van der Sluis, P.; Spek, A. L. *Acta Cryst*. **1990**, *A46*, 194.

••••

Chapter-4

D–π–A–A–π–D Prototype 2,2'–Bipyridine Dyads Exhibiting Large Structure and Environment Sensitive Fluorescence: Synthesis, Photophysics and Computation

ABSTRACT: A series of 4,4'–π–conjugated–2,2'–bipyridine chromophores (**MS 1**–**8**) were synthesized and their photophysical and thermal properties studied. The title 'push-pull' chromophores, except **MS 1**, are integrated with both alkoxy and alkylamino donor functionalities which differ in their donation capabilities. The oligophenylenevinylene (OPV) chromophores **MS 4**–**8** are associated with a π–extended backbone in which the position and the number of alkoxy donors have been systematically varied. All the studied systems possess a D–π–A–A–π–D dyad archetype in which the A–A is the central 2,2'–bipyridine acceptor core which is electronically attached with the donor termini through π–linkers. The fluorescence quantum yields of the synthesized chromophores are found to be sensitive to the molecular archetype and the solvent medium. Among the eight fluorophores described in this chapter, compound **MS 5** exhibits fluorescence in the solid state too. The modulating effect of the nature, position and number of donor functionalities on the optical properties of these classes of compounds has further been comprehended on the basis of DFT and TD–DFT computation in solvent model.

● 4.1. INTRODUCTION

In the contemporary era, fluorescence has turned out to be an indispensable analytical technique in the various branches of science, most prominently, in the fields of analytical, biological and medical sciences etc.[1] Among the diverse classes of organic π–systems, the materials that absorb electromagnetic radiation by virtue of an intramolecular charge transfer (ICT) and emit from the corresponding photoexcited state, are the most fascinating because of their notable applications in the field of molecular electronics, integrated photonic devices and nonlinear optics (NLO),[2] etc. The elegant fabrication of an electron donor-acceptor (DA) or 'push-pull' architecture can be carried out *via* the electronic unification between the donor and acceptor mesomeric units in a chromophore which is in turn, linked with spontaneous charge redistribution between the functionalities (ICT). Consequently, much research interest has been paid to the design and synthesis of diverse classes of DA-type fluorescent probes, associated with brilliant

photophysical behaviors; some typical examples of such fluorescent probes being acridine,[3] fluorescein,[4] cyanine,[5] rhodamine,[6] coumarin,[7] BODIPY,[8] squarines,[9] oligophenylenevinylenes (OPVs),[10] etc.

The beauty of organic chemistry to devise a wide variety of chromophores lies in the disconnection approach, wherein the nitrogen containing heterocycles act as very promising building blocks to synthesize diverse classes of strongly emissive materials.[11] The 2,2'–bipyridine derivatives are endowed with an extensive coordination / supramolecular chemistry.[12] However, in photoscience, it is advantageous to employ this N–heterobiaryl compound because of the fact that, easy derivatization of the pyridine rings offers introduction of an assorted class of donor end-capping functionalities to tune the optical properties of the relevant 2,2'–bipyridine based dyads. Since the past two decades, many research groups including Le Bozec, Beer, Abbotto and others have accounted for the diverse end-capped 2,2'–bipyridine chromophores with moderate to strong emission responses.[13–15] Recently, Ajayaghosh and co-workers have exemplified the chemo-sensing properties of the 2,2'–bipyridine based luminophores.[16] The transition metal complexes of the 2,2'–bipyridine based DA systems are of topical interest due to their potential applicability in octupolar nonlinearity.[17] The heteroleptic *bis*–thiocyanato ruthenium complexes, bearing a TiO_2 anchoring 2,2'–bipyridine ligand along with another auxiliary 2,2'–bipyridine ligand (known as antenna), have proved to be very promising photosensitizers for building high–performance dye sensitized solar cell modules.[18]

The exciting photophysical responses of the 2,2'–bipyridine based DA systems and their transition metal complexes have captured our attention.[19] The bipyridine based chromophores reported so far, are either symmetrically (point group = C_i) or disymmetrically (point group = C_1) substituted with alike donor functionalities (for example alkylamino etc.) whereas, photophysical properties of the associated hetero-donor systems have been less explored. In this chapter, a series of *styryl*– and *bistyryl*–2,2'–bipyridine luminophores (**MS 2**–**8**, Chart 1) functionalized with both the alkoxy and amino functionalities in C_i symmetrical fashion and their photophysical properties have been demonstrated. The prototype of the synthesized dyads is of D–π–A–A–π–D (D = donor, A = acceptor) in which the bipyridine moiety acts as the central acceptor core to

join the terminal donor functionalities through vinylene linkers. The Horner–Wadsworth–Emmons reaction (HWE) has been exclusively used so as to introduce electron donating groups into the bipyridine central acceptor core unit. The photophysical properties of the

Chart 1. Molecular structures of the synthesized and the parent π–conjugated–2,2'–bipyridine chromophores (MS 1–8). The two phenyl rings of the OPV chromophores have been named as A and B for easy discussion in the text.

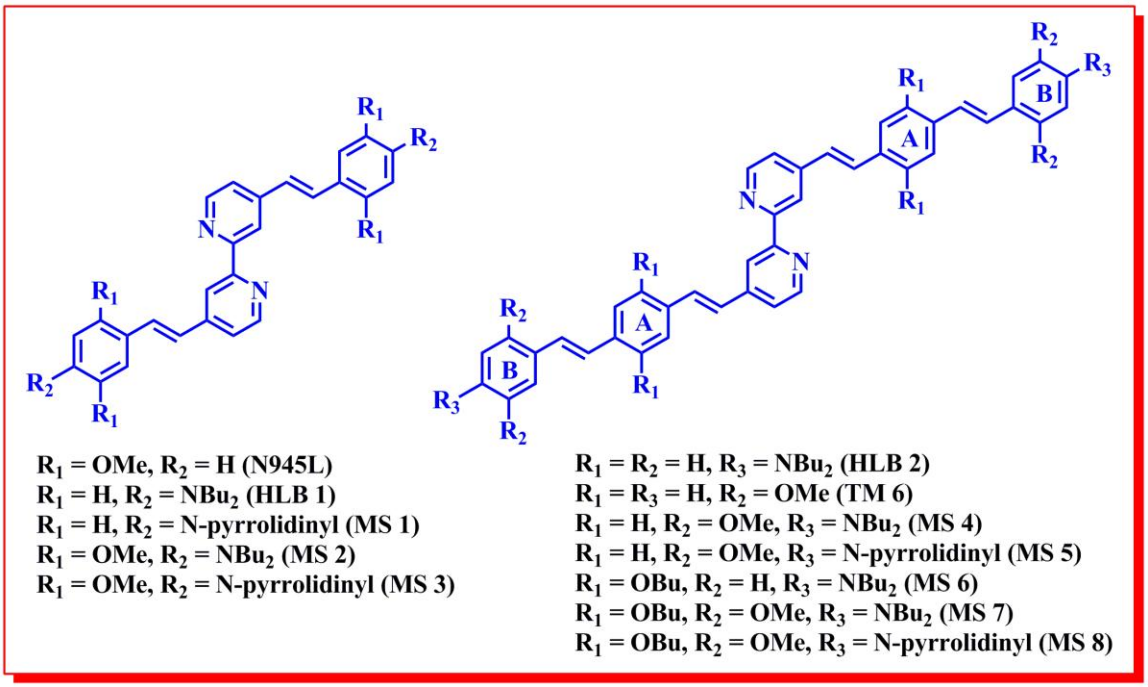

synthesized chromophores (**MS 1**–**8**, Chart 1) are compared with four reported dyes namely, (a) the blue OLED dye 4,4'–*bis*(2,5–dimethoxystyryl)–2,2'–bipyridine (known as **N945L**) reported by Nazeeruddin and Grätzel;[15a] (b) 4,4'–*bis*(4–dibutylaminostyryl)–2,2'–bipyridine (named as **HLB 1** in this chapter)[13d] and 4,4'–*bis*(4–(4–dibutylamino styryl)styryl)–2,2'–bipyridine (named as **HLB 2** in this chapter)[13h] reported by Le Bozec; and the 4,4'–*bis*(4–(2,5–dimethoxystyryl)styryl)–2,2'–bipyridine (named as **TM 6**) reported by us[19a] (see Chart 1). A pragmatic observation points up that the introduction of the amino donor functionalities to **N945L** / **TM 6** or alkoxy donors to **HLB 1** / **HLB 2** have induced a significant alteration of the photonic responses in the present chromophores. In addition, the position of the alkoxy functionalities attached to the conjugated backbone of the OPV derivatives, **MS 4**–**8**, greatly influences their photophysical properties. Furthermore, a thorough computational analysis in the level of

Density Functional Theory (DFT) in solvent model was applied to scrutinize the effect of donor positions on the geometrical and electronic parameters of the reference and the synthesized chromophores. All the synthesized π–conjugated molecules **MS 1–8** fluoresce at room temperature with large Stokes shift while the emissive behavior of the OPV chromophores **MS 4–8** epitomizes a large sensitivity to the solvent polarity. Amongst eight fluorescent compounds accounted here, the compound, **MS 5** is emissive in the solid state too.

Scheme 1. Convenient synthetic protocols to access the symmetrical bipyridine chromophores.

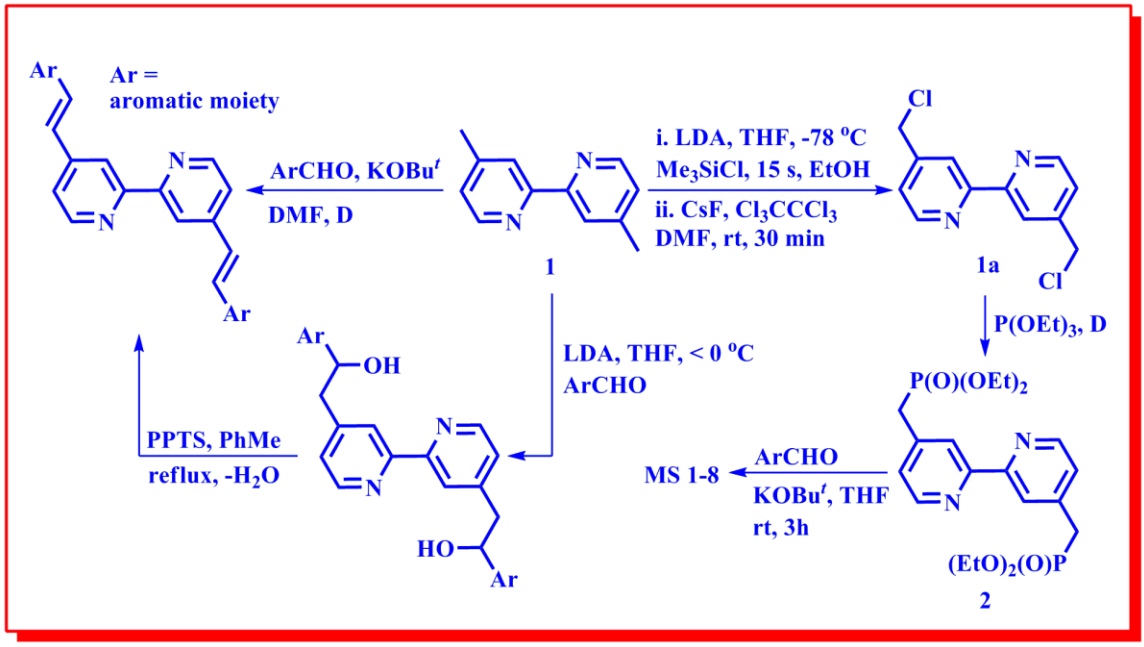

● 4.2. RESULTS AND DISCUSSION

● 4.2.1. Synthesis and characterization

The bench–top syntheses of the 4,4'–π–conjugated–2,2'–bipyridine chromophores can be accomplished via highly efficient synthetic protocols (see Scheme 1). The symmetrically substituted 2,2'–bipyridine derivatives (point symmetry =C_i) can, indeed, be easily derived either through (a) a Knoevenagel type reaction between the doubly deprotonated 4,4'–dimethyl–2,2'–bipyridine (**1**) and suitable aromatic aldehydes or (b) a Horner–Wadsworth–Emmons (HWE) reaction between the *bis*–phosphonate (**2**) and aromatic aldehydes. The Knoevenagel type reaction in fact, triggers at the acidity of the 4–picolyl

protons of the bipyridine starting precursor (**1**). A two-step synthetic approach that was developed, entailed the deprotonation of **1** by a strong base e.g. lithium diisopropylamide (LDA) at low temperature followed by nucleophilic addition of the resulting carbanion to an aromatic aldehyde to form a secondary alcohol. The resulting alcohol is then dehydrated, usually, by pyridinium *p*-toluene sulfonate (PPTS) to convert it to the corresponding alkene (Scheme 1).[14a] An alternative one-step protocol which directly yielded the desired alkenes, involved heating of a mixture of **1** and an aromatic aldehyde in presence of a strong and hindered base e.g. KOBu^t in DMF.[13d] The donor end-capping functionalities in the present bipyridine chromophores (**MS 1**–**8**) were, however, introduced by the HWE protocol due to its better performance (high yield, *E*–selectivity etc.) in comparison with the two other methodologies as described in Scheme 1. Also, the

Scheme 2. Synthesis of the alkylamino benzaldehydes.

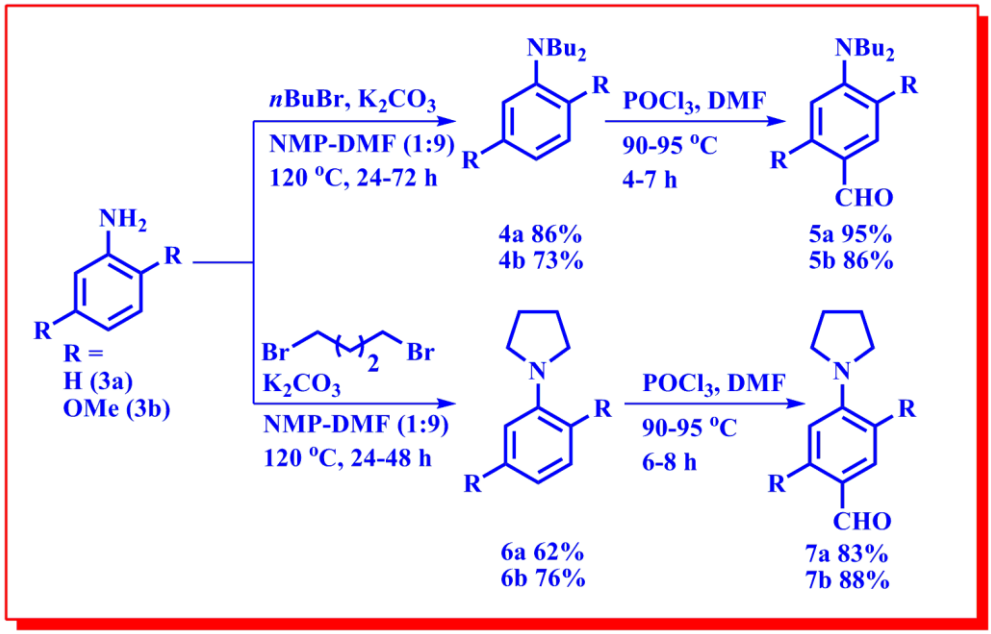

conventional Wittig pathway was avoided due to the undesired trouble with the coproduct, triphenylphosphine oxide, during work-up and purification. The key intermediate of the HWE pathway is the phosphonate **2** which has been extensively used in literature to synthesize a diverse class of symmetrically substituted 2,2'–bipyridine chromophores. The concerned intermediate (**2**) was easily derived from the corresponding halomethyl derivatives through an Arbuzov reaction. An initial attempt to

Table 1. Synthesis of the 4–styrylbenzaldehydes.

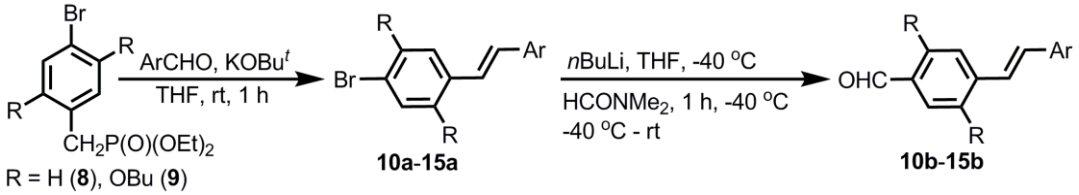

Phosphonate	ArCHO	Bromostilbenes	Styrylbenzaldehydes
8	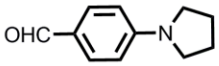 **7a**	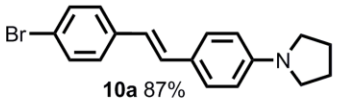 **10a** 87%	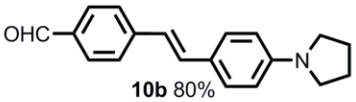 **10b** 80%
8	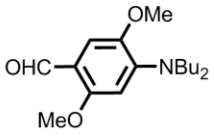 **5b**	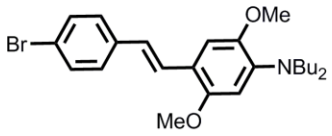 **11a** 91%	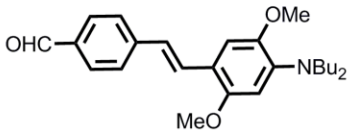 **11b** 68%
8	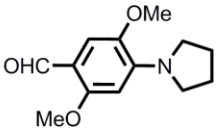 **7b**	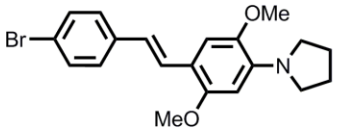 **12a** 94%	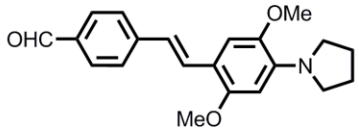 **12b** 70%
9	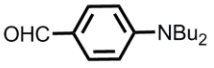 **5a**	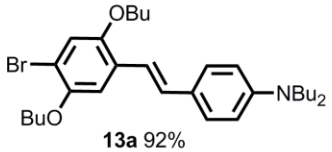 **13a** 92%	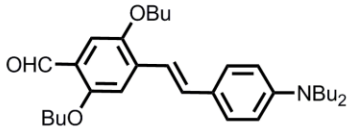 **13b** 57%
9	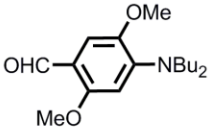 **5b**	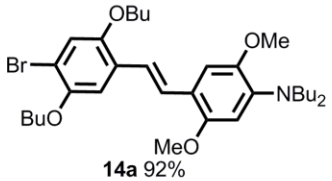 **14a** 92%	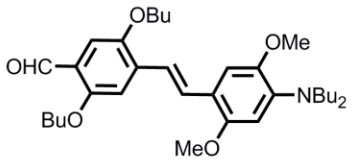 **14b** 47%
9	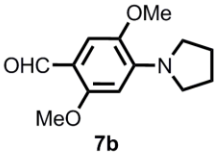 **7b**	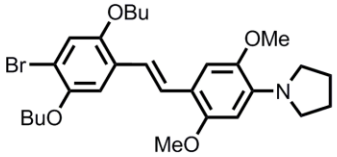 **15a** 88%	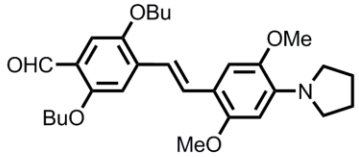 **15b** 50%

brominate **1** through a radical mechanized reaction route (NBS/benzoylperoxide or AIBN) was unsatisfactory for obtaining 4,4'–*bis*–bromomethyl–2,2'–bipyridine. However, the corresponding chloromethyl derivative, **1a**, was used throughout the present work which had been synthesized following an efficient synthetic protocol

developed by Fraser and co-workers. The concerned two-step approach involved deprotonation of **1** with LDA and trapping of the resulting carbanion with chlorotrimethylsilane, followed by subsequent chlorination with hexachloroethane in presence of a dry fluoride source, cesium fluoride (CsF).[20] The aldehydes used in the present study were not commercially accessible and therefore, were synthesized as described in the following sections.

The anilines **3a**–**b** were alkylated in presence of the suitable electrophiles in N-methylpyrrolidinone (NMP)–DMF solvent system to obtain the desired *N*,*N*–dialkyl anilines (**4a–b**, **6a**–**b**) in good yield (Scheme 2). Our experimental observation suggested that usage of 10% N–methylpyrrolidinone (NMP) in DMF as solvent afforded the corresponding N,N–dialkylanilines in better yield compared to other reagents and/or solvent combinations such as K_2CO_3–acetone/ethanol/DMF/THF or NaH–THF/DMF etc. Subsequently, the Vilsmeier–Haack formylation of the *N*,*N*–dialkyl anilines (**4a–b**, **6a–b**) converted them to the corresponding benzaldehydes (**5a–b**, **7a–b**) with excellent *para*–selectivity.

The π–conjugated benzaldehydes bearing different substitutions were obtained through a two–step synthetic approach as depicted in Table 1. The introduction of different donor functionalities in the corresponding aldehydes **10b–15b** was executed *via* the appropriate selection of the starting materials. The usage of an alkoxy derivatized phosphonate precursor (**9**) allowed the introduction of the alkoxy functionalities in the formylated phenyl rings. At the outset, the HWE reaction between the appropriate phosphonate (**8–9**) and the alkylaminobenzaldehydes (**5a–b**, **7a–b**) afforded the corresponding bromostilbenes (**10a–15a**) in excellent yield with the *E*–selectivity of the C=C bonds. Subsequent lithium–halogen exchange reaction followed by electrophilic quenching with dimethylformamide converted the bromostilbenes (**10a–15a**) to the corresponding benzaldehydes (**10b–15b**) in moderate to good yields (Table 1).

● 4.2.2. NMR spectroscopy

The molecular structures of all the synthesized bipyridine chromophores (**MS 1**–**8**) were unambiguously determined through NMR (^{1}H and ^{13}C) and mass (LC–MS and MALDI–TOF/TOF) spectroscopy. The presence of only one set of ^{1}H and ^{13}C signals in the NMR spectra evidently demonstrates the symmetrical nature of the chromophores. The ^{1}H

NMR resonances of the pyridine rings and that of the vinylic protons for the chromophores, **MS 1**–**8** are summarized in Table 2. The pyridine–$H^{6,6'}$ protons, being largely deshielded by the adjacent electronegative nitrogen atom appear as the most downfield shifted signal while the pyridine–$H^{5,5'}$ protons, owing to their meta–orientation with respect to the nitrogen atom, resonate in the benzene region (Table 2). The downfield shift of the pyridine–$H^{3,3'}$ protons compared to the pyridine–$H^{5,5'}$ protons can be attributed to the *transoid*– arrangement of the two pyridine rings in the relevant bipyridine chromophores.[13f] All the vinylic C=C bonds are found to be in *E*–geometry as

Table 2. Selected ^{1}H NMR chemical shifts for MS 1–8. All the spectra were recorded at 400 MHz working frequency in $CDCl_3$ at 298±2 K. The resonances are reported in ppm with respect to the TMS signal.

Compound	Py–$H^{6,6'}$ [a]	Py–$H^{3,3'}$	Py–$H^{5,5'}$ [b]	CH=CH [c]
MS 1	8.625 (d)	8.48 (s)	7.35–7.34	7.41 (d), 6.91 (d)
MS 2	8.635 (d)	8.48 (d)	7.44–7.43	7.75 (d), 7.05 (d)
MS 3	8.605 (d)	8.46 (s)	7.43–7.41	7.75 (d), 6.98 (d)
MS 4	8.695 (d)	8.56 (s)	7.42–7.40	7.50 (d), 7.47 (d), 7.14 (d), 7.00 (d)
MS 5	8.680 (d)	8.56 (s)	7.42–7.40	7.50 (d), 7.47 (d), 6.94 (d)
MS 6	8.675 (d)	8.52 (s)	7.46–7.45	7.80 (d), 7.28 (d), 7.20 (d), 7.10 (d)
MS 7	8.675 (d)	8.51 (s)	not resolved	7.80 (d), 7.37 (d), 7.21 (d)
MS 8	8.675 (d)	8.51 (s)	not resolved	7.80 (d), 7.49 (d), 7.32 (d), 7.20 (d)

[a] $^3J_{HH}$ = 4 Hz except in **MS 5** for which J = 8 Hz; [b] could be either doublet or doublet of doublet; [c] coupling constant ($^3J_{HH}$) ≈ 16 Hz, for **MS 5** and **MS 6** one signal is overlapped with others and could not be separately detected. **MS 1**–**3** contains only two vinylic protons in their molecular structure.

indicated by the splitting of each of the CH resonances by the neighbouring protons with a $^3J_{HH}$ coupling constant of *ca*. 16 Hz. However, no trace of the *Z*–isomer has been signified in the relevant ^{1}H NMR spectra. A comparison between the ^{1}H NMR signals due to the aromatic protons of the open chain amino donor end-capped chromophore **MS 2** (dibutylamino donor) and its cyclic analogue i.e. **MS 3** (pyrrolidine donor) reveals that the protons attached *ortho*– to the amino functionalities have a larger chemical shift in case of **MS 2** as compared to **MS 3** (see Figure 1). The figure herein evidently shows that all the aromatic protons of the two chromophores, except those attached to the *ortho*–position with respect to the amino functionality ($H^{11,11'}$), have almost similar chemical

shifts. The $H^{11,11'}$ nuclei of **MS 2** resonate at δ 6.50 while those corresponding to **MS 3** has been upfield shifted to δ 6.27 in the NMR spectra. This is clearly indicative of a more shielded environment around the relevant protons in the cyclic amino donor end-capped chromophore **MS 3** in comparison to the open chain analogue **MS 2**. The electron donating mesomeric effect of the amino groups makes the corresponding *ortho*– position

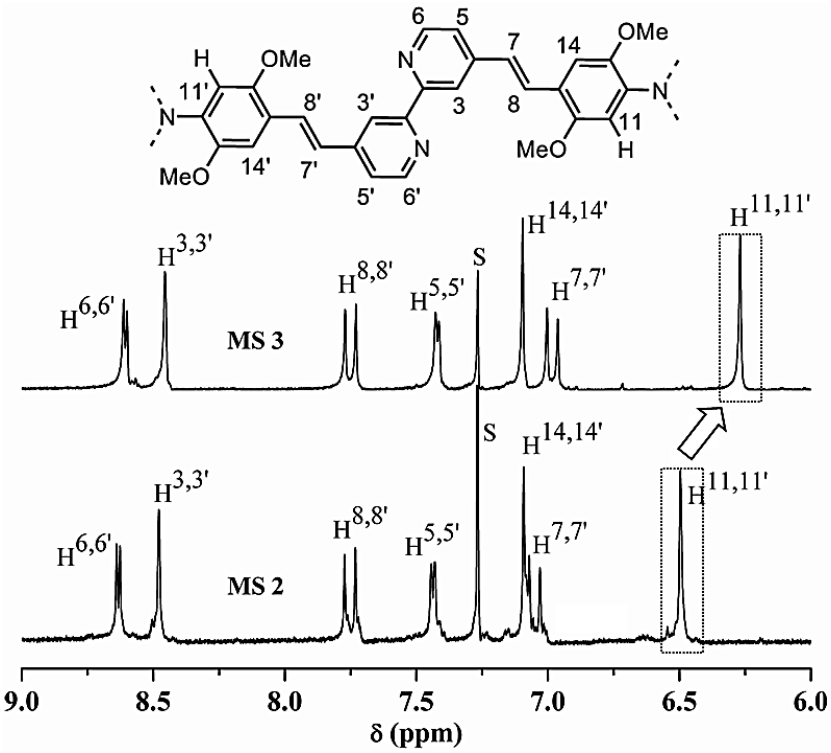

Figure 1. ^{1}H NMR signals of MS 2 and MS 3 in the aromatic region of the spectra (400 MHz, $CDCl_3$, 298 ±2 K) showing the difference in chemical shift of the proton adjacent to the amino donor ($H^{11,11'}$). S = solvent signal.

of the phenyl rings more electron rich thereby exerting greater shielding effect on the relevant protons ($H^{11,11'}$). Thus, it can be aptly said that the pyrrolidine moiety has a greater donation capability than the corresponding open chain amino donor, dibutylamine. The concerned protons in the other open chain/cyclic amino donor pairs *viz.* **MS 4**/**MS 5** and **MS 7**/**MS 8** resonates at δ 6.55/6.31 and δ 6.53/6.31 respectively. A similar trend has also been observed for resonances of the carbon atoms *ortho*– to both the amine and the alkoxy functionalities (e.g. $C^{11,11'}$ in **MS 2**/**MS 3**) in the relevant ^{13}C NMR spectra which display upfield shifted signals in the pyrrolidine end-capped chromophores as compared to the dibutylamino end-capped systems.

Table 3. Summary of the optical data of the synthesized chromophores (MS 1–8).

Compound	Solvent [a]	λ_{max} (nm)	ε (±500-1000) [b] ($L.mol^{-1}.cm^{-1}$)	λ_{em} [c] (nm)	Φ_{em}(±0.1) [d]	$\bar{\Delta\nu}$ [e] (cm^{-1})
MS 1	Toluene	390		448	0.05	3320
	THF	393		485	0.09	4827
	DCM	396		498	0.09	5172
MS 2	Toluene	392		472	0.09	4324
	THF	396		507	0.17	5529
	DCM	399	60000	533	0.20	6301
	MeCN	397		550	0.03	7007
MS 3	Toluene	408		480	0.10	3677
	THF	410		516	0.18	5010
	DCM	414	84000	543	0.17	5738
	MeCN	408		560	0.04	6653
MS 4	Toluene	409	114000	540	0.55	5931
	THF	409	100000	615	0.64	8190
	DCM	413	95000	644	0.37	8685
	MeCN	405		585	0.07	7597
MS 5	Toluene	427		552	0.85	5303
	THF	426		630	0.72	7601
	DCM	430	122000	662	0.21	8150
	MeCN	428		603	0.17	6781
MS 6	Toluene	436	116000	538	0.66	4348
	THF	437	99000	575	0.81	5492
	DCM	442	95000	598	0.65	5902
	MeCN	433		641	0.19	7494
MS 7	Toluene	432	100400	550	0.63	4966
	THF	431	96000	591	0.62	6281
	DCM	435	87000	648	0.35	7556
	MeCN	430		650	0.03	7871
MS 8	Toluene	445	131000	556	0.59	4486
	THF	445	100000	627	0.61	6523
	DCM	448	98500	660	0.23	7170
	MeCN	428		640	0.07	7740

[a] $E_T(30)$ values of the used solvents are as follows: Toluene (33.9), THF (37.4), DCM (40.7), MeCN (45.6).[21] [b] Data is represented as the average of five measurements. In cases where no data are reported, this is due to low solubility. [c] The solutions were excited at the corresponding lowest energy absorption maxima. [d] Fluorescence relative quantum yield of the compound **MS–1** was measured using quinine sulfate (in 1N H_2SO_4) as the reference (Φ_{em} = 0.545)[22] and that of rest of the compounds (**MS 2–8**) were performed using DCM–Pyran as the reference in MeOH (Φ_{em} = 0.435)[23]. Comparable result was obtained using fluorescein (in 0.1N NaOH) as the standard substance too. Optically matched solutions (OD ≈ 0.05) of the samples and that of the standards were excited at identical operating condition. The data is presented as an average of two measurements. [e] Stokes shift $\bar{\Delta\nu} = \bar{\nu}_{abs} - \bar{\nu}_{em}$.

● 4.2.3. Steady-state absorption and emission properties

(a) Nature of substituents. The steady-state one photon absorption and emission properties of the synthesized chromophores **MS 1**–**8** have been investigated in four different solvents (see Table 3 and Figure 2). The nature and position of the donor functionalities in the molecular conjugated backbone and the polarity of the fluid medium in which the compounds are dissolved, were observed to have a profound effect on the absorption and emission properties of the synthesized chromophores. As shown in Figure 2, broad structureless bands of the absorption and emission spectra in the visible region are the chief characteristic features of all the chromophores in the present study. The molar extinction coefficient (ε) of the lowest energy absorption band of all the chromophores is fairly high and though it varies only slightly with the solvent polarity, the nature of the donor functionality has an immense influence on it (see Table 3). The low solubility of **MS 1** precluded measurement of the molar absorptivity with a better accuracy. The origination of the lowest energy band in the absorption spectra of **MS 1**–**8**, however, is due to an intramolecular π→π* charge transfer (ICT) from the donor based molecular orbitals to the acceptor (pyridine) based molecular orbitals in the relevant dipolar chromophores which in fact, is firmly affirmed owing to the sensitivity of the relevant absorption band on the solvent polarity (see Table 3). In addition, the ICT band maxima undergoes a bathochromic shift by *ca.* 15 nm for the pyrrolidine end-capped (cyclic amino donor) chromophores as compared to that of the dibutylamino (open chain amino donor) analogues *viz.* **MS 2**/**MS 3**, **MS 4**/**MS 5** and **MS 7**/**MS 8** in the same solvent medium (Table 3). The rationale for this observation might be due to the greater donation capability of the cyclic pyrrolidine donor compared to the open chain dibutylamino donor. This context has already been discussed in the previous section by the up-field shift of the ^{1}H NMR signal of the proton attached *ortho*– to both the amino and the methoxy functionalities in the relevant chromophores (*vide supra*).

Upon excitation at the lowest energy absorption maxima, the chromophores **MS 1**–**8** exhibit a bright fluorescence at room temperature with a large Stokes shift from the relevant absorption maxima (see Table 3). The positions of the corresponding emission maxima are found to be independent of the excitation wavelength thereby indicating that the photoluminescent nature of the synthesized chromophores holds concurrence with

Kasha's law of photochemistry. Likewise, an excellent overlapping of the excitation spectra with the relevant lowest energy absorption maxima for the title chromophores **MS 1**–**8** has been observed (see Figure 2a and 2b). The effect of solvent polarity on the emission property of the present chromophores is found to be more pronounced as compared to the absorption spectra (see Table 3). For instance, increasing the solvent polarity from toluene to DCM induces a bathochromic shift of *ca*. 6–7 nm in the electronic absorption spectra of the first homologues **MS 1**–**3**, whereas the corresponding emission maxima are red–shifted by about 50–63 nm due to the same polarity increment. This observation is indicative of the fact that the photo–excited state of the concerned luminophores is markedly polar than the ground electronic state. The effect of solvent polarity on the emission properties is even more profound in case of the OPV derivatives **MS 4**–**8** compared to the *styryl*– analogues **MS 1**–**3** (see Table 3 and Figure 2c). For example, alteration of the solvent polarity from toluene to DCM brings about 61–63 nm bathochromic shift of the emission maxima for the first homologues **MS 2**–**3** but as large as 104–110 nm shift of the emission maxima to the longer wavelength has been observed in case of the second homologues **MS 4**–**5** under the same polarity deviation (see Table 3) and the emission color changes from deep green to orange-red (see Figure 2c). The general tendency of the dipolar fluorophores is the shifting of their emission maxima to lower energy (longer wavelength) as they approach more polar solvents owing to the fact that they exhibit a large change in dipole moment during the photo–excitation process. Thus, the excited state is stabilized by the solvent molecules via solvation through the dipole–dipole interactions and this reduces the energy gap between the emitting state and the ground electronic state of the fluorophore in the more polar solvents. However, on increasing the solvent polarity from DCM to acetonitrile, the hipsochromic shift of the emission maxima by ~60 nm for **MS 4**–**5** and ~ 20 nm for **MS 8** in contrast to the 43 nm and 2 nm bathochromic shift of the same for **MS 6** and **MS 7** respectively is not fully understood. The variation in the photoluminescent quantum yield of all the title fluorophores were examined with the same set of solvents and are compiled in Table 3. The OPV derivatives, **MS 4**–**8**, exhibit brighter fluorescence in comparison with the first homologues, **MS 1**–**3** (see Table 3). The relative quantum yield of the title chromophores is however, strongly dependent on the fluid medium and an irregular alteration of the

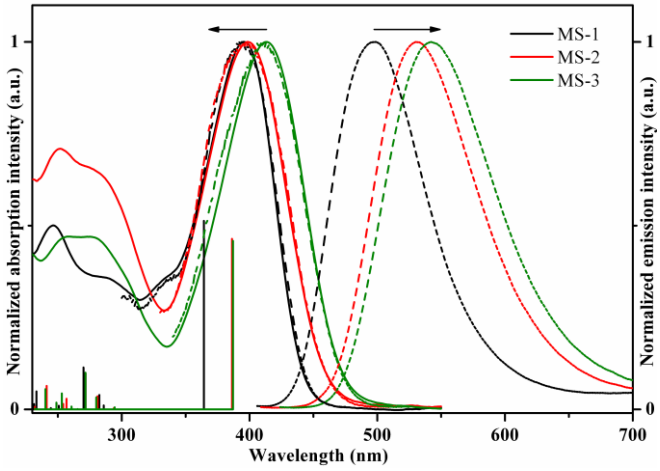

(**a**)

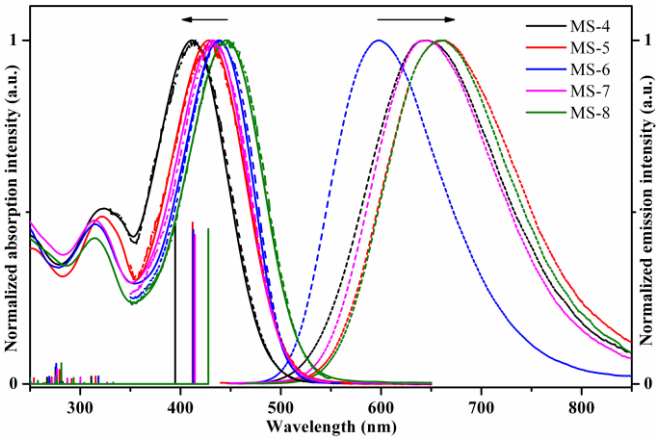

(**b**)

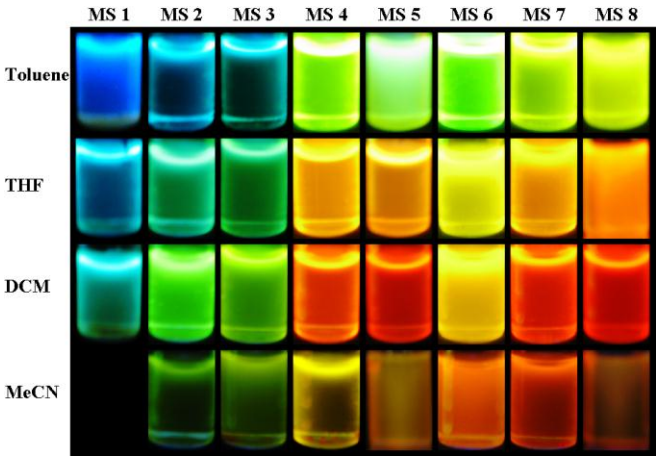

(**c**)

Figure 2. Normalized absorption (solid lines, concentration of the samples being ~1x10^{-5} M), emission (dashed lines) and excitation spectra (overlapped with the absorption spectra) together with the computed vertical excitation energies (stick lines) of (a) **MS 1**–**3** and (b) **MS 4**–**8** in DCM at 298±2K. All the solutions were excited at the lowest energy absorption maxima. Heights of the vertical lines have been adjusted so as to obtain a viewing lucidity; the relative heights are however in scale. (c) Photographs showing photoluminescence behavior of the **MS 1**–**8** in four different solvents illuminated under an UV lamp (excitation 365 nm) in the dark.

same with the solvent polarity is observed (see Table 3). The sensitivity of the absorption and emission properties of the title choromophores to the fluid medium evidently portrays the 'push–pull' architecture of **MS 1**–**8**. Apart from all the above mentioned observations, some unique spectroscopic features were explored while altering the substituents and these have been addressed in the following sections, taking into account the spectral behavior of **N945L**, **HLB 1**, **HLB 2** and **TM 6**.

The 4–dibutylaminostyryl chromophore **HLB 1** absorbs at 401 nm (ε = 65000 $L.mol^{-1}.cm^{-1}$) due to an ICT and emits at 497 nm (Φ_{em} = 0.230) from the corresponding excited state in DCM.[13d] Similarly, the 2,5–dimethoxystyryl chromophore **N945L** absorbs and emits at 358 nm (ε = 40410 $L.mol^{-1}.cm^{-1}$) and 450 nm (Φ_{em} = 0.430) respectively in DCM involving the ground and excited ICT states.[15a] However, the chromophore **MS 2** which was designed and synthesized by introducing both methoxy as well as dibutylamino donor substituents together in the same ring positions as in **HLB 1** and **N945L**, exhibits a modulated photophysical behavior compared to the two concerned reported chromophores **HLB 1** and **N945L**. A comparison of the photophysical parameters of **MS 2** with that of its parents **HLB 1**[13d] and **N945L**[15a] shows that the ground state property of **MS 2** is comparable with that of **HLB 1**. Even though it was expected that the coexistence of the amino and the alkoxy donor functionalities in the same chromophore would lead to a bathochromic shift of the corresponding charge transfer band, this was not actually found to be the case with **MS 2**. Our observation rather suggests that, owing to the greater donation capability of the amino donor functionality, it has a dominant contribution in the respective π(phenyl)→π*(pyridine) charge transfer interaction since the optical response of the ground state of **MS 2** resembles that of **HLB 1** and not of **N945L**. Thus, the presence of methoxy groups together with the amino substituent has a little influence on the electronic absorption properties of the chromophore. However, a significant variation in the emission color is observed for **MS 2** as compared to **HLB 1** or **N945L**. The chromophore **MS 2** exhibits a deep green emission at 533 nm in DCM which occurs at a considerable longer wavelength than the emission due to **HLB 1** (497 nm) or **N945L** (450 nm). The addition of the amino functionality to **N945L** or two methoxy donors to **HLB 1** generates **MS 2** which exhibits a significant weaker fluorescence compared to **N945L** though the

fluorescence quantum yields of **MS 2** and **HLB 1** are reasonably comparable. Hence, it can be said that presence of both the amino and methoxy functionalities in the same chromophore has more profound effect on the emitting state compared to the ground state of the aforementioned luminophores. At this juncture, it is worth mentioning that the position of the donor functionalities plays a crucial role for the variation of the quantum efficiency in the 4,4'–π–conjugated–2,2'–bipyridine fluorophores.

The absorption and emission behaviour of the OPVs, **HLB 2**, **TM 6** and **MS 4** follow an almost similar trend as the first homologues *viz.* **HLB 1**, **N945L** and **MS 2** respectively. In contrast to the first homologues, where the donor substituted phenyl ring and the pyridine acceptor sub–chromophore are separated by an olefinic spacer, the corresponding OPV chromophores **HLB 2**, **TM 6** and **MS 4** are associated with an extended π–skeleton involving an additional styryl spacer in between the donor–acceptor fragments. For a convenient discussion in the text, the two phenyl rings of the OPV chromophores are named as ring–A and ring–B (see Chart 1). The absorption and emission spectra of **HLB 2** consisting of the dibutylamino donor functionality at ring–B ($R_3 = NBu_2$, see Chart 1) are characterized by the relevant maxima at 420 nm (ε = 78000 $L.mol^{-1}.cm^{-1}$) and 598 nm (Φ_{em} = 0.700) respectively in DCM with a Stokes shift of 7087 cm^{-1}.[13h] The OPV chromophore **TM 6** bearing two methoxy functionalities at the 2,5–positions of ring–B has recently been reported by us.[19a] This chromophore exhibits an absorbance maximum at 380 nm (ε = 45900 $L.mol^{-1}.cm^{-1}$) and emission maximum at 488 nm (Φ_{em} = 0.730) in DCM with a Stokes shift of 5824 cm^{-1}. Under similar experimental conditions, the hybrid chromophore **MS 4**, which comprises both the $–NBu_2$ and the –OMe functionalities in the same positions as in **HLB 2** and **TM 6**, absorbs at 413 nm (ε = 95000 $L.mol^{-1}.cm^{-1}$) due to an ICT and exhibits an orange–red emission (λ_{em} = 644 nm, Φ_{em} = 0.365) with a very large Stokes shift (8685 cm^{-1}) from the relevant absorption maximum. Thus, alike the first homologues, coexistence of the methoxy donors along with the dibutylamino groups in **MS 4** has a very little influence on the absorption wavelength. The molar extinction coefficient of the ICT band of **MS 4** is however, significantly larger than that of **HLB 2**. The influence of methoxy donors is found to be rather dramatic on the fluorescence behavior of the relevant OPV chromophores. It has been observed that compared to **HLB 2** and **TM 6**, the fluorophore **MS 4** emits at a

considerably longer wavelength, but with almost half quantum efficiency. In other words, both the approaches, *viz.* (a) attaching methoxy donors to **HLB 2** at ring–B or (b) introducing amino donor to **TM 6** at ring–B render a significant bathochromic shift of the emission wavelength in the resultant chromophore with the concomitant diminution of the fluorescence brightness. In this context, some important experimental observations need to be addressed. The fluorescence quantum yields of both the chromophores, **HLB 2** and **TM 6** are almost similar (Φ_{em} = 0.700 vs 0.730 respectively) which signifies that the fluorescence brightness of the OPV chromophores, containing donor functionalities at the ring–B, is not much sensitive to the nature of the donor, as far as the chromophore is associated with similar type of electron pushing moiety. An almost identical situation is observed with the OPV chromophores containing two methoxy donors at the 2,4– and 2,5– positions of ring–B (Φ_{em} = 0.700 vs 0.730 respectively) thereby indicating that the quantum efficiency of the related chromophores is independent of the position of the donor functionalities.[19a] However, the effect of nature and position of the donor sub–chromophores on the fluorescence brightness of the first homologues is remarkably different. The divergence in quantum yield of **HLB 1** (Φ_{em} = 0.230) and **N945L** (Φ_{em} = 0.430) is noteworthy.

(b) Position of substituents. A careful analysis of the optical data presented in Table 3 reveals some interesting features. The influence of the nature of donor and conjugation length on the photophysical behavior of the bipyridine chromophores has already been addressed in the previous section. The OPV chromophores **MS 4**, **MS 6** and **MS 7** were designed and synthesized in order to investigate the outcome of varying the position and number of alkoxy donors on the absorption and emission properties of the relevant chromophores. In **MS 4**, two methoxy donors are attached with the ring–B at 2,5–positions along with the dibutylamino donor at 4–position (Chart 1). In case of **MS 6,** two butyloxy donors were used for the aid of solubility in contrast to the two methoxy donors in **MS 4.** Moreover, the alkoxy donors have been moved to ring–A (2,5– positions) in case of **MS 6** as compared to **MS 4**, the total number of donor units being same for both the chromophores. The alkyl chain length in the alkoxy donors is not expected to alter the +I effect to a very significant extent and therefore, spectroscopic features of any chromophore bearing methoxy or butyloxy donor functionalities would be almost

identical. Hence, the variation in the absorption and emission properties of **MS 4** and **MS 6** is administered only by the position of the alkoxy donors in the conjugation backbone of the relevant chromophores. The absorption due to an intramolecular charge transfer in

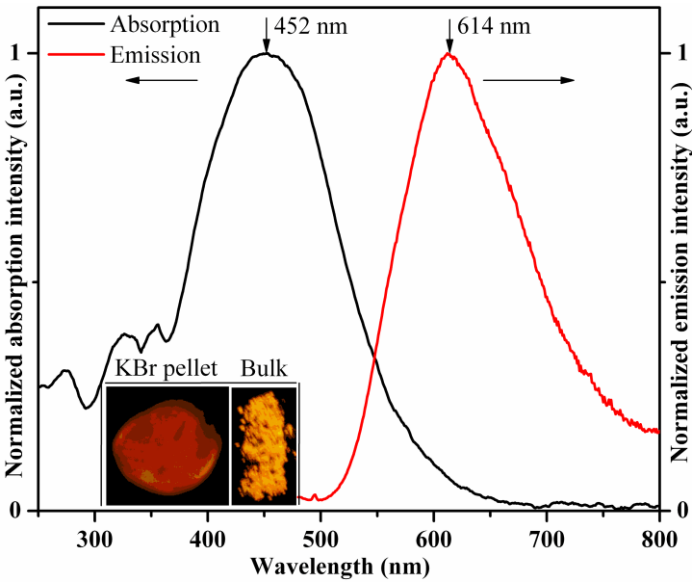

Figure 3. Solid state absorption (black) and emission (red) spectra of **MS 5** at room temperature (KBr pellet, arbitrary concentration). The inset shows photographs of the relevant KBr pellet and bulk sample illuminated with a 365 nm UV lamp.

MS 6 (442 nm in DCM) is shifted to longer wavelength by *ca.* 30 nm compared to that in **MS 4** (413 nm in DCM) and the reason behind this might probably be due to the greater extent of conjugation between the alkoxy donor and pyridine acceptor functionalities in **MS 6** due to a smaller separation between the donor-acceptor moieties. On the contrary, the emission spectrum of **MS 6** exhibits almost 45 nm hypsochromic shift compared to **MS 4** in DCM and furthermore, the fluorescence quantum yield of **MS 6** is considerably larger than that of **MS 4** (Φ_{em} = 0.65 for **MS 6** and 0.37 for **MS 4** in DCM). The chromophores **MS 7** and **MS 8** bear the highest number of donor units among all the compounds discussed in this chapter. Most surprisingly, in spite of attaching extra alkoxy donors with the ring–B of **MS 6,** a further shift of the ICT absorption to the longer wavelength has not been induced but instead a hypsochromic shift of *ca.* 7 nm of the relevant band position is observed for **MS 7**. The emission properties of the luminophores **MS 4** and **MS 7** are almost similar except in MeCN in which the former exhibits yellow emission but the latter exhibits red emission (see Table 3 and Figure 2c).

● 4.2.4. Solid state emission of MS 5

Among all the studied 'push-pull' chromophores in the present work, **MS 1**–**8**, the compound **MS 5** fluoresces even in the solid state. The solid state absorption and emission spectra of the pertinent compound were recorded in dilute KBr matrix and the relevant spectra are presented in Figure 3. The absorption spectrum is characterized by a broad band centered at 442 nm which is slightly red-shifted with respect to the absorption maxima of the relevant dyad in dissolved media (see Table 3). The bathochromic shift of the absorption maximum in condensed phase as compared to that of the solution state is presumably due an aggregation. When excited at the relevant absorption maximum, the chromophore **MS 5** exhibits orange emission with the maximum intensity at 614 nm (see Figure 3).

● 4.2.5. Computational analysis

(a) General considerations. To gain insight into the effect of various substituents on the geometrical and electronic outcome of the 2,2'–bipyridine chromophores, Density Functional Theory (DFT) and Time Dependent DFT (TD–DFT) were applied on the synthesized compounds **MS 1**–**8** along with **HLB 1**, **N945L**, **HLB 2**, **TM 6**, *styryl*– and *bistyryl*– derivatives without any donor substituent using the Gaussian09 program package.[24] The fundamental aim of the current work is to understand the influence of the nature and position of the various donor functionalities on the electronic properties of the 4,4'–π–conjugated–2,2'–bipyridine dyads functionalized with two dissimilar donor units. As a result, more emphasis is given to the electronic structures of the studied systems instead of their geometrical parameters in this section. In a nutshell, we have made an attempt to draw a correlation between the structural and electronic aspects of the related systems. Our computational analysis begins with the *styryl*– and *bistyryl*– 2,2'–bipyridine skeleton without any donor functionality. In addition, computational investigation has been carried out with **HLB 1**, **N945L**, **HLB 2** and **TM 6** along with the synthesized dyads of the present work. Although the DFT analysis of **N945L** has already been reported,[15a] we reproduced the same with our own computational set-up for the purpose of ready comparison. A semi-empirical calculation on **HLB 2** was earlier reported by Hernández and co-workers (named as **SY187**).[25] However, the absence of any X-ray crystal structure for the dye molecules of the present work impelled us to optimize the

geometries of all the studied systems, which in fact, was accomplished using the CAM-B3LYP exchange–correlation hybrid functional together with the 6–31+g(d) basis set imposing C_i symmetry constraint. As the donation strength of butyl and methyl groups is not supposed to differ much, all the butyl chains of the OPV derivatives (**MS 4**, **MS 6** and **MS 7**) were truncated to the methyl groups in an attempt to reduce the number of basis functions and consequently to increase the computational speed. The relevant geometrical structures were modelled by applying the Self–Consistent Reaction Field (SCRF) under Polarizable Continuum Model (C–PCM) incorporating DCM as the solvent. For the purpose of ready comparison between the various computed parameters, an identical theoretical set-up was maintained throughout the course of the computational investigations. As the *transoid*– conformation is energetically more favorable for the free bipyridine derivatives, all the geometry optimizations were carried out on *transoid*– input structures and no attempt was made to optimize the *cisoid*– input geometries. The DFT computed HOMO and LUMO Frontier Molecular Orbitals (FMOs) of the chromophores **MS 1**–**8** are presented in Figure 4. A scrutiny on the computer modelled structures of the studied systems reveals some common features such as, almost coplanar structures of the systems which are devoid of any alkoxy functionality, out–of–plane displacement of the phenyl rings bearing the alkoxy substituents from the planes containing the pyridine ring and the C=C vinylic bonds etc. Hence, these matters have not been individually addressed over again for the systems used in this study.

(b) Electronic aspects. An investigation on the electronic structures reveals that an almost similar type of localization and nature of HOMO and LUMO are retained among the individual homologues (see Figure 4), the only difference being in the energy of these FMOs, which in turn, depend on the system architecture. The HOMO of the relevant chromophores is associated with the in–phase and out–of–phase π–bonding combination and consists of major coefficients at the phenyl rings containing the donor substituents and at the C=C vinylic bonds. On the contrary, the LUMO of the model structures stems from the π*–type combination of the molecular orbitals (MOs), mainly contributed by the C=C bonds and the two pyridine rings along with a sizeable coefficient on the C–C bond joining the two pyridine rings. The modulation of energy for the four occupied (HOMO–3, HOMO–2, HOMO–1, HOMO) and four virtual (LUMO, LUMO+1, LUMO+2, LUMO

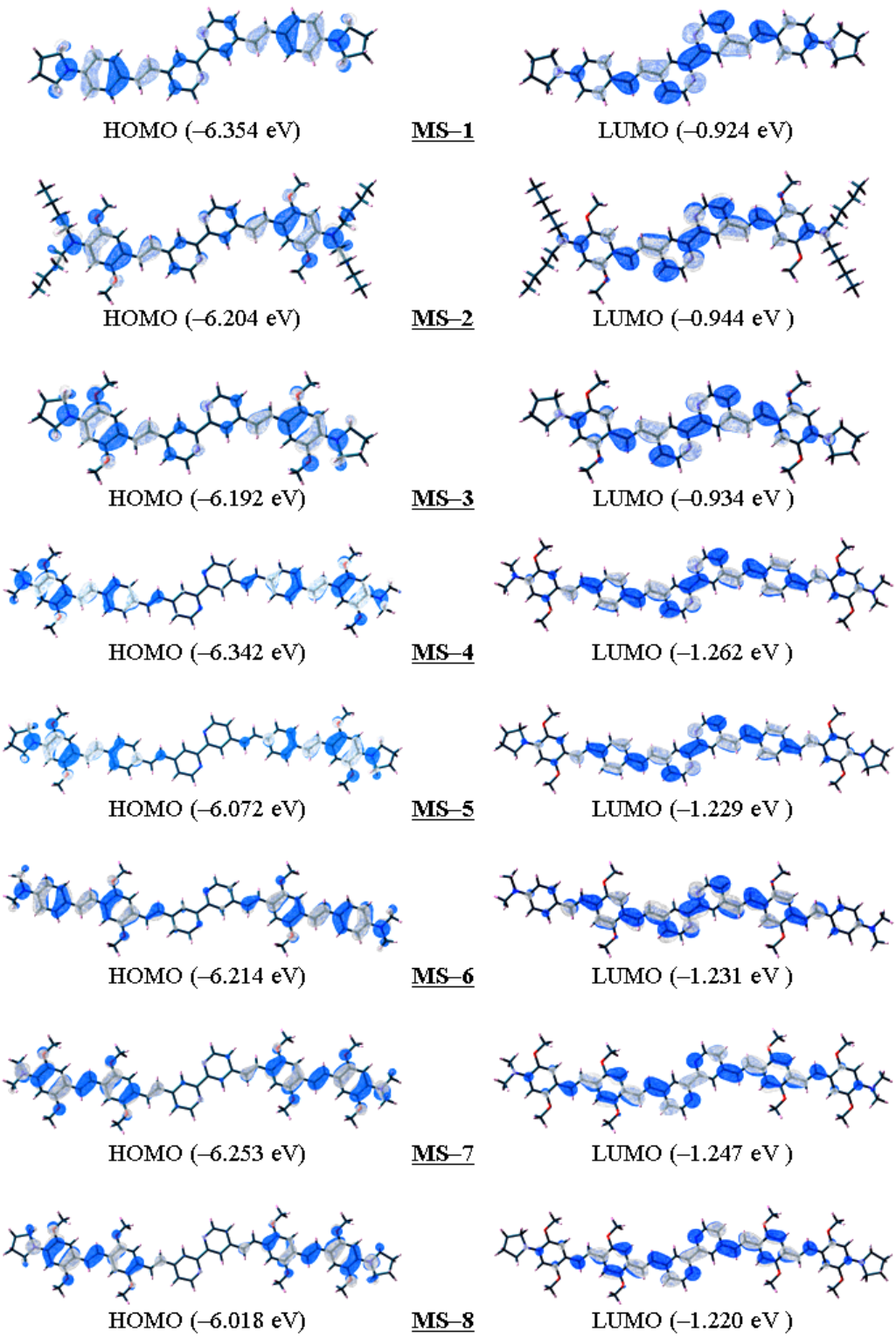

Figure 4. Isodensity plots of HOMO and LUMO frontier molecular orbitals of the bipyridine chromophores **MS 1–8** as computed by the CAM-B3LYP/6–31+g(d) level of theory (isodensity value = 0.02). The butyl chains of **MS 4** and **MS 6–8** were truncated to the methyl groups.

+3) molecular orbitals upon alteration of the core architecture in the studied systems is presented in Table 4. The HOMO–1 and HOMO occupied MOs of all the studied systems constitute an almost degenerate couple. Such pairs in 4,4'–distyryl–2,2'–bipyridine and 4,4'–*bis*(4–styrylstyryl)–2,2'–bipyridine which are devoid of any donor functionality are most stabilized among all the model structures and are computationally estimated at –7.524/–7.470 and –6.921/–6.897 eV respectively. A considerable destabilization of the HOMO and HOMO–1 by 1.153 and 1.180 eV respectively is observed on introduction of the $–NBu_2$ functionality (**HLB 1**) with concomitant lowering of the HOMO–LUMO gap by 0.945 eV. An identical donor alteration from **MS 2** to **MS 3** results in destabilization of the HOMO as well as lowering of the E_g value by 0.030 and 0.030 eV respectively for **MS 3**, thereby pinpointing to the greater electron pushing effect of the pyrrolidine donor compared to that of the $–NBu_2$ functionality in **MS 2**. The HOMO of **N945L** (–6.99 eV) is stabilized by 0.660 eV with respect to **HLB 1** (E_{HOMO} = –6.33 eV) and hence, the E_g value of **N945L** is elevated by 0.390 eV as compared to **HLB 1**. This observation is in concurrence with the stronger donation propensity of the amino functionality in **HLB 1** than the methoxy donor in **N945L**. However, when both the methoxy and the amino functionalities are positioned together in **MS 2**, an attenuation of the E_g value by 0.130 eV with respect to **HLB 1** is computed thereby signifying to the greater electron pushing influence of the mixed donor system, **MS 2** as compared to the single donor systems **N945L** or **HLB 1.** Overall, a varying degree of destabilization of the HOMO–1 and HOMO occupied levels along with alteration of the HOMO–LUMO gap has been observed upon introduction of the donor substituents to the 2,2'–bipyridine core skeleton (see Table 4). The consequence of conjugation length on the electronic structure of the bipyridine dyads is evidently comprehended in the computer modelled structures. For example, expansion of conjugation from **MS 3** to **MS 5** results in destabilization of the HOMO by 0.11 eV and a sizable shrinking of the HOMO–LUMO gap by 0.40 eV in **MS 5** with respect to **MS 3**. As depicted in Figure 4, the π–character of the two phenyl rings and that of the two C=C vinyl linkages of the OPV derivatives attribute to the HOMO, the extent of localization being dependent upon the position and number of alkoxy donors. For instance in **MS 4**, the HOMO has larger coefficients at ring–B and C=C linkage between rings A and B with a relatively smaller contribution from the ring A.

Table 4. Energy (eV) of four higher occupied (HOMO–3, HOMO–2, HOMO–1, HOMO) and four lower virtual (LUMO, LUMO+1, LUMO+2, LUMO+3) molecular orbitals of the studied systems as computed in CAM-B3LYP/6-31+G(d) level of Theory (in DCM). H = HOMO, L = LUMO.

	H–3	H–2	H–1	H	L	L+1	L+2	L+3
HLB1	–8.19	–7.96	–6.36	–6.33	–0.93	–0.63	0.22	0.71
MS1	–8.19	–7.97	–6.37	–6.34	–0.90	–0.63	0.22	0.71
MS2	–7.62	–7.62	–6.20	–6.20	–0.93	–0.68	0.19	0.73
MS3	–7.64	–7.64	–6.20	–6.17	–0.93	–0.65	0.22	0.73
N945L	–7.92	–7.89	–7.02	–6.99	–1.09	–0.87	0.02	0.60
HLB2	–7.43	–7.40	–6.23	–6.23	–1.22	–1.09	–0.33	0.05
MS4	–7.37	–7.34	–6.34	–6.34	–1.25	–1.14	–0.38	–0.03
MS5	–7.29	–7.26	–6.06	–6.06	–1.22	–1.09	–0.33	0.02
MS6	–7.10	–7.10	–6.20	–6.20	–1.22	–1.12	–0.33	0.05
MS7	–7.07	–7.05	–6.26	–6.23	–1.22	–1.14	–0.38	0.05
MS8	–6.96	–6.94	–6.01	–6.01	–1.20	–1.09	–0.33	0.03
TM6	–7.43	–7.43	–6.75	–6.72	–1.31	–1.20	–0.46	–0.11

Modification of the dyad skeleton from **MS 4** to **MS 6** increases the localization on ring–A and a subsequent destabilization of the HOMO by 0.14 eV and a declination of the E_g value by 0.110 eV with respect to **MS 4** is computed. Further substitution at ring–B leads to a stabilization of the HOMO by 0.03 eV and an increment of the HOMO–LUMO gap by 0.03 eV in **MS 7** with respect to **MS 6**. However, the nature of LUMO in all the OPV derivatives are almost similar and are attributed from the π*–combinations with major localization on the bipyridine central acceptor core and on the 2,2'- C–C bond between the two pyridine rings. Thus, it is obvious that, the modification of the archetype of the π–conjugated 2,2'–bipyridine dyad systems offer a systematic variation of the orbital energies and the HOMO–LUMO gap which are the direct consequences of their photophysical responses. The computational parameters discussed in this section are carried forward in the next section to comprehend the various TD-DFT outputs.

(c) TD-DFT. The inspection of the vertical electronic excitations between the various occupied and virtual energy levels of the studied chromophores as computed by the TD-DFT method reveals a fair agreement between computation and the experimentally observed absorption spectra (see Figure 2a and 2b). The various vertical Frank-Condon electronic excitations were computed by the TD-DFT formalism in order to comprehend the nature of electronic transitions responsible for appearance of the absorption bands in

Table 5. TD-DFT computed (CAM-B3LYP, 6-31+g(d)) representative intense vertical excitations (λ_{calcd}), associated oscillator strengths (*f*) and the experimentally observed band positions (λ_{obs}) for MS 1–8 in DCM.

Compound	Transition (symmetry)	λ_{calcd} (*f*) (nm)	λ_{obs} (nm)
MS 1	HOMO–1(A_g)→LUMO(A_u)	364 (2.873)	396
	HOMO(A_u)→LUMO+1(A_g)		
	HOMO–1(A_g)→LUMO+4(A_u)	282 (0.220)	335
	HOMO–2(A_g)→LUMO(A_u)	270 (0.640)	292
	HOMO–1(A_g)→LUMO+2(A_u)	233 (0.274)	245
MS 2	HOMO–1(A_g)→LUMO(A_u)	386 (2.600)	399
	HOMO(A_u)→LUMO+1(A_g)		
	HOMO–2(A_u)→LUMO+1(A_g)	281 (0.200)	285
	HOMO–4(A_g)→LUMO(A_u)	272 (0.547)	
	HOMO–1(A_g)→LUMO+2(A_u)	241 (0.358)	250
MS 3	HOMO–1(A_g)→LUMO(A_u)	387 (2.568)	414
	HOMO(A_u)→LUMO+1(A_g)		
	HOMO–2(A_u)→LUMO+1(A_g)	280 (0.182)	275
	HOMO–4(A_g)→LUMO(A_u)	272 (0.560)	
	HOMO–1(A_g)→LUMO+2(A_u)	240 (0.308)	257
MS 4	HOMO–1(A_g)→LUMO(A_u)	395 (4.208)	413
	HOMO(A_u)→LUMO+1(A_g)		
	HOMO–3(A_g)→LUMO(A_u)	311 (0.194)	323
	HOMO–2(A_u)→LUMO+1(A_g)		
MS 5	HOMO–1(A_g)→LUMO(A_u)	412 (4.229)	430
	HOMO(A_u)→LUMO+1(A_g)		
	HOMO–3(A_g)→LUMO(A_u)	315 (0.197)	322
	HOMO–2(A_u)→LUMO+1(A_g)		
MS 6	HOMO–1(A_g)→LUMO(A_u)	413 (4.037)	442
	HOMO(A_u)→LUMO+1(A_g)		
	HOMO–3(A_g)→LUMO(A_u)	318 (0.200)	315
	HOMO–2(A_u)→LUMO+1(A_g)		
MS 7	HOMO–1(A_g)→LUMO(A_u)	414 (3.903)	435
	HOMO(A_u)→LUMO+1(A_g)		
	HOMO–7(A_g)→LUMO(A_u)	300 (0.173)	314
	HOMO–6(A_u)→LUMO+1(A_g)		
	HOMO(A_u)→LUMO+3(A_g)	277 (0.393)	
MS 8	HOMO–1(A_g)→LUMO(A_u)	428 (4.058)	448
	HOMO(A_u)→LUMO+1(A_g)		
	HOMO–7(A_g)→LUMO(A_u)	293 (0.159)	314
	HOMO–6(A_u)→LUMO+1(A_g)		
	HOMO(A_u)→LUMO+3(A_g)	281 (0.544)	

the relevant electronic spectra. Some representative excited states for **MS 1**–**8** are presented in Table 5.

The computed vertical excitations for **MS 1**–**8** in DCM are shown in Figures 2a and 2b. An initial attempt to compute the excited states (TD-DFT) using the B3LYP hybrid functional had resulted in large overestimation of the absorption bands, mostly for the OPV analogues. In particular, the well-celebrated TD-DFT method is often known to produce flawed results in case of computation on the excited states of molecules with extended π–systems and those which involve a charge transfer character.[26] This method (TD–DFT) is also known to be sensitive to the functional to gain the correct long-range 1/R dependence on the donor–acceptor distance in the π–expanded systems.[26] The Configuration Interaction Singles (CIS) is a promising method to compute the excited states of such systems but our attempts to calculate the absorption spectra of the present OPV chromophores at this level could not improve the situation. This prompted us to use the recently developed coulomb–attenuated long-range corrected version of B3LYP i.e. CAM–B3LYP hybrid functional which indeed turned out to be very promising as this functional recovers the long-range 1/R behavior.[27]

The lowest energy intense absorption band in all the cases are due to the involvement of two excited states *viz.* HOMO–1→LUMO and HOMO→LUMO+1 excitations with high oscillator strength ($f > 1$) indicating a π→π* charge transfer (ICT) from the donor based molecular orbitals to the pyridine (acceptor) centered molecular orbitals. The HOMO(A_u)→LUMO(A_u) excitation in all the studied systems is symmetrically forbidden and does not contribute to the electronic absorption spectra in the relevant bipyridine dyads. The scenario of the computed electronic excitations thereby essentially points about the 'push-pull' architecture of the pertinent systems. Unfortunately, ~15 nm bathochromic shift of the ICT absorption maximum of **MS 3** in comparison with **MS 2** could not be reproduced through our computational set-up. However, an ~18 nm red-shift of the ICT absorption maximum for **MS 6** has been computed as compared to **MS 4**, very similar to the experimentally observed ~30 nm bathochromic shift upon identical alteration of the donor position (see Table 3). Alteration of the substitution pattern from **MS 4** to **MS 6** causes more destabilization of the HOMOs as compared to the LUMOs resulting in attenuation of the HOMO–LUMO gap in **MS 6** as compared to that in **MS 4**

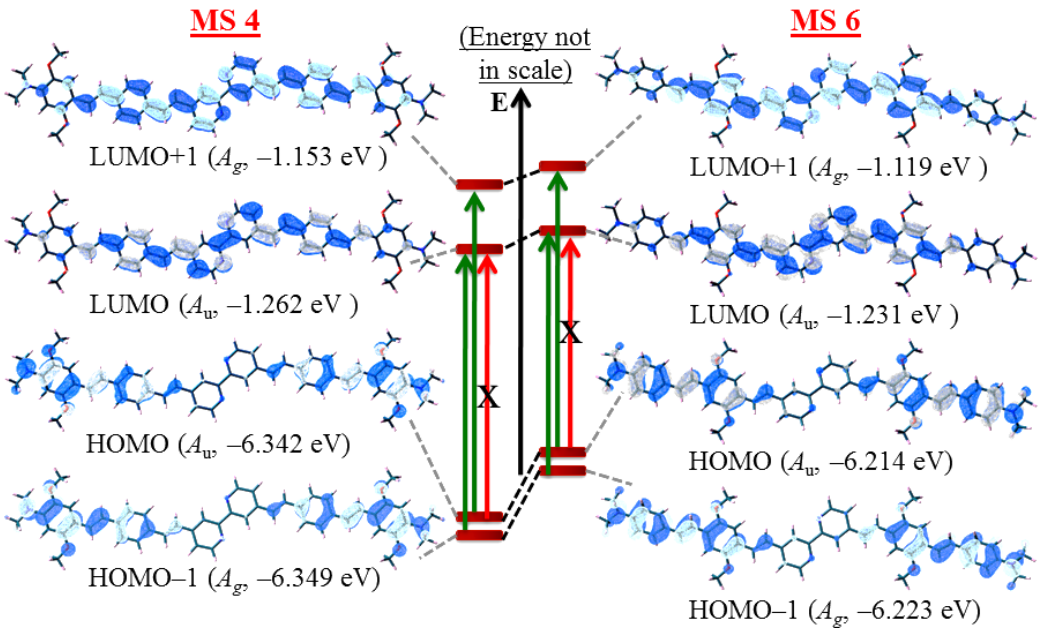

Figure 5. Pictorial representation of the alteration of energies of HOMOs and LUMOs while changing the substitution pattern from **MS 4** to **MS 6**.

(Figure 5). However, the experimentally observed ~7 nm hypsochromic shift of the ICT band maximum upon increment of the number of alkoxy donors from **MS 6** to **MS 7** could not be reproduced.

● 4.2.6. Thermal stability

Thermal durability is one of the most significant and essential parameters for the custom–tailored applications of the bench-top synthesized compounds. The thermal decay/weight loss of the compounds **MS 1**–**8** were examined by heating the solid samples in an analyzer under a flow of nitrogen. The thermal weight loss behavior of the chromophores **MS 3**, **MS 5**, **MS 6**–**8** are shown in Figure 6 which depicts very high thermal stability of the relevant 'push–pull' chromophores. The 10% weight loss temperature (Td_{10}) for these chromophores is evidently high (~ 350 ºC) as shown in Figure 6. No significant weight loss occurs even up to 250 ºC. However, the Td_{10} value for the compounds **MS 1**–**2** and **MS 4** are found to be relatively low (*ca*. 150 ºC).

● 4.3. SUMMARY AND CONCLUSION

In summary, a series of 4,4'–π–conjugated–2,2'–bipyridine dyads having a D–π–A–A–π–D architecture were synthesized wherein the 2,2'–bipyridine heterocycle acts as the central acceptor core to join the donor termini through olefinic spacers. The photophysi-

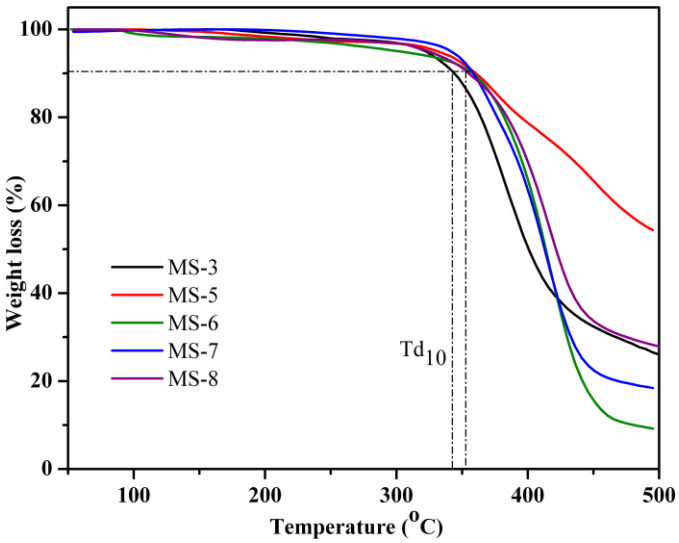

Figure 6. Thermogravimmetric behavior of **MS 3**, **MS 5** and **MS 6**–**8**.

-cal properties (absorption and emission) of the synthesized chromophores are governed by the intramolecular charge separation from the donor end-capping functionalities to the pyridine acceptor heterocycle. This observation is in line with the photophysics of previously reported related dyes. The emitting state of the fluorophores is substantially more polar than the ground electronic state which is affirmed by the large solvent sensitive photoluminescent behavior of the synthesized compounds. The absorptive and emissive nature of the present chromophores are enormously dependent on the conjugation backbone i.e. the nature, position and number of donor functionalities, the parameters which act as the function of their photophysical outcome. The computational analyses of the absorption properties of the synthesized chromophores clearly depicts an alteration of the various occupied and virtual energy levels with the structure of the synthesized chromophores and is in fair agreement with the variation trend of the experimentally observed absorption spectra.

In this work, we have demonstrated optical properties of the 4,4'–π–conjugated–2,2'–bipyridine dyes which are fabricated with hetero-donor functionalities. We have shown how simple modification of the π–skeleton of these dyes modulates their fluorescence behavior. For example, among the eight dye stuffs described in this chapter, the compound, **MS 5** fluoresce even in the condensed phase which is one of the pre-requirements for possible application in light emitting devices. Thus, changing the amino donor from open chain dibutylamino in **MS 4** to the cyclic pyrrolidine donor in **MS 5**

results in this differing photophysical behavior. Although, the 4,4'–π–conjugated–2,2'–bipyridine derivatives have been extensively studied in terms of devising nonlinear optical and solar energy harvesting materials, our systematic study on the photophysical properties of the hetero-donor systems in comparison with the parent chromophores bearing alike donor functionalities approaches a structure-function relationship which would be useful for choosing the proper material for practical applications. Accordingly, the findings of the present study in conjunction with the photophysics of the previously reported parent dye molecules construct a library of such systems in which, the present investigation finds some notable differences in the fluorescence responses compared to the parent molecules functionalized with only one kind of donor sub-chromophores. The present work reveals that the coexistence of both the alkoxy and amino functionalities in the same phenyl ring modulates the emitting state of **MS 2** and **MS 4** which exhibit considerable bathochromic shifted fluorescence with respect to the reported chromophores having either alkoxy (**N945L**, **TM 6**) or amino (**HLB 1-2**) donor groups. Furthermore, moving the alkoxy donors from ring–B (**MS 4**) to ring–A (**MS 6**) results in a large bathochromic shift of the absorption wavelength presumably due to the enhanced participation of the alkoxy groups in the charge transfer process when placed in ring-A than in ring-B. The introduction of additional alkoxy donor functionalities has not induced further bathochromic shift of the absorption maxima.

● 4.4. EXPERIMENTAL SECTION

● 4.4.1. Materials and methods

All the reactions were performed under either ultra high pure nitrogen or argon atmosphere unless mentioned elsewhere. The commercially procured chemicals were used as received. Triethylphosphite was distilled prior to use. THF, diethyl ether was freshly distilled over Na / Benzophenone under nitrogen until a deep purple color persists and used either immediately (THF) or stored over sodium wire in the dark (ether). Triethylamine, diisopropylamine were distilled thrice over calcium hydride under nitrogen and stored over KOH/NaOH pellets in a $CaCl_2$ desiccator. Aniline was distilled over KOH and used immediately. All the deuteriated NMR solvents were purchased from Acros Organics and used as received. Column chromatography was performed with silica gel (100–200 mesh) (SRL, India) unless mentioned. All the solvents used for the

chromatographic purifications were distilled prior to use. NMR spectra (^{1}H and ^{13}C) were recorded by Bruker AV–400 MHz spectrometer using tetramethylsilane (TMS) as internal standard in case of $CDCl_3$ solvent. Signal multiplicities are reported as follows: s = singlet, d = doublet, t = triplet, m = multiplet, br = broad. Elemental analyses were performed by FLASH EA series 1112 CHNS analyzer. The infrared spectra were recorded on a JASCO–5300 FT-IR spectrophotometer. Thermogravimetric analyses were carried out on a STA 409 PC analyzer under the flow of nitrogen. HRMS (MALDI-TOF/TOF) spectra of **MS 4**–**8** were recorded in α-cyanocinnamic acid matrix. Cary 100 Bio UV-visible spectrophotometer and Shimadzu UV–3600 spectrophotometer was used to record the electronic absorption spectra. The emission spectra were recorded on a Fluromax–4 (Jobin Yvon) spectrofluorometer and corrected for the instrumental response. Dilute solutions with OD ≈ 0.05 at the excitation wavelength were used for the quantum yield measurements (error limit ±10%). Optically matched solutions of the sample and the reference were measured under the same operating condition and instrumental settings.

● 4.4.2. Synthesis and characterization data

***N,N*–dibutylaniline (4a).** A mixture of aniline (19 mL, 200 mmol), 1–bromo butane (65 mL, 600 mmol) and Na_2CO_3 (84 g, 800 mmol) in 100 mL of 90:10 v/v DMF/NMP was heated at 120 ºC for 24 h. The reaction mixture was then cooled to room temperature and filtered to remove the insoluble material. The precipitate was washed with ethyl acetate and the combined filtrate was evaporated to dryness. Water was then added and the aqueous phase was extracted with ethyl acetate. After a silica gel filtration using hexane as the mobile phase, the pure compound was obtained as a pale yellow liquid. Yield: 35.3 g (86%).

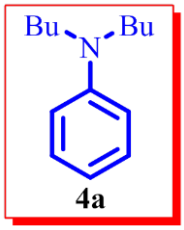

4a

^{1}H NMR (400 MHz, $CDCl_3$): δ 7.25–7.21 (unresolved, 2H), 6.68 (unresolved, 3H), 3.29 (t, 4H), 1.58 (unresolved, 4H), 1.41–1.35 (m, 4H), 1.00 (t, 6H).

^{13}C NMR (100 MHz, $CDCl_3$): δ 129.2, 115.1, 111.7, 50.8, 29.4, 20.4, 14.0.

LC–MS (positive mode): *m*/*z* 206 $(M+H)^+$.

Anal. calcd. for $C_{14}H_{23}N$: C, 81.89; H, 11.29; N, 6.82. Found: C, 81.83; H, 11.33; N, 6.84.

***N*,*N*–dibutyl–2,5–dimethoxyaniline (4b).** This compound was synthesized using the same procedure as described for compound **4a**. 2,5–dimethoxy aniline (**3b**, 30.6 g, 200 mmol) was used instead of aniline (**3a**) and the reaction time was 72 h at 120 ºC. The black crude liquid was subjected to silica gel filtration using hexane as the eluent to obtain the pure product **4b** as a light sensitive pale yellow liquid. Yield: 38.7 g (73%).

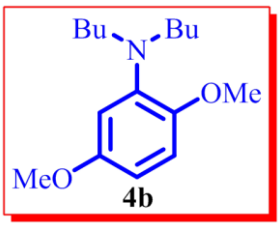

4b

^{1}H NMR (400 MHz, $CDCl_3$): δ 6.76 (d, J = 8 Hz, 1H), 6.54 (d, $^{4}J_{HH}$ = 4 Hz, 1H), 6.46–6.43 (dd, J = 8 Hz, $^{4}J_{HH}$ = 4 Hz, 1H), 3.80 (s, 3H), 3.78 (s, 3H), 3.08 (t, 4H), 1.45 (p, 4H), 1.28 (sextet, 4H), 0.88 (t, 6H).

^{13}C NMR (100 MHz, $CDCl_3$): δ 153.9, 147.9, 141.3, 112.8, 108.7, 104.7, 56.2, 55.5, 52.4, 26.9, 20.5, 14.1.

LC–MS (positive mode): m/z 266 $(M+H)^{+}$.

Anal. calcd. for $C_{16}H_{27}NO_2$: C, 72.41; H, 10.25; N, 5.28. Found: C, 72.47; H, 10.11; N, 5.32.

4–(dibutylamino)benzaldehyde (5a). $POCl_3$ (5.5 mL, 60 mmol) was slowly added to a DMF (20 mL, excess) solution of *N*,*N*–dibutyl aniline (**4a**, 10.25 g, 50 mmol) with cooling in an ice bath under an inert atmosphere. The resulting orange–red viscous liquid was then stirred at this temperature for 15 min, slowly warmed up to room temperature and then heated at 90–95 ºC for 7 h. The dark reaction mixture was then cooled in an ice bath and carefully quenched with water, followed by neutralization with aqueous Na_2CO_3 solution. The aqueous layer was extracted with dichloromethane. The combined organic layer was washed with water, brine, dried (anhydrous Na_2SO_4) and evaporated. Chromatographic purification of the crude mixture in a silica gel (100–200 mesh) column eluting with EtOAc/Hexane 15:85 v/v gave the product **5a** as a yellow viscous liquid. Yield: 11.16 g (95%).

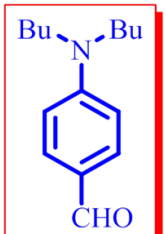

5a

^{1}H NMR (400 MHz, $CDCl_3$): δ 9.69 (s, 1H), 7.69 (d, J = 8 Hz, 2H), 6.64 (d, J = 8 Hz, 2H), 3.35 (t, 4H), 1.60 (p, 4H), 1.36 (hextet, 4H), 0.97 (t, 6H).

^{13}C NMR (100 MHz, $CDCl_3$): δ 189.9, 152.6, 132.2, 124.5, 110.7, 50.8, 29.3, 20.3, 20.25, 13.9.

IR (neat, cm^{-1}): υ_{max} 1680 (>C=O).

LC–MS (positive mode): *m/z* 234 $[M+H]^+$.

Anal. calcd. for $C_{15}H_{23}NO$: C, 77.21; H, 9.93; N, 6.00. Found: C, 77.27; H, 9.84; N, 6.12.

4–(dibutylamino)–2,5–dimethoxybenzaldehyde (5b). This compound was synthesized using the same procedure as described for **5a**. *N*,*N*–dibutyl–2,5–dimethoxyaniline (**2b**, 13.25 g, 50 mmol) was used instead of *N*,*N*–dibutyl aniline (**2a**). Reaction time at 90–95 ºC: 4 h. The product **5b** was isolated as an orange–yellow viscous liquid after silica gel (100–200 mesh) filtration of the crude with EtOAc/Hexane 20:80 v/v as the mobile phase. Yield: 12.60 g (86%).

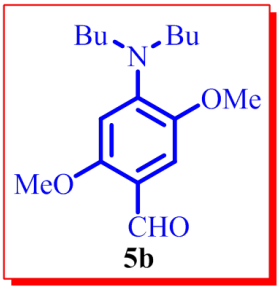

5b

^{1}H NMR (400 MHz, $CDCl_3$): δ 10.20 (s, 1H), 7.25 (s, 1H), 6.27 (s, 1H), 3.85 (s, 3H), 3.79 (s, 3H), 3.30 (t, 4H), 1.55 (p, 4H), 1.31 (hextet, 4H), 0.90 (t, 6H).

^{13}C NMR (100 MHz, $CDCl_3$): δ 187.3, 158.6, 147.9, 145.3, 115.9, 110.1, 100.6, 55.98, 55.90, 52.2, 29.8, 20.4, 14.0.

IR (neat, cm^{-1}): υ_{max} 1660 (>C=O).

LC–MS (positive mode): *m/z* 294 $[M+H]^+$.

Anal. calcd. for $C_{17}H_{27}NO_3$: C, 69.59; H, 9.28; N, 4.77. Found: C, 69.51; H, 9.33; N, 4.70.

1–phenylpyrrolidine (6a). A mixture of aniline (4.6 mL, 50 mmol), 1,4–dibromobutane (6.5 mL, 55 mmol) and K_2CO_3 (28 g, 200 mmol) in 90:10 v/v DMF/N–methylpyrrolidinone (NMP) was heated at 120 ºC for 24 h after which it was cooled to room temperature and filtered. The precipitated solid was washed with ethyl acetate and the combined filtrate was evaporated to dryness. Water was then added and the aqueous phase was extracted with ethyl acetate. The crude product was purified on short silica gel column eluting with EtOAc/Hexane 1:99 v/v to yield the pure product **6a** as a light sensitive yellow liquid. Yield: 4.7 g (62%).

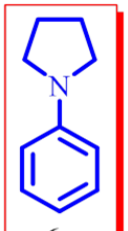

6a

^{1}H NMR (400 MHz, $CDCl_3$): δ 7.29–7.25 (unresolved, 2H), 6.70–6.61 (m, 3H), 3.32 (unresolved, 4H), 2.04 (unresolved, 4H).

^{13}C NMR (100 MHz, $CDCl_3$): δ 148.2, 129.2, 115.6, 111.8, 47.7, 25.5.

LC–MS (positive mode): *m*/*z* 148 $(M+H)^+$.

Anal. calcd. for $C_{10}H_{13}N$: C, 81.59; H, 8.90; N, 9.51. Found: C, 81.48; H, 9.04; N, 9.48.

1–(2,5–dimethoxyphenyl)pyrrolidine (6b). This compound was prepared using the same procedure as described for the synthesis of compound **6a**. 7.6 g (50 mmol) 2,5–dimethoxy aniline was used instead of aniline and the reaction mixture was heated at 120 ºC for 48 h. Silica gel filtration using EtOAc/Hexane 5:95 v/v as the mobile phase afforded the pure compound **6b** as a yellow light sensitive liquid. Yield: 7.9 g (76%).

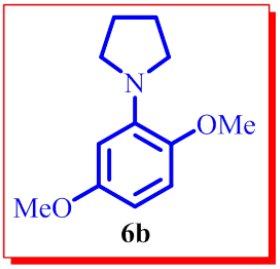

6b

^{1}H NMR (400 MHz, $CDCl_3$): δ 6.78 (d, J = 8 Hz, 1H), 6.38 (d, $^4J_{HH}$ = 4 Hz, 1H), 6.34–6.31 (dd, J = 8 Hz, $^4J_{HH}$ = 4 Hz, 1H), 3.79 (s, 3H), 3.78 (s, 3H), 33.2 (unresolved, 4H), 19.4 (unresolved, 4H).

^{13}C NMR (100 MHz, $CDCl_3$): δ 154.5, 144.8, 141.1, 113.0, 103.1, 101.6, 56.6, 55.5, 50.4, 24.5.

LC–MS (positive mode): *m*/*z* 208 $(M+H)^+$.

Anal. calcd. for $C_{12}H_{17}NO_2$: C, 69.54; H, 8.27; N, 6.76. Found: C, 69.41; H, 8.23; N, 6.73.

4–(pyrrolidin–1–yl)benzaldehyde (7a). This compound was synthesized using the same procedure as described for **5a**. 1–phenylpyrrolidine (**6a**, 7.35 g, 50 mmol) was used instead of *N*,*N*–dibutyl aniline (**4a**). Reaction time at 90–95 ºC: 6–7 h. Column chromatographic (silica gel, 100–200 mesh) purification of the crude product using EtOAc/Hexane 20:80 v/v as the eluent afforded the desired product **7a** as a white crystalline solid. Yield: 7.26 g (83%). Mp: 81–83 ºC.

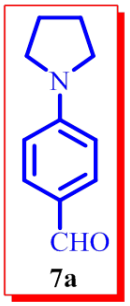

7a

^{1}H NMR (400 MHz, $CDCl_3$): δ 9.72 (s, 1H), 7.73 (d, J = 8 Hz, 2H), 6.57 (d, J = 8 Hz, 2H), 3.41–3.37 (m, 4H), 2.07–2.04 (m, 4H).

^{13}C NMR (100 MHz, $CDCl_3$): δ 190.2, 152.0, 132.1, 124.9, 111.2, 47.7, 25.4.

IR (KBr, cm^{-1}): υ_{max} 1674 (>C=O).

LC–MS (positive mode): *m*/*z* 176 $[M+H]^+$.

Anal. calcd. for $C_{11}H_{13}NO$: C, 75.40; H, 7.48; N, 7.99. Found: C, 75.45; H, 7.39; N, 8.07.

2,5–dimethoxy–4–(pyrrolidin–1–yl)benzaldehyde (7b). This compound was synthesized using the same procedure as described for **5a**. 1–(2,5–dimethoxyphenyl)pyrrolidine (**6b**, 10.35 g, 50 mmol) was used instead of *N*,*N*–dibutyl aniline (**4a**). Reaction time at 90–95 ºC: 7–8 h. The crude product was purified by silica gel (100–200 mesh) column eluting with EtOAc/Hexane 20:80 v/v as the mobile phase to obtain the pure aldehyde **7b** as a light sensitive cream colored solid. Yield: 10.34 g (88%). Mp: 120–121 ºC.

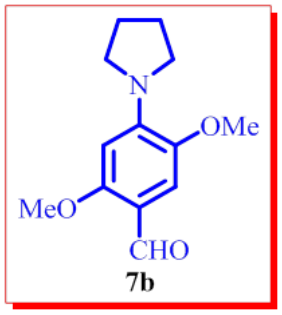

7b

^{1}H NMR (400 MHz, $CDCl_3$): δ 10.13 (s, 1H), 7.23 (s, 1H), 6.00 (s, 1H), 3.85 (s, 3H), 3.76 (s, 3H), 3.55 (unresolved, 4H), 1.93 (unresolved, 4H).

^{13}C NMR (100 MHz, $CDCl_3$): δ 186.7, 159.5, 146.7, 142.9, 113.8, 110.1, 96.2, 56.4, 55.8, 50.7, 25.5.

IR (KBr, cm^{-1}): υ_{max} 1639 (>C=O).

LC–MS (positive mode): *m*/*z* 236 $[M+H]^+$.

Anal. calcd. for $C_{13}H_{17}NO_3$: C, 66.36; H, 7.28; N, 5.95. Found: C, 66.28; H, 7.25; N, 6.11.

(*E*)–4–(4–(pyrrolidin–1–yl)styryl)bromobenzene (10a). Solid potassium *t*–butoxide (1.68 g, 15 mmol) was added at once to an ice–cooled THF solution (30 mL) containing 3.68 g of phosphonate **8** (12 mmol) and 1.75 g of aldehyde **7a** (10 mmol) under an inert atmosphere. The resulting slurry was warmed up to room temperature and stirred for 1 h before the reaction was quenched with water. The precipitated yellow solid was collected by filtration, washed several times with water and dried in air. It was re–dissolved in dichloromethane (*ca*. 600 mL) and the solvent was rotavaporated to *ca*. 15 mL and filtered to obtain the pure product **10a** as a yellow solid. Yield: 2.85 g (87%). Mp: more than 200 ºC.

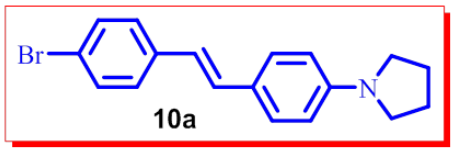

10a

^{1}H NMR (400 MHz, $CDCl_3$): δ 7.43 (d, J = 8 Hz, 2H), 7.39 (d, J = 8 Hz, 2H), 7.33 (d, J = 8 Hz, 2H), 7.03 (d, J = 16 Hz, 1H), 6.81 (d, J = 16 Hz, 1H), 6.55 (d, J = 8 Hz, 2H), 3.33 (unresolved, 4H), 2.02 (unresolved, 4H).

^{13}C NMR was not possible because of low solubility.

LC–MS (positive mode): *m*/*z* 328 $(M)^+$, 330 $(M+2H)^+$.

Anal. calcd. for $C_{18}H_{18}BrN$: C, 65.86; H, 5.53; N, 4.27. Found: C, 65.69; H, 5.48; N, 4.30.

(*E*)–4–(4–(dibutylamino)–2,5–dimethoxystyryl)bromobenzene (11a). Under nitrogen, solid potassium *t*–butoxide (1.68 g, 15 mmol) was added at once to a THF solution (30 mL) containing 3.68 g of phosphonate **8** (12 mmol) and 2.93 g of aldehyde **5b** (10 mmol) pre–cooled at 0 ºC. The ice bath was removed and the reaction mixture was allowed to stir at room temperature for 60 min. It was subsequently quenched with water and then extracted with dichloromethane. The combined organic phase was washed with brine, dried over anhydrous Na_2SO_4 and evaporated to dryness. Purification of the crude product through column chromatography (silica gel, 100–200 mesh) using EtOAc/Hexane 5:95 v/v as the eluent afforded the product **11a** as a dark yellow solid. Yield: 4.06 g (91%). Mp: 76–78 ºC.

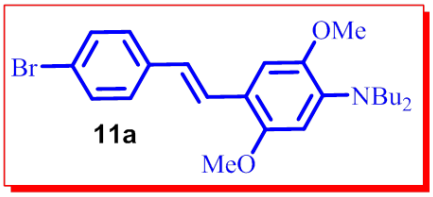

11a

^{1}H NMR (400 MHz, $CDCl_3$): δ 7.46–7.37 (m, 5H), 7.06 (s, 1H), 6.89 (d, J = 16 Hz, 1H), 6.50 (s, 1H), 3.87 (s, 3H), 3.85 (s, 3H), 3.16 (t, 4H), 1.51 (p, 4H), 1.33 (m, 4H), 0.90 (t, 6H).

^{13}C NMR (100 MHz, $CDCl_3$): δ 151.8, 147.4, 141.4, 137.4, 131.6, 127.7, 125.0, 124.1, 120.4, 118.4, 110.3, 105.2, 52.3, 29.3, 20.6, 14.1.

LC–MS (positive mode): m/z 446 $(M)^+$, 448 $(M+2H)^+$.

Anal. calcd. for $C_{24}H_{32}BrNO_2$: C, 64.57; H, 7.23; N, 3.14. Found: C, 64.43; H, 7.16; N, 3.16.

(*E*)–4–(2,5–dimethoxy–4–(pyrrolidin–1–yl)styryl)bromobenzene (12a). This compound was prepared using the same procedure as described for **11a** using 3.68 g of phosphonate **8** (12 mmol), 2.35 g of aldehyde **7b** (10 mmol) and 1.68 g of potassium *t*–butoxide (15 mmol) in 30 mL of THF. Column chromatographic purification on silica gel (100–200 mesh) using EtOAc/Hexane 20:80 v/v as the mobile phase afforded the product **12a** as fluorescent yellow needles. Yield: 3.65 g (94%). Mp: 128–130 ºC.

12a

^{1}H NMR (400 MHz, $CDCl_3$): δ 7.45–36 (m, 5H), 7.07 (s, 1H), 6.85 (d, J = 16 Hz, 1H), 6.29 (s, 1H), 3.86 (s, 3H), 3.84 (s, 3H), 3.41 (unresolved, 4H), 1.96 (unresolved, 4H).

^{13}C NMR (100 MHz, $CDCl_3$): δ 152.5, 144.1, 141.1, 137.7, 131.6, 127.6, 124.2, 123.5, 120.0, 115.3, 110.8, 99.6, 56.9, 56.4, 50.5, 25.1.

LC–MS (positive mode): m/z 388 $(M)^+$, 390 $(M+2H)^+$.

Anal. calcd. for $C_{20}H_{22}BrNO_2$: C, 61.86; H, 5.71; N, 3.61. Found: C, 62.01; H, 5.64; N, 3.55.

(*E*)–2,5–dibutoxy–4–(4–(dibutylamino)styryl)bromobenzene (13a). This compound was prepared using the same procedure as described for **11a** using 2.3 g of phosphonate **7** (5 mmol), 1.1 g of aldehyde **5a** (4.8 mmol) and 0.7 g of potassium *t*–butoxide (6 mmol) in 25 mL of THF. The product **13a** was isolated as a fluorescent yellow solid after column chromatography on silica gel (100–200 mesh) using EtOAc/Hexane 5:95 v/v as the mobile phase. Yield: 2.34 g (92%). Mp: 84–86 ºC.

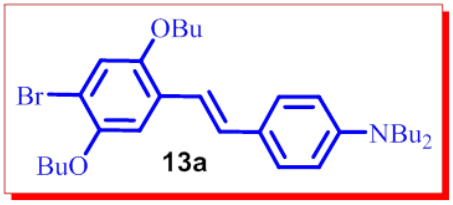

^{1}H NMR (400 MHz, $CDCl_3$): δ 7.39 (d, J = 8 Hz, 2H), 7.16 (d, J = 16 Hz, 1H), 7.12 (s, 1H), 7.06 (s, 1H), 7.02 (d, J = 16 Hz, 1H), 6.54 (d, J = 8 Hz, 2H), 4.05 (t, 2H), 3.95 (t, 2H), 3.30 (t, 4H), 1.82 (p, 4H), 1.63–1.52 (m, 8H), 1.36 (t, 4H), 1.03–0.96 (m, 12H).

^{13}C NMR (100 MHz, $CDCl_3$): δ 150.7, 149.9, 147.9, 129.6, 127.8, 124.9, 117.8, 111.6, 111.2, 110.3, 70.0, 69.3, 50.8, 31.5, 29.5, 20.4, 19.4, 14.0.

LC–MS (positive mode): m/z 531 $(M)^+$, 533 $(M+2H)^+$.

Anal. calcd. for $C_{30}H_{44}BrNO_2$: C, 67.91; H, 8.36; N, 2.64. Found: C, 68.02; H, 8.25; N, 2.69.

(*E*)–2,5–dibutoxy–4–(4–(dibutylamino)–2,5–dimethoxystyryl)bromobenzene (14a). This compound was prepared using the same procedure as described for **11a** using 2.3 g of phosphonate **7** (5 mmol), 1.4 g of aldehyde **5b** (4.8 mmol) and 0.7 g of potassium *t*–butoxide (6 mmol) in 25 mL of THF. The product **14a** was isolated as a yellow solid after chromatographic purification on silica gel stationary phase (100–200 mesh) using EtOAc/Hexane 5:95 v/v as the mobile phase. Yield: 2.61 g (92%). Mp: 58–60 ºC.

^{1}H NMR (400 MHz, $CDCl_3$): δ 7.41 (d, J = 16 Hz, 1H), 7.26 (d, J = 16 Hz, 1H), 7.15 (s, 1H), 7.10 (s, 1H), 7.07 (s, 1H), 6.51 (s, 1H), 4.05 (t, 2H), 3.96 (t, 2H), 3.86–3.85 (m, 6H),

3.15 (t, 4H), 1.85–1.78 (m, 4H), 1.60–1.43 (m, 8H), 1.29 (m, 4H), 0.99 (t, 6H), 0.91 (t, 6H).

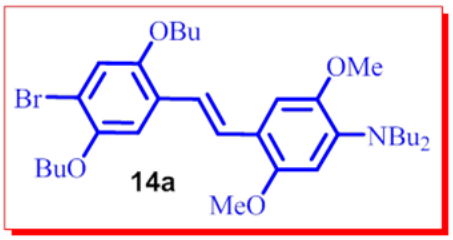

14a

^{13}C NMR (100 MHz, $CDCl_3$): δ 151.7, 150.9, 149.9, 147.6, 141.1, 127.8, 123.9, 120.8, 119.4, 117.9, 111.7, 110.9, 110.5, 105.4, 70.0, 69.3, 56.5, 56.3, 52.4, 31.5, 29.4, 20.6, 19.4, 19.3, 14.0, 13.9.

LC–MS (positive mode): *m*/*z* 590 $(M)^+$, 592 $(M+2H)^+$.

Anal. calcd. for $C_{32}H_{48}BrNO_4$: C, 65.07; H, 8.19; N, 2.37. Found: C, 65.10; H, 8.08; N, 2.43.

(*E*)–2,5–dibutoxy–4–(2,5–dimethoxy–4–(pyrrolidin–1–yl)styryl)bromobenzene (15a). This compound was synthesized by the same procedure as described for **11a** using 2.3 g of phosphonate **7** (5 mmol), 1.1 g of aldehyde **7b** (4.8 mmol) and 0.7 g of potassium *t*–butoxide (6 mmol) in 25 mL of THF. Chromatographic purification using silica gel stationary phase (100–200 mesh) and EtOAc/Hexane 10:90 v/v as the mobile phase afforded the product **15a** as a fluorescent yellow solid. Yield: 2.25 g (88%). Mp: 116–118 ºC.

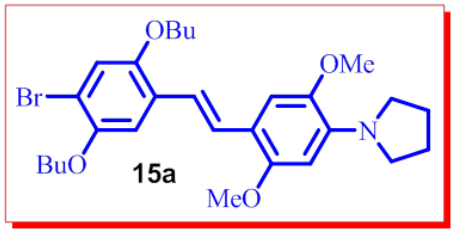

15a

^{1}H NMR (400 MHz, $CDCl_3$): δ 7.40 (d, *J* = 16 Hz, 1H), 7.20 (d, *J* = 16 Hz, 1H), 7.15 (s, 1H), 7.10 (s, 1H), 7.06 (s, 1H), 6.30 (s, 1H), 4.05 (t, 2H), 3.96 (t, 2H), 3.86 (s, 3H), 3.83 (s, 3H), 3.41 (unresolved, 4H), 1.95 (unresolved, 4H), 1.81 (p, 4H), 1.56 (m, 4H), 1.00 (t, 6H).

^{13}C NMR (100 MHz, $CDCl_3$): δ 152.4, 150.8, 149.9, 144.2, 140.8, 128.0, 124.0, 119.2, 117.9, 116.3, 111.4, 110.8, 110.4, 99.8, 70.0, 69.4, 56.8, 56.5, 50.5, 31.5, 25.1, 19.4, 19.3, 14.0.

LC–MS (positive mode): *m*/*z* 532 $(M)^+$, 534 $(M+2H)^+$.

Anal. calcd. for $C_{28}H_{38}BrNO_4$: C, 63.15; H, 7.19; N, 2.63. Found: C, 63.21; H, 7.22; N, 2.68.

(*E*)–4–(4–(pyrrolidin–1–yl)styryl)benzaldehyde (10b). A solution of bromostilbene **10a** (0.98 g, 3 mmol) in 110 mL of THF was cooled to –40 ºC and then 2.2 mL of 1.6 M *n*BuLi (3.6 mmol) was added dropwise. The heterogeneous mixture was stirred at this

temperature for 60 min, 0.4 mL of dry DMF (5 mmol) was subsequently added followed by stirring at this temperature for additional 60 min. The cooled reaction mixture was then slowly warmed up to room temperature, quenched with saturated ammonium chloride solution and extracted with dichloromethane. The organic layer was washed twice with water, then with brine, dried (Na_2SO_4) and evaporated to dryness. The crude product was purified by column chromatography on silica gel (100–200 mesh) using dichloromethane as the mobile phase to obtain the pure aldehyde **10b** as an orange yellow solid. Yield: 0.66 g (80 %). Mp: more than 200 ºC.

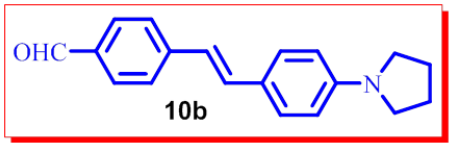

10b

^{1}H NMR (400 MHz, $CDCl_3$): δ 9.96 (s, 1H), 7.83 (d, J = 8 Hz, 2H), 7.60 (d, J = 8 Hz, 2H), 7.43 (d, J = 8 Hz, 2H), 7.22 (d, J = 16 Hz, 1H), 6.92 (d, J = 16 Hz, 1H), 6.57 (d, J = 8 Hz, 2H), 3.33 (unresolved, 4H), 1.58 (unresolved, 4H).

^{13}C NMR (100 MHz, $CDCl_3$): δ 191.7, 148.1, 144.8, 134.3, 132.9, 130.3, 129.4, 128.4, 126.2, 121.9, 111.8, 47.6, 25.5.

IR (KBr, cm^{-1}): υ_{max} 1691 (>C=O).

LC–MS (positive mode): m/z 278 $(M+H)^+$.

Anal. calcd. for $C_{19}H_{19}NO$: C, 82.28; H, 6.90; N, 5.05. C, 88.23; H, 6.88; N, 5.12.

(*E*)–4–(4–(dibutylamino)–2,5–dimethoxystyryl)benzaldehyde (11b). This compound was synthesized by the same procedure as described for aldehyde **10b**. Reactant amount is as follows: bromostilbene **11a** (1.34 g, 3 mmol), 1.6 M *n*BuLi (2.2 mL, 3.6 mmol), DMF (0.4 mL, 5 mmol), 20 mL of THF was used instead. Chromatographic purification using silica gel stationary phase (100–200 mesh) and EtOAc/Hexane 10:90 v/v mobile phase rendered the aldehyde **11b** as a vermillion red gummy mass. Yield: 0.81 g (68%).

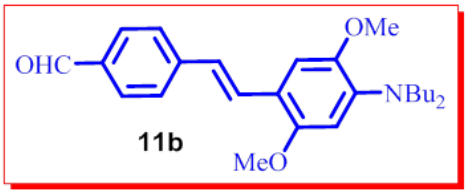

11b

^{1}H NMR (400 MHz, $CDCl_3$): δ 9.97 (s, 1H), 7.84 (d, J = 8 Hz, 2H), 7.65 (d, J = 8 Hz, 2H), 7.61 (d, J = 16 Hz, 1H), 7.09 (s, 1H), 7.01 (d, J = 16 Hz, 1H), 6.49 (s, 1H), 3.87 (unresolved, 6H), 3.18 (t, 4H), 1.52–1.47 (p, 4H), 1.33–1.26 (m, 4H), 0.91 (t, 6H).

^{13}C NMR (100 MHz, $CDCl_3$): δ 191.7, 152.3, 147.8, 144.8, 142.2, 134.6, 130.2, 127.0, 126.5, 124.6, 117.6, 110.5, 104.6, 56.40, 56.35, 52.2, 29.4, 20.5, 14.1.

IR (KBr, cm^{-1}): υ_{max} 1695 (>C=O).

LC–MS (positive mode): *m*/*z* 396 $(M+H)^+$.

Anal. calcd. for $C_{25}H_{33}NO_3$: C, 75.91; H, 8.41; N, 3.54. Found: C, 76.09; H, 8.35; N, 3.58.

(*E*)–4–(2,5–dimethoxy–4–(pyrrolidin–1–yl)styryl)benzaldehyde (12b). This compound was synthesized by the same procedure as described for aldehyde **10b** using bromostilbene **12a** (1.16 g, 3 mmol), 1.6 M *n*BuLi (2.2 mL, 3.6 mmol), DMF (0.4 mL, 5 mmol) in 20 mL of THF. Purification of the crude product by column chromatography using silica gel (100–200 mesh) and EtOAc/Hexane 10:90 v/v mobile phase afforded the aldehyde **12b** as a vermillion orange solid. Yield: 0.71 g (70%). Mp: 120–122 ºC.

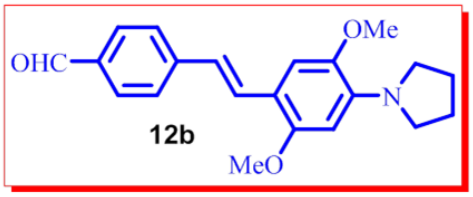

12b

^{1}H NMR (400 MHz, $CDCl_3$): δ 9.96 (s, 1H), 7.82 (d, *J* = 8 Hz, 2H), 7.64–7.59 (m, 3H), 7.09 (s, 1H), 6.95 (d, *J* = 16 Hz, 1H), 6.26 (s, 1H), 3.88 (s, 3H), 3.84 (s, 3H), 3.44 (unresolved, 4H), 1.96 (unresolved, 4H).

^{13}C NMR (100 MHz, $CDCl_3$): δ 191.7, 153.1, 145.1, 143.9, 141.8, 134.3, 130.3, 127.2, 126.3, 123.0, 114.6, 111.0, 99.1, 57.0, 56.3, 50.5, 25.2.

IR (KBr, cm^{-1}): υ_{max} 1689 (>C=O).

LC–MS (positive mode): *m*/*z* 338 $(M+H)^+$.

Anal. calcd. for $C_{21}H_{23}NO_3$: C, 74.75; H, 6.87; N, 4.15. Found: C, 74.62; H, 6.84; N, 4.13.

(*E*)–2,5–dibutoxy–4–(4–(dibutylamino)styryl)benzaldehyde (13b). This compound was synthesized by the same procedure as described for aldehyde **10b** using bromostilbene **13a** (1.6 g, 3 mmol), 1.6 M *n*BuLi (2.2 mL, 3.6 mmol), DMF (0.4 mL, 5 mmol) in 20 mL of THF. Chromatographic purification of the crude product on silica gel (100–200 mesh) using EtOAc/Hexane 5:95 v/v as the eluent afforded the aldehyde **13b** as a thick red gum. Yield: 0.82 g (57%).

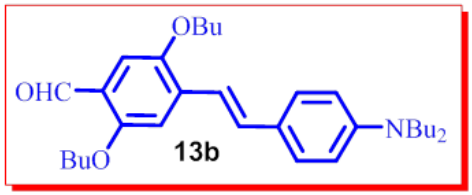

13b

^{1}H NMR (400 MHz, $CDCl_3$): δ 10.44 (s, 1H), 7.43 (d, *J* = 8 Hz, 2H), 7.31 (s, 1H), 7.23

(d, *J* = 16 Hz, 1H), 7.16 (s, 1H), 6.65 (d, *J* = 8 Hz, 2H), 4.13 (t, 2H), 4.03 (t, 2H), 3.32 (t, 4H), 1.86–1.83 (m, 4H), 1.59–1.53 (m, 8H), 1.41–1.37 (m, 4H), 1.04–0.96 (m, 12H).

^{13}C NMR (100 MHz, $CDCl_3$): δ 189.0, 156.5, 150.3, 148.3, 135.8, 132.7, 128.4, 124.4, 123.2, 117.4, 111.6, 110.0, 109.6, 68.9, 68.7, 50.8, 31.4, 29.5, 20.4, 19.4, 14.0.

IR (KBr, cm^{-1}): υ_{max} 1672 (>C=O).

LC–MS (positive mode): *m*/*z* 481 $(M+H)^+$.

Anal. calcd. for $C_{31}H_{45}NO_3$: C, 77.62; H, 9.46; N, 2.92. Found: C, 77.51; H, 9.42; N, 3.00.

(*E*)–2,5–dibutoxy–4–(4–(dibutylamino)–2,5–dimethoxystyryl)benzaldehyde (14b).

This compound was synthesized by the same procedure as described for aldehyde **10b** using bromostilbene **14a** (1.8 g, 3 mmol), 1.6 M *n*BuLi (2.2 mL, 3.6 mmol), DMF (0.4 mL, 5 mmol) in 20 mL of THF. The crude product was subjected to column chromatography on silica gel (100–200 mesh) using EtOAc/Hexane 5:95 v/v as the mobile phase to afford the aldehyde **14b** as a thick red gum. Yield: 0.76 g (47%).

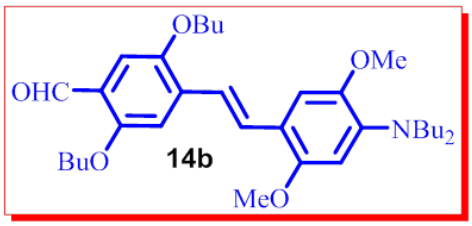

^{1}H NMR (400 MHz, $CDCl_3$): δ 10.42 (s, 1H), 7.58 (d, *J* = 16 Hz, 1H), 7.55 (d, *J* = 16 Hz, 1H), 7.30 (s, 1H), 7.19 (s, 1H), 7.12 (s, 1H), 6.50 (s, 1H), 4.12 (t, 2H), 4.02 (t, 2H), 3.86 (s, 6H), 3.18 (t, 4H), 1.83 (p, 4H), 1.58–1.48 (m, 8H), 1.31 (m, 4H), 1.00 (t, 6H), 0.91 (t, 6H).

^{13}C NMR (100 MHz, $CDCl_3$): δ 189.1, 156.4, 152.2, 150.5, 147.2, 141.9, 135.7, 126.9, 123.5, 120.2, 118.5, 110.6, 110.0, 109.9, 104.7, 68.8, 68.7, 56.4, 56.2, 52.2, 31.4, 31.3, 29.4, 20.5, 19.5, 19.3, 14.1, 14.0, 13.9.

IR (KBr, cm^{-1}): υ_{max} 1674 (>C=O).

LC–MS (positive mode): *m*/*z* 541 $(M+H)^+$.

Anal. calcd. for $C_{33}H_{49}NO_5$: C, 73.43; H, 9.15; N, 2.60. Found: C, 73.57; H, 9.09; N, 2.53.

(*E*)–2,5–dibutoxy–4–(2,5–dimethoxy–4–(pyrrolidin–1–yl)styryl)benzaldehyde (15b).

This compound was synthesized by the same procedure as described for aldehyde **10b** using bromostilbene **15a** (1.6 g, 3 mmol), 1.6 M *n*BuLi (2.2 mL, 3.6 mmol), DMF (0.4 mL, 5 mmol) in 20 mL of THF. Purification of the crude product by silica gel (100–200

mesh) column chromatography using EtOAc/Hexane 10:90 v/v as the mobile phase afforded the aldehyde **15b** as a vermillion orange solid. Yield: 0.72 g (50%). Mp: 103–105 ºC.

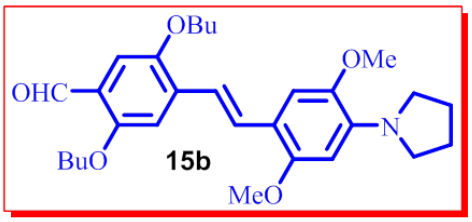

^{1}H NMR (400 MHz, $CDCl_3$): 10.42 (s, 1H), 7.58 (d, *J* = 16 Hz, 1H), 7.30 (d, *J* = 16 Hz, 1H), 7.29 (s, 1H), 7.19 (s, 1H), 7.12 (s, 1H), 6.27 (s, 1H), 4.42 (t, 2H), 4.43 (t, 2H), 3.88 (s, 3H), 3.82 (s, 3H), 3.43 (unresolved, 4H), 1.95 (unresolved, 4H), 1.84 (p, 4H), 1.56 (m, 4H), 0.99 (t, 6H).

^{13}C NMR (100 MHz, $CDCl_3$): δ 156.5, 153.0, 150.4, 143.9, 141.5, 136.1, 127.1, 123.3, 118.6, 115.5, 111.1, 110.0, 109.8, 99.3, 68.9, 68.8, 56.9, 56.3, 50.4, 31.4, 25.2, 19.5, 19.4, 13.9.

IR (KBr, cm^{-1}): υ_{max} 1670 (>C=O).

LC–MS (positive mode): *m*/*z* 483 $(M+H)^+$.

Anal. calcd. for $C_{29}H_{39}NO_5$: C, 72.32; H, 8.16; N, 2.91. C, 72.27; H, 8.19; N, 3.01.

4,4'–*bis*(4–(pyrrolidin–1–yl)styryl)–2,2'–bipyridine (MS 1). Under nitrogen, solid potassium *tert*–butoxide (0.45 g, 4 mmol) was added at a time to a THF solution (50 mL) of the *bis*–phosphonate (**2**, 0.46 g, 1 mmol) and the aldehyde (**7a**, 0.39 g, 2.2 mmol) at room temperature and the resulting heterogeneous reaction mixture was stirred at this temperature for 3 h. The reaction mixture was subsequently quenched with water (25 mL), evaporated to dryness and methanol 50 mL was added to cause precipitation of the product. It was collected by filtration, washed several times with water, methanol and a small amount of ether and dried in air. It was re-dissolved in dichloromethane (*ca*. 500 mL) and the yellow solution was concentrated to almost 20 mL. The bright yellow precipitated material was collected by filtration and dried thoroughly. The compound **MS 1** was isolated as a yellow microcrystalline solid. Yield: 0.46 g (92%). Mp (Differential Thermal Analysis, DTA): 357 ºC.

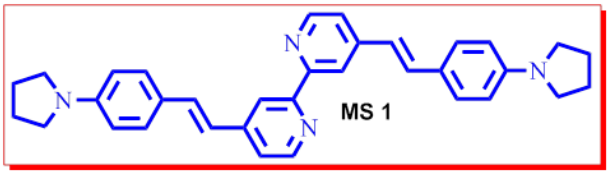

^{1}H NMR (400 MHz, $CDCl_3$): δ 8.615 (d, *J* = 4 Hz, 2H), 8.48 (s, 2H), 7.46 (d, *J* = 8 Hz, 4H), 7.41 (d, *J* = 16 Hz, 2H), 7.345 (d, *J* = 4 Hz, 2H), 6.90 (d, *J* = 16 Hz, 2H), 6.58 (d, *J* = 8 Hz, 4H), 3.35 (unresolved, 8H), 2.03 (unresolved, 8H).

^{13}C NMR was not possible because of low solubility.

LC–MS (positive mode): *m*/*z* 499 $(M+H)^+$.

Anal. calcd. for $C_{34}H_{34}N_4$: C, 81.89; H, 6.87; N, 11.24. Found: C, 81.72; H, 6.81; N, 11.15.

4,4'–*bis*(4–dibutylamino–2,5–dimethoxystyryl)–2,2'–bipyridine (MS 2). Neat potassium *t*–butoxide (0.45 g, 4 mmol) was added at once to a mixture of the *bis*–phosphonate (**2**, 0.46 g, 1 mmol) and the aldehyde (**5b**, 0.64 g, 2.2 mmol) dissolved in 50 mL of THF at room temperature under an inert atmosphere and the dark colored reaction mixture thus obtained was stirred at this temperature for 3 h. It was then quenched with water (25 mL) and the product was extracted with dichloromethane. The organic layer was washed with brine, dried over anhydrous Na_2SO_4 and subjected to chromatographic purification over silica gel (100–200 mesh) column using methanol/chloroform 5:95 v/v as the eluent to obtain the compound **MS 2** as a dark colored thick gum. Yield: 0.66 g (90%).

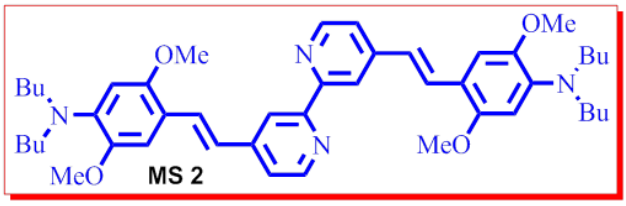

MS 2

^{1}H NMR (400 MHz, $CDCl_3$): δ 8.635 (d, J = 4 Hz, 2H), 8.48 (s, 2H), 7.75 (d, J = 16 Hz, 2H), 7.435 (d, J = 4 Hz, 2H), 7.09 (s, 2H), 7.05 (d, J = 16 Hz, 2H), 6.50 (s, 2H), 3.88 (unresolved, 12H), 3.19 (t, 8H), 1.53–1.47 (p, 8H), 1.34–1.26 (m, 8H), 0.91 (t, 12H).

^{13}C NMR (100 MHz, $CDCl_3$, C-type based on DEPT-135 spectrum): δ 156.6 (C), 152.5 (C), 149.3 (CH), 147.1 (C), 146.9 (C), 142.3 (C), 128.2 (CH), 123.7 (CH), 120.3 (CH), 118.5 (CH), 117.4 (C), 111.0 (CH), 104.6 (CH), 56.3 (OMe), 52.2 (CH_2), 29.4 (CH_2), 20.5 (CH_2), 14.0 (CH_3).

LC–MS (positive mode): *m*/*z* 736 $(M+H)^+$.

Anal. calcd. for $C_{46}H_{62}N_4O_4$: C, 75.17; H, 8.50; N, 7.62. Found: C, 75.23; H, 8.41; N, 7.56.

4,4'–*bis*(2,5–dimethoxy–4–(pyrrolidin–1–yl)styryl)–2,2'–bipyridine (MS 3). This compound was obtained using the same procedure as described for **MS 2**. The aldehyde **7b** (0.52 g, 2.2 mmol) was used instead of aldehyde **5b**. Column chromatographic purification (silica gel, 100–200 mesh) using methanol/chloroform 5:95 v/v as the mobile

phase resulted in the isolation of the pure compound **MS 3** as a brown microcrystalline solid. Yield: 0.56 g (91%). Mp (DTA): 250 ºC.

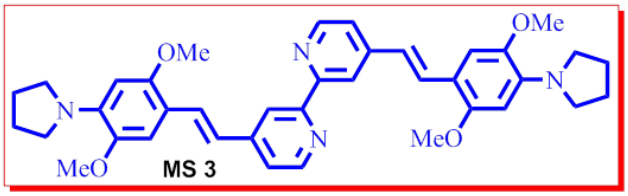

^{1}H NMR (400 MHz, $CDCl_3$): δ 8.605 (d, J = 4 Hz, 2H), 8.46 (s, 2H), 7.75 (d, J = 16 Hz, 2H), 7.42 (d, J = 8 Hz, 2H), 7.10 (s, 2H), 6.98 (d, J = 16 Hz, 2H), 6.27 (s, 2H), 3.89 (s, 3H), 3.84 (s, 3H), 3.44 (unresolved, 8H), 1.95 (unresolved, 8H).

^{13}C NMR (100 MHz, $CDCl_3$, C-type based on DEPT-135 spectrum): δ 153.3 (C), 149.1 (CH), 147.4 (C), 143.8 (C), 141.8 (C), 128.4 (CH), 122.1 (CH), 120.2 (CH), 118.4 (CH), 114.4 (C), 111.4 (CH), 99.1 (CH), 56.9 (OMe), 56.2 (OMe), 50.5 (CH_2), 25.2 (CH_2).

LC–MS (negative mode): m/z 618 $(M–H)^+$.

Anal. calcd. for $C_{38}H_{42}N_4O_4$: C, 73.76; H, 6.84; N, 9.05. Found: C, 73.61; H, 6.78; N, 9.15.

4,4'–bis(4–(2,5–dimethoxy–4–dibutylaminostyryl)styryl)–2,2'–bipyridine (MS 4).

The synthesis of this compound follows the same procedure as described for **MS 2**. Aldehyde **11b** (0.86 g, 2.2 mmol) was used instead of aldehyde **5b**. The crude product was purified through column chromatography using silica gel (100–200 mesh) stationary and methanol/chloroform 5:95 v/v as the mobile phases to obtain the compound **MS 4** as a thick red gum that solidified after standing at room temperature for a few days. Yield: 0.87 g (93%). Mp: was not measured.

^{1}H NMR (400 MHz, $CDCl_3$): δ 8.695 (d, J = 4 Hz, 2H), 8.56 (s, 2H), 7.59–7.53 (m, 8H), 7.50 (d, J = 16 Hz, 2H), 7.47 (d, J = 16 Hz, 2H), 7.41 (d, J = 8 Hz, 2H), 7.16–7.11 (m, 2H), 7.00 (d, J = 16 Hz, 2H), 6.55 (s, 2H), 3.88 (s, 6H,), 3.86 (s, 3H), 3.17 (t, 8H), 1.54–1.46 (p, 8H), 1.36–1.26 (m, 8H), 0.91 (t, 12H).

^{13}C NMR (100 MHz, $CDCl_3$, C-type based on DEPT-135 spectrum): δ 156.3 (C), 151.8 (C), 149.5 (CH), 147.5 (C), 146.0 (C), 138.9 (C), 134.8 (C), 133.2 (CH), 127.4 (CH), 126.7 (CH), 126.0 (C), 125.8 (CH), 125.3 (CH), 123.9 (CH), 121.1 (CH), 119.0 (C),

118.3 (CH), 110.3 (CH), 105.4 (CH), 56.5 (OMe), 56.3 (OMe), 52.4 (CH_2), 29.3 (CH_2), 20.5 (CH_2), 14.1 (CH_3).

HRMS (MALDI–TOF/TOF, positive mode): *m*/*z* calcd. 938.571 (M^+). Found: 939.673 $(M+H)^+$.

Anal. calcd. for $C_{62}H_{74}N_4O_4$: C, 79.28; H, 7.94; N, 5.96. Found: C, 79.35; H, 7.89; N, 5.88.

4,4'–*bis*(4–(2,5–dimethoxy–4–(pyrrolidin–1–yl)styryl)styryl)–2,2'–bipyridine (MS 5). The synthesis of this compound follows the same procedure as described for **MS 1**. Aldehyde **12b** (0.74 g, 2.2 mmol) was used instead of aldehyde **7a**. The compound **MS 5** was isolated as orange microcrystalline solid. Yield: 0.72 g (87%). Mp (DTA): 274 ºC.

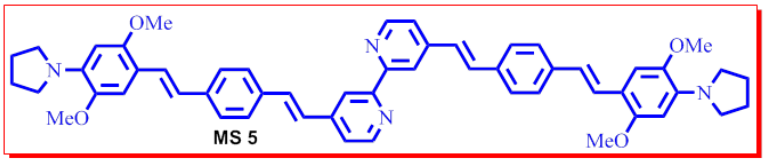

MS 5

^{1}H NMR (400 MHz, $CDCl_3$): δ 8.68 (d, J = 8 Hz, 2H), 8.56 (s, 2H), 7.54 (s, 8H), 7.50 (d, J = 16 Hz, 2H), 7.47 (d, J = 16 Hz, 2H), 7.41 (d, J = 8 Hz, 2H), 7.16–7.11 (unresolved, 4H), 6.94 (d, J = 16 Hz, 2H), 6.31 (s, 2H), 3.88 (s, 6H), 3.86 (s, 6H), 3.41 (unresolved, 8H), 1.96 (unresolved, 8H).

^{13}C NMR was not possible because of low solubility.

HRMS (MALDI–TOF/TOF, positive mode): *m*/*z* calcd. 822.415 (M^+). Found: 823.575 $(M+H)^+$.

Anal. calcd. for $C_{54}H_{54}N_4O_4$: C, 78.80; H, 6.61; N, 6.81. Found: C, 78.96; H, 6.54; N, 6.68.

4,4'–*bis*(2,5–dibutoxy–4–(4–dibutylaminostyryl)styryl)–2,2'–bipyridine (MS 6). The synthesis of this compound follows the same procedure as described for **MS 2**. Aldehyde **13b** (1.0 g, 2.2 mmol) was used instead of aldehyde **5b**. The crude product was purified by a short silica gel column (100–200 mesh) eluting with methanol/chloroform 5:95 v/v as the mobile phase. The compound **MS 6** was isolated as a thick red gel that solidified to an orange

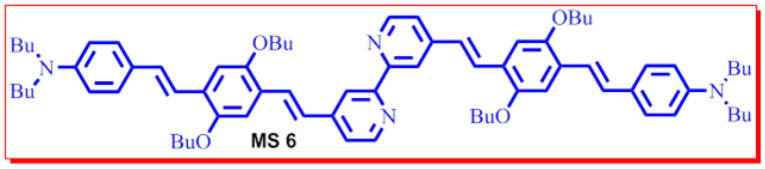

MS 6

solid after standing overnight at room temperature. Yield: 1.1 g (95%). Mp: was not measured.

^{1}H NMR (400 MHz, $CDCl_3$): δ 8.675 (d, J = 4 Hz, 2H), 8.52 (s, 2H), 7.80 (d, J = 16 Hz, 2H), 7.455 (d, J = 4 Hz, 2H), 7.42 (d, J = 8 Hz, 4H), 7.28 (d, J = 16 Hz, 2H), 7.20 (d, J = 16 Hz, 2H), 7.15 (s, 2H), 7.14 (s, 2H), 7.10 (d, J = 16 Hz, 2H), 6.66 (d, J = 8 Hz, 4H), 4.11 (t, 4H), 4.07 (t, 4H), 3.31 (t, 8H), 1.93–1.87 (p, 8H), 1.66–1.57 (m, 16H), 1.41–1.36 (m, 8H), 1.08 (t, 12H), 0.99 (t, 12H).

^{13}C NMR (100 MHz, $CDCl_3$, C-type based on DEPT-135 spectrum): δ 156.6 (C), 151.8 (C), 150.6 (C), 149.4 (CH), 147.9 (C), 146.6 (C), 129.8 (CH), 129.4 (C), 128.4 (CH), 128.0 (CH), 125.6 (CH), 125.1 (C), 124.3 (C), 120.3 (CH), 118.9 (CH), 118.2 (CH), 111.7 (CH), 111.1 (CH), 109.8(CH), 69.2 (CH_2), 50.8 (CH_2), 31.7 (CH_2), 29.6 (CH_2), 20.4 (CH_2), 19.6 (CH_2), 14.1 (CH_3).

HRMS (MALDI–TOF/TOF, positive mode): m/z calcd. 1106.759 (M^+). Found: 1107.748 $(M+H)^+$.

Anal. calcd. for $C_{74}H_{98}N_4O_4$: C, 80.25; H, 8.92; N, 5.06. Found: C, 80.15; H, 8.78; N, 4.91.

4,4'–*bis*(2,5–dibutoxy–4–(2,5–dimethoxy–4–dibutylaminostyryl)styryl)–2,2'–bipyridine (MS 7). This compound was synthesized following the same procedure as described for **MS 2**. The aldehyde **14b** (1.2 g, 2.2 mmol) was used instead of aldehyde **5b**. The crude product was purified by a short silica gel column (100–200 mesh) eluting with methanol/chloroform 5:95 v/v as the mobile phase. The compound **MS 7** was isolated as a red gum that solidified to a red solid after standing for five days at room temperature. Yield: 1.1 g (90%). Mp: was not measured.

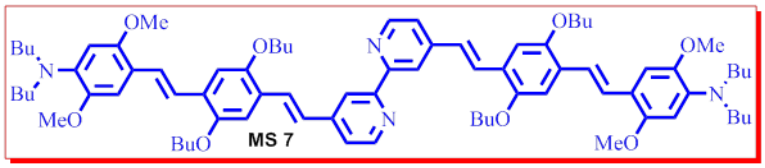

MS 7

^{1}H NMR (400 MHz, $CDCl_3$): δ 8.675 (d, J = 4 Hz, 2H), 8.51 (s, 2H), 7.80 (d, J = 16 Hz, 2H), 7.51–7.46 (m, 4H), 7.37 (d, J = 16 Hz, 2H), 7.21 (d, J = 16 Hz, 2H), 7.18 (s, 2H), 7.14 (s, 4H), 6.53 (s, 2H), 4.12 (t, 4H), 4.08 (t, 4H), 3.88 (s, 6H), 3.87 (s, 6H), 3.17 (t, 8H), 1.92–1.86 (m, 8H), 1.66–1.59 (m, 8H), 1.54–1.47 (m, 8H), 1.34–1.27 (m, 8H), 1.08–1.01 (m, 12H), 0.92 (t, 12H).

^{13}C NMR (100 MHz, $CDCl_3$, C-type based on DEPT-135 spectrum): δ 156.5 (C), 151.8 (C), 151.7 (C), 150.8 (C), 149.3 (CH), 147.6 (C), 146.6 (C), 140.9 (C), 129.3 (C), 128.4 (CH), 125.8 (CH), 124.8 (C), 124.0 (CH), 121.1 (CH), 120.4 (CH), 119.7 (C), 118.9 (CH), 111.2 (CH), 110.5 (CH), 110.3 (CH), 105.4 (CH), 69.1 (CH_2), 56.4 (OMe), 56.2 (OMe), 52.4 (CH_2), 31.7 (CH_2), 31.6 (CH_2), 29.4 (CH_2), 20.6 (CH_2), 19.6 (CH_2), 14.1 (CH_3).

HRMS (MALDI–TOF/TOF, positive mode): *m*/*z* calcd. 1226.801 (M^+). Found: 1227.884 $(M+H)^+$.

Anal. calcd. for $C_{78}H_{106}N_4O_8$: C, 76.31; H, 8.70; N, 4.56. Found: C, 76.25; H, 8.78; N, 4.46.

4,4'–*bis*(2,5–dibutoxy–4–(2,5–dimethoxy–4–(pyrrolidin–1–yl)styryl)styryl)–2,2'–bipyridine (MS 8). This compound was synthesized following the same procedure as described for **MS 2**. The aldehyde **15b** (1.1 g, 2.2 mmol) was used instead of aldehyde **5b**. The crude product was purified by a short silica gel column (100–200 mesh) eluting with methanol/chloroform 5:95 v/v as the mobile phase. The compound **MS 8** was isolated as a red–brown solid. Yield: 1.0 g (89%). Mp (DTA): 202 ºC.

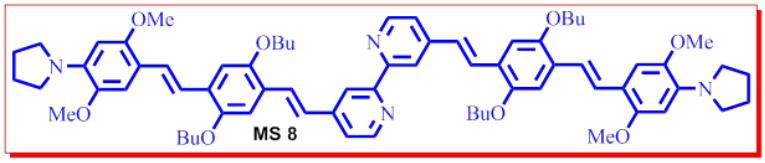

MS 8

^{1}H NMR (400 MHz, $CDCl_3$): δ 8.675 (d, *J* = 4 Hz, 2H), 8.51 (s, 2H), 7.80 (d, *J* = 16 Hz, 2H), 7.49 (d, *J* = 16 Hz, 2H), 7.45 (unresolved, 2H), 7.32 (d, *J* = 16 Hz, 2H), 7.22–7.14 (m, 8H), 6.32 (s, 2H), 4.12 (t, 4H), 4.07 (t, 4H), 3.88 (s, 6H), 3.85 (s, 6H), 3.42 (unresolved, 8H), 1.96 (unresolved, 8H), 1.92–1.87 (m, 8H), 1.66–1.60 (m, 8H), 1.06 (t, 12H).

^{13}C NMR (100 MHz, $CDCl_3$, C-type based on DEPT-135 spectrum): δ 156.6 (C), 152.5 (C), 151.8 (C), 150.7 (C), 149.4 (CH), 146.6 (C), 144.2 (C), 140.8 (C), 129.7 (C), 128.4 (CH), 125.7 (CH), 124.5 (C), 124.1 (CH), 120.3 (CH), 119.6 (CH), 118.9 (CH), 116.5 (C), 111.3 (CH), 110.8 (CH), 110.2 (CH), 99.8 (CH), 69.3 (CH_2), 69.2 (CH_2), 56.8 (OMe), 56.5 (OMe), 50.5 (CH_2), 31.7 (CH_2), 31.6 (CH_2), 25.1 (CH_2), 19.5 (CH_2), 14.0 (CH_3).

HRMS (MALDI–TOF/TOF, positive mode): *m*/*z* calcd. 1110.645 (M^+). Found: 1111.670 $(M+H)^+$.

Anal. calcd. for $C_{70}H_{86}N_4O_8$: C, 75.64; H, 7.80; N, 5.04. Found: C, 75.49; H, 7.68; N, 5.12.

● 4.5. REFERENCES

1. (a) Lakowicz, J. R. in *Principles of Fluorescence Spectroscopy: 3rd edition*, **2006**, Springer Sciences and Business Media, New York. (b) *Springer Series on Fluorescence: Methods and Applications*, Wolfbeis, O. S. Ed., Springer Sciences and Business Media, Springer–Verlag Berlin Heidelberg, **2010**. (c) *Topics in Fluorescence Spectroscopy*, Lakowicz, J. R. Ed., Vol. 1–4, Kluwer Academic Publishers, **2002**, New York.
2. (a) Meier, H. *Angew. Chem. Int. Ed.* **2005**, *44*, 2482 and references therein. (b) Grimsdale, A. C.; Chan, K. L.; Martin, R. E.; Jokisz, P. G.; Holmes, A. B. *Chem. Rev.* **2009**, *109*, 897 and references therein. (c) Li, C.; Liu, M.; Pschirer, N. G.; Baumgarten, M.; Müllen, K. *Chem. Rev.* **2010**, *18*, 4619 and references therein. (d) Arias, A. C.; MacKenzie, J. D.; McCulloch, I.; Rivnay, J.; Salleo, A. *Chem. Rev.* **2010**, *110*, 3 and references therein.
3. (a) Campbell, N. H.; Smith, D. L.; Reszka, A. P.; Neidle, S.; O' Hagan, D. *Org. Biomol. Chem.* **2011**, *9*, 1328. (b) Janovec, L.; Kožurková, M.; Sabolová, D.; Ungvarský, J.; Paulíková, H.; Plšíková, J.; Vantová, Z.; Imrich, J. *Bioorg. Med. Chem.* **2011**, *19*, 1790. (c) Sparapani, S.; Haider, S. M.; Doria, F.; Gunaratnam, M.; Neidle, S. *J. Am. Chem. Soc.* **2010**, *132*, 12263. (d) Würdemann, M.; Christoffers, J. *Org. Biomol. Chem.* **2010**, *8*, 1894. (e) Rogness, D. C.; Larock, R. C. *J. Org. Chem.* **2010**, *75*, 2289.
4. (a) Egawa, T.; Koide, Y.; Hanaoka, K.; Komatsu, T.; Terai, T.; Nagano, T. *Chem. Commun.* **2011**, 4162. (b) Li, T.; Yang, Z.; Li, Y.; Liu, Z.; Qi, G.; Wang, B. *Dyes and Pigments* **2011**, *88*, 103. (c) Shi, W.; Sun, Z.; Wei, M.; Evans, D. G.; Duan, X. *J. Phys. Chem. C* **2010**, *114*, 21070. (d) McQueen, P. D.; Sagoo, S.; Yao, H.; Jockusch, R. A. *Angew. Chem. Int. Ed.* **2010**, *49*, 9193. (e) Santra, M.; Ko, S. –K.; Shin, I.; Ahn, K. H. *Chem. Commun.* **2010**, *46*, 3964.
5. (a) Zanotti, K. J.; Silva, G. L.; Creeger, Y.; Robertson, K. L.; Waggoner, A. S.; Berget, P. B.; Armitage, B. A. *Org. Biomol. Chem.* **2011**, *9*, 1012. (b) Fischer, G. M.; Daltrozzo, E.; Zumbusch, A. *Angew. Chem. Int. Ed.* **2011**, *50*, 1406. (c) Yuan,

L.; Lin, W.; Song, J. *Chem. Commun.* **2010**, *46*, 7930. (d) Samanta, A.; Vendrell, M.; Das, R.; Chang, Y. –T. *Chem. Commun.* **2010**, *46*, 7406. (e) Pandey, A. K.; Deakin, P. C.; Jansen–Van Vuuren, R. D.; Burn, P. L.; Samuel, I. D. W. *Adv. Mater.* **2010**, *22*, 3954.

6. (a) Bag, B.; Pal, A. *Org. Biomol. Chem.* **2011**, *9*, 4467. (b) Wang, C.; Wong, K. M. –C. *Inorg. Chem.* **2011**, *50*, 5333. (c) Beija, M.; Afonso, C. A. M.; Martinho, J. M. G. *Chem. Soc. Rev.* **2009**, *38*, 2410. (d) Kim, H. N.; Lee, M. H.; Kim, H. J.; Kim, J. S.; Yoon, J. *Chem. Soc. Rev.* **2008**, *37*, 1465. (e) Koide, Y.; Urano, Y.; Hanaoka, K.; Terai, T.; Nagano, T. *J. Am. Chem. Soc.* **2011**, *133*, 5680.
7. (a) Wu, W.; Wu, W.; Ji, S.; Guo, H.; Zhao, J. *Dalton Trans.* **2011**, *40*, 5953. (b) Semeniuchenko, V.; Groth, U.; Khilya, V. *Synthesis* **2009**, 3533. (c) Jana, R.; Partridge, J. J.; Tunge, J. A. *Angew. Chem. Int. Ed.* **2011**, *50*, 5157. (d) Shiraishi, Y.; Sumiya, S.; Hirai, T. *Chem. Commun.* **2011**, *47*, 4953. (e) Dong, Y.; Li, J.; Jiang, X.; Song, F.; Cheng, Y.; Zhu, C. *Org. Lett.* **2011**, *13*, 2252.
8. (a) Nepomnyashchii, A. B.; Bröring, M.; Ahrens, J.; Bard, A. J. *J. Am. Chem. Soc.* **2011**, *133*, 8633. (b) Chase, D. T.; Young, B. S.; Haley, M. M. *J. Org. Chem.* **2011**, *76*, 4043. (c) Chase, D. T.; Young, B. S.; Haley, M. M. *Inorg. Chem.* **2011**, *50*, 4392. (d) Khan, T. K.; Rao, M. R.; Ravikanth, M. *Eur. J. Org. Chem.* **2010**, 2314. (e) Rao, M. R.; Mobin, S. M.; Ravikanth, M. *Tetrahedron* **2010**, *66*, 1728.
9. (a) Arun, K. T.; Jayaram, D. T.; Avirah, R. R.; Ramaiah, D. *J. Phys. Chem. B.* **2011**, *115*, 7122. (b) Jisha, V. S.; Arun, K. T.; Hariharan, M.; Ramaiah, D. *J. Phys. Chem. B* **2010**, *114*, 5912. (c) Sreejith, S.; Divya, K. P.; Ajayaghosh, A. *Angew. Chem. Int. Ed.* **2008**, *47*, 7883. (d) Sreejith, S.; Carol, P.; Chithra, P.; Ajayaghosh, A. *J. Mater. Chem.* **2008**, *18*, 264. (e) Ajayaghosh, A. *Acc. Chem. Res.* **2005**, *38*, 449.
10. (a) Vijayakumar, C.; Praveen, V. K.; Kartha, K. K.; Ajayaghosh, A. *Phys. Chem. Chem. Phys.* **2011**, *13*, 4942. (b) Dasgupta, D.; Srinivasan, S.; Rochas, C.; Thierry, A.; Schröder, A.; Ajayaghosh, A.; Guenet, J. M. *Soft Mater.* **2011**, *7*, 2797. (c) Babu, S. S.; Kartha, K. K.; Ajayaghosh, A. *J. Phys. Chem. Lett.* **2010**, *1*, 3413. (d) Prasanthkumar, S.; Gopal, A.; Ajayaghosh, A. *J. Am. Chem. Soc.* **2010**, *132*, 13206. (e) Mahesh, S.; Thirumalai, R.; Yagai, S.; Kitamura, A.; Ajayaghosh, A. *Chem. Commun.* **2009**, 5984.

11. (a) Hu, B.; Fu, S. –J.; Xu, F.; Tao, T.; Zhu, H. –Y.; Cao, K. –S.; Huang, W.; You, X. –Z. *J. Org. Chem.* **2011**, *76*, 4444. (b) Lee, H. –S.; Kim, H. –J.; Kang, J. –G. *Photochem. Photobiol. Sci.* **2011**, *10*, 1338. (c) Peng, X.; Wu, T.; Fan, J.; Wang, J.; Zhang, S.; Song, F.; Sun, S. *Angew. Chem. Int. Ed.* **2011**, *50*, 4180. (d) Cao, X.; Lin, W.; Ding, Y. *Chem. –Eur. J.* **2011**, *17*, 9066. (e) Yuasa, J.; Mitsui, A.; Kawai, T. *Chem. Commun.* **2011**, *47*, 5807. (f) Ulrich, G.; Goeb, S.; Nicola, A. D.; Retailleau, P.; Ziessel, R. *J. Org. Chem.* **2011**, *76*, 4489. (g) Mahmood, T.; Paul, A.; Ladame, S. *J. Org. Chem.* **2010**, *75*, 204. (h) Bürckstümmer, H.; Weissenstein, A.; Bialas, D.; Würthner, F. *J. Org. Chem.* **2011**, *76*, 2426. (i) Chen, Y.; Wang, H.; Wan, L.; Bian, Y.; Jiang, J. *J. Org. Chem.* **2011**, *76*, 3774.

12. (a) Kaes, C.; Katz, A.; Hosseini, M. W. *Chem. Rev.* **2000**, *100*, 3553. (b) Schubert, U. S.; Eschbaumer, C. *Angew. Chem. Int. Ed.* **2002**, *41*, 2892. (c) Smith, A. P.; Fraser, C. L. *Comprehensive Coordination Chemistry II*; Elsevier, **2003**, Vol. *1*, 1–23.

13. (a) Maury, O.; Bozec, H. L. *Acc. Chem. Res.* **2005**, *38*, 691 and the references therein. (b) Bouder, T. L.; Viau, L.; Guégan, J. –P.; Maury, O.; Bozec, H. L. *Eur. J. Org. Chem.* **2002**, 3024. (c) Aubert, V.; Ishow, E.; Ibersiene, F.; Boucekkine, A.; Williams, J. A. G.; Toupet, L.; Métivier, R.; Nakatani, K.; Guerchais, V.; Bozec, H. Le *New. J. Chem.* **2009**, *33*, 1320. (d) Maury, O.; Guégan, J. –P.; Renouard, T.; Hilton, A.; Dupau, P.; Sandon, N.; Toupet, L.; Bozec, H. Le *New J. Chem.* **2001**, *25*, 1553. (e) Araya, J. C.; Gajardo, J.; Moya, S. A.; Aguirre, P.; Toupet, L.; Williams, J. A. G.; Escadeillas, M.; Bozec, H. Le; Guerchais, V. *New. J. Chem.* **2010**, *34*, 21. (f) Bourgault, M.; Renouard, T.; Lognoné, B.; Mountassir, C.; Bozec H. L. *Can. J. Chem.* **1997**, *75*, 318. (g) Lohio, O.; Viau, L.; Maury, O.; Bozec, H. Le *Tetrahedron Lett.* **2007**, *48*, 1229. (h) Viau, L.; Maury, O.; Bozec, H. Le *Tetrahedron Lett.* **2004**, *45*, 125.

14. (a) Kocian, O.; Mortimer, R. J.; Beer, P. D. *J. Chem. Soc. Perkin Trans. 1* **1990**, 3203. (b) Abdel–Shafi, A. A.; Beer, P. D.; Mortimer, R. J.; Wilkinson, F. *J. Phys. Chem. A* **2000**, *104*, 192. (c) Beer, P. D.; Kocian, O.; Mortimer, R. J.; Ridgway, C. *J. Chem. Soc. Dalton Trans.* **1993**, 2629. (d) Beer, P. D.; Kocian, O.; Mortimer, R. J.; Ridgway, C. *J. Chem. Soc. Faraday Trans.* **1993**, *89*, 333. (e) Beer, P. D.;

Kocian, O.; Mortimer, R. J.; Ridgway, C. *Analyst*, **1992**, *117*, 1247. (f) Beer, P. D.; Kocian, O.; Mortimer, R. J.; Ridgway, C. *J. Chem. Soc. Chem. Commun.* **1991**, 1460. (g) Abbotto, A.; Bellotto, L.; Angelis, F. De; Manfredi, N.; Marinzi, C. *Eur. J. Org. Chem.* **2008**, 5047. (h) An, B. –K.; Burn, P. L.; Meredith, P. *Chem. Mater.* **2009**, *21*, 3315. (i) Grabulosa, A.; Martineau, D.; Beley, M.; Gros, P. C.; Cazzanti, S.; Caramori, S.; Bignozzi, C. A. *Dalton Trans.* **2009**, 63.

15. (a) Berner, D.; Klein, C.; Nazeeruddin, M. K.; Angelis, F. D.; Castellani, M.; Scopelliti, P. B. R.; Zuppirolid, L.; Grätzel, M. *J. Mater. Chem.* **2006**, *16*, 4468. (b) Klein, C.; Baranoff, E.; Nazeeruddin, Md. K.; Grätzel, M. *Tetrahedron Lett.* **2010**, *51*, 6161.

16. (a) Sreejith, S.; Divya, K. P.; Ajayaghosh, A. *Chem. Commun.* **2008**, 2903. (b) Ajayaghosh, A.; Carol, P.; Sreejith, S. *J. Am. Chem. Soc.* **2005**, *127*, 14962. (c) Divya, K. P.; Sreejith, S.; Balakrishna, B.; Jayamurthy, P.; Aneesa, P.; Ajayaghosh, A. *Chem. Commun.* **2010**, *46*, 6069.

17. (a) Bozec, H. Le; Renouard, T. *Eur. J. Inorg. Chem.* **2000**, 229. (b) Sénéchal, K.; Maury, O.; Bozec, H. Le; Ledoux, I.; Zyss, J. *J. Am. Chem. Soc.* **2002**, *124*, 4560. (c) Maury, O.; Viau, L.; Sénéchal, K.; Corre, B.; Guégan, J. –P.; Renouard, T.; Ledoux, I.; Zyss, J.; Bozec, H. Le *Chem. Eur. J.* **2004**, *10*, 4454. (d) Aubert, V.; Guerchais, V.; Ishow, E.; Hoang–Thi, K.; Ledoux, I.; Nakatani, K.; Bozec, H. Le *Angew. Chem. Int. Ed.* **2008**, *47*, 577. (e) Coe, B. J.; Fielden, J.; Foxon, S. P.; Brunschwig, B. S.; Asselberghs, I.; Clays, K.; Samoc, A.; Samoc, M. *J. Am. Chem. Soc.* **2010**, *132*, 3496.

18. (a) O'Regan, B.; Grätzel, M. *Nature* **1991**, *353*, 737. (b) Campbell, W. M.; Burrell, A. K.; Officer, D. L.; Jolley, K. W. *Coord. Chem. Rev.* **2004**, *248*, 1363. (c) Shao, W.; Gu, F.; Gai, L.; Li, C. *Chem. Commun.* **2011**, *47*, 5046. (d) Monari, A.; Assfeld, X.; Beley, M.; Gros, P. C. *J. Phys. Chem. A* **2011**, *115*, 3596. (e) Jennings, J. R.; Liu, Y.; Wang, Q.; Zakeeruddin, S. M.; Grätzel, M. *Phys. Chem. Chem. Phys.* **2011**, *13*, 6637. (f) Koster, L. J. A.; Kemerink, M.; Wienk, M. M.; Maturová, K.; Janssen, R. A. J. *Adv. Mater.* **2011**, *23*, 1670. (g) Lee, C. –H.; Chiu, W. –H.; Lee, K. –M.; Hsieh, W. –F.; Wu, J. –M. *J. Mater. Chem.* **2011**, *21*, 5114. (h) Fabregat–Santiago, F.; Bisquert, J.; Cevey, L.; Chen, P.; Wang, M.; Zakeeruddin, S. M.;

Grätzel, M. *J. Am. Chem. Soc.* **2009**, *131*, 558. (i) Listorti, A.; O'Regan, B.; Durrant, J. R. *Chem. Mater.* **2011**, *23*, 3381. (j) Clifford, J. N.; Martínez-Ferrero, E.; Viterisi, A.; Palomares, E. *Chem. Soc. Rev.* **2011**, *40*, 1635. (k) Vougioukalakis, G. C.; Philippopoulos, A. I.; Stergiopoulos, T.; Falaras, P. *Coord. Chem. Rev.* **2011**, *255*, 2602. (l) Reynal, A.; Palomares, E. *Eur. J. Inorg. Chem.* **2011**, 4509.

19. (a) Chatterjee, T.; Sarma, M.; Das, S. K. *Tetrahedron Lett.* **2010**, *51*, 1985. (b) Chatterjee, T.; Sarma, M.; Das, S. K. *Tetrahedron Lett.* **2010**, *51*, 6906. (c) Chatterjee, T.; Sarma, M.; Das, S. K. *Tetrahedron Lett.* **2011**, *52*, 5460.
20. (a) Smith, A. P.; Lamba, J. J. S.; Fraser, C. L. *Org. Synth.* **2004**, *10*, 107. (b) Fraser, C. L.; Anastasi, N. R.; Lamba, J. J. S. *J. Org. Chem.* **1997,** *62*, 9314.
21. Reichardt, C. *Chem. Rev.* **1994,** *94*, 2319.
22. (a) Parker, C. A. in *Measurement of Fluorescence Efficiency*, Elsevier Publishing Co, 1968. (b) Kartens, T.; Kobs, K. *J. Phys. Chem.* **1980**, *84*, 1871.
23. Rurack, K.; Spieles, M. *Anal. Chem.* **2011**, *83*, 1232.
24. Frisch, M. J. *et al*. GAUSSIAN09, revision B.01, Gaussian, Inc., Wallingford, CT, **2010**.
25. Toro, C.; Boni, L. D.; Yao, S.; Belfield, K. D.; Hernández, F. E. *J. Phys. Chem. B* **2008**, *112*, 12185.
26. Dreuw, A.; Head-Gordon, M. *J. Am. Chem. Soc.* **2004**, *126*, 4007 and references therein.
27. Yanai, T.; Tew, D.; Handy, N. *Chem. Phys. Lett.* **2004**, *393*, 51.

Spectrum 4.1. ^{1}H NMR spectrum of MS 1

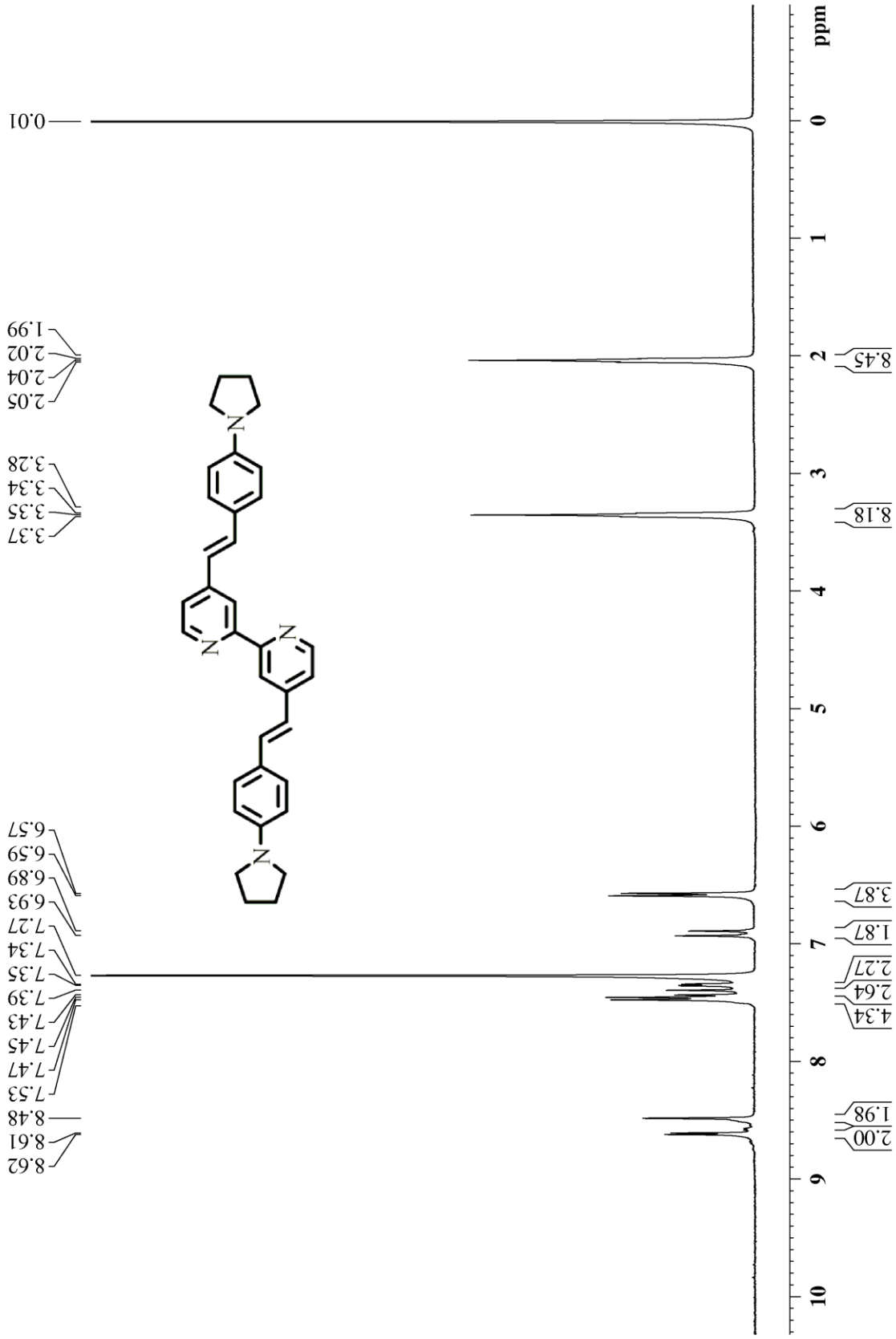

Spectrum 4.2. ^{1}H NMR spectrum of MS 2

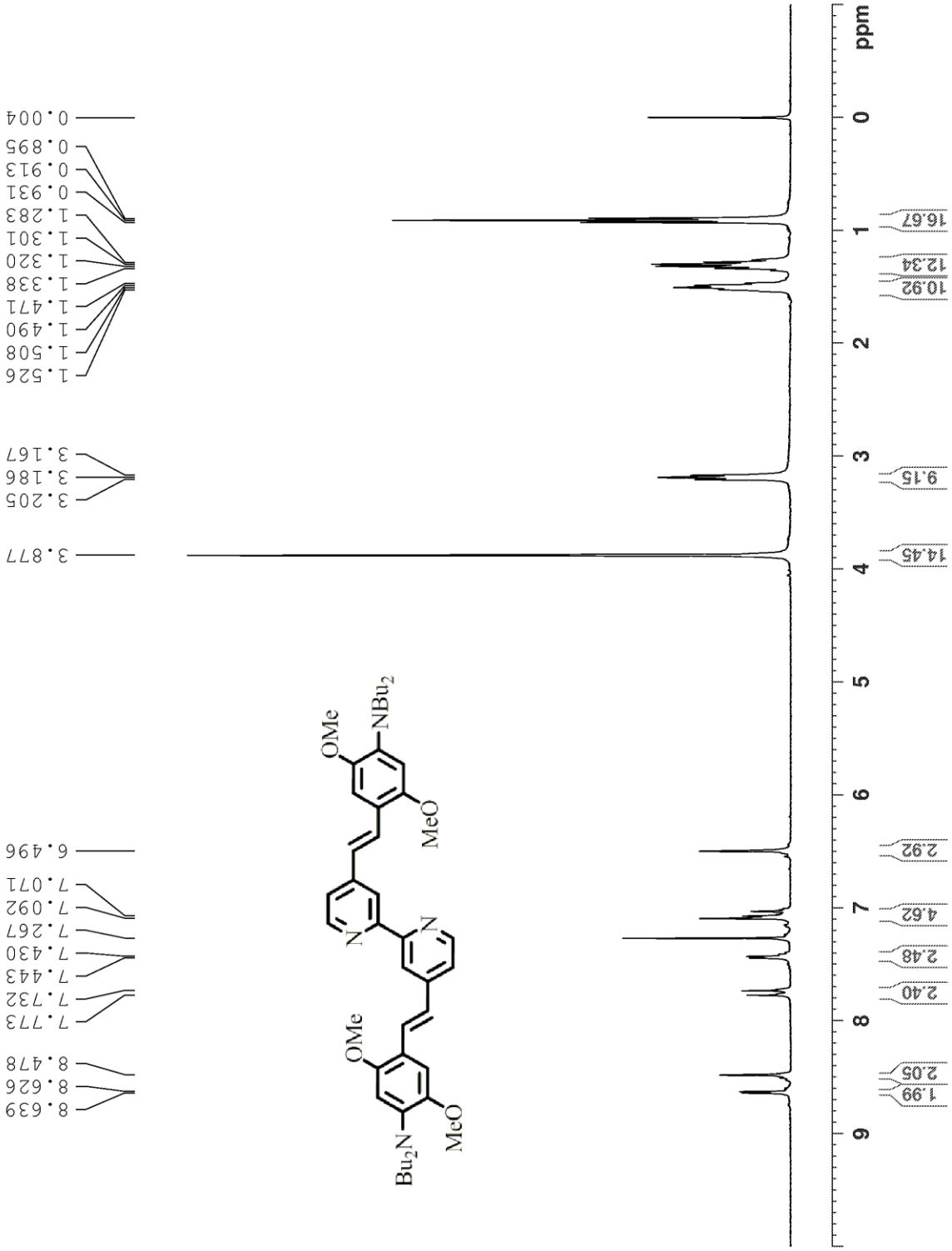

Spectrum 4.3. ^{13}C NMR spectrum of MS 2

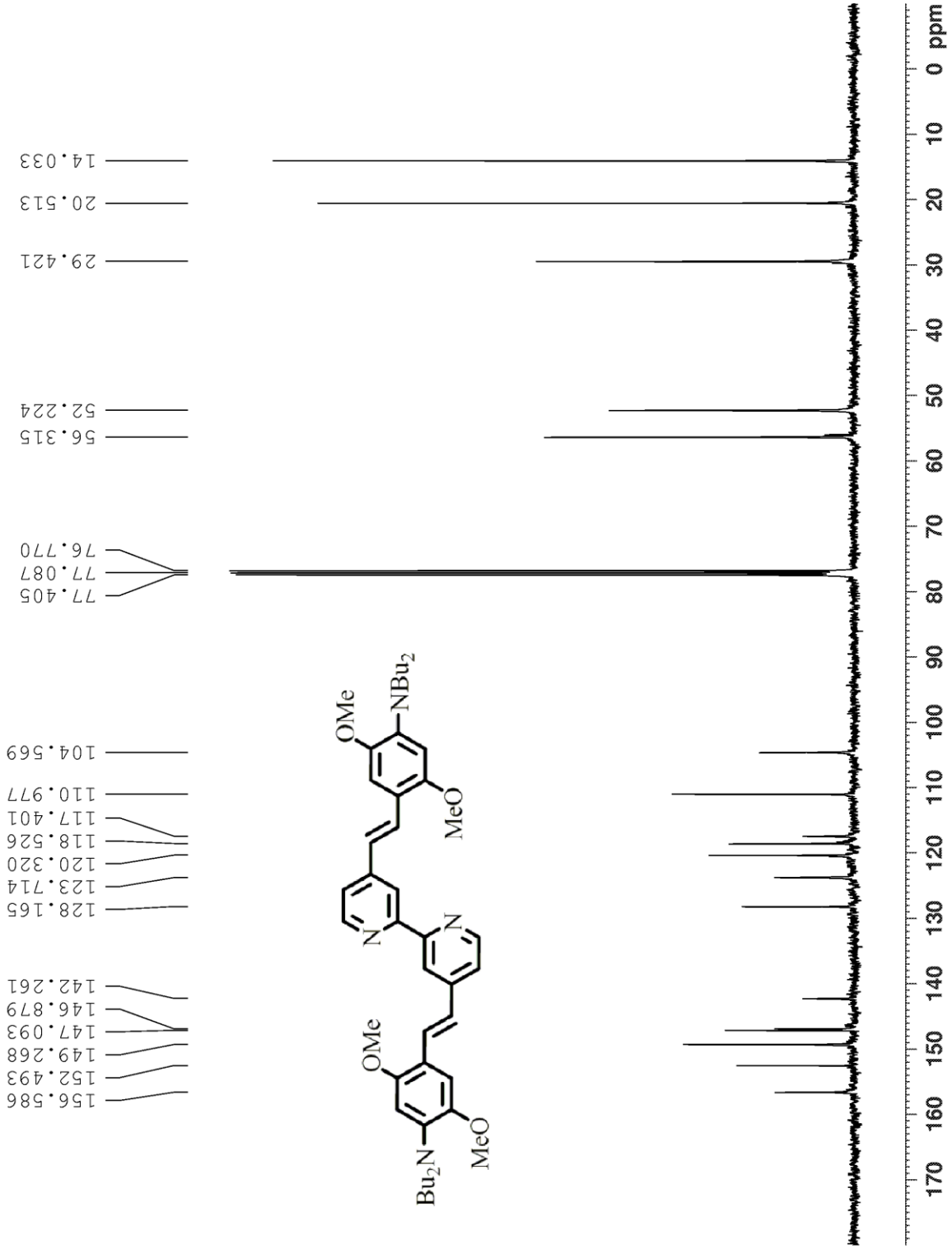

Spectrum 4.4. ^{1}H NMR spectrum of MS 3

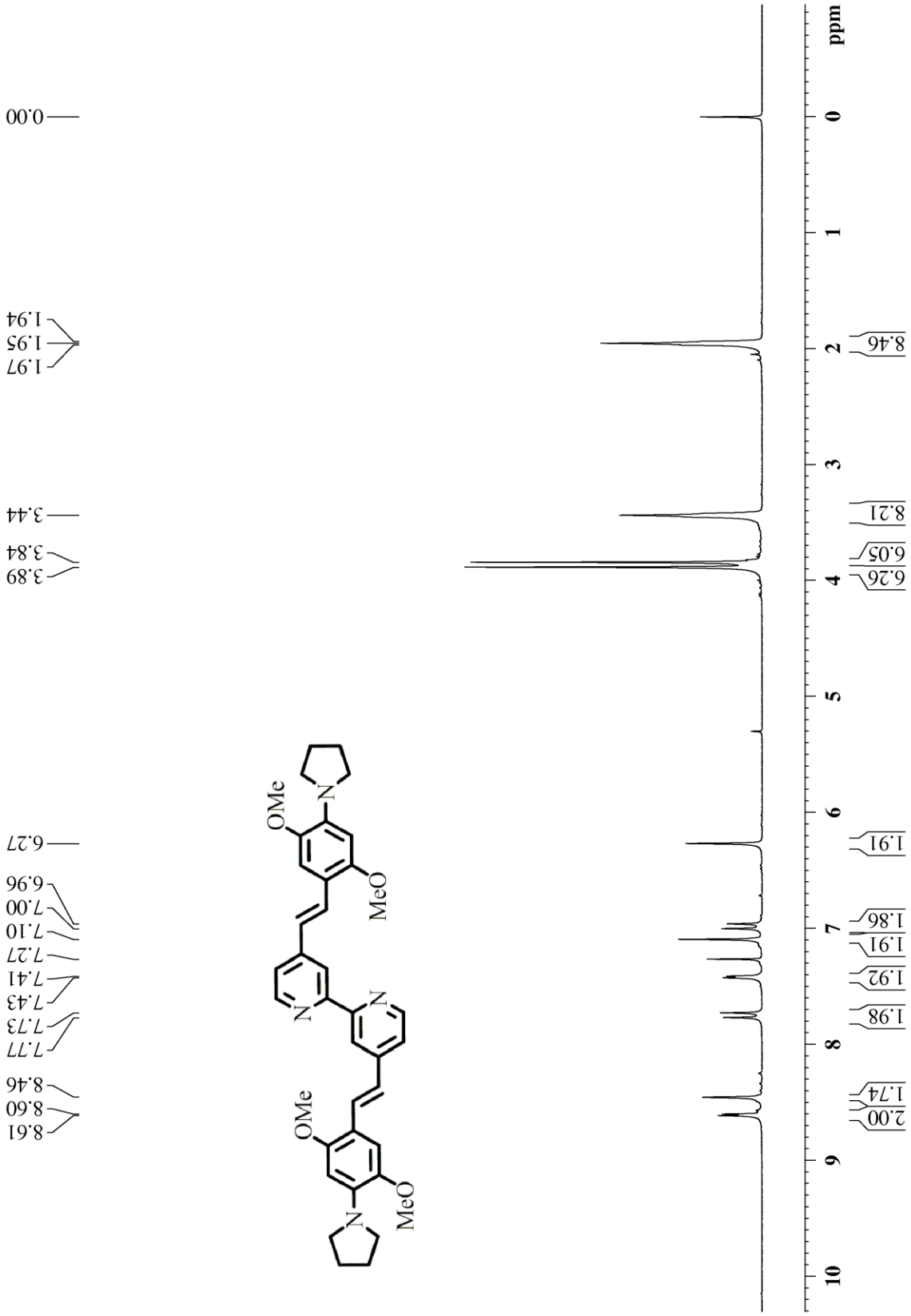

Spectrum 4.5. ^{13}C NMR spectrum of MS 3

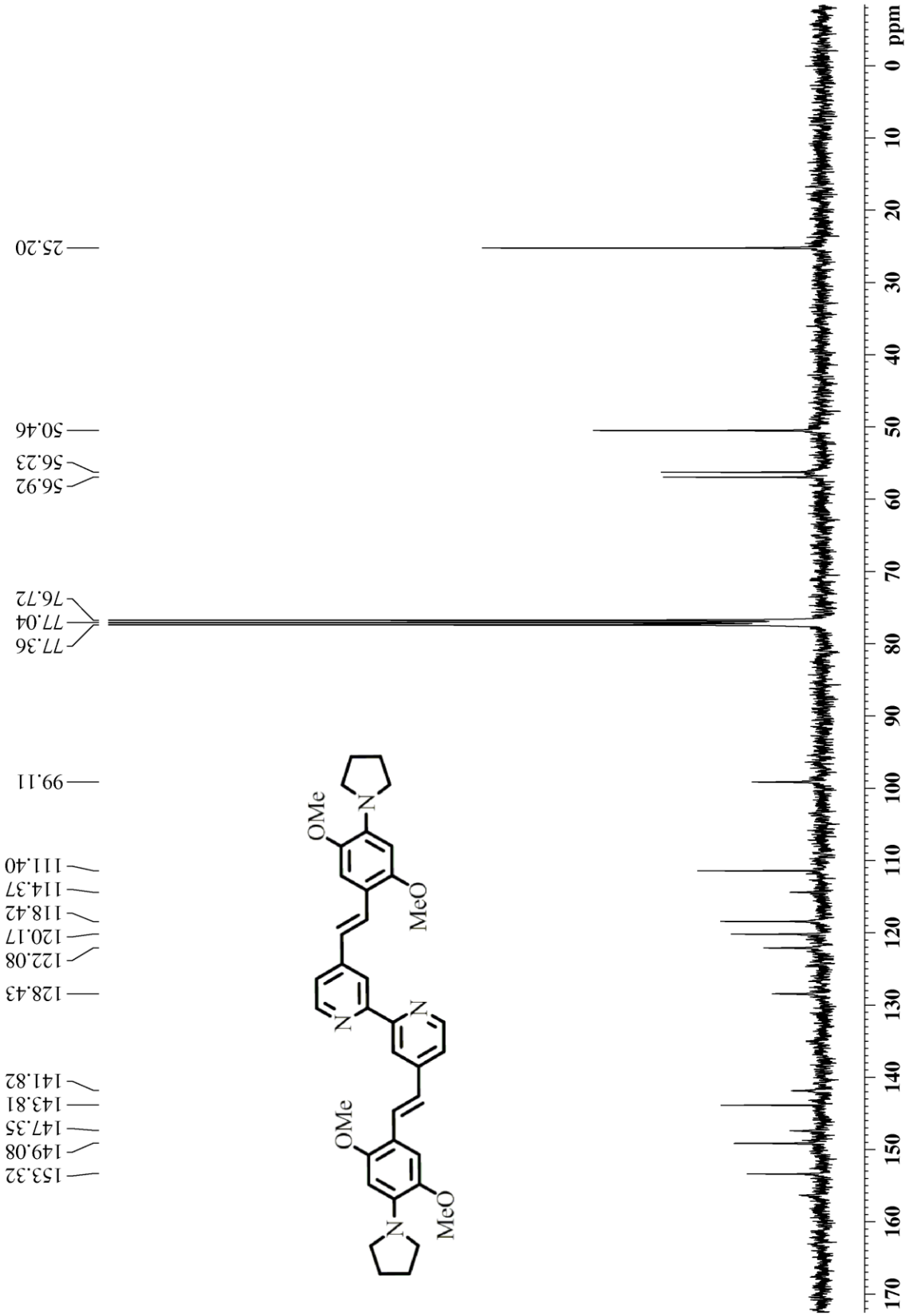

Spectrum 4.6. ^{1}H NMR spectrum of MS 4

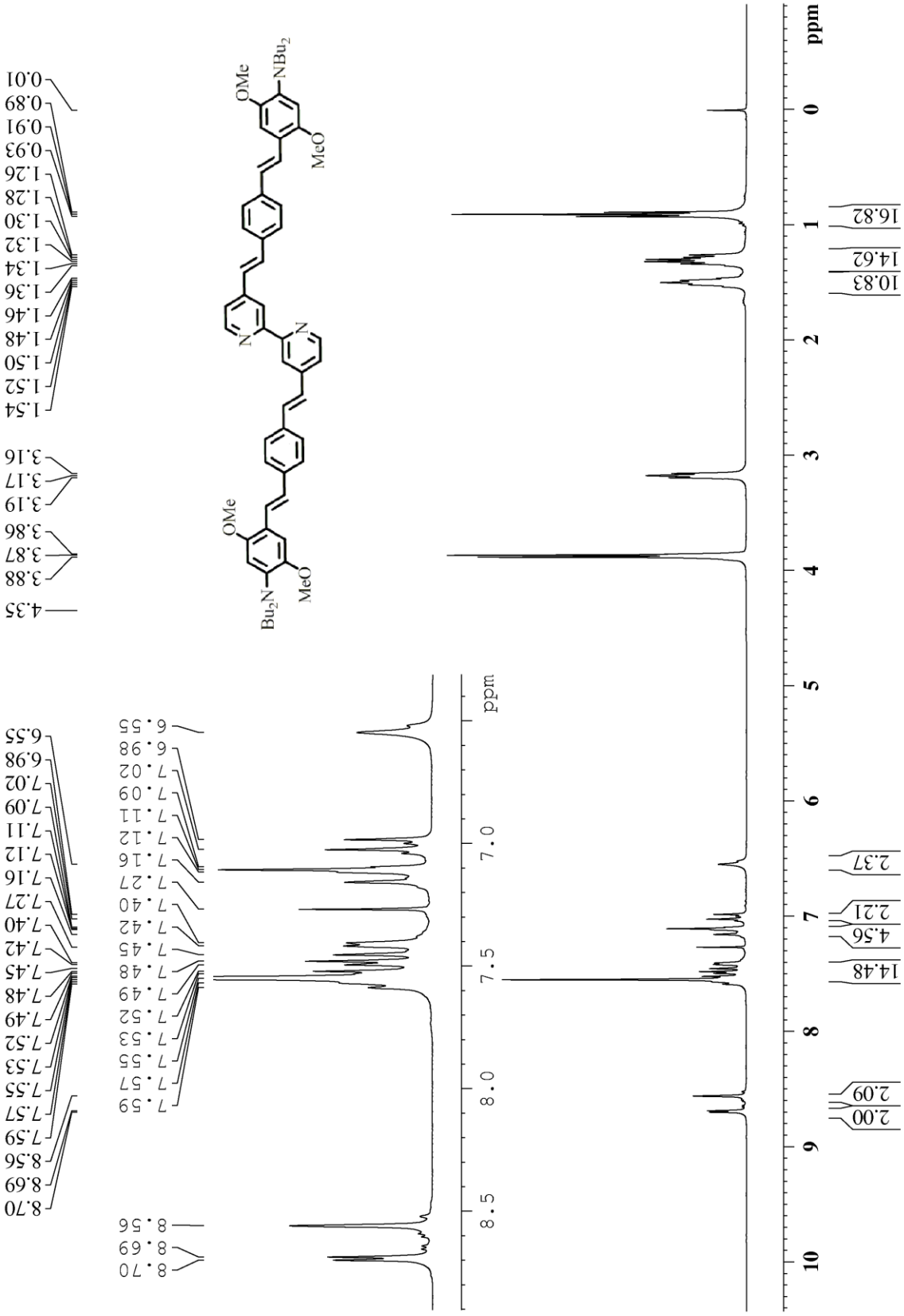

Spectrum 4.7. ^{13}C NMR spectrum of MS 4

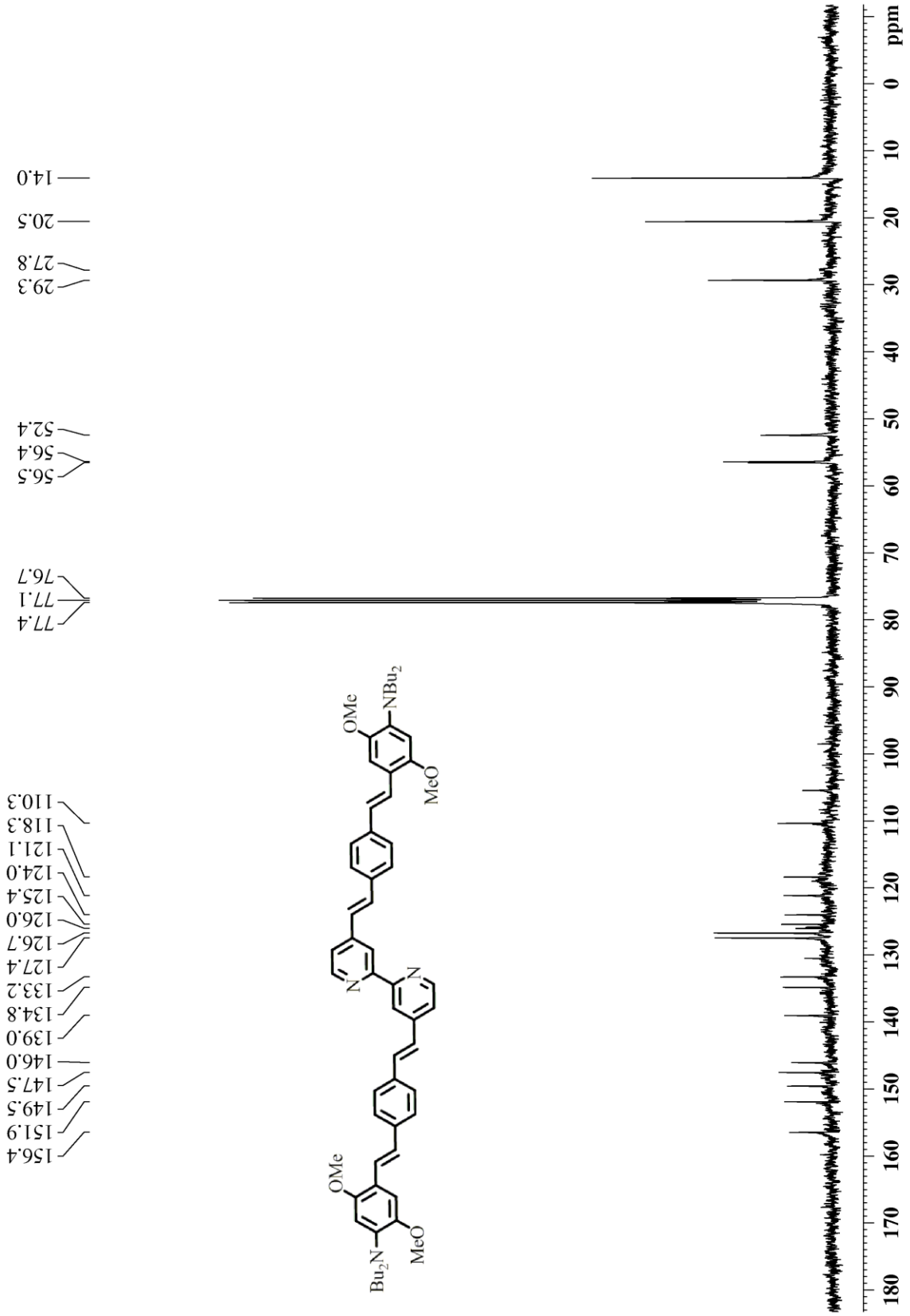

Spectrum 4.8. ^{1}H NMR spectrum of MS 5

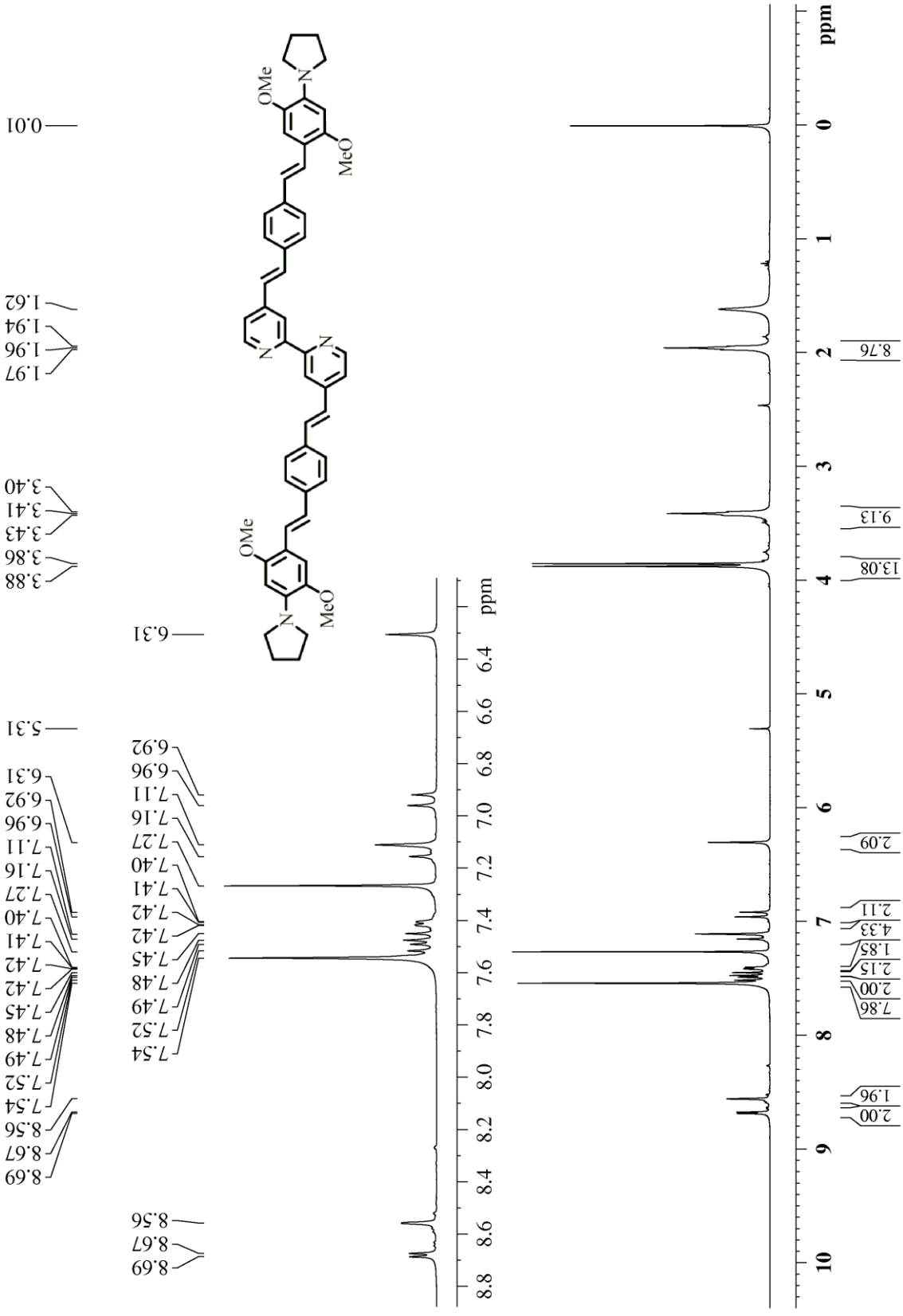

Spectrum 4.9. ^{1}H NMR spectrum of MS 6

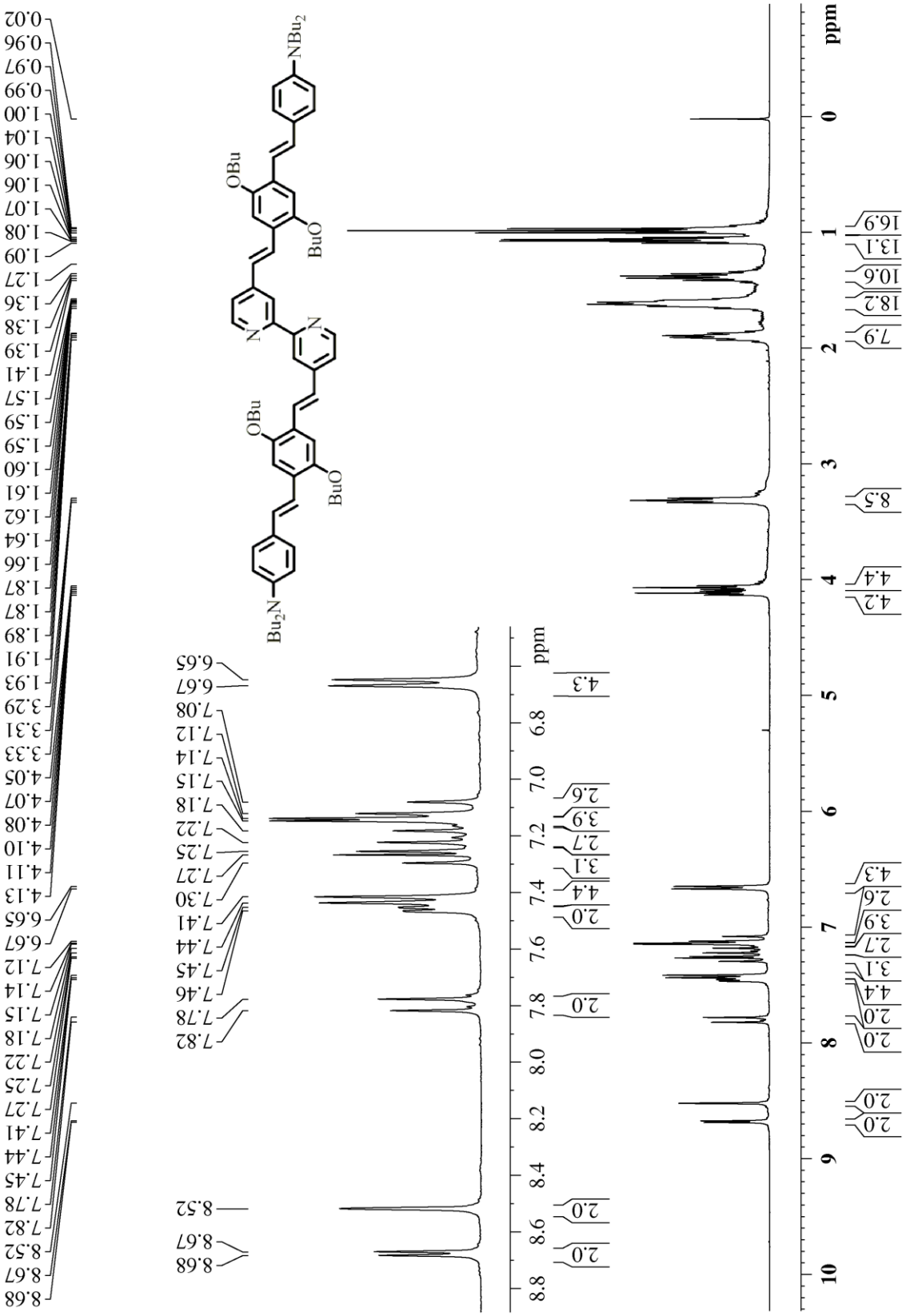

Spectrum 4.10. ^{13}C NMR spectrum of MS 6

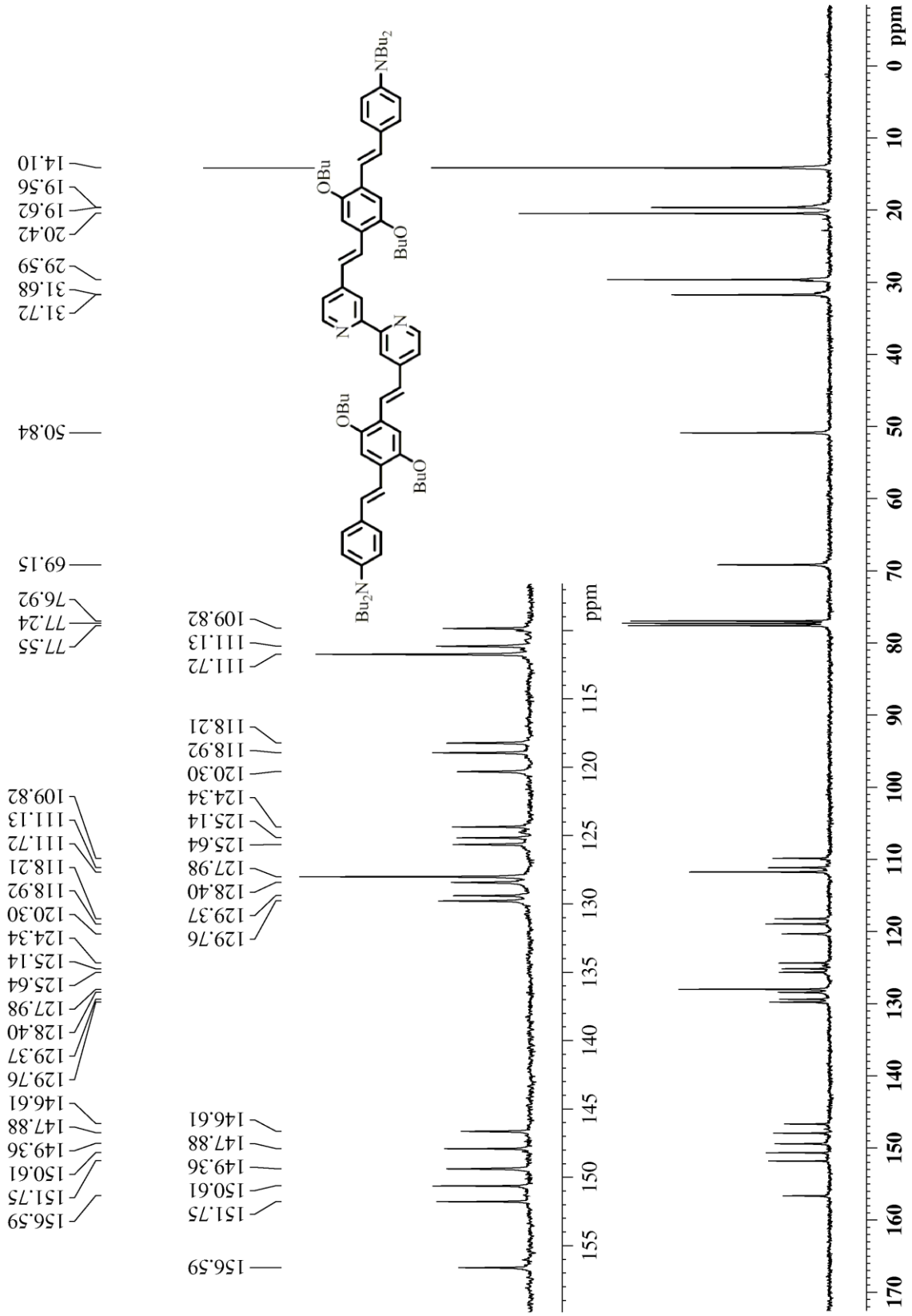

Spectrum 4.11. ^{1}H NMR spectrum of MS 7

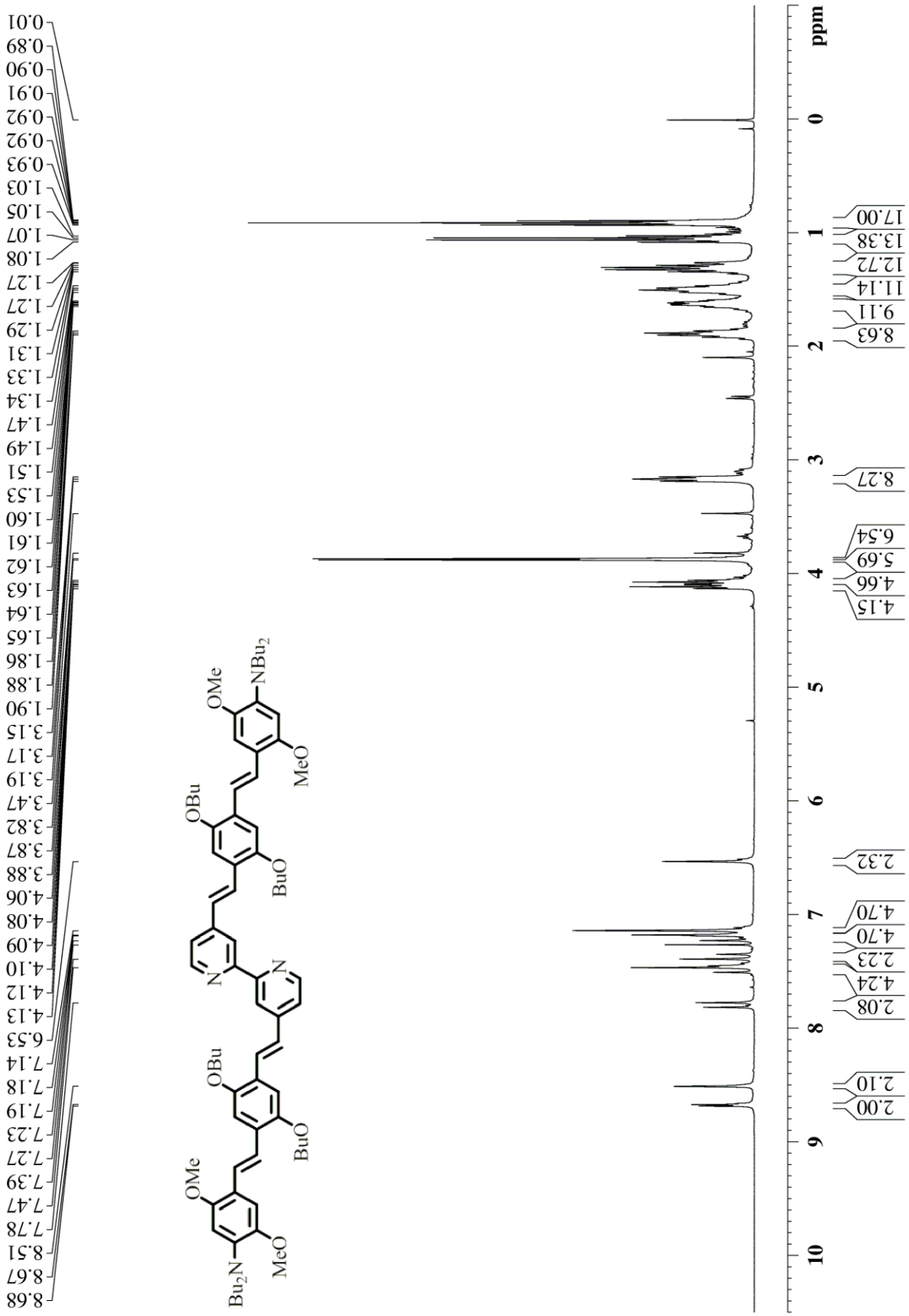

Spectrum 4.12. ^{13}C NMR spectrum of MS 7

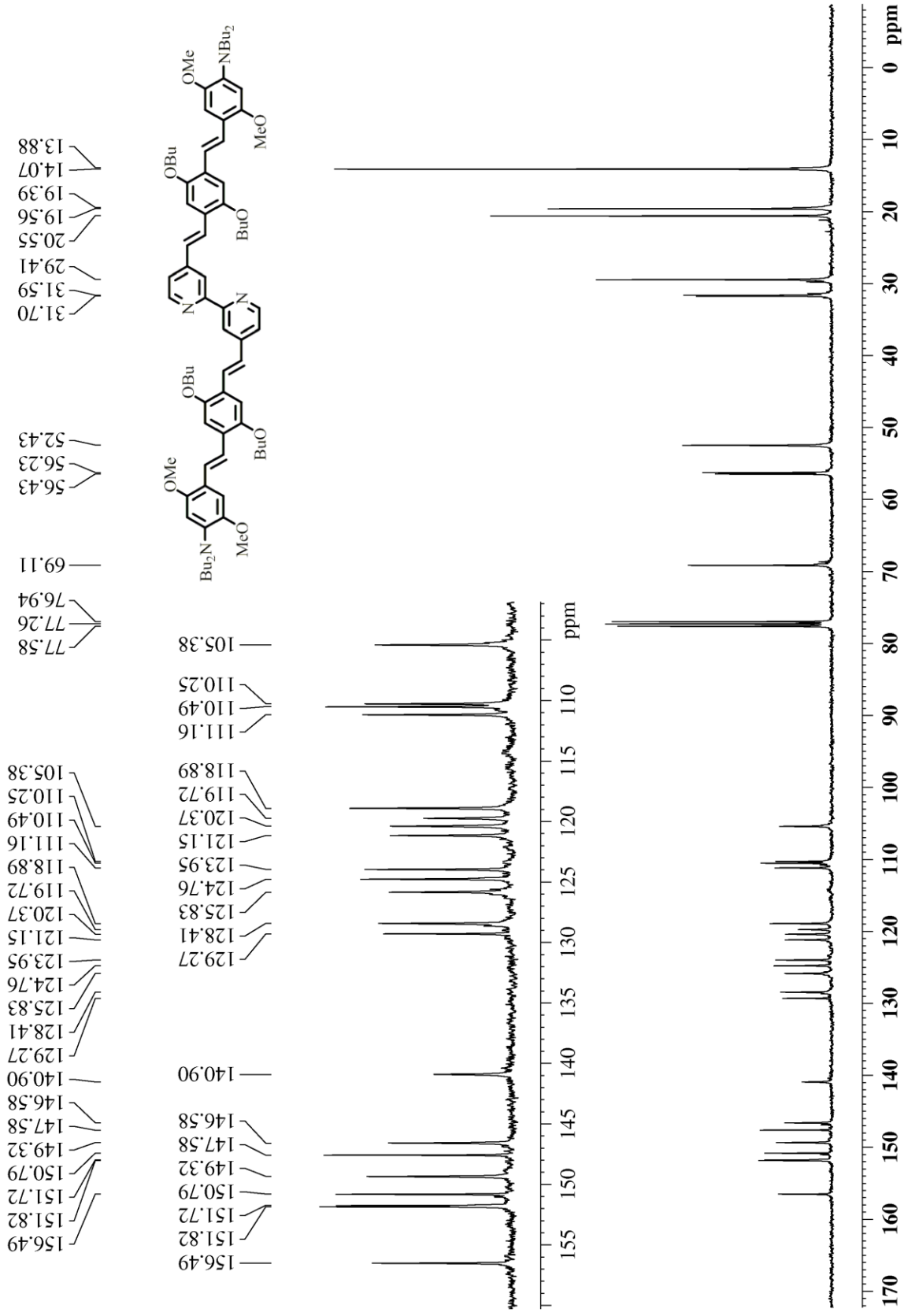

Spectrum 4.13. ^{1}H NMR spectrum of MS 8

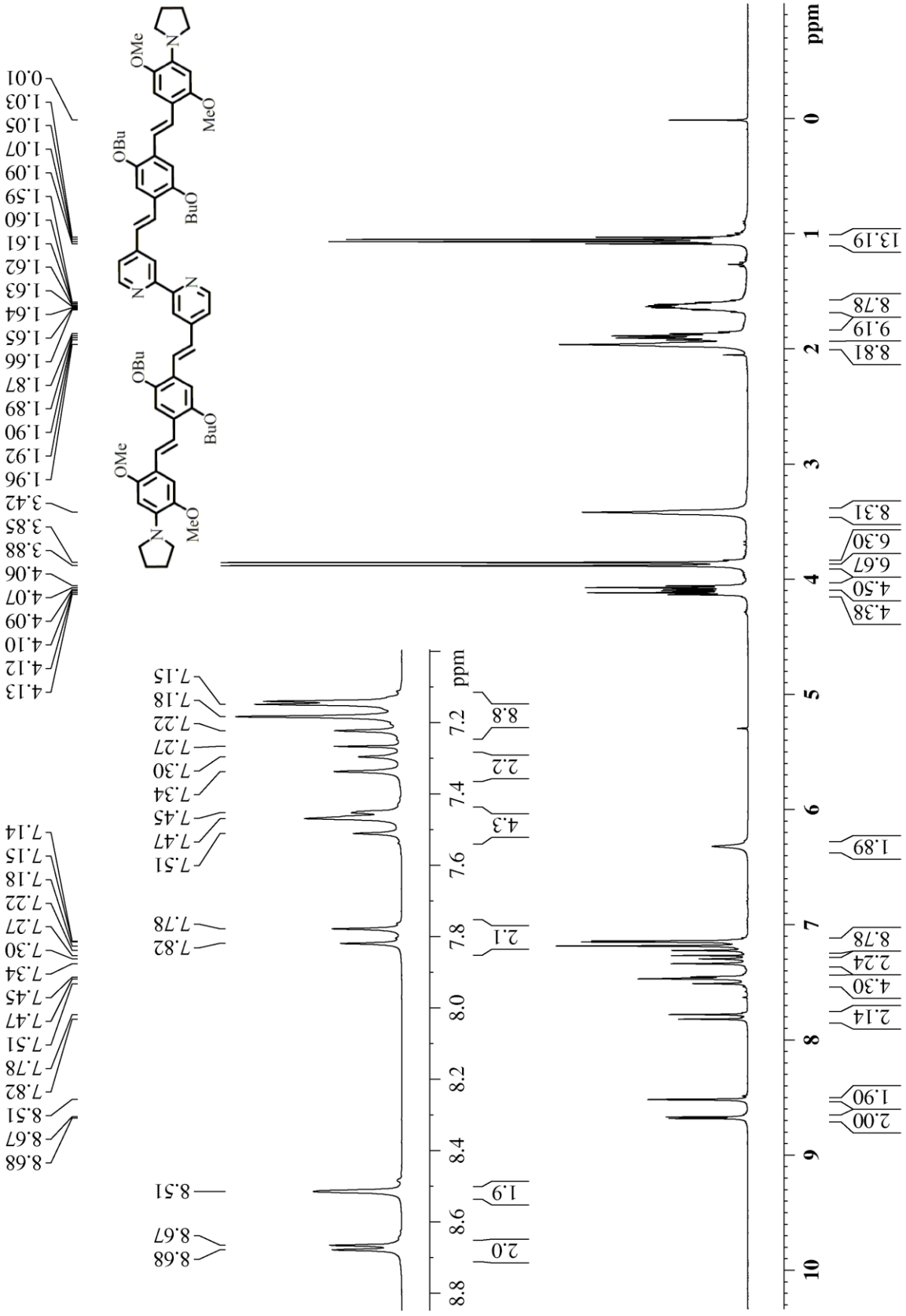

Spectrum 4.14. ^{13}C NMR spectrum of MS 8

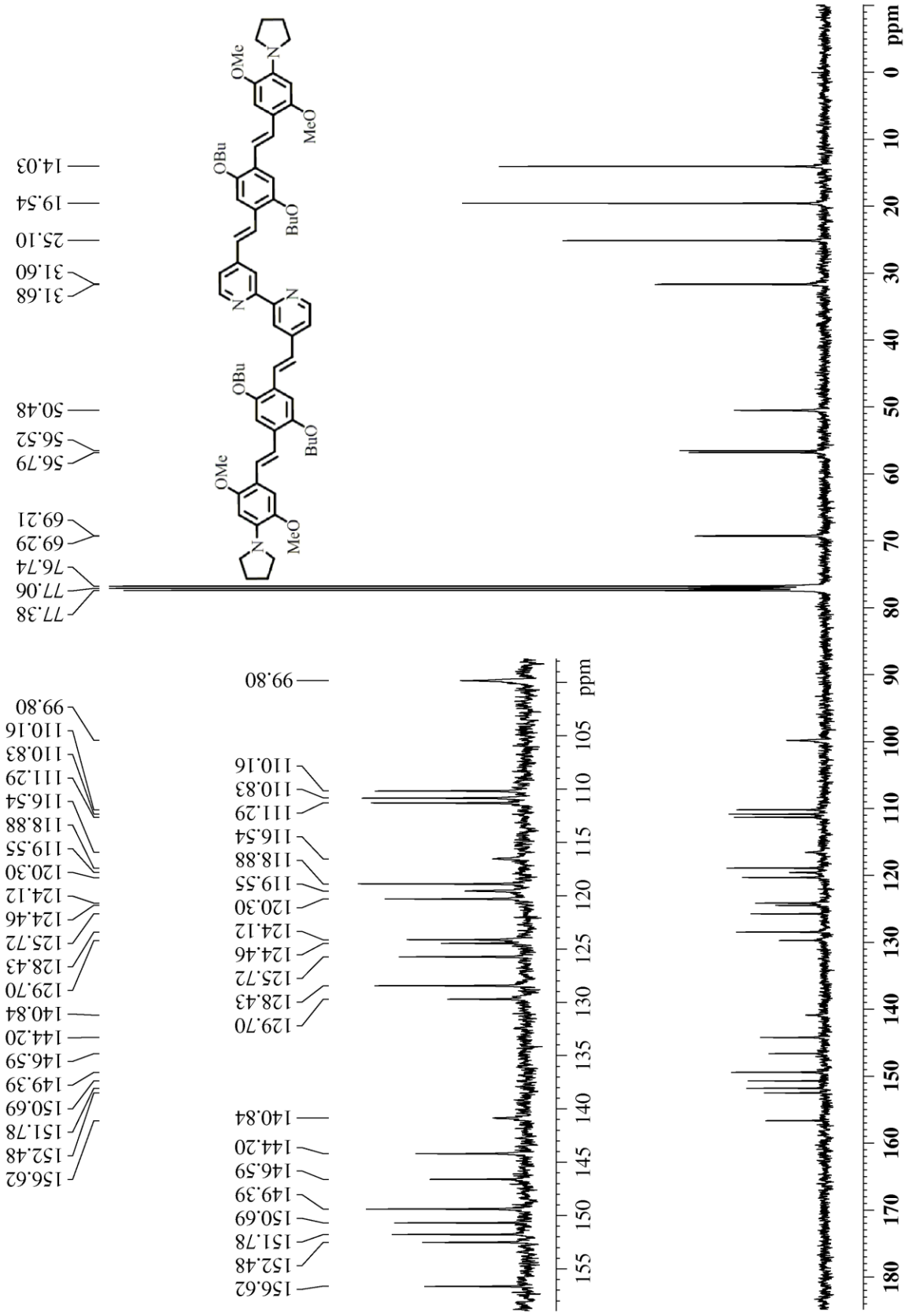

Chapter-5

Cyclometalated Iridium(III) Complexes Containing 4,4'–π–Conjugated–2,2'–bipyridine Derivatives as the Ancillary Ligands: Synthesis, Photophysics and Computational Studies

ABSTRACT: The synthesis, photophysical and computational studies of a new series of cyclometalated Ir^{III} complexes of the type $[Ir(C^N)_2(N^N)](PF_6)$, where, C^N is 2-phenylpyridine and N^N corresponds to the 4,4'–π–conjugated–2,2'–bipyridine ligands, i.e., **Ir(MS 3)**–**Ir(MS 8)**, are discussed in this chapter. All these complexes were synthesized through splitting of the binuclear dichloro-bridged complex precursor, $[Ir(C^N)_2$-μ-$Cl]_2$, with the appropriate bipyridine ligands followed by the anion exchange reaction. The linear and nonlinear absorption properties of the synthesized complexes have been investigated. The absorption spectra of all the title complexes exhibit a broad structureless feature in the 350–700 nm spectral region with two bands being well-resolved in most of the cases. The structures of all the complexes have been modeled in dichloromethane using the DFT algorithm. The nature of electronic transitions has further been comprehended on the basis of TD-DFT analysis which indicates that the origins of various bands are primarily due to intraligand charge transfer (ILCT) transitions and mixed metal and ligand centered transitions (ILCT, LL'CT, MLCT, IL etc.). All the complexes are non-emissive at room temperature; only **Ir(MS 3)** and **Ir(MS 5)** phosphoresce at low temperature in the near infrared region. The two-photon absorption studies were conducted on the title complexes in dichloromethane solvent using the Z–scan technique.

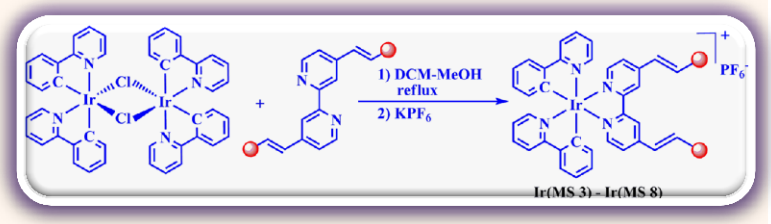

• 5.1. INTRODUCTION

Coordination complexes of iridium have gained enormous interest in recent times due to their potential applications in multidisciplinary areas such as, organic light emitting diodes (OLEDs),[1] biological imaging,[2] sensory materials,[3] dye-sensitized solar cells (DSSC),[4] and nonlinear optics[5] etc. The strong spin–orbit coupling caused by the heavy metal ion, iridium, in the complexes results in efficient $S_0 \rightarrow T_1$ intersystem crossing (ISC) upon photoexcitation thereby making majority of the complexes to follow the phosphorescence deactivation pathway of the photoexcited state. The coordination complexes of Ir^{III}, Ru^{II} and Os^{II} exhibit almost similar type of photophysical properties. However, a majority of the previously reported studies involve complexes of Ru^{II} and

Os^{II} compared to Ir^{III} complexes and the reason for this is probably the synthetic challenges associated with the kinetic inertness of Ir^{III} with respect to substitution.[6] Among the diverse classes of iridium complexes, the heteroleptic systems containing a combination of 2,2'–bipyridine (N^N) and cyclometalating phenylpyridine (ppy, C^N) ligands have gained special notice due to their synthetic ease compared to the *tris*-chelated homoleptic complexes. The general formulation of these heteroleptic complexes is $(C^N)_2Ir^{III}(N^N)$. It has been observed that, the photophysical and electrochemical properties of similar complexes are usually governed by substitution in the individual C^N and/or N^N ligands, which therefore opens up a scope for synthesizing a large number of related derivatives through the variation of functionalization either in the C^N or N^N fragments.

Martin *et al.* synthesized the *tris*-2,2'–bipyridine (bpy) complex of iridium way back in 1958.[7] Initially, the formulation of the obtained complex was thought to be $[Ir(bpy)_3]^{3+}$ i.e. $[Ir(N^N)_3]^{3+}$, but later, question arose regarding the binding modes of one of the bpy ligands. It was determined that although two bpy ligands were attached in N^N fashion to the metal center, the third ligand was bound in C^N fashion using C3 of one of the pyridine rings.[8] This was in fact, a clear instance of cyclometalation reaction and although rare for bipyridine ligands, it was found to be quite familiar in ligands which contain a benzene ring attached to a functional group having a coordinating donor atom, usually nitrogen. This was indeed the beginning of a new era in the chemistry of Iridium.[9]

Cyclometalated Ir^{III} complexes are generally characterized by an octahedral coordination environment with strong Ir–C bonds between the cyclometalating ligands and the metal ion. Therefore, a good thermal and photo-stability is expected for such complexes owing to their compact framework. Moreover, these complexes are encountered with a strong electronic interaction between the metal d–orbitals and the p–orbitals of the ligands, thereby enhancing the d–d energy gap and eventually preventing radiationless quenching. In cyclometalated Ir^{III} complexes, the electron density at the iridium center is increased due to the strong σ–donating effect of the metal–carbon bond thereby making the metal center more oxidizable compared to its isoelectronic system Ru^{II}.[10] Furthermore, the mixed ligand cationic complexes of the type $[Ir(C^N)_2(N^N)]^+$ are generally characterized by tunable color and emission quantum yields. This is usually

done by varying the electron-withdrawing/releasing character of the two types of ligands so as to increase the HOMO–LUMO gaps and consequently the emission energies. It has been observed that electron-withdrawing substituents on the (C^N) ligands decrease the electron donation to the metal and therefore stabilize the metal-based HOMO, while electron releasing substituents on the (N^N) ligand, destabilize the (N^N) ligand-based LUMO. In either of the two cases, there is an increase in the HOMO–LUMO energy gaps.[11] As a result such types of mixed ligand complexes have been drawing more interest as compared to the solo ligand systems since their photophysical properties can be easily tuned through substitution on either of the ligand systems.

Preliminary investigation by Watts *et al.* on the complex $[Ir(ppy)_2(bpy)]^+$ revealed that when both cyclometalating C^N and N^N coordinating ligands are present, then the metal–carbon bonds exert a strong *trans*–influence on the complex resulting in the Ir–N(bpy) bonds to be significantly longer than the Ir–N(ppy) bonds.[12a] An additional investigation also pointed out that in substituted $[Ir(ppy)_2(bpy)]^+$ complexes, where the ppy ligands bear electron donating methyl groups, the electron density at the metal center is enhanced to facilitate MLCT transitions. However, the poorer π–accepting ability of the methylated ppy ligand counteracts this effect with the overall outcome being only little change in the energy of MLCT transitions when compared to the unsubstituted parent Ir^{III} complex.[12b] Constable and co-workers demonstrated that promising electroluminescent devices or light-emitting electrochemical cells (LECs) could be easily synthesized by incorporating the ionic transition metal complexes, such as $[Ir(ppy)_2(bpy)](PF_6)$ and $[Ir(ppy)_2(phen)](PF_6)$ as the primary active components. Infact, the performance of the optimized devices incorporating such simple complexes are found to be amongst some of the best examples reported till date.[13] Bryce and co-workers recently reported a series of cationic cyclometalated Ir^{III} complexes having general formula $[Ir(ppy)_2(phen)](PF_6)$ where, ppy = 2-phenylpyridine and phen = a substituted phenanthroline.[14] The phenanthroline ligand was substituted with 9,9-dihexylfluorene units so as to enhance the solubility as well as to extend the ligand π–system. These complexes were used in LECs producing good efficiencies. Moreover, these devices operated in air and no sign of reduction in efficiency was detected even after storing them for one week in the same conditions.

A new class of cationic cyclometalated Ir^{III} complexes with the *N^N* ligand being substituted phenananthrolines was reported by Roberto and co-workers.[15] These complexes were found to display strong absorption bands in the ultraviolet region of the spectrum, which were attributed to π–π^* ligand-centered (LC) transitions of the π–systems of 1,10–phenanthroline and of the cyclometalated ligands. However, the weaker absorption bands at longer wavelengths were attributed to metal-to-ligand charge-transfer transitions (MLCT), predominantly from the Ir^{III} metal center to the vacant π^*–orbitals of the phenanthroline ligand. Another observation pointed out that if the 1,10–phenanthroline ligand carried an $–NR_2$ donor group, then the absorption spectrum of the complex would consist of an additional band in the visible region, *i.e.* intraligand charge transfer (ILCT) from the $–NR_2$ group to the π^* orbitals of the phenanthroline ligand.[15] These complexes were reported to exhibit good second-order nonlinear responses. Thus, it was concluded that these responses could be modulated by controlling in parallel the nature of the substituents on the 1,10–phenanthroline ligand as well as the choice of the cyclometalated ligands. Moreover, ion–pairing in such complexes was also observed to exert a significant influence on the NLO properties.[15]

A new series of Ir^{III} complexes of the type $[Ir(C^N)_2(N^N)]^+$ incorporating π–extended bipyridine ancillary ligands was reported by Guerchais and co-workers.[16] It was observed that the systematic variation of end groups of the *N^N* ligand not only modulated absorption and emission properties of the resulting complexes but also their second order nonlinear optical properties. Moreover, concentration and counterions were also observed to play a crucial role in enhancing the second order nonlinear response. In fact, an increase of the second order nonlinear response was observed (i) on increasing the π delocalization of the 2,2′–bipyridine ligand, (ii) upon dilution due to an increase of the percentage of free ions and, (iii) when ion-pairs were not too tight, for instance, usage of a weakly interacting counter anion PF_6^-.[16]

It is thus evident that, cyclometalated Ir^{III} complexes have mostly been explored in the areas of OLEDs, LECs, second order nonlinear optics, etc. whereas, reports associated with such complexes being used as two-photon absorbers (third order nonlinear process) are very scarce. Beeby and coworkers recently reported the near-infrared two-photon absorption (TPA) of a series of neutral cyclometalated iridium com-

Chart 1. Molecular structures of the synthesized cyclometalated Ir^{III} complexes.

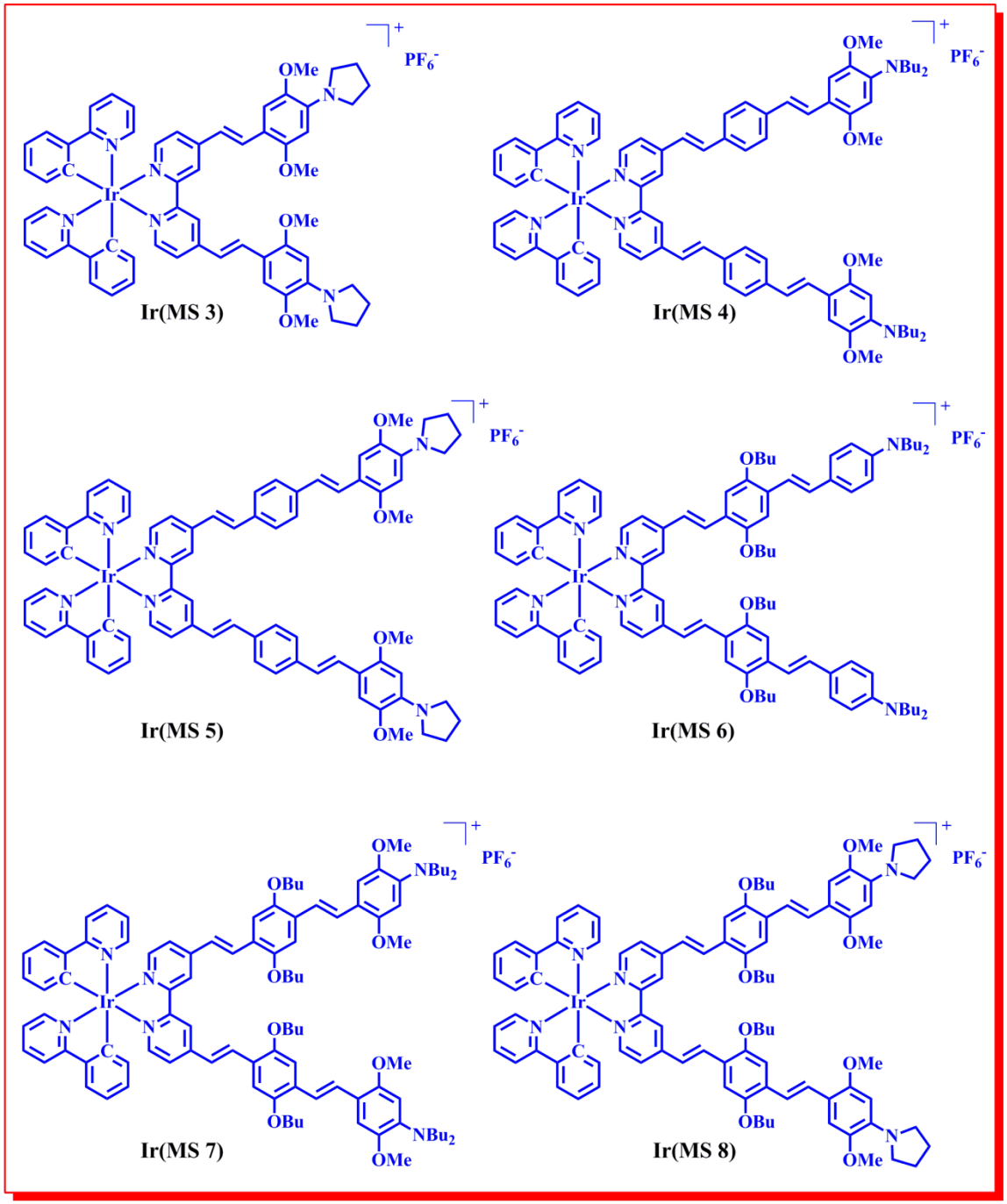

-plexes using substituted phenylpyridines as the cyclometalated ligands and acetylacetonate as the ancillary ligand. These complexes in fact exhibited moderately good values of TPA cross-section.[17]

With such enticing literature reports in hand, we developed interest to find out whether increasing the conjugation and varying the donor substituents on the ancillary

ligands could tune the optical properties of the complexes. Continuing our effort to probe the structural factors that could improve the linear and nonlinear optical properties of π-conjugated bipyridyl metal complexes, we describe in this chapter, synthesis of a new series of cyclometalated Ir^{III} complexes of the type $[Ir(C^N)_2(N^N)](PF_6)$ where, C^N is 2-phenylpyridine and N^N corresponds to the 4,4'–π–conjugated–2,2'–bipyridine ligands (**MS 3**–**8**) demonstrated in Chapter 4 (see Chart 1). These complexes were easily synthesized using proper metal precursor and the bipyridine derivatives and isolated as their hexafluorophosphate salts. For easy discussion in the text, the complexes are named as **Ir(MS 3)-Ir(MS 8)** based on the bipyridine ligand used. All these compounds were isolated as dark colored powders and characterized by NMR and mass (HRMS) spectroscopic techniques and elemental analysis. Photophysical properties of the synthesized compounds have been investigated in a set of solvents with varying polarity. The geometric and electronic structures of the compounds have been theoretically modeled in solvent medium. Finally, two-photon absorption properties of the synthesized complexes were conducted in dichloromethane at room temperature.

● 5.2. RESULTS AND DISCUSSION

● 5.2.1. Synthesis

The synthesis of homoleptic iridium complexes is more complicated and tedious as compared to that of the heteroleptic complexes. As such, we have focused our attention to the synthesis of cyclometalated Ir^{III} complexes of the type $[Ir(C^N)_2(N^N)](PF_6)$, where C^N represents a cyclometalating 2-phenylpyridine ligand and N^N represents an ancillary bipyridine ligand. The cyclometalating ligand, 2-phenylpyridine (ppy) is analogous to the 2,2'–bipyridine ligand, the only difference being the replacement of the N-center of one of the pyridine rings by a carbon atom. As such, it binds to the metal ion via the nitrogen atom and also cyclometalate through the carbon atom at the 2-position in the adjacent benzene ring. This ligand has a propensity to form a binuclear dichloro-bridged metal complex, $[Ir(C^N)_2\text{-}\mu\text{-}Cl]_2$, which is handily synthesized from a reaction of the respective phenylpyridine ligand and $IrCl_3{\cdot}xH_2O$. This dimeric species can easily be split by chelating ligands resulting in neutral or charged homoleptic or heteroleptic cyclometalated complexes. This species was in fact, used as the starting precursor to obtain the desired complexes described in this chapter. The styryl appended bipyridine

Scheme 1. Synthetic pathway to obtain the complexes Ir(MS 3)–Ir(MS 8).

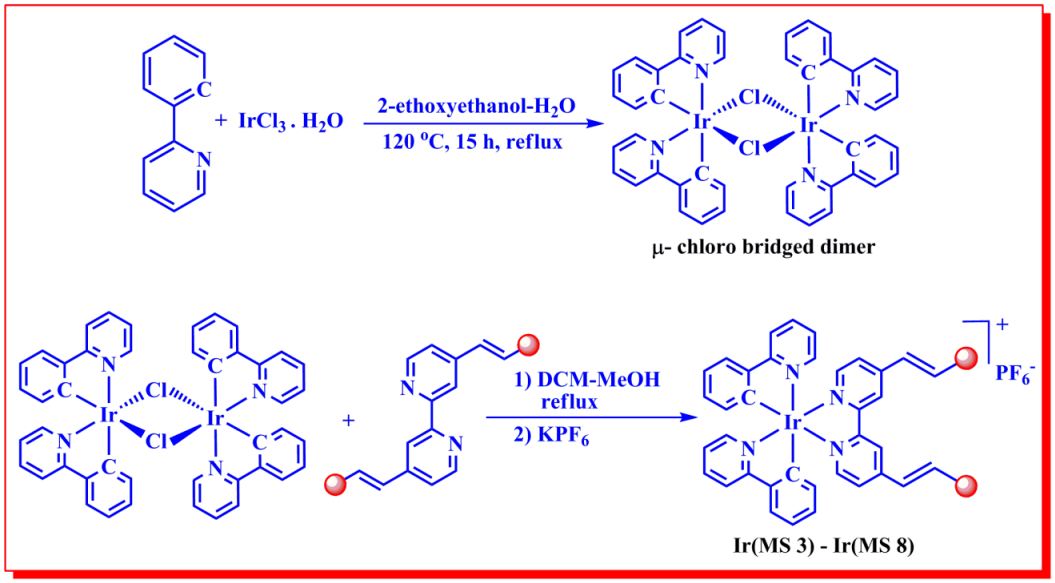

ligands demonstrated in Chapter 4 (**MS 3**–**8**) were used as the ancillary ligands in the present work. The synthetic pathway to obtain the desired iridium complexes in the present work is shown in Scheme 1. The reaction between hydrated iridium trichloride and 2-phenylpyridine in 2-ethoxyethanol-water solvent mixture under refluxing condition formed the μ-chloro bridged dimer which, as stated earlier, served the role of the starting precursor. The ancillary bipyridine ligand was then introduced by splitting the bridged dimer with appropriate bipyridine ligands (**MS 3**–**8**) in the DCM-MeOH solvent system. The chloride counter anion of the complexes, thus obtained, was replaced by hexafluorophosphate anion through a simple anionic metathesis reaction with KPF_6 (see Scheme 1). The crude products were subsequently purified through column chromatography to obtain the desired complexes as dark red solids in good yield (see experimental section). All these complexes were characterized through IR, NMR and mass (HRMS) spectroscopic techniques and elemental analysis. In all the synthesized Ir^{III} complexes, the vinylic C=C bonds are found to have *E*– configuration which is indicated by the splitting of each of the CH resonances by the neighboring protons with a $^3J_{HH}$ coupling constant of *ca*. 16 Hz.

5.2.2. Computational analysis

In order to comprehend the origins of various electronic transitions responsible for absorption of electromagnetic radiation by the Ir^{III} complexes, *ab initio* calculations were

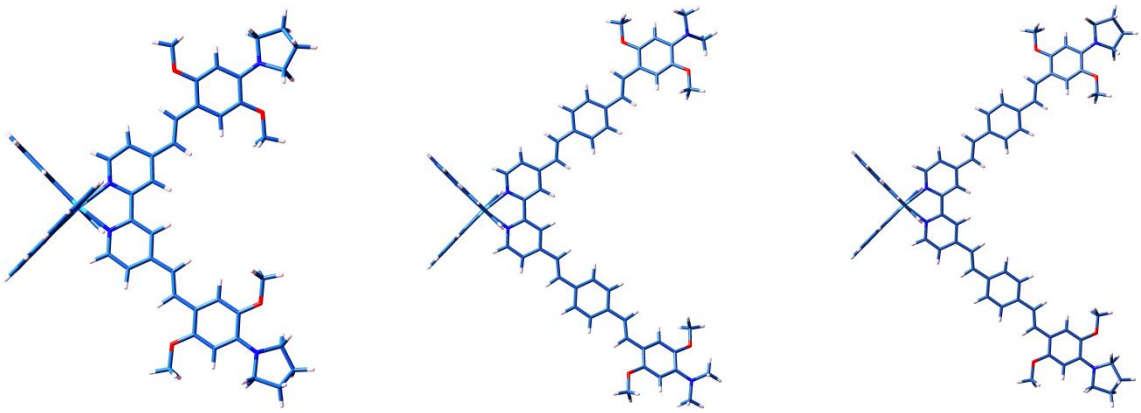

Ir(MS 3) **Ir(MS 4)** **Ir(MS 5)**

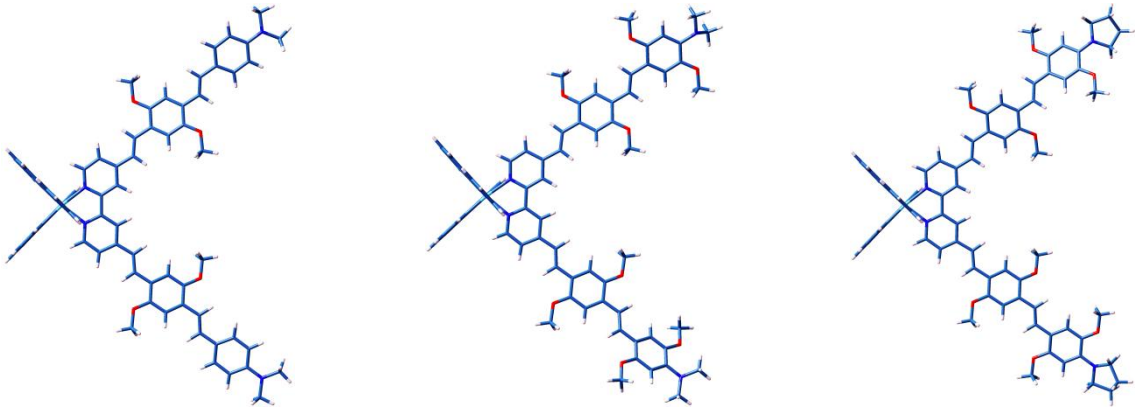

Ir(MS 6) **Ir(MS 7)** **Ir(MS 8)**

Figure 1. Energy minimized structures of the synthesized iridium complex cations in their ground state in dichloromethane. All the butyl chains were truncated to methyl groups to reduce the computational cost.

carried out on the molecular structures of the cationic counterpart of the synthesized complexes at the DFT and TD-DFT level of theory using the Gaussian 09 program package.[18] The ground state geometry of the title complex cations were optimized applying the CAM-B3LYP exchange correlation functional and LANL2DZ basis set for Iridium atom and 6-31g(d) basis set for the rest of the atoms in dichloromethane solvent reaction field. As already mentioned in Chapter 4, the CAM-B3LYP hybrid functional was preferred over the conventional B3LYP functional because, the charge-transfer character in π–expanded systems can be more accurately reproduced using the Coulomb attenuated version of B3LYP.[19] Effective Core Potential (ECP) correction for the iridium heavy atom was included and an identical computational set-up was used throughout the simulation studies. In all the cases, the accuracy of the energy minimized structures was scrutinized by a performing stability test of the relevant wave function. The total energy

Table 1. Selected bond lengths and dihedral angles of the energy minimized structures in the Iridium complexes.

	Bond length (Å, ±0.001)			Dihedral angle (°, ±0.1)		
Compound	Ir–C(ppy)	Ir–N(ppy)	Ir–N(bpy)	Bpy-Ph(A)	Bpy-Ph(B)	Py-Py
Ir(MS 3)	2.02	2.07	2.18	8, 8		4
Ir(MS 4)	2.02	2.07	2.18	9, 5	31, 23	4
Ir(MS 5)	2.02	2.07	2.18	0, 8	12, 24	4
Ir(MS 6)	2.02	2.07	2.18	11, 11	10, 10	4
Ir(MS 7)	2.02	2.07	2.18	10, 11	41, 11	4
Ir(MS 8)	2.02	2.07	2.18	10, 4	11, 25	4

A and B refer to the two phenyl rings in the OPV bipyridine ligands.

of all the optimized structures was corrected over the zero-point energy and the TD-DFT computation was also performed at the same level of theory. The energy minimized structures of all the relevant metal complex cations are shown in Figure 1.

The simulated structures of the title complexes exhibit some common features: (a) the calculated bond lengths, *viz.* Ir–C(ppy), Ir–N(ppy) and Ir–N(bpy) are found to be *ca*. 2.02, 2.07 and 2.18 Å respectively in all the complexes (see Table 1); (b) the two pyridine rings of the bipyridine ligands in all the structures are twisted by ~4° and (c) the two phenyl rings of the individual distyryl arms of the complexes comprising the oligophenylenevinylene (OPV) bipyridine ligands (except **Ir(MS 6)**) are found to be out-of-plane displaced in differing degrees with respect to the pyridine plane (see Table 1).

The planarity of a molecule generally plays a crucial role in determining the charge transfer character between the donor and acceptor moieties. Conjugation between the concerned functionalities becomes more facile with the increase in planarity of the molecules which directly affect the charge transfer process. The order of planarity between the various functionalities of the 2,2'–bipyridine ligands in the optimized structure of the title complexes has been analyzed on the basis of out-of-plane displacement of the phenyl rings from the bipyridine plane (see Table 1). It is found that the dibutylamino donors in the complexes, **Ir(MS 4)** and **Ir(MS 7)** are strongly rotated with respect to the phenyl rings they are attached with whereas, they are found to be almost planar in case of the complex **Ir(MS 6)**. In contrast, the pyrrolidine donor systems

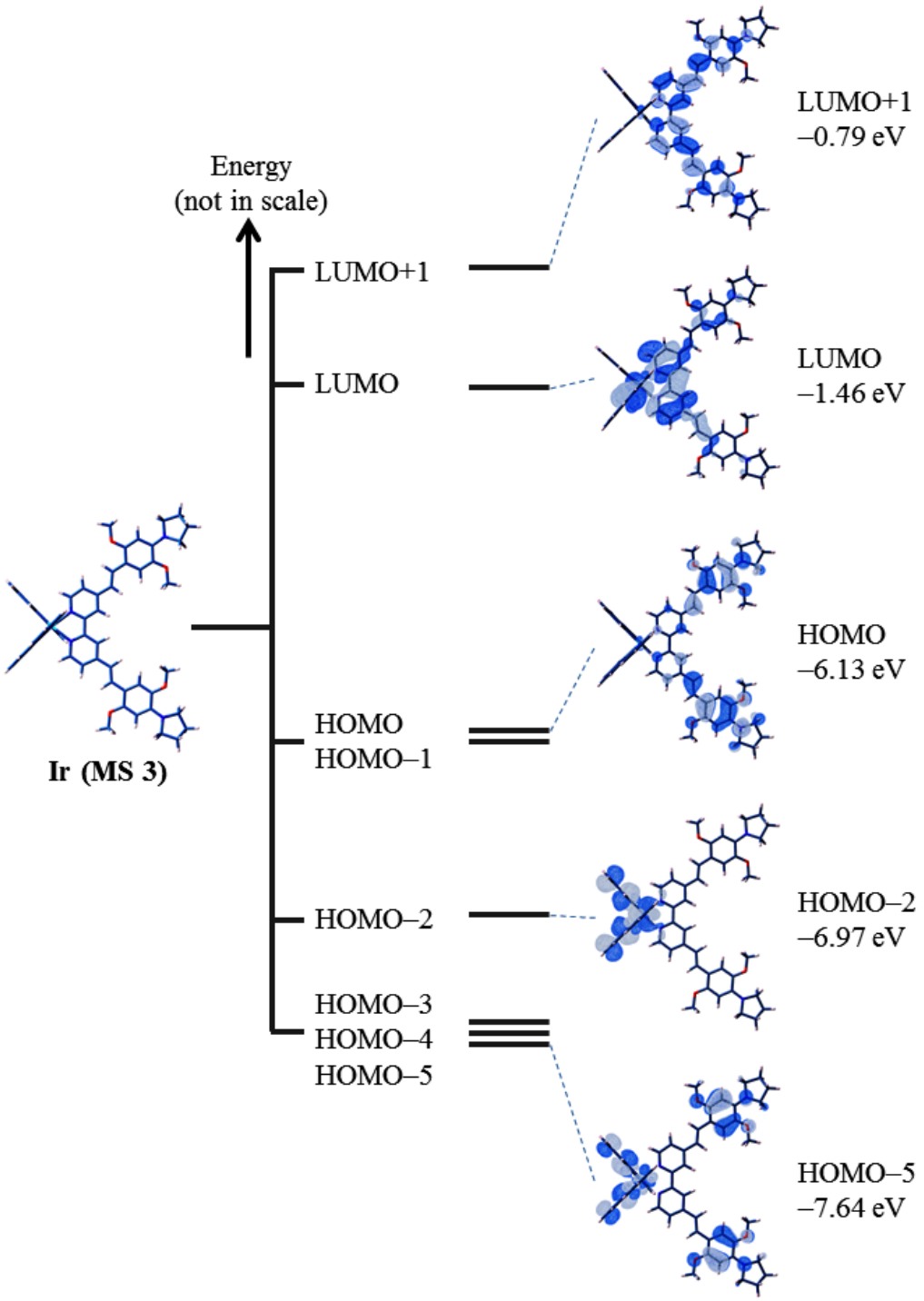

Figure 2. Representation of various energy levels in **Ir(MS 3)**.

in all the complexes **Ir(MS 3)**, **Ir(MS 5)** and **Ir(MS 8)** are found to be almost in plane with the adjacent phenyl rings. It is thus evident that, based on the computed molecular geometries, differing degree of conjugation or donor-acceptor interaction between the amino donor functionalities and pyridine acceptor core is present in the title complexes.

Table 2. Summary of the most relevant electronic excitations with the oscillator strengths responsible for the appearance of Band–I and Band–II in the absorption spectra of the synthesized Iridium complexes in dichloromethane.

Compound	Transition (contribution)	λ_{calcd} (*f*) (nm)	Assignment	λ_{obs} (nm)
Ir(MS 3)	HOMO→LUMO (65%)	434 (1.43)	ILCT+LL'CT	503
	HOMO–1→LUMO (67%)	416 (1.47)	ILCT+LL'CT	
	HOMO–2→LUMO+2 (85%)	330 (0.14)	IL+MLCT	400
	HOMO–1→LUMO+1 (37%)	327 (0.21)	ILCT	
	HOMO→LUMO+1 (41%)	325 (0.15)	ILCT	
Ir(MS 4)	HOMO→LUMO (37%)	417 (2.214)	ILCT+LL'CT	465
	HOMO–1→LUMO (38%)	407 (2.192)	ILCT+LL'CT	
	HOMO–2→LUMO+3 (77%)	328 (0.15)	IL+MLCT	390
	HOMO→LUMO (37%)	313 (0.22)	ILCT+LL'CT	
	HOMO–1→LUMO (34%)	311 (0.47)	ILCT+LL'CT	
Ir(MS 5)	HOMO→LUMO (39%)	441 (2.16)	ILCT+LL'CT	500
	HOMO–1→LUMO (41%)	430 (2.16)	ILCT+LL'CT	
	HOMO→LUMO (25%)	342 (0.09)	ILCT+LL'CT	390
	HOMO→LUMO+1(25%)		ILCT	
	HOMO–1→LUMO (25%)	341(0.11)	ILCT+LL'CT	
	HOMO–2→LUMO+3 (70%)	328 (0.14)	IL+MLCT	
	HOMO–3→LUMO+1 (29%)	324 (0.31)	ILCT	
	HOMO–2→LUMO+4 (65%)	316 (0.17)	MLCT+LL'CT	
Ir(MS 6)	HOMO→LUMO (44%)	442(2.222)	ILCT+LL'CT	515
	HOMO–1→LUMO+1 (27%)		ILCT	
	HOMO–1→LUMO (45%)	429 (2.027)	ILCT+LL'CT	
	HOMO→LUMO+1 (27%)		ILCT	
	HOMO–3→LUMO (20%)	335 (0.13)		415
	HOMO→LUMO+1 (26%)		ILCT	
	HOMO–1→LUMO+1 (26%)	334 (0.15)	ILCT	
	HOMO–4→LUMO+3 (32%)	329 (0.14)	IL+MLCT	
	HOMO–2→LUMO+3 (35%)		IL+MLCT	
Ir(MS 7)	HOMO–1→LUMO+1 (19%)	444(2.226)	ILCT	500
	HOMO→LUMO (34%)		ILCT+LL'CT	
	HOMO–1→LUMO (34%)	431 (1.946)	ILCT+LL'CT	
	HOMO→LUMO (9 %)		ILCT+LL'CT	
	HOMO→LUMO+1 (19%)		ILCT	
	HOMO→LUMO (35%)	329(0.06)	ILCT+LL'CT	415
	HOMO–4→LUMO+3 (70%)	328 (0.14)	IL+MLCT	
Ir(MS 8)	HOMO–1→LUMO+1(18%)	464(2.251)	ILCT	524
	HOMO→LUMO (32%)		ILCT+LL'CT	
	HOMO–1→LUMO (34%)	450 (2.0184)	ILCT+LL'CT	
	HOMO→LUMO+1 (18%)		ILCT	

Table 2. Continued…

HOMO→LUMO+1 (22%)	350 (0.06)	ILCT	425
HOMO–1→LUMO+1 (20%)	349 (0.05)	ILCT	
HOMO→LUMO (29%)	342 (0.15)	ILCT+LL'CT	
HOMO–2→LUMO (15%)		ILCT+LL'CT	
HOMO–2→LUMO+1 (23%)	340 (0.06)	ILCT	
HOMO–1→LUMO (29%)		ILCT+LL'CT	
HOMO–4→LUMO+2 (22%)	329 (0.14)	ILCT+LL'CT	
HOMO–4→LUMO+3 (70%)		ILCT	

Alternatively, it can be said that, a greater degree of conjugation between the donor and acceptor functionalities makes the intramolecular charge transfer more feasible and thus, the complexes, the geometry of which fulfills this criteria, would absorb at a lower energy region of the electromagnetic radiation compared to those with lesser extent of conjugation.

The examination of electronic structures of the title complexes reveal that the HOMO and HOMO–1 molecular orbitals (MOs) form an almost degenerate pair and are predominantly localized on the donor substituted phenyl rings and the vinylic C=C bonds of the 2,2'–bipyridine ligands while, the LUMO and LUMO+1 orbitals have major coefficients at the bipyridine and phenylpyridine cores. The localization of the various MOs in the electronic structure of **Ir(MS 3)** is presented in Figure 2 as an illustrative example and the TD-DFT computed various relevant electronic transitions are collected in Table 2.

It is observed that the calculated electronic excitation wavelengths are under-estimated by ~60–70 nm as compared to the observed absorption maxima under the present theoretical level. The variation of the estimated transition wavelengths with alteration of the molecular structure, however, follows a similar trend with the observed spectroscopic behavior of the pertinent complexes. No attempt was however made to improve the theoretical set-up so as to increase the accuracy of the calculated absorption wavelengths. A similar type of distribution of the coefficients has also been observed in all the other systems, the only difference being energy of the representative MOs. As can be seen from Figure 2, the contribution due to the metal ion in HOMO or HOMO–1 is very less. In case of **Ir(MS 3)** it has been found that, the iridium metal center has a significant contribution in HOMO–2 orbital.

5.2.3. UV-visible spectroscopy

The electronic absorption properties of all the synthesized cyclometalated complexes have been investigated in five different solvents at room temperature (298±2 K). The absorption spectra of the compounds in dichloromethane are shown in Figure 3 and the corresponding optical data are summarized in Table 3. As shown in Figure 3a, the absorption spectra of all the title complexes exhibit a broad structureless feature in the 350–700 nm spectral region. Although, in most of the cases, the two bands are well-resolved in this region, however, in some cases, the shorter wavelength band appears as a shoulder. The lowest energy and second lowest energy absorption bands are hereafter represented as Band–I and Band–II respectively for easy discussion in the text. The main absorption bands are followed by moderate to intense bands at the higher energy region of the spectrum. The Band–I in all the cases is found to be more sensitive to the structure of the 2,2'–bipyridine ligands and the solvent polarity in contrast to Band–II (see Table 3). A comparison of the absorption spectra of the free ligand **MS 3** and its iridium complex **Ir(MS 3)** in dichloromethane is depicted in Figure 3b which reveals that the absorption due to an ICT in **MS 3** (414 nm) almost matches with the Band–II of **Ir(MS 3)**. This might mislead one to wrongly assign the Band–II of the complex due to an ILCT of the bipyridine ligand and the Band–I as a representative feature of the transition metal complex. This is however not the case as the Lewis acidity of the metal ions enhances electron accepting propensity of the pyridine acceptor units by lowering the energy of its LUMO.[15] A bathochromic shift of the charge transfer band of the original bipyridine chromophores upon complexation is therefore, an expected phenomenon. The polarity sensitiveness of the Band–I clearly indicates a charge transfer character in the title complexes. Moreover, quantum chemical calculations (TD-DFT) on the various excited states of the synthesized complexes clearly indicate that the appearance of the Band–I is due to an intraligand charge transfer (ILCT) within the donor functionalized bipyridine ligands (see Table 2). It is thus obvious that the ICT band of the free 2,2'–bipyridine ligands are prominently red-shifted in their complexes, *c.f.* ~90 nm bathochromic shift of **MS 3**/**Ir(MS 3)** (see Figure 3b). The origin of Band–II was also comprehended on the basis of TD-DFT (see Table 2) which suggests that the concerned band appears due to the involvement of mixed metal and ligand centered transitions (ILCT, LL'CT, MLCT, IL

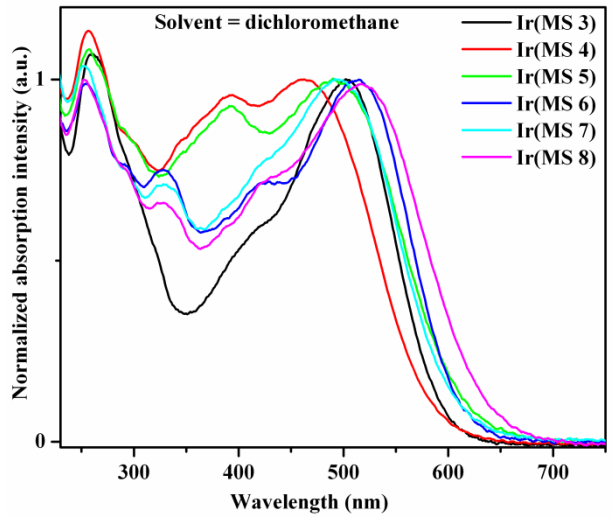

Figure 3. (a) Normalized absorption spectra of the title iridium complexes in dichloromethane at room temperature. Concentration of the solution ~ $1x10^{-5}$ M. (b) A comparison of the absorption spectra of **MS 3** and **Ir(MS 3)** in dichloromethane.

etc.). The higher energy absorption bands in the electronic absorption spectra of the complexes presumably appear due to various $\pi \rightarrow \pi^*$ transitions within the bipyridine and phenylpyridine ligands.

The analyses of the absorption spectra of the synthesized iridium complexes (Figure 3a) and the optical data, presented in Table 3, reveal some important information. The position of Band–I in the complexes with cyclic pyrrolidine donors is bathochromically shifted by almost 25–35 nm as compared to their acyclic dibutylamino analogues irrespective of the solvent i.e. **Ir(MS 4)/ Ir(MS 5)** and **Ir(MS 7)/Ir(MS 8)**. The probable

Table 3. Summary of the linear optical data of the synthesized Iridium complexes.

Compd.	Solvent	λ (nm)	λ_{em} /nm	τ/μs
Ir(MS 3)	Toluene	519, 408, 285		
	THF	495, 404, 260		
	DCM	503 (56200), 410 (33100), 260 (59500)	725	86.7
	DMSO	487, 406, 230		
	EtOH	491, 408, 260		
Ir(MS 4)	Toluene	460, 387, 232		
	THF	454, 386, 255		
	DCM	465 (58,600), 390 (57,100), 260 (70000)		
	DMSO	450, 389, 262		
	EtOH	432, 390, 260		
Ir(MS 5)	Toluene	492, 393, 236		
	THF	480, 391, 235		
	DCM	500 (52400), 395 (48900), 260 (59000)	775	44.6
	DMSO	470, 394, 262		
	EtOH	460, 395, 259		
Ir(MS 6)	Toluene	516, 417, 235		
	THF	500, 418, 255		
	DCM	515 (61,000), 415 (42200), 255 (61000)		
	DMSO	490, 416, 230		
	EtOH	490, 415, 255		
Ir(MS 7)	Toluene	505, 420, 240		
	THF	490, 420, 255		
	DCM	500 (68200), 415 (51600), 253 (73000)		
	DMSO	474 (unresolved), 235		
	EtOH	468 (unresolved), 254		
Ir(MS 8)	Toluene	530, 426, 240		
	THF	508, 422, 254		
	DCM	524 (65700), 423 (46200), 256 (66000)		
	DMSO	492 (unresolved), 260		
	EtOH	488, 416, 254		

reason behind this observation can be explained on the basis of the energy minimized structures of the concerned complex cations (see section 5.2.2). The cyclic amino groups are found to be more conjugated with the π–framework as compared to the open chain dialkylamines thereby reducing the energy of the charge transfer transition. Another important observation is that the position of Band–I in the spectra of **Ir**(**MS 4)**, **Ir**(**MS 6)** and **Ir**(**MS 7)** maintains a similar trend as noticed in case of the free ligands (described in

chapter 4). However, the extent of spectral shifts in the complexes is found to be greater compared to the free ligands. The maximum of Band–I in **Ir**(**MS 6)** is shifted to longer wavelength compared to **Ir**(**MS 4)** and **Ir**(**MS 7**) (see Table 3). This is again explained taking into account the quantum chemical calculation which compute more planar structure of **Ir**(**MS 6)** compared to **Ir**(**MS 4)** and **Ir**(**MS 7**). The HOMO–LUMO energy gap for the three pertinent complexes vary in the order: **Ir(MS 4)** > **Ir(MS 7)** > **Ir(MS 6)**, which justifies the shifts in the λ_{max} of Band–I in the absorption spectra. The position of the Band–II follows an almost similar trend as the Band–I which is the direct outcome of the variation of the energy of metal and ligand centered transitions with the molecular architecture as revealed by DFT and TD-DFT.

A general observation on the spectral data of the title compounds (Table 3) demonstrates a negative solvatochromic effect on increasing the solvent polarity. A plausible rationale for this observation is probably due to the more polar nature of the ground state as compared to the excited state.

5.2.4. Emission spectroscopy

The ancillary 2,2'–bipyridine ligands (**MS 3**–**8**) used in the present study are highly fluorescent in organic solvents at room temperature. However, no fluorescence could be detected for the title iridium complexes under similar experimental condition. The deactivation channel of the fluorescence emission from S_1 state in majority of the iridium complexes is the fast $S_1 \rightarrow T_1$ intersystem crossing induced by the strong spin–orbit coupling due to the heavy atom effect of iridium. The photoexcited state of the Ir^{III} complexes is thus expected to decay through a phosphorescence emission pathway and in majority of the complexes this phenomenon is observed even at room temperature. Unfortunately, none of the title Ir^{III} complexes displayed detectable luminescence at room temperature when excited at the corresponding absorption maxima. It is in fact known that, such type of complexes containing styryl functionalities in their π–backbones undergo competitive deactivation of the excited state due to $E \leftrightarrow Z$ isomerization of the styryl groups which quenches the emission at room temperature in solution.[15] As such, experiments were conducted at low temperature (77 K) in EtOH-MeOH solvent system (glass) so as to impede the isomerization process in the present work. Under this experimental condition, only **Ir(MS 3)** and **Ir(MS 5)** are found to display broad

structureless phosphorescence emission at the near-infrared region with long lifetimes (see Table 3). The emission maximum of **Ir(MS 5)** is found to be red-shifted compared to that of **Ir(MS 3)** probably due to the greater conjugation length in the OPV ligand **MS 5** compared to **MS 3** as shown in Figure 4.

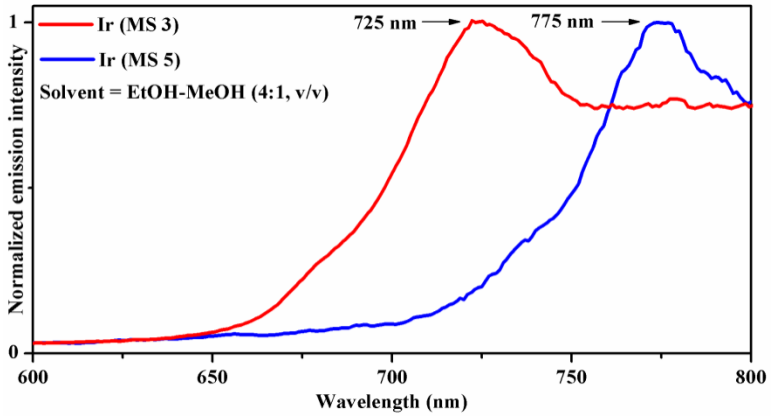

Figure 4. Normalized phosphorescence emission spectra of the complexes, **Ir(MS 3)** and **Ir(MS 5)** in EtOH-MeOH (4:1, v/v) at 77 K.

5.2.5. Two-photon absorption spectroscopy

The nonlinear optical response of a variety of materials has been studied over the past decade and a full portrayal of this response can be obtained from the Z–scan or TREF (two-photon excited fluorescence) techniques.[20,21] As the investigated complexes are non-emissive at room temperature, we used the Z–scan method (open and closed aperture) for recording the two-photon absorption properties of the synthesized complexes in dichloromethane. The pulse energies during the close-aperture Z–scan were maintained low so as to cut down contributions from any higher order nonlinearities. The open-aperture Z–scan data (recorded at a peak intensity of ~100 GW/cm^2) provide the information that the relevant molecules exhibit moderately strong two-photon absorption (2PA) with the nonlinear absorption cross-sections in the range of 300–1000 GM. The 2PA cross-section, σ_2 (in units of cm^4 s per photon or GM) are calculated using the formula:

$h\nu\beta = \sigma_2 N_0 = h\nu\sigma_2 N_A d_0 \times 10^{-3}$, where, d_0 (in units of mol L^{-1}) denotes the concentration of the solution, β represents the TPA coefficient, $h\nu$ is the energy of the incident photon and N_A is Avogadro's constant.

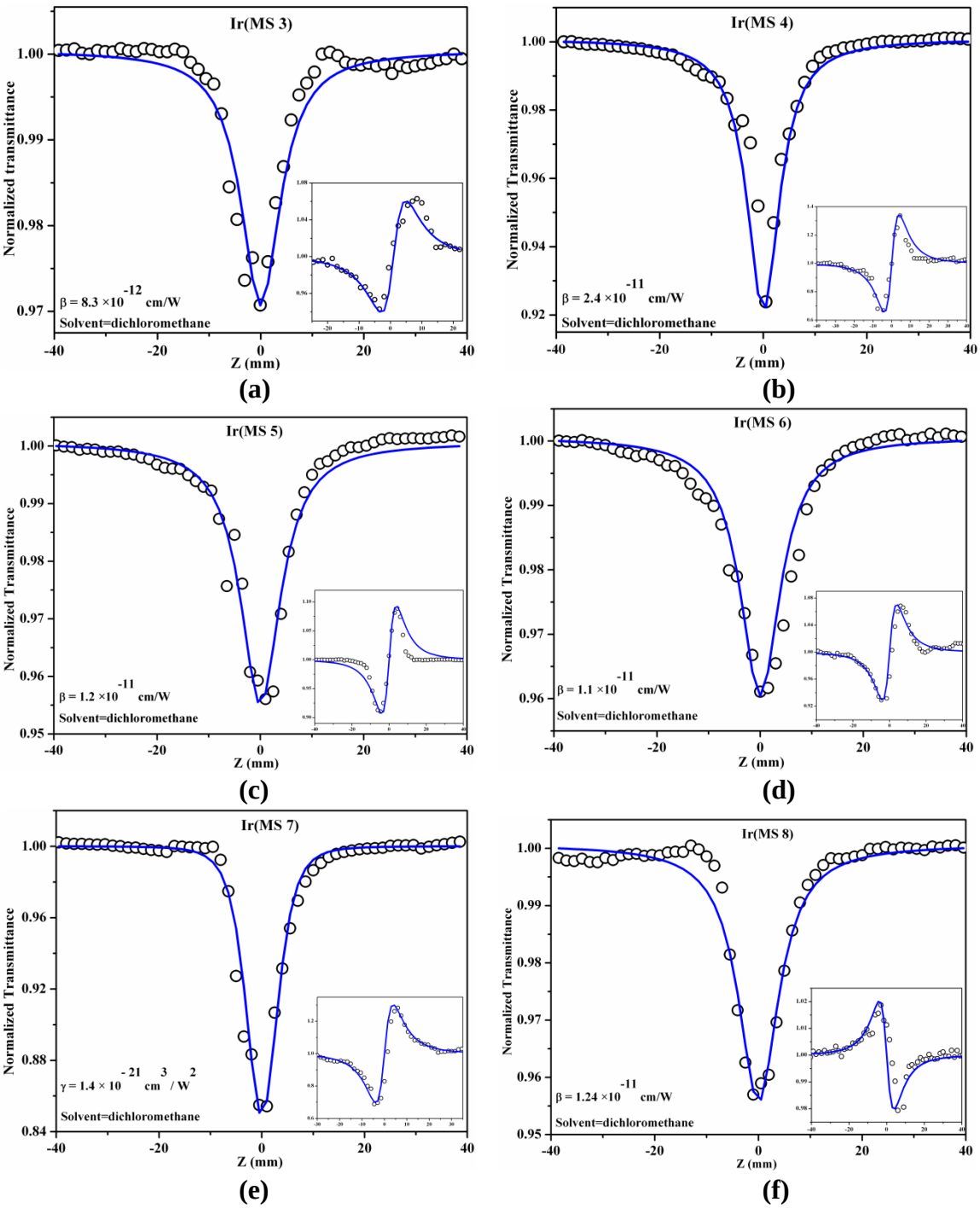

Figure 5. The open aperture Z–scan curves (at I_{00} = 100 GW/cm^2) of the iridium complexes, **Ir(MS 3)–Ir(MS 8)**. Open circles represent experimental data for the solutions while solid lines correspond to theoretical data. The inset shows the curves corresponding to the closed aperture Z–scan data (at I_{00} = 28 GW/cm^2).

The sign and magnitude of the real part of third order nonlinearity is however projected from the closed aperture data. The relevant spectra are displayed in Figures 5a-f and the

experimentally observed two-photon absorption cross-sections (σ_2) of the title complexes are tabulated in Table 4. In all the cases, except **Ir(MS 7)**, a good fit was obtained between the predicted and experimentally observed data and the two photon absorption coefficient (β) for the samples is estimated to be ~10^{-11} cm/W while the same due to the solvents is found to be as low as 0.2×10^{-11} cm/W at a peak intensity of ~100 GW/cm^2. Surprisingly, three-photon absorption (3PA) is observed as the dominant nonlinear absorption process for only **Ir(MS 7)** while the two-photon absorption is the chief nonlinear phenomenon in all the other cases. The three-photon absorption coefficient (γ) for **Ir(MS 7)** is found to be ~1.4×10^{-21} cm^3/W^2 (the solvent contribution was found to be negligible in this case).

The closed aperture scans for all the complexes were recorded with a peak intensity of 28 GW/cm^2. The valley followed by the peak in the normalized transmittance data of all the complexes [except **Ir(MS 8)**] is clearly an indicative feature showing the presence of a positive type of nonlinearity. In all the cases, the best fit between the theoretical and experimental data was obtained and the value of the nonlinear refractive index, η_2 was found to be in the order of ~10^{-15} cm^2/W (η_2 for solvent ~10^{-16} cm^2/W). The closed aperture scans for all the complexes are shown at the inset of the figures 5a-f.

It has already been suggested in literature that the same design principles can be applied to inorganic materials akin to organic chromophores, for obtaining large TPA σ_2 values. These values can further be increased with increase in conjugation and/or by increasing the donor/acceptor strength.[17] It has also been suggested that when the ancillary ligands bear weak electron donors, e.g. alkyloxy or alkylthio groups, then upon metal coordination, an increase in the TPA cross-section is observed while with ancillary ligands bearing strong electron donors, such as, dialkylamino group, the TPA cross-section has been observed to decrease.[22]

The synthesized cyclometalated Ir^{III} complexes described in this chapter contain both weak (alkoxy) and strong donor (dialkylamino) groups in the backbones of the ancillary ligand. In case of the cyclic donor systems, we have observed an increase in the TPA cross-section, σ_2 on increasing the π−conjugation from **Ir(MS 3)** to **Ir(MS 5)**. A further increase in TPA cross-section is observed for **Ir(MS 8)** i.e. on introducing weak alkoxy donors to the ring–A of **Ir(MS 5)**. However, the same trend has not been observed in case

Table 4. Summary of nonlinear optical data of the synthesized iridium complexes.

Compd.	Solvent	λ (nm)	η (cm^2/W)	β (cm/W)	σ_2(GM)
Ir(MS 3)	DCM	503, 410, 285	$1.4x10^{-15}$	$8.3x10^{-12}$	342
Ir(MS 4)	DCM	465, 390, 260	$6.2x10^{-15}$	$2.4x10^{-11}$	990
Ir(MS 5)	DCM	500, 395, 260	$2.0x10^{-15}$	$1.2x10^{-11}$	495
Ir(MS 6)	DCM	515, 415, 255	$1.6x10^{-15}$	$1.1x10^{-11}$	454
Ir(MS 7)	DCM	500, 415, 253	$7.0x10^{-15}$	—	—
Ir(MS 8)	DCM	524, 423, 256	$-5x10^{-15}$	$1.24x10^{-11}$	511

of the acyclic donor systems. Three-photon absorption is observed in case of **Ir(MS 7)** in contrast to the two-photon absorption for the analogous cyclic system, **Ir(MS 8)**. Moreover, a very high two-photon absorption cross-section is observed for **Ir(MS 4)** as compared to its cyclic analogue **Ir(MS 5)**.

5.3. SUMMARY AND CONCLUSION

In summary, we have demonstrated a new series of cyclometalated Ir^{III} complexes of the type $[Ir(C\hat{}N)_2(N\hat{}N)](PF_6)$, which includes extended Ar-vinyl−π systems on the ancillary bipyridine core. The linear and nonlinear optical properties of the synthesized complexes have been investigated and their photophysical properties are found to be governed by ILCT, LL′CT and MLCT transitions as depicted by the DFT and TD-DFT calculations. From the computational studies, it is quite apparent that in contrast to the complex **Ir(MS 6)**, the dibutylamino donor groups in the complexes **Ir(MS 4)** and **Ir(MS 7)** are strongly rotated with respect to the phenyl rings in which they are attached. However, the pyrrolidine donor systems in all the complexes **Ir(MS 3)**, **Ir(MS 5)** and **Ir(MS 8)** are found to be almost planar with the adjacent phenyl rings. In addition, a systematic variation in the nature, position and number of donor groups modulate their absorption behavior and a negative solvatochromic effect is observed on increasing the solvent polarity. Also, the position of Band–I (lowest energy band) in the title complexes with cyclic pyrrolidine donors is found to be bathochromically shifted by almost 25-35 nm as compared to their acyclic dibutylamino analogues irrespective of the solvent i.e. **Ir(MS 4)/Ir(MS 5)** and **Ir(MS 7)/Ir(MS 8)**. The compounds **Ir(MS 3)** and **Ir(MS 5)** exhibit phosphorescence emission in the NIR region. Finally, the two-photo cross-sections of the

synthesized complexes were conducted and a value in the range 300−1000 GM is obtained. Such classes of cyclometalated iridium complexes can open up new and exciting opportunities to have a better control over the photophysical aspects intended to be used for a wide variety of applications.

5.4. EXPERIMENTAL SECTION

5.4.1. Materials and methods

All the reactions were performed under ultra high pure nitrogen atmosphere unless mentioned elsewhere. All the deuteriated NMR solvents were purchased from Acros Organics and the other commercially procured chemicals were used as received. Column chromatography was performed with silica gel (100–200 mesh) (SRL, India) unless mentioned. All the solvents used for the chromatographic purification were distilled prior to use. The NMR spectra were recorded by Bruker AV-400 400 MHz spectrometer using tetramethylsilane (TMS) as internal standard in case of $CDCl_3$ solvent. Signal multiplicities are reported as follows: s = singlet, d = doublet, t = triplet, m = multiplet, br = broad. Elemental analysis was carried out by FLASH EA series 1112 CHNS analyzer. HRMS spectra were recorded on Bruker Maxis spectrophotometer. Cary 100 Bio UV-visible spectrophotometer was used to record the electronic absorption spectra, while the emission (phosphorescence) spectra were recorded on a Fluorolog-3 (Jobin Yvon) spectrofluorimeter.

The nonlinear optical experiments were performed in dichloromethane using 1 mm optical path length. A Ti-sapphire laser (Coherent, Legend amplifiers) source was used operating at a repetition rate of 1 kHz with a pulse durations ~2 ps at 800 nm. The amplifiers were seeded with ~15 fs pulses from the oscillator (Coherent, Micra). The input beam was spatially filtered to obtain a pure Gaussian profile in the far field. Z–scan studies were performed by focusing the 3-mm diameter input beam using a 200 mm focal length convex lens into the sample in both ps domain. The sample was placed on a high resolution translation stage and the detector (Si photodiode, SM1PD2A, Thorlabs) output was connected to a lock-in amplifier. Both the stage and lock-in were controlled by a computer program. The picosecond studies were performed with solutions having the concentration of 1 mM providing 92-96 % (for all samples) linear transmittance at 800 nm wavelength. Closed aperture scans were performed at intensities where the

contribution from the higher order nonlinear effects is negligible (the value of ΔΦ estimated in all the cases was < π). The experiments were repeated more than once and the best data were used for obtaining the nonlinear optical coefficients from the best fits.

5.4.2. Synthesis and characterization data

A mixture of the bridged dimer, $[Ir(C\text{^}N)_2\text{-}\mu\text{-}Cl]_2$ (0.075 mmol) and the corresponding bipyridine derivatives (MS 3 – MS 8) (0.15 mmol), taken in 30 mL DCM - MeOH (2:1) degassed solvent system, was heated under reflux in an inert atmosphere of N_2 in the dark for 4 h. The red colored solution was then brought to room temperature and a five-fold excess of saturated KPF_6 in degassed MeOH was added to it with an additional stirring for 2 h. The solvent was then evaporated to dryness. The crude product was extracted with dichloromethane and the organic layer was washed several times with water. Evaporation of the solvent gave a dark red colored compound, which was finally purified by column chromatography over silica using acetone/$CHCl_3$, 5:95 v/v as the eluent.

Ir(MS 3). Red microcrystalline solid. Yield: 73 %.

^{1}H NMR (400 MHz, $CDCl_3$): δ 8.66 (s, 2H), 7.91 (d, J = 8 Hz, 2H), 7.79−7.61 (m, 10H), 7.50 (d, J = 8 Hz, 2H), 7.35 (s, 2H), 7.28 (d, J = 8 Hz, 2H), 7.05−6.99 (m, 4H), 6.93−6.91 (m, 2H), 6.345 (d, J = 4 Hz, 2H), 6.16 (s, 2H), 3.95 (s, 6H), 3.82 (s, 6H), 3.46 (unresolved, 8H), 1.93 (unresolved, 8H).

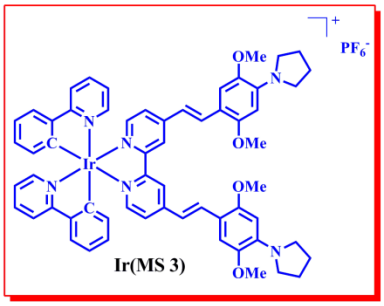

IR (KBr, cm^{-1}): υ_{max} 841 (P–F).

HRMS: (m/z) calcd. 1119.415 $(M-PF_6)^+$. Found: 1119.426.

Anal. calcd. for $C_{60}H_{58}F_6IrN_6O_4P$: C, 57.00; H, 4.62; N, 6.65. Found: C, 57.12; H, 4.56; N, 6.75.

Ir(MS 4). Red microcrystalline solid. Yield: 71 %.

^{1}H NMR (400 MHz, $CDCl_3$): δ 8.77 (s,2H), 7.93 (d, J = 8 Hz, 2H), 7.79−7.74 (m, 4H), 7.69−7.65 (m, 4H), 7.61 (d, J = 8 Hz, 4H), 7.52−7.30 (m, 12H), 7.10−6.91 (m, 10H), 6.52 (s, 2H), 6.34 (d, 8 Hz, 2H), 3.88 (s, 6H), 3.86 (s, 6H), 3.17 (t, 8H), 1.54–1.47 (m, 8H), 1.34−1.26 (m, 8H),

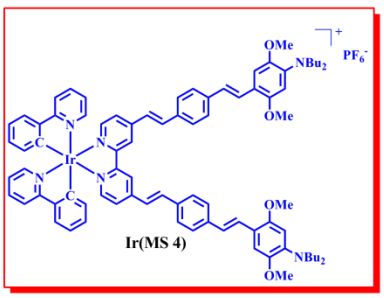

0.91 (t, 12H).

IR (KBr, cm^{-1}): υ_{max} 839 (P–F).

HRMS: (*m*/*z*) calcd. 1439.665 $(M-PF_6)^+$. Found: 1439.660.

Anal. calcd. for $C_{84}H_{90}F_6IrN_6O_4P$: C, 63.66; H, 5.72; N, 5.30. Found: C, 63.56; H, 5.64; N, 5.41.

Ir(MS 5). Red microcrystalline solid. Yield: 77 %.

^{1}H NMR (400 MHz, $CDCl_3$): δ 8.85 (s, 2H), 8.02 (s, 2H), 7.94 (d, *J* = 8 Hz, 2H), 7.79−7.34 (m, 22H), 7.25–6.89 (m, 10H), 6.34 (d, *J* = 8 Hz, 2H), 6.30 (s, 2H), 3.88 (s, 6H), 3.86 (s, 6H), 3.42 (unresolved, 8H), 2.36−2.33 (m, 8H).

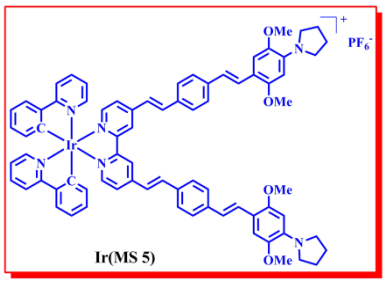

IR (KBr, cm^{-1}): υ_{max} 839 (P–F).

HRMS: (*m*/*z*) calcd. 1323.508 $(M-PF_6)^+$. Found: 1323.507.

Anal. calcd. for $C_{76}H_{70}F_6IrN_6O_4P$: C, 62.16; H, 4.80; N, 5.72. Found: C, 62.25; H, 4.87; N, 5.65.

Ir(MS 6). Red microcrystalline solid. Yield: 80 %.

^{1}H NMR (400 MHz, $CDCl_3$): δ 8.82 (s, 2H), 7.92 (d, *J* = 8 Hz, 2H), 7.87 (d, *J* = 16 Hz, 2H), 7.78–7.70 (m, 6H), 7.61 (d, *J* = 8 Hz, 2H), 7.55−7.28 (m, 10H), 7.13−6.92 (m, 10H), 6.64 (d, *J* = 8 Hz, 4H), 6.35 (d, *J* = 8 Hz, 2H), 4.24 (t, 4H), 4.05 (t, 4H), 3.30 (t, 8H), 1.89−1.27 (m, 32H), 1.05−0.96 (m, 24H).

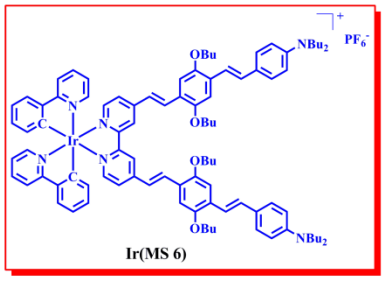

IR (KBr, cm^{-1}): υ_{max} 839 (P–F).

HRMS: (*m*/*z*) calcd. 1607.853 $(M-PF_6)^+$. Found: 1607.831.

Anal. calcd. for $C_{96}H_{114}F_6IrN_6O_4P$: C, 65.77; H, 6.55; N, 4.79. Found: C, 65.87; H, 6.51; N, 4.86.

Ir(MS 7). Red microcrystalline solid. Yield: 75 %.

^{1}H NMR (400 MHz, $CDCl_3$): δ 8.84 (s, 2H), 7.93 (d, *J* = 8 Hz, 2H), 7.87 (d, *J* = 16 Hz, 2H), 7.79–7.75 (m, 4H), 7.71 (d, *J* = 8 Hz, 2H), 7.62–7.39 (m, 12H), 7.13 (d, *J* = 8 Hz,

4H), 7.07–7.01 (m, 4H), 6.96–6.92 (m, 2H), 6.52 (s, 2H), 6.35 (d, 8 Hz, 2H), 4.25 (t, 4H), 4.05 (t, 4H), 3.88 (s, 6H), 3.85 (s, 6H), 3.15 (t, 8H), 1.90−1.26 (m, 34H), 1.05–0.98 (m, 12H), 0.91 (t, 12H).

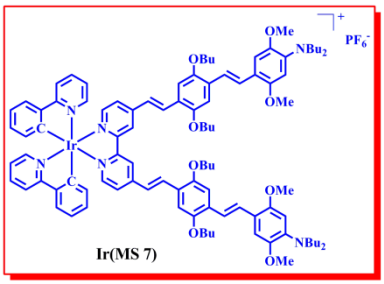

Ir(MS 7)

IR (KBr, cm^{-1}): υ_{max} 839 (P–F).

HRMS: (*m*/*z*) calcd. 1727.895 $(M-PF_6)^+$. Found: 1727.879.

Anal. calcd. for $C_{100}H_{122}F_6IrN_6O_8P$: C, 64.12; H, 6.56; N, 4.49. Found: C, 64.25; H, 6.67; N, 4.41.

Ir(MS 8). Red microcrystalline solid. Yield: 79 %.

^1H NMR (400 MHz, $CDCl_3$): δ 8.81 (s, 2H), 7.92 (d, J = 8 Hz, 2H), 7.87 (d, J = 16 Hz, 2H), 7.78−7.69 (m, 6H), 7.61 (d, J = 8 Hz, 4H), 7.55−7.48 (m, 8H), 7.36 (d, J = 16 Hz, 2H), 7.13 (d, J = 8 Hz, 4H), 7.06–7.00 (m, 4H), 6.95–6.91 (m, 2H), 6.34 (d, J = 8 Hz, 2H), 6.31 (s, 2H), 4.25 (t, 4H), 4.06 (t, 4H), 3.86 (s, 6H), 3.84 (s, 6H), 3.4 (unresolved, 8H), 1.97−1.51 (m, 24H), 1.05−0.96 (m, 12H).

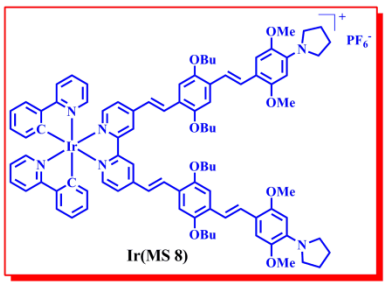

Ir(MS 8)

IR (KBr, cm^{-1}): υ_{max} 839 (P–F).

HRMS: (*m*/*z*) calcd. 1611.739 $(M-PF_6)^+$. Found: 1323.507.

Anal. calcd. for $C_{92}H_{102}F_6IrN_6O_8P$: C, 62.89; H, 5.85; N, 4.78. Found: C, 62.75; H, 5.81; N, 4.63.

5.5. REFERENCES

1. Baldo, M. A.; Thompson, M. E.; Forrest, S. R. *Nature* **2000**, *403*,750.
2. Zhang, K. Y.; Lo, K. K. –W. *Inorg. Chem.* **2009**, *48*, 6011.
3. Chen, H.; Zhao, Q.; Wu, Y.; Li, F.; Yang, H.; Yi, T.; Huang, C. *Inorg. Chem.* **2007**, *46*, 11075.
4. Mayo, E. I.; Kilså, K.; Tirrell, T.; Djurovich, P. I.; Tamayo, A.; Thompson, M. E.; Lewis, N. S.; Gray, H. B. *Photochem. Photobiol. Sci.* **2006**, *5*, 871.
5. (a) Dragonetti, C.; Righetto, S.; Roberto, D.; Ugo, R.; Valore, A.; Fantacci, S.; Sgamellotti, A.; Angelis, F. D. *Chem. Commun.* **2007**, 4116. (b) Valore, A.; Cariati,

E.; Dragonetti, C.; Righetto, S.; Roberto, D.; Ugo, R.; Angelis, F. D.; Fantacci, S.; Sgamellotti, A.; Macchioni, A.; Zuccaccia, D. *Chem. Eur. J.* **2010**, *16*, 4814.

6. Dixon, M.; Collin, J. –P.; Sauvage, J. –P.; Flamigni, L.; Encinas, S.; Barigelletti, F. *Chem. Soc. Rev.* **2000**, *29*, 385.
7. Martin, B.; Waind, G. M. *J. Chem. Soc.* **1958**, 4284.
8. Wickramasinghe, W. A.; Bird, P. H.; Serpone, N. *J. Chem. Soc. Chem. Commun.* **1981**, 1284.
9. Garces, F. O.; Watts, R. J. *Inorg. Chem.* **1990**, *29*, 582.
10. Sprouse, S.; King, K. A.; Spellane, P. J.; Watts, R. J. *J. Am. Chem. Soc.* **1984**, *106*, 6647.
11. Fantacci, S.; Angelis, F. D. *Coord. Chem. Rev.* **2011**, *255*, 2704.
12. (a) King, K. A.; Watts, R. J. *J. Am. Chem. Soc.* **1987**, *109*, 1589. (b) Garces, F. O.; King, K. A.; Watts, R. J. *Inorg. Chem.* **1988**, *27*, 3464.
13. Costa, R. D.; Ortí, E.; Bolink, H. J.; Graber, S.; Schaffner, S.; Neuburger, M.; Housecroft, C. E.; Constable, E. C. *Adv. Funct. Mater*. **2009**, *19*, 3456.
14. Zeng, X.; Tavasli, M.; Perepichka, I. F.; Batsanov, A. S.; Bryce, M. R.; Chiang, C. –J.; Rothe, C.; Monkman, A. P. *Chem. Eur. J.* **2008**, *14*, 933.
15. Aubert, V.; Ordronneau, L.; Escadeillas, M.; Williams, J. A. G.; Boucekkine, A.; Coulaud, E.; Dragonetti, C.; Righetto, S.; Roberto, D.; Ugo, R.; Valore, A.; Singh, A.; Zyss, J.; Ledoux-Rak, I.; Bozec, H. L.; Guerchais, V. *Inorg. Chem.* **2011**, *50*, 5027.
16. Lepeltier, M.; Lee, T. K. –M.; Lo, K. K. –W.; Toupet, L.; Bozec, H. L.; Guerchais, V. *Eur. J. Inorg. Chem.* **2005**, 110.
17. Edkins, R. M.; Bettington, S. L.; Goeta, A. E.; Beeby, A. *Dalton Trans*. **2011**, *40*, 12765.
18. Frisch, M. J. *et al*. GAUSSIAN09, revision B.01, Gaussian, Inc., Wallingford, CT, 2010.
19. (a) Dreuw, A.; Head-Gordon, M. *J. Am. Chem. Soc*. **2004**, *126*, 4007 and references therein. (b)Yanai, T.; Tew, D.; Handy, N. *Chem. Phys. Lett.* **2004**, *393*, 51.
20. (a) Guliano, C. R.; Hess, L. D. *IEEE J. Quantum Electron.***1967**, *QE-3*, 358. (b) Sheik-Bahae, M.; Said, A. A.; Van Stryland, E. W. *Opt. Lett.* **1989**, *14*, 955.

21. (a) Rao, S. V.; Rao, D. N. *Chem. Phys. Lett.* **1998**, *283(3-4)*, 227. (b) Rao, D. N.; Rao, S. V.; Blanco, E.; Aranda, F. J.; Rao, D. V. G. L. N.; Akkara, J. A. *J. Sci. Ind. Res.* **1998**, *57(10,11)*, 664. (c) Rao, S. V.; Rao, D. N.; Akkara, J. A.; DeCristofano, B. S.; Rao, D. V. G. L. N. *Chem. Phys. Lett.* **1998**, *297*, 491. (d) Gangopadhyay, P.; Rao, S. V.; Rao, D. N.; Radhakrishnan, T. P.; *J. Mater. Chem*. **1999**, *9(8)*, 1699. (e) Rao, S. V.; Srinivas, N. K. M. N.; Giribabu, L.; Maiya, B. G.; Rao, D. N.; Philip, R.; Kumar, R. G. *Opt. Commun*. **2000**, *182*, 255. (f) Srinivas, N. K. M. N.; Rao, S. V.; Rao, D. N. *Journal of Porphyrins and Phthalocyanines* **2001**, *5(7)*, 549.

22. Zheng, Q.; He, G. S.; Prasad, P. N. *J. Mater. Chem*. **2005**, *15*, 579.

Spectrum 5.1. ^{1}H NMR spectrum of Ir(MS 3)

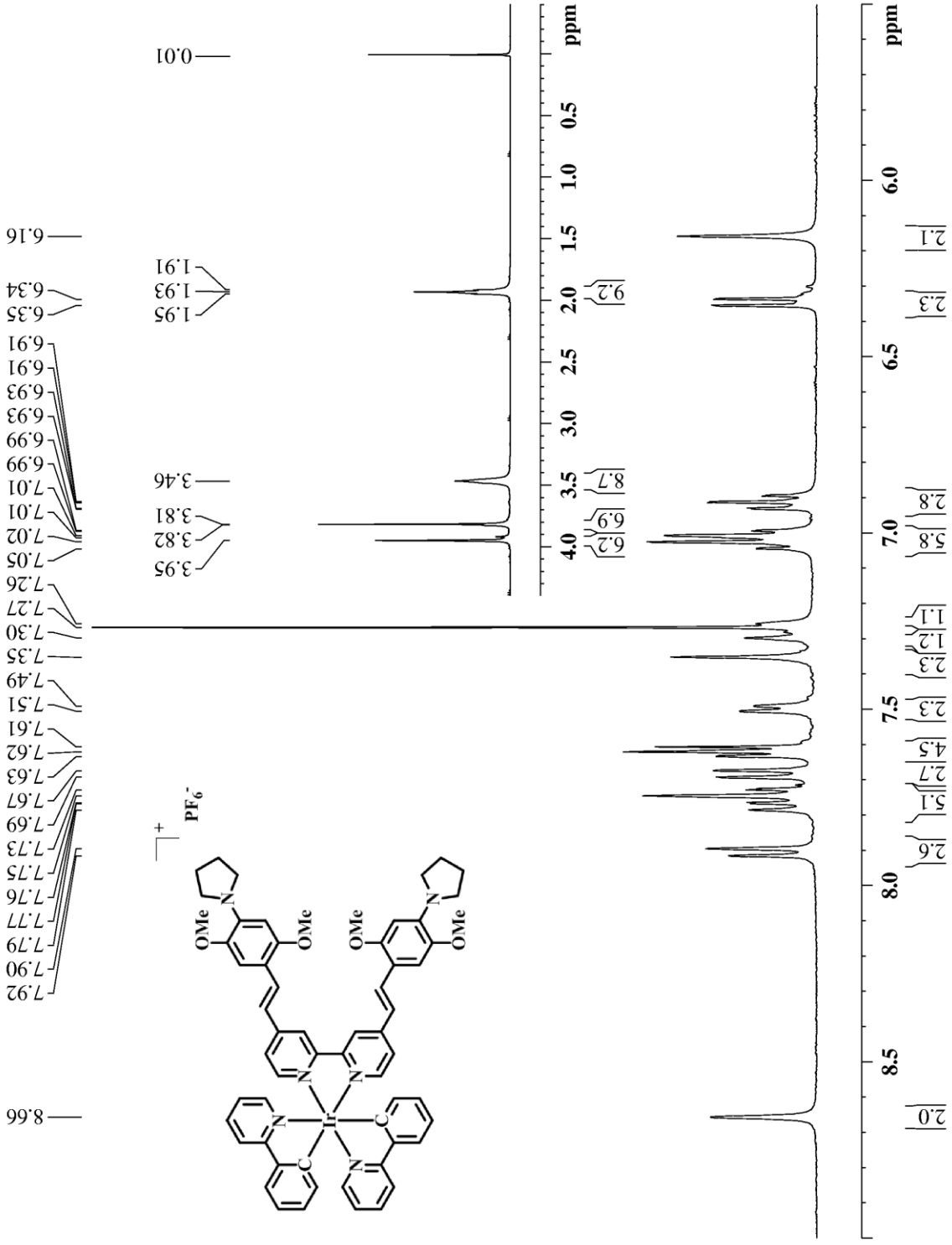

Spectrum 5.2. ^{1}H NMR spectrum of Ir(MS 4)

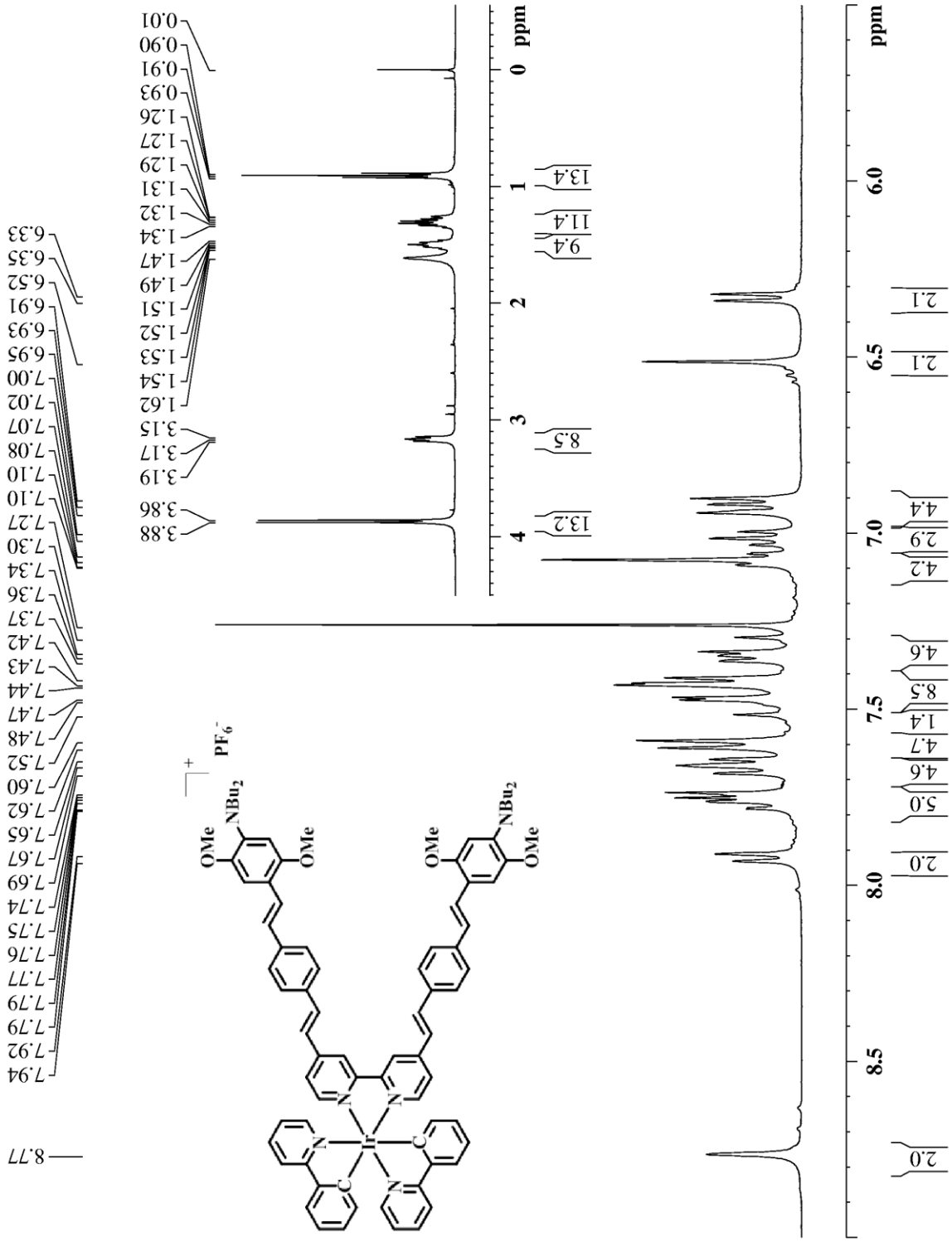

Spectrum 5.3. ^{1}H NMR spectrum of Ir(MS 5)

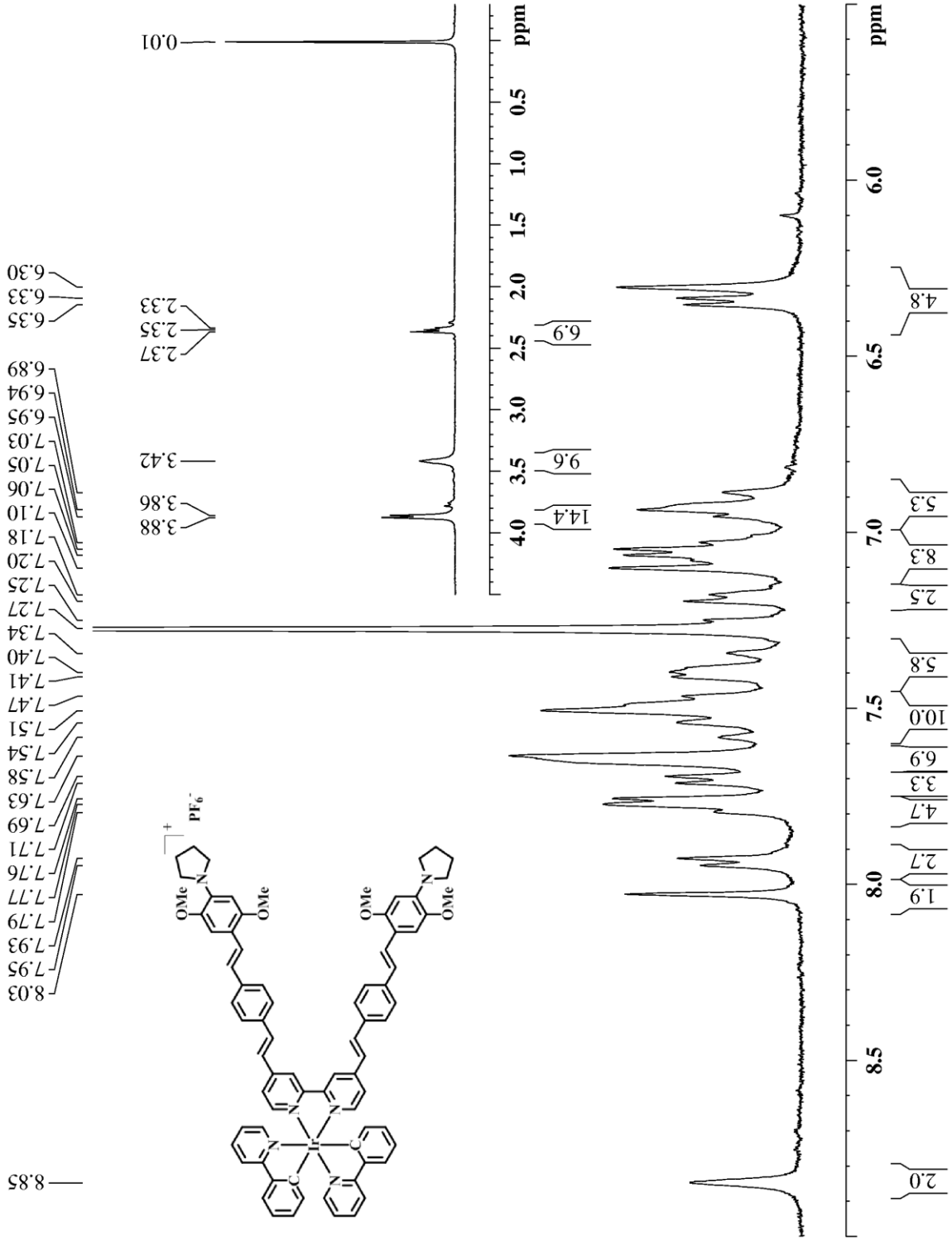

Spectrum 5.4. ^{1}H NMR spectrum of Ir(MS 6)

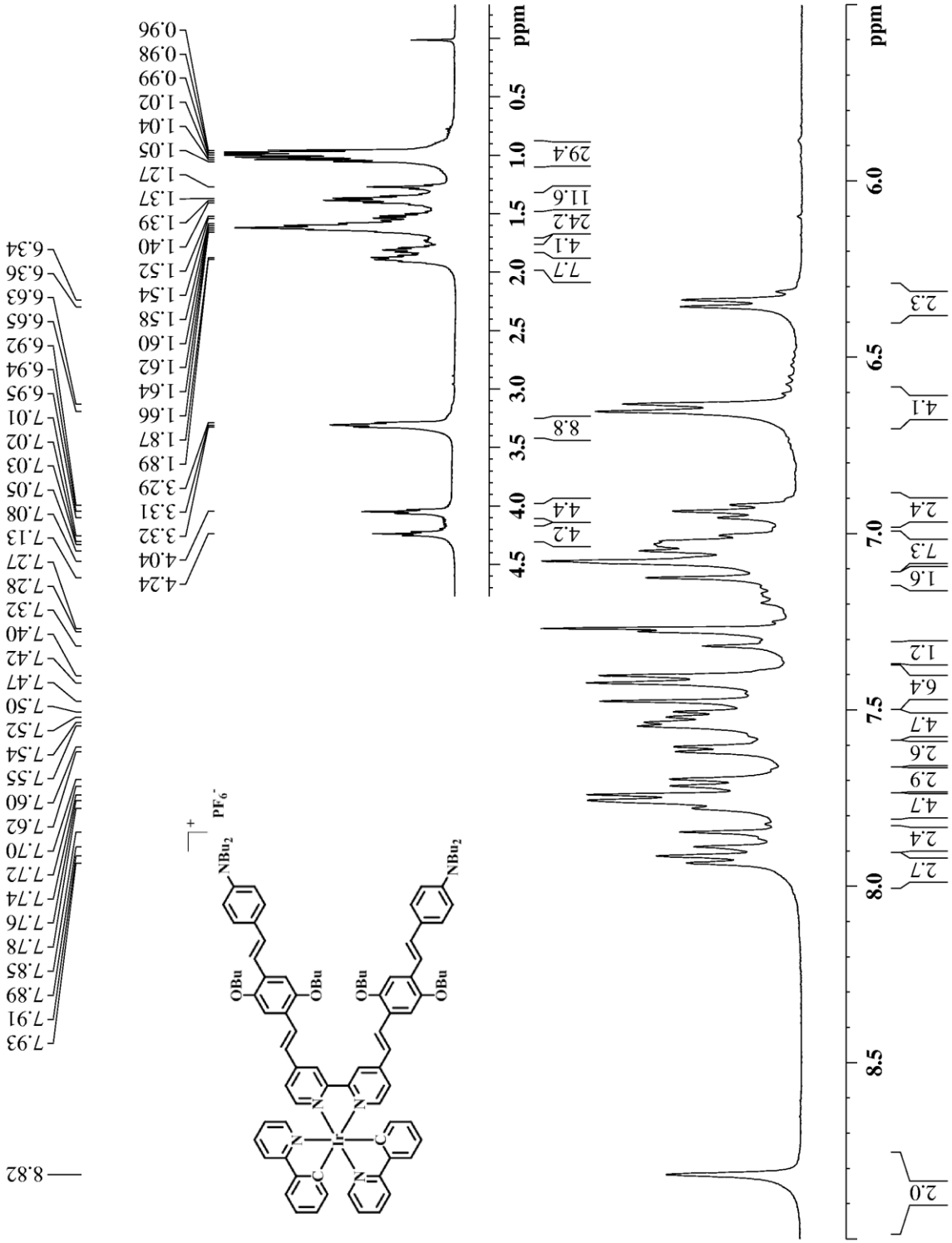

Spectrum 5.5. ^{1}H NMR spectrum of Ir(MS 7)

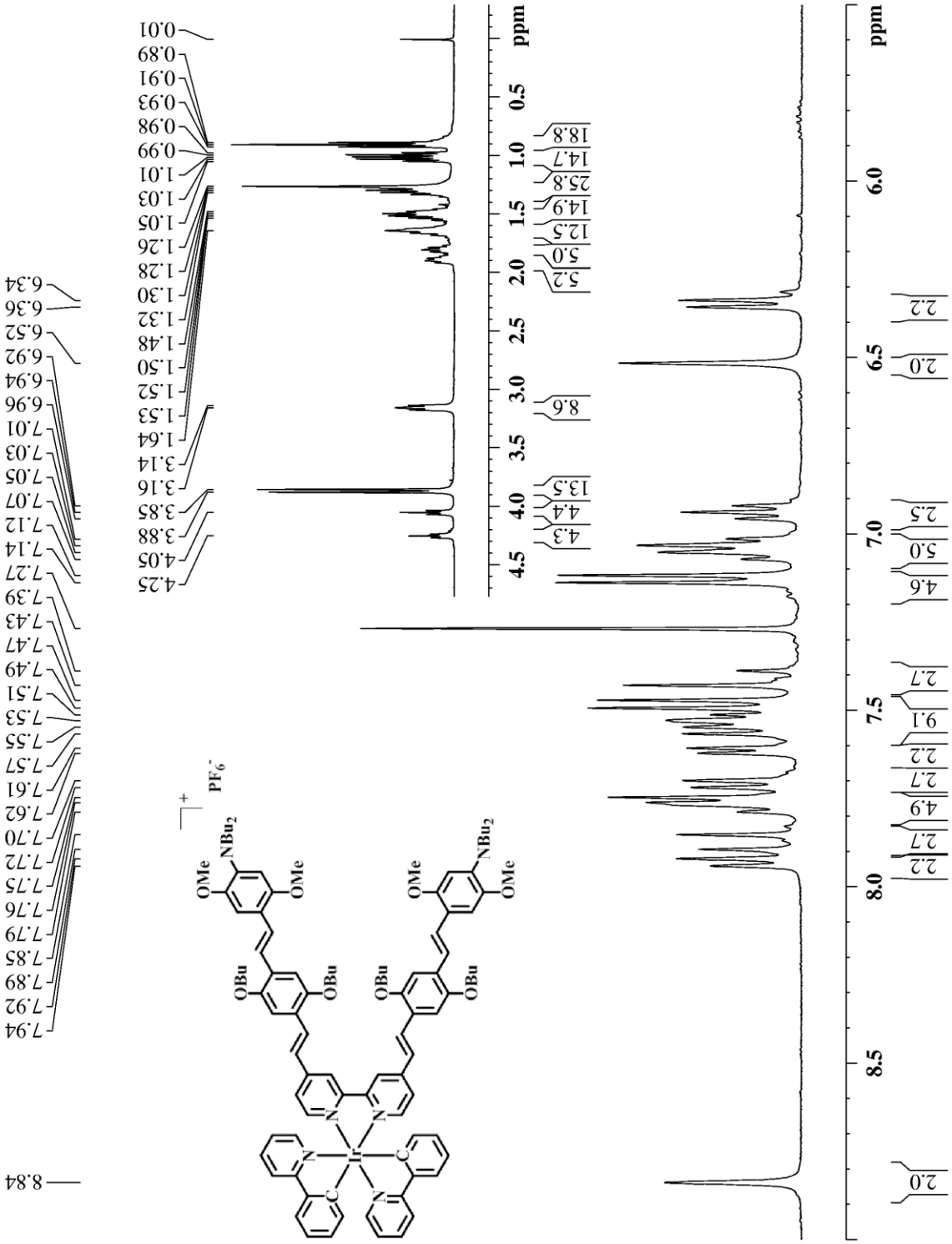

Spectrum 5.6. ^{1}H NMR spectrum of Ir(MS 8)

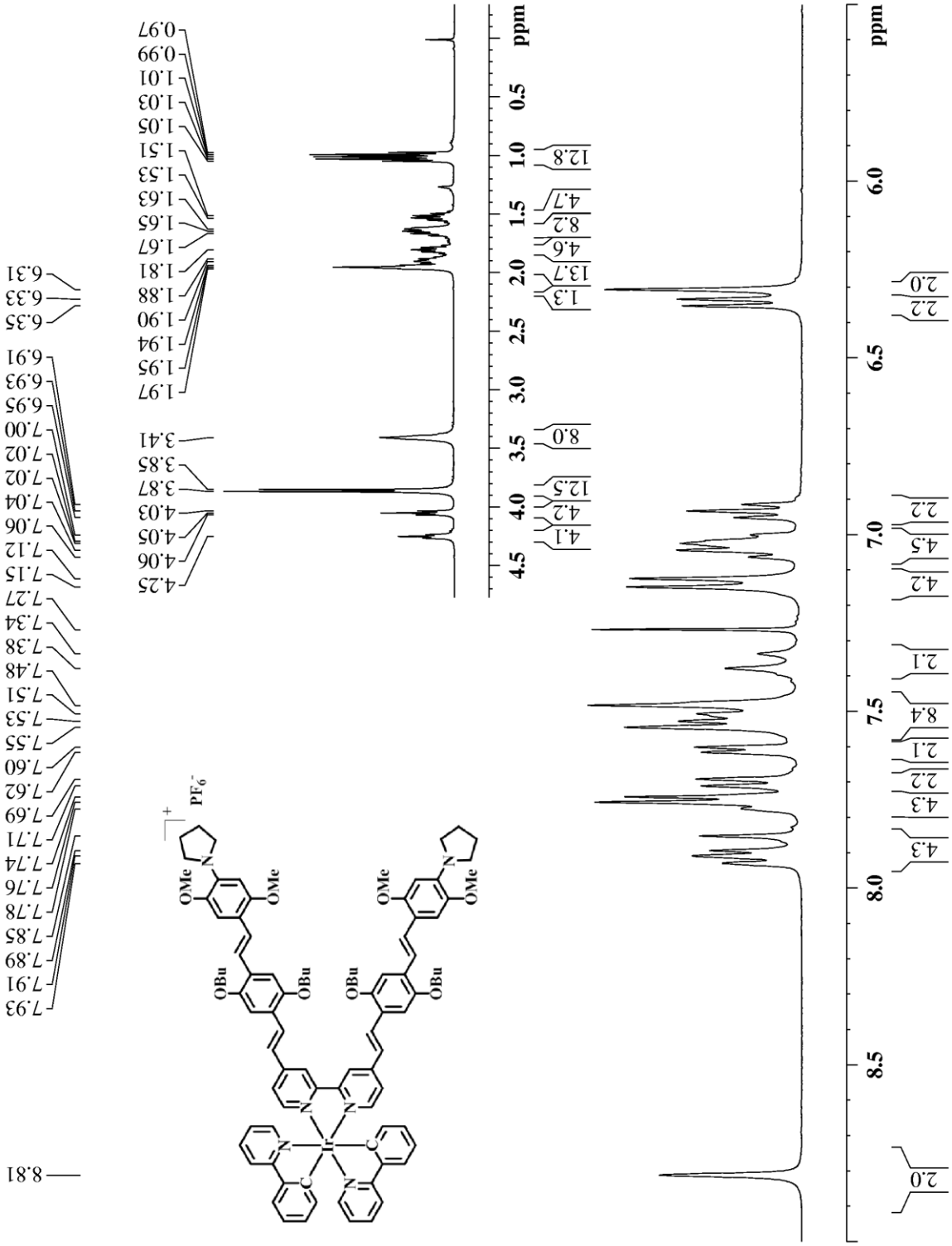

••••

Chapter-6

Concluding Remarks and Future Scopes of the Present Work

• 6.1. SUMMARY AND CONCLUSION

The present thesis incorporates macrocycles and 4,4'–π–conjugated–2,2'–bipyridine derivatives as the major research substrates. The introductory notes on the relevant systems have been summarized in Chapter 1, i.e., this chapter embodies an introduction to the chemistry of macrocycles and bipyridine derivatives while the motivation of the work has been outlined in the last section of the chapter. The major focus of this chapter is only on the significant aspects of the aforesaid materials. Macrocycles are the potential hosts for diverse classes of ionic species whereas the bipyridines are well-known in the area of Coordination Chemistry. Aza-macrocycles and crown ethers are the widely acclaimed building blocks in the area of Supramolecular Chemistry. Although, the two aforementioned classes of substrates have been the subject of various novel research articles till date, many important facets of the interlaying chemical aspects of these two classes of substances are yet to be explored. For instance, the macrocycle Transdiene, has been known since the 1960s and its transition metal complexes are reported to have potential biological and catalytic activities, but the chiral behavior of the pertinent complexes have been paid least attention.

Similarly, the π–extended organic molecules have enticed the scientific community due to their versatile applications in the area of integrated electronics; the Liquid Crystal Display (LCD), Thin Film Transistors (TFT) and Organic Light Emitting Diodes (OLED) being the most common. The heterocyclic organic compounds are promising materials in organic electronics. The 2,2'–bipyridines containing a π–conjugated framework and their transition metal complexes belong to another class of important materials and have been explored in various branches of photosciences e.g., nonlinear optics, dye sensitized solar cells, OLEDs, etc. The spectral feature of these materials is a direct outcome of the nature of substituents in their π–skeleton and their photonic behavior could merely be tuned through judicious selection of the end-capping functionalities. It is thus, worth mentioning that, the design and synthesis of such materials which respond in the longer wavelength region of the electromagnetic spectrum would be an interesting topic of research.

Some queries which cropped up in our minds during rigorous literature survey instigated us to accomplish the present work. A few vital points which have never been emphasized, such as, (i) the chiral resolution of transition metal complexes of the macrocycle, Transdiene; (b) whether supramolecular complexes of crown ethers with angular shaped guests would lead to a helical crystal packing or not and, (c) the difference in photophysical behavior of 2,2'–bipyridines end-capped with hetero-donor functionalities against the known homo-donor derivatives, etc. are the key aspects for which we initiated our work in this direction.

The intermolecular non-covalent association between transition metal complexes of two tetra-aza macrocyclic systems (transdiene and cyclen) and Lindqvist type polyoxometalate (POM) cluster anions has been illustrated in Chapter 2. The various complexes were isolated as their hexametalate salts and their spectroscopic and crystallographic aspects have been illustrated in details. The non-covalent weak interactive forces between various functionalities of the structural motifs are mainly responsible for building the crystals in a three-dimensional array, the hydrogen bonding interactions being the most important due to their directional nature. It is nonetheless important to mention that, hydrogen bonds play a major role in the biological systems, the interaction between the various nucleic bases in the double helical structure of DNA being one of the brightest instances. The double helical architecture of DNA is an excellent example of chiral packing feature, which in most cases, is achieved through hydrogen bonding interactions between the structural motifs in the crystal lattices. The helical packing of the supramolecular building blocks is primarily sub-grouped in two categories: homochiral and heterochiral. In the first case, similar chirality is transmitted through the adjacent helices while in the latter case the adjacent helices of opposite chirality are usually linked by the solvent molecules, anions etc. Each of the crystals containing right and left handed homochiral packing motifs are chiral and they form a bulk condensate with equal distribution, the separation of the individual crystals (i.e. the enantiomers) being known as the Spontaneous Resolution. On the contrary, heterochirality turns the individual crystals optically inactive. The present work aims at understanding as to whether the transition metal complexes of transdiene (*racemic* form) can be spontaneously resolved or not. The *racemic*– isomers essentially have a 50:50

distribution of the *RR*– and *SS*– enantiomers which mostly form racemic condensates. However, only the conglomerate formation involves spontaneous resolution of the enantiomers which in turn occurs with 5–10% of the racemates only. Thus, chiral resolution seems to be a very challenging task and this is what is portrayed in Chapter 2.

The most important finding of the work carried out in the Chapter 2, is the occurrence of spontaneous resolution of the copper complex of transdiene with the POM anions during crystallization whereas the other six compounds crystallize in centrosymmetric space groups (Chapter 2). The *rac*– diastereomer of $[Cu(L)](ClO_4)_2$ has been observed to crystallize as a racemate (space group = $P2_1/c$) from methanol, wherein the perchlorate counter anion acts as a mediator for transferring opposite chirality between the two opposite handed Cu^{II}–L helical chains. The same result is also obtained upon crystallization of $[Cu(L)](ClO_4)_2$ from acetonitrile. However, replacing the perchlorate counter anion with the hexatungstate anion leads to the occurrence of spontaneous resolution during crystallization in acetonitrile solvent. Both the enantiomorphs of compound $[Cu(L)(MeCN)][W_6O_{19}]$ (**P** and **M**) have been structurally elucidated which clearly reveals that the principal reason behind this occurrence is the transmittance of interstrand chirality through hydrogen bonding interactions throughout the network. In addition, the occurrence of spontaneous resolution has also been firmly confirmed on the basis of CD spectra of the relevant compounds which exhibit opposite Cotton effects. Therefore, the POM anion participation as well as acetonitrile coordination to the copper center is strongly believed to play an important role in this unique spontaneous resolution process. In order to further comprehend whether the macrocycle, the POM or solvent coordination plays the major role in the occurrence of spontaneous resolution, we have also studied another copper macrocycle assisted by a POM cluster anion, $[Cu(cyclen)(MeCN)][W_6O_{19}]$. This complex also has a copper coordinated acetonitrile molecule, but it does not crystallize in any chiral space group.

We have also tried to explore if the angular geometry of guest molecules leads to any helical crystal packing. In an endeavour to do so, we have demonstrated in Chapter 3, seven host–guest complexes in which ammonium–type cationic guests are incorporated with various crown ethers. In the pertinent study, we have used doubly protonated 3–amino pyridine ($3AmPyH_2$), diamino diphenyl ether ($DADPEH_2$) and diamino diphenyl

methane ($DADPMH_2$) that serve the role of anchoring units to the crown ethers. Among all the supramolecular complexes demonstrated in this chapter, only the compound $[3AmPyH_2(12C4)_2](ClO_4)_2]$ crystallizes in a chiral space symmetry ($P2_1$). The differing behavior of 12C4 in this compound (chiral packing) is not very clear to us at this level of investigation. The crystallographic analysis of all the compounds discussed in the Chapter 3 reveals that the crown ethers play a dual role, i.e., hydrogen bonding acceptance as well as donation. The guest integration within the host cavity is mainly governed by the N–H···O hydrogen bridges between the ammonium functionalities and the oxygen acceptor heteroatoms of the crown ethers, while the weak C–H···O interaction between the crown ethers and the perchlorate counter anions in the crystal lattice of the aforementioned compounds concurrently plays an important role in packing the host-guest complexes. However, owing to the failure of crystallization attempts, the complete set of crystal data regarding complexation of the same crown ether with all the three ammonium systems is unavailable. Hence, drawing a straightforward structure–packing correlation is beyond the scope of the present work.

In the Chapter 4, we have shown how simple modification of the π–skeleton of donor-acceptor based bipyridine derivatives modulates their fluorescence behavior. In an endeavor to do so, a series of *styryl*– and *bistyryl*– 2,2'–bipyridine chromophores functionalized with both the alkoxy and amino functionalities were synthesized and their photophysical properties have been demonstrated. The prototype of the synthesized dyads is of D–π–A–A–π–D (D = donor, A = acceptor) in which the bipyridine moiety acts as the central acceptor core to join the terminal donor functionalities through vinylene linkers. The 2,2'–bipyridine derivatives are generally endowed with an extensive coordination / supramolecular chemistry. This N–heterobiaryl compound has been employed in our study because the pyridine rings can be easily derivatized thereby paving the way for the introduction of an assorted class of donor end-capping functionalities to tune the optical properties of the relevant 2,2'–bipyridine based dyads. The transition metal complexes of the 2,2'–bipyridine based DA systems are of topical interest due to their potential applicability in octupolar nonlinearity and this is what has drawn our attention and motivated us to carry forward our research in this direction. The photophysical properties (absorption and emission) of the synthesized chromophores are

found to be governed by the intramolecular charge separation between the donor end-capping functionalities and the pyridine acceptor heterocycle as depicted by the computational studies. A large solvent sensitive photoluminescent behavior has been observed for the synthesized compounds which clearly indicate that the emitting state of the fluorophores is more polar than the ground electronic state. Furthermore, it has been observed that the conjugation backbone i.e. the nature, position and number of donor functionalities modulate the absorptive and emissive nature of the title chromophores. For instance, among the eight dye stuffs described in the Chapter 4, the compound, **MS 5** fluoresce even in the condensed phase which is one of the prerequisite for possible application in light emitting devices. It is thus quite apparent that, variation of the amino donor from open chain dibutylamino in **MS 4** to the cyclic pyrrolidine donor in **MS 5** results in such differing photophysical behavior. In short, our systematic study on the photophysical properties of the 4,4'–π–conjugated–2,2'–bipyridine based hetero-donor systems in comparison with the parent chromophores bearing alike donor functionalities approaches a structure-function relationship which would be useful for choosing the materials for practical applications (in terms of devising nonlinear optical and solar energy harvesting materials). In view of that, the findings of the current study in conjunction with the photophysics of the earlier reported parent dye molecules construct a library of such systems wherein, the present exploration finds some remarkable diversities in the fluorescence responses compared to the parent molecules functionalized with only one kind of donor sub-chromophores.

As already mentioned, the transition metal complexes of 2,2'–bipyridine based DA systems are useful in various fields, such as, nonlinear optics, photonic devices, etc. As such, in order to check out whether the structural factors would improve the linear and nonlinear optical properties of the extended π–conjugated bipyridyl metal complexes or not, we synthesized a new series of cyclometalated Ir^{III} complexes which has been described in Chapter 5. Since the synthesis of homoleptic Iridium complexes seems to be more intricate and tedious as compared to that of the heteroleptic complexes, therefore, the synthesis of heteroleptic cyclometalated Ir^{III} complexes was preferred in our study. The absorption spectra of the synthesized complexes have been found to display a broad structureless feature in the 350–700 nm spectral region, but in most of the cases, the two

bands are well resolved in this region. These two bands are due to the intraligand charge transfer (ILCT) transitions and due to the involvement of mixed metal and ligand centered transitions (ILCT, LL'CT, MLCT, IL etc.) respectively as depicted by the computational studies. A systematic variation in the nature, position and number of donor groups has been observed to modulate their electronic absorption behavior and a negative solvatochromic effect has been observed on increasing the solvent polarity. A bathochromic shift (*ca.* 25–35 nm) of the highest energy band has been observed for the cyclic pyrrolidine donors as compared to their acyclic dibutylamino analogues in the title complexes irrespective of the solvent. Also, it has been observed that only two metal complexes containing cyclic donor systems emit in the NIR region. Eventually, the two-photon absorption cross-sections of the synthesized complexes were measured in dichloromethane solvent using the Z–scan technique yielding a moderately good value of σ_2. Such classes of cyclometalated iridium complexes can herald new and exciting opportunities to have a better control over the photophysical aspects intended to be used for a wide variety of applications.

• 6.2. FUTURE SCOPES

It has already been stated that isolation of the spontaneously resolved crystals from a bulk conglomerate is a difficult task. The occurrence of spontaneous resolution of the individual enantiomorphs is affected by several factors which lead to the isolation of achiral crystals. The competition between homochirality and heterochirality in the crystal lattice often hinders this process and hence a straightforward prediction about the occurrence of this phenomenon is complicated a priori. As such, it is quite evident that special attention is needed while working in this direction.

Although a large number of publications have demonstrated diverse properties of the transition metal complexes of the macrocycle Transdiene till date, the chirality of the relevant systems have not been depicted yet. Hence, in the quest for isolation of individual enantiomorphs of the pertinent macrocyclic complexes through spontaneous resolution, we have made use of the polyoxometalate cluster anions as described in Chapter 2. In spite of the fact that we were able to isolate individual enantiomorphic crystals of one of the complexes through spontaneous resolution, the interlaying phenomenon responsible for the negative outcome in the rest of the complexes is not very

clear to us at this level and this issue needs to be resolved in the near future. In a nutshell, rigorous analysis of the structural data of related systems are needed to address a straightforward explanation for the occurrence of this phenomenon in such complexes which has not been hitherto addressed. We anticipate that usage of chiral polyoxometalates in conjunction with the transition metal complexes of Transdiene could make the scenario vivid. Some of the chiral POM structures include $[H_4Co_2Mo_{10}O_{38}]^{6-}$, $[P_6W_{18}O_{79}]^{20-}$, $[P_2Mo_5O_{23}]^{6-}$, etc. The association of the macrocycles (used in Chapter 2) and the host-guest complexes (used in Chapter 3) with chiral POMs have not been explored yet. The work to be accomplished in this direction would be performed in the near future in our laboratory.

While the Chapters 2 and 3 are motivated by single crystal X-ray crystallography, the Chapters 4 and 5 deal with the chemistry associated with the widely acclaimed ligand 2,2'–bipyridine. This ligand and its several derivatives have already been widely studied for a diverse class of applications. However, the scope of the present work was limited to only synthesis and photophysical characterizations of some of the related compounds. We have demonstrated, in this thesis, how simple modification of the conjugated backbone of the relevant bipyridine dyads modulates their photophysical behavior. Nevertheless, it is important to mention that, a series of transition metal complexes of the synthesized bipyridine ligands could be synthesized for custom tailored applications. However due to certain limitations, we had to restrain ourselves to explore only a few numbers of such complexes. However, from the relevant study, we have learnt how to tune the optical properties of the pertinent ligands and their metal complexes. It is a known fact that, coordination of a metal to donor end-capped, extended π–conjugated chromophores such as conjugated bipyridine, phenanthroline or terpyridine ligands produces a significant augmentation of their NLO response. This is for the reason that the metal acts as a Lewis acceptor, thereby causing a red-shift of the intraligand charge transfer transition (ILCT). Though Ir^{III} cyclometalated complexes have only recently received attention as NLO materials, they have been characterized as exhibiting one of the highest second order NLO responses ever reported for a transition metal complex. High NLO response for cationic Ir^{III} complexes is generally reached without any cost in transparency because these complexes exhibit relatively high energy absorptions, which is a crucial feature in

the design of NLO–phores. We strongly believe that the Iridium complexes demonstrated in the Chapter 5 would exhibit high second order NLO response. Besides the nonlinear optical responses of the related transition metal complexes, their electroluminescent behavior has been a subject of considerable interest in recent times. The photon emission efficiency in response to the electric field is dependent on several parameters. The electroluminescent quantum yield is usually optimized on the basis of several trial and error experimentations. The cyclometalated Iridium complexes of 2,2'–bipyridines are excellent emitters under the influence of electric field. We believe that, in future, we would be able to contribute in this area via the improvement of the photophysical behavior of related complexes.